UNIVERSITY OF LONDON THESIS

Degree PhD Year 2007 Name of Author RICKETTS, Claire Louise

The reactions of the molecular nitrogen doubly charged ion with neutral molecules of relevance to planetary ionospheres

by

Claire Louise Ricketts

A thesis submitted for the degree of Doctor of Philosophy

University College London

University of London

2007

ProQuest LLC
789 East Eisenhower Parkway
P.O. Box 1346
Ann Arbor, MI 48106-1346

Abstract

Diatomic dications (e.g. CO^{2+}) have been known to exist for several decades and are believed to be important components of energised media. Molecular dications possess significant internal energy due to the Coulombic repulsion of their two positive charges, meaning that many possible reaction channels are available to dications in a collision with a neutral molecule. Modellers have recently predicted that N_2^{2+} is present in the ionosphere of Earth and Titan as well as the dications O_2^{2+} and O^{2+} in the ionosphere of Earth and CO_2^{2+} in the ionosphere of Mars. These recent predictions, of dications in planetary ionospheres, imply that dications, and processes involving dication-neutral collisions, may have more significance than previously thought in the upper atmospheres of planets. Therefore this thesis describes a study of the reactions between N_2^{2+}dications and neutrals, potentially of relevance to the ionosphere of Earth and Titan.

A position sensitive coincidence (PSCO) time-of flight (TOF) mass spectrometer is used to probe the reactivity, energetics and dynamics of the bimolecular reactions of N_2^{2+}. Dication-neutrals reactions often result in a pair of singly charged ions. The PSCO experiment is used to collect these pairs of singly-charged ions in coincidence. From the position-sensitive data we extract the velocity vectors of the product ions, and if the reaction of interest involves the formation of a third, undetected, neutral species, its velocity can be determined via conservation of momentum.

The electron transfer reactions between dications and neutrals have been well rationalized previously, so only the electron transfer reactions of N_2^{2+} with Ne and NO are discussed in this thesis. This thesis concentrates on probing the less well rationalized, bond-forming reactions between dications and neutrals. The bond-forming reactions of N_2^{2+} with O_2, CO_2, H_2O, C_2H_2, CH_4, H_2 and Ar have been investigated and discussed. Several new bond-forming reactions mechanisms are derived for example, the bond-forming reactions of N_2^{2+} with O_2 proceed via a 'long' lived complex which dissociates via loss of a neutral and then charge separation, a mechanism which is also operating for one of the bond-forming reactions of N_2^{2+} with CO_2 and N_2^{2+} with H_2O. Additional bond-forming reactions are detected for N_2^{2+} with CO_2 and H_2O, which proceed via shorter lived collision complexes. The reactions of N_2^{2+} with C_2H_2, CH_4, H_2 and Ar all proceed via a variety of mechanisms involving short-lived collision complexes or H and electron stripping.

Acknowledgements

I would like to express my thanks and gratitude to the following people for their help with this thesis;

Steve Price for his excellent supervision, and in particular his unwavering patience, throughout the course of my PhD.

Detlef Schroder, for his suggestions and correction of my final draft.

Sarah Harper, for voluntarily helping to teach me to use the PSCO in my first year.

Anna Kenyon, for undertaking with great care, the arduous task of proof reading.

Richard Underwood, for dealing with the final stages of printing and binding while I was out of the country.

My father Christopher, my mother Christine, my brother Paul, my sister Kathryn and all my grandparents, for their belief, encouragement and support.

Table of Contents

List of Figures

Chapter 1 Introduction

Chapter 2 Experimental Arrangement and Data Processing

Chapter 3 Introduction to the Nitrogen Dication and the PSCO spectra

Chapter 4 The reactions of the Nitrogen Dication Part I: Electron Transfer Reactions of N_2^{2+} with Ne and NO

Chapter 5 The reactions of the Nitrogen Dication Part II: Bond-forming reactions of N_2^{2+} with O_2, CO_2 and H_2O

Chapter 6 The reactions of the Nitrogen Dication Part III: Bond-forming reactions of N_2^{2+} with C_2H_2, H_2, CH_4 and Ar

Appendix A

Appendix B Other bond-forming reactions of dications with neutrals

List of Tables

Chapter 3 Introduction to the Nitrogen Dication and the PSCO spectra

Chapter 4 The reactions of the Nitrogen Dication Part I: Electron Transfer Reactions of N_2^{2+} with Ne and NO

Chapter 6 The reactions of the Nitrogen Dication Part III: Bond-forming reactions of N_2^{2+} with C_2H_2, H_2, CH_4 and Ar

Chapter 1 Introduction

Diatomic dications have been known to exist for several decades. One of the earliest observations of a molecular dication was that of CO^{2+} in mass spectrometric experiments in 1930. [1] The importance of monocations in energised environments, and their reactions within these environments, was quickly realised. [2] However, when molecular dications were first detected, they were regarded simply as a curiosity. But the fact these dications had lived for the time it took to cover the distance from the ion source to the mass spectrometer's detector proved these doubly-charged molecules must have a lifetime of at least the order of 10^{-6} seconds. Some notable early work includes the first measurements of the double ionisation energies of N_2 and CO in the early 1930s and the first theoretical prediction of a stable dicationic species, He_2^{2+}, made by Pauling, in 1933. [3-7] Over the past 70 years a range of experimental and computational techniques have revealed detailed information concerning the properties of molecular dications. [8-11] However, it was not until the 1980s that the first real studies of the reactivity of molecular dications were made.

The first studies of dication reactivity involved collisions with rare gas atoms in conventional or adapted mass spectrometers. [12-17] The products identified revealed a significant level of electron transfer from the neutral to the dication. In the last decade purpose built spectrometers have been developed for the study of the chemical reactivity between dications and neutrals. [18-20] Such investigations were stimulated by the first recorded observation of a bond-forming reaction (equation (1.1)) from a molecular dication-neutral collision, which was detected in a drift tube experiment. [21]

First observed bond-forming reaction: $O_2^{2+} + NO \rightarrow NO_2^{+} + O^{+}$ (1.1)

An understanding of the properties and reactions of dications is important for the study of a wide variety of energised media, such as plasmas, planetary ionospheres and the interstellar medium (ISM). [22, 23] Indeed, there is a discussion of the role of dications in some techniques for biological diagnosis. [24] Hence, to improve our understanding of these varied environments it is necessary to study the properties and reactions of dications.

This thesis presents the results of an investigation of the reactivity of gas phase dications with neutrals of relevance to planetary ionospheres, with particular attention paid to the bond-forming reactions that are observed. The experiment used for this investigation is a

Position Sensitive Coincidence (PSCO) experiment, which involves the position-sensitive detection of the product ion pairs from individual dicationic reactive events using time-of-flight mass spectrometry (TOFMS). This PSCO technique allows the detailed study of the reactivity for each collision system studied. As well as identifying the individual reactive channels, the coincidence data provides a powerful mechanistic and energetic probe of each individual reactive process. In order to put these PSCO investigations into context, this chapter will discuss the role of dications in different media, with particular attention paid to planetary ionospheres followed by a discussion of the properties of molecular dications and what is known of their reactivity. A review of the experimental techniques used to form dications and probe their properties and reactivity is then presented.

1.1 The role of dications in energized media

The experiments presented in this thesis concentrate on reactions of potential ionospheric interest between dications and neutrals. The following section briefly describes some of the roles dications in a variety of media and then focuses on a discussion of recent work modelling the chemistry of dications in planetary ionospheres.

1.1.1 Astrochemical and industrial roles of dications

Signatures of large polycyclic aromatic hydrocarbons (PAH) have been detected in the ISM via infra-red (IR) emission and absorption features in the visible region of the spectrum. [25-27] One suggested mechanism of formation, fragmentation and eventual destruction of a particular PAH in the ISM involves a number of excitation processes that can lead to dicationic species. Molecular dications have also been proposed for uses such as rocket propellants. [28] For example the lifetime of He_2^{2+} is found to be relatively long with a lifetime of 220 minutes before unimolecular dissociation to $He^+ + He^+$. [28] The dissociation of He_2^{2+} can release between 230 and 1000 kcal/mol of energy, which has meant that He_2^{2+} has attracted interest in dications as rocket propellants, especially given the long length of the He_2^{2+} lifetime, combined with its low mass and large energy content. In principle such dicationic fuels have many advantages over the existing liquid hydrogen and oxygen rocket fuels. Reactions of N_2^{2+} in bow shock waves of re-entry vehicles are also of interest. [29]

Industrially, knowledge of the properties of dications is important to understand their contribution to the properties of plasmas (ionised gases composed of ions, electrons, and neutral particles), used for example in plasma etching and fusion, and for use in lasers. With regards to industrial plasma, it is important that the plasma is operated with the optimal conditions. To attain the optimal conditions an accurate knowledge of molecular partial ionisation cross sections is important. Accurate partial ionisation cross sections allow the ionic abundances in the plasma to be precisely modelled, helping a theoretical understanding of the plasma. [30-32] However, currently, these molecular partial ionisation cross sections have a level of ambiguity and inconsistency, which leads to major problems in the theoretical modelling of plasma processes. One reason for the uncertainty in molecular partial ionisation cross sections is that dications were commonly believed to only account for a very small percentage of the total ionisation yield and so their contribution to the ion yields above the double ionisation potential was thought unnecessary. Accurate measurement of partial ionisation cross sections, where all energetic fragment ions are detected, has now shown that multiple ionisation contributes significantly to the total ion yield above the relevant ionisation potential. For example, at 100 eV Cl_2^{2+} has been shown to contribute up to 26% of the ion yield following ionisation of the chlorine molecule. [30] A second potential application of dication properties is in excimer, or excited dimer, lasers. Excimer lasers use a diatomic molecule, usually involving an inert gas atom and a halide atom, which is bound in an excited state. Emission from the dicationic states of diatomic dications has been proposed as a potential excimer laser medium. [33]

Dications have also proved to be involved in biological diagnostic techniques. [24, 34] Atrazine, a cyclic organic molecule, is used widely in agriculture in low concentrations as a herbicide to kill grassy weeds and can be used in higher concentrations as a biological weapon to kill all plant life. Atrazine and other compounds with the same functionality are water pollutants, so monitoring the water supply for atrazine contamination is imperative. In the relevant mass spectra, singly charged fragments of atrazine are absent or of very low abundance; the same is true for compounds with related structures. However, intense and distinctive dication fragments are observed in the Mass Spectra (MS) of these compounds, and so can be used as a signal of the presence of these contaminants. Thus, an understanding of the properties of dications is even relevant in analytical chemistry.

1.1.2 Dications in planetary ionospheres

This thesis concentrates on the study of reactions of dication–neutral interactions that potentially have a role in planetary ionospheres. An ionosphere is defined as the region of an atmosphere where the number of free electrons and ions present is significant. Ionospheres have been observed to be associated with all the bodies in the solar system that are surrounded by a neutral gas atmosphere. [35] This includes seven of the eight classical planets; excluded is Mercury because it has very little atmosphere. In addition to the seven planets, ionospheres have been observed on several moons including Io, Europa, Titan and Triton, and comets including the famous Halley and Hale-Bopp.

Ionospheric modellers have recently demonstrated that CO_2^{2+} should be present in the ionosphere of Mars, and this prediction stimulated interest in the role of dications in other planetary ionospheres, including that of Earth, Venus and Titan. [22, 36-38] The existence of metastable dications in planetary ionospheres had not been considered to any significant extent previously as, again, double ionisation was considered to be negligibly important in these media. As described above, recent experimental measurements have shown that metastable dications can be a significant ionic product, and dissociative double ionisation can contribute significantly to the ion yield from electron-molecule collisions at energies above the double ionisation energy. Indeed, modellers have also recently predicted non-negligible abundances of several dications in the ionospheres of Earth and the moon Titan. This interest in the involvement of dications in ionospheric chemistry has become a topic of current interest in the field. The next sections discuss these recent modelling results.

1.1.2.1 Earth

The nature of the Aurora Borealis, the Northern Lights, and Aurora Australis, the Southern Lights has invoked interest for thousands of years. Even today the ion chemistry of the terrestrial auroral ionosphere still retains some mysteries, particularly where the involvement of dications is concerned. Interest in the presence of dications in the terrestrial ionosphere was in fact stimulated over half a century ago by Vegard's identification of the O^{2+} line at 500.8 nm in the auroral spectrum. However, because the 496.0 nm line which should accompany this 500.8 nm line did not appear in the spectrum, Vegards assignment was subsequently rejected. [36] Then in the late 1960s Hoffman reported the detection of O^{2+} in the ionosphere by the mass spectrometer on board the

satellite Explorer 31. [39] In the mid 1970s Prasad and Furman suggested that O_2^{2+} dications in the ionosphere could provide an explanation for the large inconsistencies found between the observations and theoretical predictions in the density of auroral O^+ ions. [40] The presence of dications provided a very simple explanation for the inconsistencies, as the dications would be indistinguishable from the singly charged atoms of O^+ in the mass spectrometric satellite measurements since O_2^{2+} and O^+ have the same mass to charge ratio of 16. Breig *et al* produced the first model of ionospheric O^{2+} densities using the Atmosphere Explorer C satellite data recorded in 1974. [41, 42] The dots in Figure 1.1 are plotted from the Atmosphere Explorer C satellite data for the O^{2+} density, by Simon *et al*.

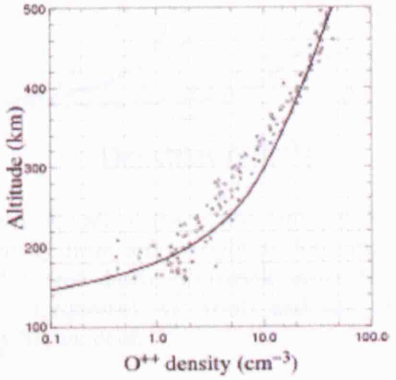

Figure 1.1 The dots show the O^{2+} density in the range 100 to 500 km from the Atmosphere Explorer C satellite data from Simon *et al*.[36]

In addition to the detection of O^{2+} ions in the terrestrial ionosphere, N^{2+} ions have also been detected. [43] These ions can be detected by on board satellite mass spectrometers experiments, since O^{2+} (m/q=8) and N^{2+} (m/q=7) do not overlap with any other significant species. However, mass spectrometry is not suitable for the detection of N_2^{2+} and O_2^{2+} since N^+ and O^+ have, respectively, the same mass to charge ratio. These molecular dications could be detected by optical methods; for example fluorescence has been experimentally detected from N_2^{2+}. [44, 45] Indeed it has been predicted that N_2^{2+} fluorescence should be observable from the terrestrial ionosphere. [36]

Avakyan first modelled the density profiles of N_2^{2+}, O_2^{2+} and O^{2+} in the Earths ionosphere at altitudes of 100-500 km, predicting a peak in dicationic abundances between 100 and 200 km and outlining the need for further investigation of these concentrations. [46, 47] Simon *et al* recently modelled the density of N_2^{2+}, O_2^{2+} and O^{2+} in the Earth's ionosphere over the altitude range 100–500 km and presented calculated density profiles. [36] Although there are no ionospheric measurements for N_2^{2+} and O_2^{2+}, the model was

validated by comparison of the predicted abundances for other ions to the measurements of the satellite Atmosphere Explorer. Figure 1.2 shows the density profiles for the major ionic species in the ionosphere, including dications, from the calculations of Simon *et al.* [36]

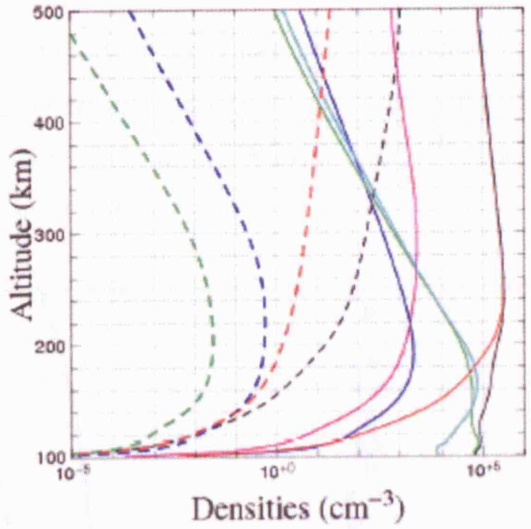

Figure 1.2 Density profiles for all of the major ionic species in the ionosphere, in increasing density from left to right at 200 km; O_2^{2+} (green dash), N_2^{2+} (blue dash), O^{2+} (red dash), H^+ (black dash), N^+ (pink), N_2^+ (blue), O_2^+ (green), NO^+ (turquoise), O^+ (red) and the electron density (black) determined by Simon *et al.* [36]

Simon *et al* showed that the production rates of the doubly-charged ions are smaller than those for singly-charged ions by a factor of approximately 100, with the exception of the production rate of O^{2+} which can represent up to 10% of that of O^+ above 600 km. In fact O^{2+} has the highest density amongst the dications, reaching 60 to 100 ions per cm^3 at 500 km, and hence becoming the ion with the fourth highest density, after O^+, H^+ and N^+. The abundances of N_2^{2+} and O_2^{2+} peak at 1 cm^{-3} and 0.01 cm^{-3} respectively at altitudes between 200 km and 250 km. However, increased solar activity increases the density of the dications. During increased solar activity O^{2+} densities increase by a factor of 2.5 between 150 and 500 km, N_2^{2+} and O_2^{2+} densities increase by a factor of 3 between 100 and 300 km, and by a factor of 10 to 10^5 above 300 km, in comparison with the abundances calculated for periods of low solar activity.[36]

Simon *et al* showed that the three major dications in the earth's ionosphere, N_2^{2+}, O_2^{2+} and O^{2+}, are mainly lost by dissociative recombination and collisions with the most abundant neutral species N_2, O_2 and O. In the region of the density peak of N_2^{2+} and O_2^{2+} the plasma is only weakly ionised so collisions between charged particles are not important and so ion-neutral reactions dominate the reactivity. While the dications are

believed to be detectable under normal solar conditions, the detection of all three dications, N_2^{2+}, O_2^{2+} and O^{2+}, would be made easier in solar maximum conditions, where the sun produces more radiation, and at noon when densities are at their highest.[36]

1.1.2.2 Mars

The dication of carbon dioxide CO_2^{2+}, has been predicted to be present as a minor constituent in the atmosphere of Mars, between approximately 130 km and 230 km peaking at an altitude of 155-160 km, by Witasse *et al.* [22] The modelled concentrations of CO_2^{2+} are shown in Figure 1.3.

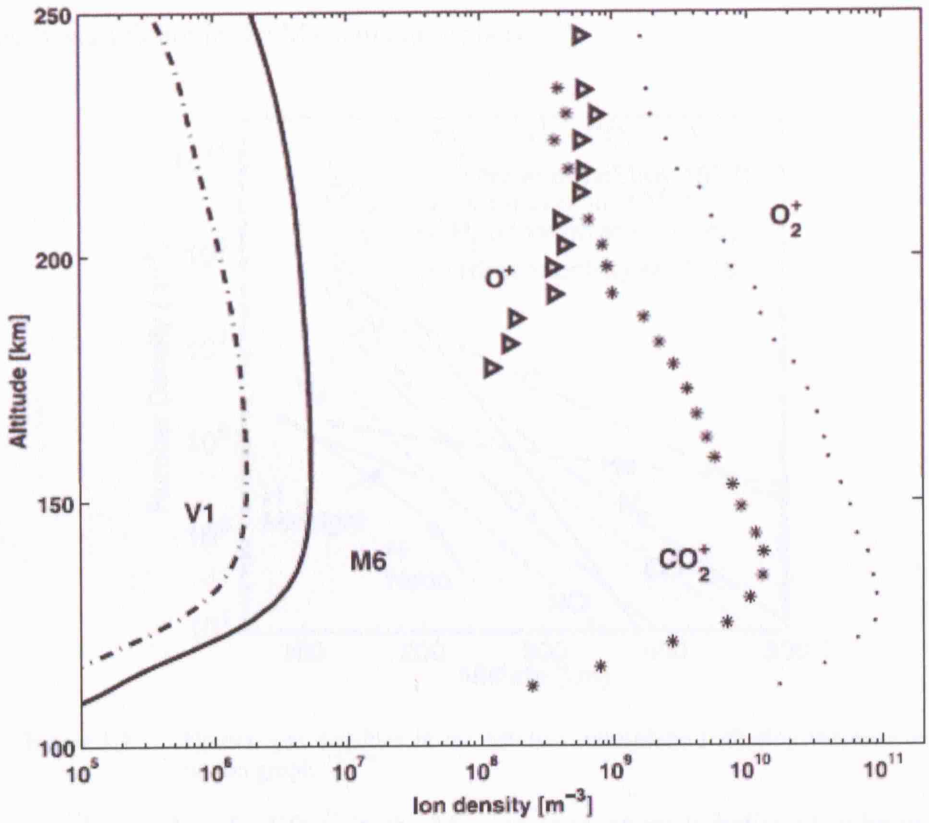

Figure 1.3 The ion densities in the Martian atmosphere determined by Witasse *et al.* The lines labelled with V1 (dash) and M6 (solid) show the calculated CO_2^{2+} densities for the conditions during the Viking 1 (V1) and Mariner 6 (M6) missions with the three ions, O_2^+ (triangle), O^+ (star) and CO_2^+ (dots), detected during the Viking 1 mission. [22]

O_2^+, O^+ and CO_2^+ were detected in the ionosphere of Mars during the Viking 1 mission, as shown in Figure 1.3. [22] Nitrogen containing species such as NO^+ and N_2^+ are also proposed to be abundant constitutions of the Martian ionosphere. [35] The CO_2^{2+} densities shown in Figure 1.3 were calculated for the conditions during the Viking 1 (V1) and Mariner 6 (M6) missions. The densities of CO_2^{2+}, of approximately 3×10^6 m^{-3} for V1 and approximately 5×10^6 m^{-3} for M6 between 155 and 160 km altitude, were calculated using

a model of the daytime Martian ionosphere based on experimental work to measure electron recombination and chemical reaction coefficient rates. [22]

CO_2^{2+} has a ground state lifetime of 4.2 seconds. [48] This lifetime is potentially long enough for this dication to affect the chemistry of the Martian ionosphere as it could be involved in collisions with electrons and neutral molecules. Reactions of neutrals with CO_2^{2+} would, as is shown below, produce pairs of singly charged ions with a high amount of kinetic energy. [49, 50] The reactions of such translationally energetic species could also have implications for ionospheric abundances. Figure 1.4 shows the main neutral gas constituents in the region of the predicted CO_2^{2+} layer are CO_2, N_2, O, CO, Ar, O_2, NO, H_2, He and H hence reactions between these neutral species and CO_2^{2+} could be potentially significant in the Martian atmosphere. [51]

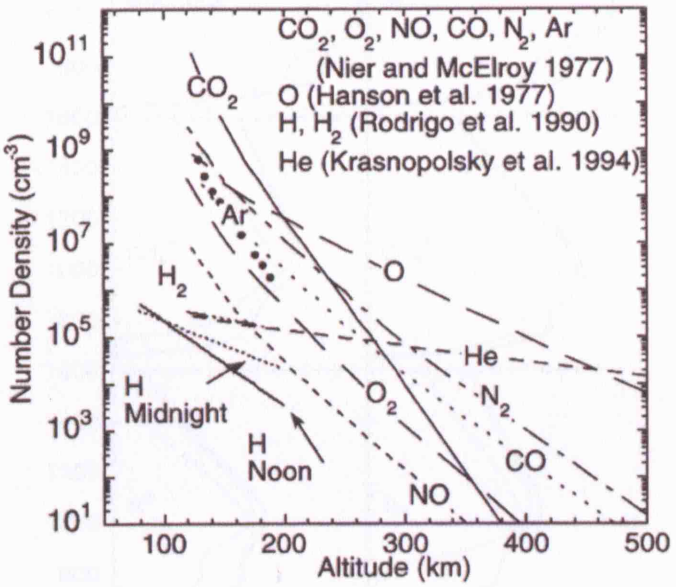

Figure 1.4 Neutral gas densities in the Martian ionosphere including the references within graph. [51-55]

Witasse *et al* state that the CO_2^{2+} in the Martian ionosphere is believed to be produced in the dayside by photoionisation of, and photoelectron impact upon, CO_2. CO_2^{2+} is modelled to be lost by dissociative recombination with electrons and chemical reactions with neutral species such as those shown in Figure 1.4.

In the next decade there will be three missions to Mars, all of which have part of their mission designated to the study of the Martian ionosphere. It is predicted that the CNES PREMIER 07 mission will be able to detect CO_2^{2+}. [22] The orbiter of this mission will include an ion spectrometer, detecting by mass to charge ratio (*m/z*). The *m/z* of CO_2^{2+} is 22. This *m/z* of 22 is relatively far away from the atmospheric species closest in *m/z* of

O^+ (m/z = 16), CO^+ and N_2^+ (m/z = 28). Given the above discussion, laboratory experiments are obviously important for investigating the reactions CO_2^{2+} that could be involved in the Martian ionosphere.

1.1.2.3 Titan

The moon Titan has a dense atmosphere consisting mainly of N_2 and a small amount of hydrocarbons. Figure 1.5 shows the calculated density of N_2^{2+} in the atmosphere of Titan, along with the densities of other ionic species and electrons by Lilensten *et al.* [37]

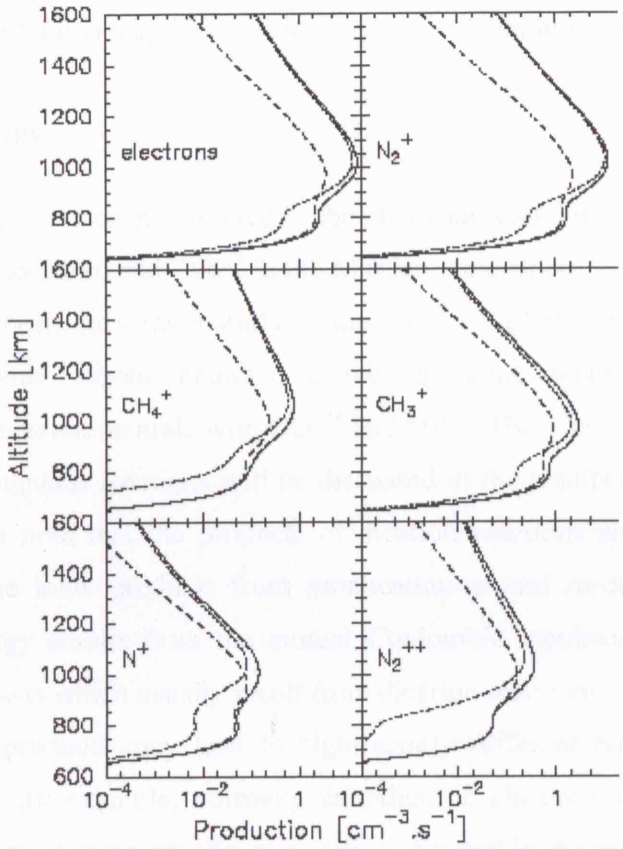

Figure 1.5 The ion densities in the atmosphere of Titan including the calculated density of N_2^{2+} by Lilensten *et al.* The three different lines for each of the ions represent; the total ion productions (full lines), the primary photoproductions (dotted lines) and the secondary electron impact productions (dashed lines). [37]

The N_2^{2+} ions in the atmosphere of Titan are thought to be produced by double photoionisation and by photoelectron impact upon N_2. [37] Lilensten *et al* showed that the N_2^{2+} layer peaks around 1100 to 1200 km altitude where the density is approximately 1×10^4 m^{-3}. While this density is low (less than 10% of the total ion density), it is larger than that of other ions which are considered important in the ionosphere of Titan such as CH^+, C_2H^+, $C_2H_6^+$ and CN^+. The lifetime of N_2^{2+} in the ground state is at least 3 seconds

which is certainly long enough for N_2^{2+} to encounter, and therefore react with, neutral species, as well as electrons. [48] Hence the N_2^{2+} is thought to be lost via dissociative recombination with electrons and by chemical reactions with the neutral species. Although the density of N_2^{2+} is low, the reactions of the energetic products of the N_2^{2+} reactions could again affect the overall chemistry of the ionosphere.

N_2^{2+} can not be detected in the atmosphere of Titan using a conventional satellite mass spectrometer because has the same *m/z* value as N^+. However, fluorescence has been observed from N_2^{2+}. [45,56] The Cassini–Huygens mission, which arrived at Titan in 2004, has an instrument which could detect this fluorescence. [37] Hence, the prediction of N_2^{2+} in the ionosphere of Titan may be confirmed by observation in the near future.

1.1.2.4 Summary

To summarise, N_2^{2+} has been predicted in the atmosphere of Titan, O^{2+}, N_2^{2+} and O_2^{2+} in the Terrestrial atmosphere and CO_2^{2+} in the Martian atmosphere. Therefore to extend our knowledge, this thesis presents a study of the reactions of the atmospherically relevant dication, N_2^{2+}, with relevant neutrals, as well as some details on the reactions of atmospherically relevant neutrals with CO_2^{2+} and O_2^{2+}. These potentially ionospherically relevant dication-neutral reactions will be discussed in the results chapters of this thesis. It is important to note that the products of dication reactions are more translationally energetic than the ionic products from monocation-neutral reactions. This increased translational energy results from the mutual Coulombic repulsion between the pair of product monocations which usually result from dication reactions. The extra translational energy of these products may lead to significantly different reactivity in subsequent collisions where, for example, normally endothermic channels can become available. Hence the reactions of the energetic monocations formed in the reaction of dications can also potentially influence ionospheric properties.

1.2 Molecular dications

The following section discusses the properties of isolated dications and the experimental techniques used to probe the properties of dications.

1.2.1 Properties of isolated dications

The process of removing two electrons from a neutral molecule, XZ, yields a resultant molecular dication, XZ^{2+}, with high potential energy, between 25 to 40 eV. [2] As a result of the high potential energy, many small molecular dications are thermodynamically unstable as the dication has more energy than a pair of separated singly charged fragments. The logical conclusion of this would be that, due the Coulomb repulsion between the two positive charges, all molecular dications are extremely short lived and rapidly fragment into a pair of singly charged cations. Such rapid fragmentation processes do occur and involve a considerable release of kinetic energy, about 6 eV for a typical pair of ions formed from a diatiomic dication. [57] While this rapid fragmentation is the fate of many electronic states of dications, it has been clear since molecular dications were first detected in mass spectrometry experiments, that this is not the case for all dication electronic states. For detection by conventional mass spectrometry it is necessary for a species to exist on the microsecond scale in order to travel from the ionisation source to the detector. Thus not all electronic states of molecular dications can be undergoing this rapid dissociation.

Many molecular dications possess at least one electronic state that has a barrier with respect to charge separating dissociation as is illustrated in Figure 1.6. [58]

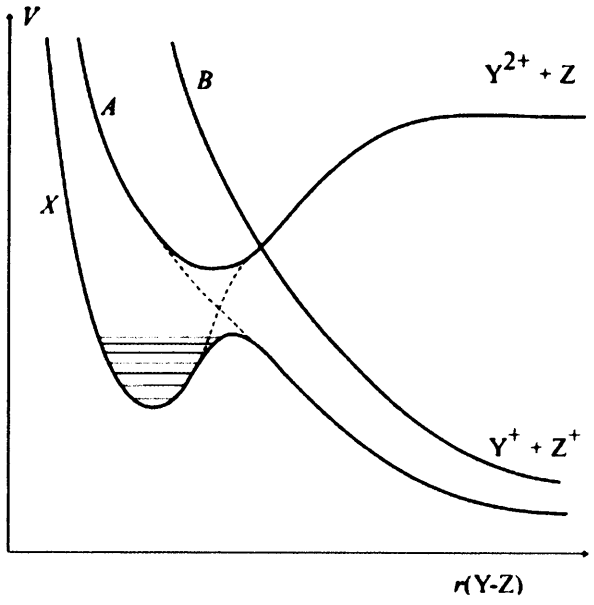

Figure 1.6 Schematic potential energy curves diagram showing the barrier to charge-separating dissociation which dication YZ^{2+} can occupy to avoid immediate dissociation to $Y^{+} + Z^{+}$ upon ionisation. [58]

State *B* in Figure 1.6 is a purely dissociative electronic state, population of which results in a translationally energetic pair of monocations, as previously mentioned. However,

states *X* and *A* in Figure 1.6 exhibit potential energy minima. These states with barriers to charge separating dissociation are usually termed metastable, since they lie at energies above the charge separation asymptote but the states are kinetically stabilised by the barrier. The barriers can be viewed as arising from the avoidance of the crossing of the $Y^{2+} + Z$ and $Y^{+} + Z^{+}$ potential energy surface asymptotes as shown in Figure 1.6. The $Y^{2+} + Z$ surface is attractive at large interspecies separation, whilst the $Y^{+} + Z^{+}$ surface is purely repulsive. Hence the avoided crossing between these surfaces results in a potential energy surface possessing a minimum separated from the $Y^{+} + Z^{+}$ asymptote by the energy barrier. It is these long-lived dication states that are important in dication-neutral reactivity, since these metastable electronic states have a sufficient lifetime to encounter neutral molecules. [58]

The depth of the potential well of the metastable state dictates how many vibrational levels the dication can support. The potential energy wells can be several eV deep and hence can support many vibrational levels. The lifetime of an isolated dication varies depending on their vibrational excitation. Dications populating high vibrational levels can tunnel through the barrier to charge separating dissociation. However dications populating lower vibrational levels are even more effectively trapped within the barrier to charge separation and hence have significantly longer lifetimes. The barrier to charge-separating dissociation rapidly broadens with decreasing vibrational energy so the tunnelling lifetime of dications increases with decreasing vibrational energy.

The differences in the lifetimes of the dication in different vibrational levels have been shown experimentally using Ion Storage Ring experiments for molecules such as N_2^{2+}, as is discussed in section 1.2.4.4. [48] The detection of fluorescence from excited dications states also serves as a lifetime indication as discussed in sections 1.2.4.3. Fluorescence has been detected from several dications, including N_2^{2+}, NO^{2+}, CS_2^{2+}, N_2O^{2+} and CO^{2+}. [56, 59-62] Simple optical spectrometry can be used to observe the fluorescence emitted from a plasma and the presence of dications can be determined via analysis of the wavelengths of the fluorescence emitted. This is discussed in more detail in section 1.2.4.2.

The main decay route of dications is via a curve crossing to a dissociative electronic state, particularly for dicationic states which are not the ground state. For non-ground state dications the probability of a predissociative curve crossing onto a dissociative potential, which correlates with a lower dissociation asymptote, is significant. Therefore the lifetime of an individual vibrational level of an excited metastable state usually depends

on the coupling of that level to the available dissociation continua via predissociative interactions. [58]

1.2.2 Experimental methods to probe the properties of dications

In order to fully understand the reactivity of dications it is essential that we understand the dications themselves. Sophisticated techniques, as briefly described below, are employed to give an insight into the properties of doubly-charged ions. This section describes some of the techniques used to probe the properties of dications. Two of the areas of interest regarding isolated dications are the electronic and vibrational structures of the dications themselves and the lifetimes of these species. These aspects of dicationic structure are particularly pertinent to the experiments described in this thesis. Firstly, we need knowledge of the electronic structure of the dications in order to understand the energetics of dication-neutral reactions. Secondly, only dicationic states with significant lifetimes will encounter neutral molecules, so in general we need information regarding the lifetimes of the dicationic states.

1.2.2.1 Collisional ionisation experiments

Several collisional methods have been used to study dications; Electron ionisation threshold measurements, Auger spectroscopy employing electron ionisation, dissociative charge transfer (DCT) spectroscopy and translational energy spectroscopy (TES).

The electron ionisation methodology was one of the earlier methods used to study dications. By monitoring the change in intensity of the ion signals as a function of electron energy the threshold of double ionisation could be determined. Many dications have been formed and studied using EI such as N_2^{2+}, CO_2^{2+}, HCl^{2+}, CF_3^{2+} and Ne^{2+}, to name just a few. To an extent an indication of the presence of an excited dication state can be obtained from simple electron ionisation techniques by monitoring a change in the ionisation cross section. However, when electron ionisation is coupled with a second technique, such as Auger spectroscopy, the electronic states of the dication can be probed in much more detail. [68, 70, 71]

Auger spectroscopy is commonly associated with surface science techniques but is also a popular probe of doubly charged ions. Auger spectroscopy often comes in hand with electron ionisation or photoionisation, and is an indirect double ionisation method. First,

an 'inner/core electron hole' is produced via photon absorption or electron ionisation. Subsequently an outer electron falls down to fill this hole and the energy released in this relaxation allows a second electron, the Auger electron, to be ejected and hence a doubly charged ion is produced. The doubly charged states of several small molecules have been studied using Auger spectroscopy including N_2, O_2, CO, NO, H_2O, CO_2, CH_4, CCl_4 and SF_6. The different electronic states of the doubly charged ion can be probed using Auger spectroscopy. This is particularly successful when the Auger electron is detected in coincidence with either the doubly charged ion of interest, or one of its fragments. The measurement of the kinetic energy of the Auger electron allows the determination of the binding energy of the dication state and hence information about that state is determined. [72-74]

Typically, Translational Energy Spectroscopy (TES) involves the collision of a fast ion (keV order) with a neutral gas in a collision cell. A monoenergetic beam of mass selected dications collides with relevant neutral at pressures below 10^{-5} Torr. The products of the reaction are commonly mass and energy analysed. One implementation of a TES uses a double focusing arrangement. In this arrangement, two symmetrically arranged cylindrical electrostatic energy analysers are used to monochromatize the reactant beam and analyse the products. Typically, TES reveals information regarding the electronic and vibrational states of the participating species. TES can also potentially reveal spectroscopic information on the rotational states of the participating species, the dynamics of the collision, lifetimes of species, collision cross-sections and populations of states. Dications such as N_2^{2+}, He_2^{2+}, NO^{2+}, CO_2^{2+}, OCS^{2+} and CS_2^{2+} have all been studied using TES. The energy change spectra are recorded following the electron transfer reactions and then the reactant and product states which can account for the intensity are determined. The energy change spectra can be recorded over a range of ionisation energies and so if the relative intensity of a particular peak decreases it can be assigned to a reaction from a dicationic excited state. Figure 1.7 shows a real TES energy change spectra recorded by Hamdan *et al* for the electron transfer reaction of N_2^{2+} with He. [75-77]

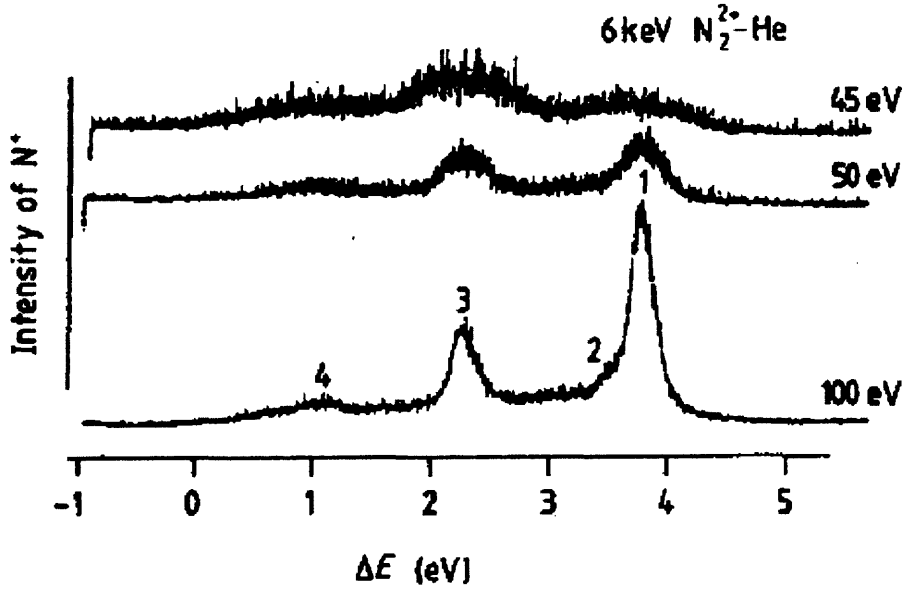

Peak	Reactants		Products	ΔE (eV)
1	$N_2^{2+}(C\,^3\Sigma_g^+) + He(1s^2\,^1S)$	→	$N_2^+(X\,^2\Sigma_g^+) + He^+(1s\,^2S)$	4.2
2	$N_2^{2+}(C\,^1\Delta_g, b\,^1\Pi_u) + He(1s^2\,^1S)$	→	$N_2^+(X\,^2\Sigma_g^+) + He^+(1s\,^2S)$	3.8
3	$N_2^{2+}(X\,^3\Pi_u) + He(1s^2\,^1S)$	→	$N_2^+(X\,^2\Sigma_g^+) + He^+(1s\,^2S)$	2.4
4	$N_2^{2+}(X\,^3\Pi_u) + He(1s^2\,^1S)$	→	$N_2^{2+}(A\,^2\Pi_u) + He^+(1s\,^2S)$	1.3

Figure 1.7 TES energy change spectra recorded by Hamdan *et al* for the electron transfer reaction of N_2^{2+} with He. It is important to note how the relative intensity of peak '1' decreases as the ionisation energy decreases and hence this peak is assigned to an excited state.

Double charge transfer (DCT) spectroscopy is based on double electron transfer reactions, as the name suggests, in the form:

Double Charge Transfer spectroscopy $X^+ + Y \rightarrow X^- + Y^{2+}$ (1.2)

X^+ is a fast moving, singly charged ion, projectile generally with an energy of the order of several keV. After the collision of X^+ with Y to form X^- and Y^{2+}, the translational energy loss of the X^- can be measured. As a result, the double ionisation energies of the Y^{2+}, in the relevant excited vibrational and electronic states, can be determined by considering the conservation of energy and momentum. Various dications have been studied using DCT including N_2^{2+}, CO^{2+}, NO^{2+}, CO_2^{2+}, SO_2^{2+}, H_2O^{2+}, $C_2H_2^{2+}$, and $C_2H_4^{2+}$. [78-84]

1.2.2.2 Optical spectroscopy

The collisions between the ions, neutrals and electrons in a gas discharge, otherwise known as a plasma, can result in a wide variety of species, including molecular dications. If the dication is created in an excited state it may live long enough to fluoresce to a lower electronic level. Simple optical spectroscopy involves the detection, and subsequent assignment, of the observed fluorescent light from the gas discharges. Carroll was the

first to observe a rotationally resolved spectrum of a molecular dication by observing fluorescence from N_2^{2+} in 1958. Carroll tentatively assigned the band to the $^1\Sigma_u^+$-$X^1\Sigma_g^+$ transition. [44] The tentative assignment made by Carroll was later confirmed by Cossart *et al* who also observed some additional, but weaker, N_2^{2+} bands. [59, 85, 86] Cossart *et al* also obtained a high resolution emission spectrum of NO^{2+} from an electrical discharge. [59, 85, 86]

Photofragment spectroscopy has also been used successfully to identify optical transitions in N_2^{2+}, HCl^{2+} and DCl^{2+}. [87] In addition attempts have been made to use photofragment spectroscopy to identify optical transitions with NO^{2+} and CO^{2+}, although there has been less success with these. [87] Typically, the dications are formed using electron ionisation and are then mass selected and accelerated into a beam before irradiation using a laser. The photofragment signal induced by the laser can then be sensitively detected by counting the fragment ions generated. With regards to N_2^{2+}, Cosby *et al*, Larsson *et al*, Sundstrom *et al*, Martin *et al* and Masters *et al*, used laser Ion Photofragment spectroscopy to study the N_2^{2+} $^1\Pi_u$–$X^1\Sigma_g^+$ transition, obtaining increasingly more resolved rovibrational photopredissociation spectra of the transition. [88-92] Szaflarski *et al* and Mullin *et al* assigned and obtained a vibrationally resolved photofragment spectrum of the transitions between the $^3\Pi_g$–$^3\Sigma_u^+$. [93, 94] Hyperfine, high resolution spectra of DCl^{2+}, $D^{35}Cl^{2+}$ and $D^{37}Cl^{2+}$ have been obtained by Cox *et al* using infra-red ion Photofragment spectroscopy. However, the assignment of the DCl^{2+} is as yet to be fully completed by Cox *et al* and the same is true for the $H^{37}Cl^{2+}$ spectrum measured by this group. [87] Photofragment spectroscopy has several advantages over simple optical spectroscopy because it can also be used to measure the lifetimes of individual rovibrational levels of electronically excited dications. Optical spectroscopy can yield very accurate spacings between the vibrational levels but does not locate the electronic states relative to the lowest electronic states.

1.2.2.3 Coincidence techniques

Several different coincidence techniques have been developed to probe dications. These techniques involved the simultaneous detection of at least two species from a double ionisation event, such as electrons, ions or even photons. The advantage of these coincidence techniques over the previously described optical techniques is that they often locate the observed electronic states relative to an accurately located ground electronic state.

The Time-Of-Flight Photoelectron-Photoelectron Coincidence (TOF-PEPECO) technique uses pulsed ultraviolet light to photoionise the neutral species. Time-of-flight analysis is then used to detect the electron pairs, in coincidence, in a magnetic bottle. The technique works by detecting all the electrons emitted in the photoionisation to produce two-electron spectra, effectively a photoelectron spectroscopy of dications. The TOF–PEPECO spectrum reveals the electronic and vibrational energy levels populated in the photoionisation process. The mechanism of the photoionisation process can also be deduced from the distribution of excess energy between the electrons. HI^{2+}, CH_3I^{2+}, CF_3I^{2+} and I^{2+} have been studied using TOF-PEPECO and the spectra have been recorded showing varying degrees of resolution. For HI^{2+}, the three lowest lying electronic states are vibrationally resolved. For CH_3I^{2+} only partial vibrational resolution has been obtained for the three lowest lying states and for CF_3I^{2+}, five electronic states, not vibrationally resolved, are observed. [95] For I^{2+} the TOF-PEPECO technique was used to accurately determine its double ionisation energy of 24.85 ± 0.02 eV. [96] In addition, the Eland group has measured the double photoionisation spectra of many molecules including CH_4, NH_3, H_2O, CO_2, SO_2, CO, C_2H_2, HBr, N_2, NO, O_2, H_2S, OCS, CS_2, N_2O, toluene, ethylene, butadiene, cyclooctatetraene, benzene and naphthalene using the TOF-PEPECO technique. For some molecules, such as N_2, highly vibrationally resolved double ionisation spectra are obtained. For others molecules, such as NH_3, the double ionisation spectra are not well resolved but still reveal the double ionisation energy of the molecule and information regarding the ionisation mechanism of the individual molecules. [9, 97-104]

Threshold Photoelectrons Coincidence Spectroscopy (TPEsCO) uses synchrotron radiation to doubly photoionise the neutral molecules. When double photoionisation occurs at the threshold of a dicationic state, two zero-energy electrons - threshold electrons - are produced and detected in coincidence. The coincidence yield, as a function of the photon energy, maps out the states of the dication. The double ionisation of N_2, CO_2, NO, CO, O_2, OCS, C_2H_2, CS_2, HI and C_6H_6 have all been studied using TPEsCO. The spectra can be resolved up to vibrational resolution depending on the molecule. For example, the vibrational levels of the three lowest HI^{2+} states have been obtained. [101, 105-109]

Often the spectra obtained by TOF-PEPECO and TPEsCO can be very similar, but sometimes one technique can reveal information that the other did not. For example the $C_2H_2^{2+}$ dication was studied using both techniques comparatively. Figure 1.8 shows a

spectrum recorded using the TOF-PEPECO technique and the TPEsCO technique for $C_2H_2^{2+}$.

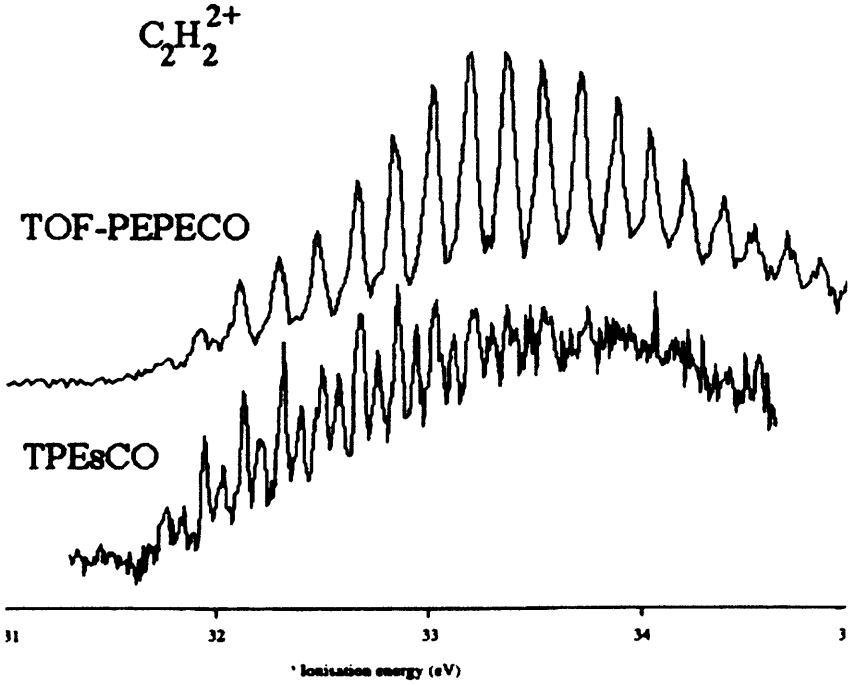

Figure 1.8 TOF–PEPECO spectrum and TPEsCO spectrum of $C_2H_2^{2+}$ recorded by Kinugawa *et al.* [101]

Generally the two spectra in Figure 1.8 provide very similar information regarding the C_2H_2 dication. However, The TOF-PEPECO spectrum shows more intense peaks above 33.5 eV than the TPEsCO spectrum, and the TPEsCO spectrum shows more intense peaks below 32.3 eV than the TOF-PEPECO spectrum does. These differences were attributed to the difference in the velocities of the ejected electron between the two techniques, which led to differences in the interaction time of the ejected electrons. [101]

Double Zero Kinetic Energy Electron (ZEKE) spectroscopy uses TOF and two electron detectors to detect, in coincidence, the near zero energy electrons formed from the double ionisation of a neutral species. The technique can vibrationally resolve molecules such as N_2^{2+}. The essence of the Double ZEKE Coincidence technique is similar to that of TPEsCO technique although the two techniques were developed independently. However, subsequently the TPEsCO technique appears to have been utilised in the study of dications significantly more than the Double ZEKE Coincidence technique. [110]

The above coincidence techniques, TOF-PEPECO, TPEsCO and double ZEKE, are all used to gain information about the dication through utilising the information intrinsically stored in the photoelectrons ejected during the ionisation event. However, the techniques

Doppler-Free Kinetic Energy Release, Photoion-Photoion Coincidence and Ion-Ion Coincidence, all study the dication via coincident detection of the ions (or photoions depending on the ionisation method) formed following the fragmentation of the dication.

The Ion-Ion Coincidence technique uses electron ionisation with TOFMS to detect fragment ions formed from dissociative double ionisation events, as well as single and triple ionisation events. In this technique ionisation is induced by a pulse of electrons and hence the absolute time of flights of the ions making up the ion pair can be determined. Various double ionisation events have been studied using the Ion-Ion coincidence technique including the fragmentation of N_2O^{2+}, BCl_3^{2+}, HCl^{2+}, ClO_2^{2+}, O_3^{2+} and $N_2O_5^{2+}$. [31,68, 69, 111-113]

The Doppler-Free Kinetic Energy Release technique (DFKER) effectively employs a coincidence technique; the source gas is ionised and the two fragment ions from dicationic dissociation are extracted into two TOF tubes mounted at 180° to one another to measure their energies. The ions are detected as a coincidence pair, one ion at the end of each flight tube. This methodology eliminates the Doppler broadening in the ionic kinetic energy release spectrum, allowing vibrational resolution to be achieved. Thus a spectrum of the dicationic vibronic levels is generated. The DFKER technique has been used to study NO^{2+}, N_2^{2+}, $CO^{2+}$and O_2^{2+}. [114-117]

In the Photoion-Photoion Coincidence technique (PIPICO) two photoions from the dissociation of a dication are detected in coincidence in a TOFMS. The kinetic energy release distributions of the fragment ions are determined. When the spectra are obtained at a range of photoionisation energies, the differences in the kinetic energy releases can be used to determine the ionisation mechanism and the electronic state in which the dication was formed. N_2^{2+}, CO_2^{2+}, SO_2^{2+}, CF_4^{2+}, NH_3^{2+}, CO^{2+}, NO^{2+}, OCS^{2+}, $C_2H_4^{2+}$, $C_2H_2D_2^{2+}$, $C_2H_2F_2^{2+}$ and CH_3I^{2+} are examples of the compounds that have been studied using PIPICO. [65, 118-126] The PIPICO technique can also been used to determine the lifetimes of dications by examination of the coincidence peak patterns. Mean lifetimes of approximately 900 ns for CO_2^{2+}, 450 ns for N_2O^{2+} and 600 ns for CO^{2+} have been determined. [127, 128]

Recently, a range of new coincidence techniques have been developed, almost all by the Eland group. The Photoelectron-Photoion-Photoion Coincidence (PEPIPICO) technique, the Photoelectron-Photoelectron-Photoion Coincidence (PEPEPICO) technique and the Photoelectron-Photoelectron-Photoion-Photoion Coincidence (PEPEPIPICO) technique

all involve the coincident detection of both photoelectrons and photoions. While the Photoelectron-Photoion-Fluorescence Coincidence (PEPIFCO) and Photoelectron-photoelectron-fluorescence coincidence (PEPEFCO) techniques involve the coincident detection of fluorescence, photoelectrons (and photoions).

In the Photoion-Photon-Fluorescence Coincidence technique (PIFCO) dications are formed by double photoionisation and if an excited dicationic state relaxes by fluorescence, coincidences are recorded between the fluorescence photon and the photoion. Hence emissions from the dications can be detected and the lifetime of the emitting state are measured. For example, the lifetime of the N_2^{2+} $D^1\Sigma_u^+$ state was measured at 8 ± 3 ns. [45]

The Photoelectron-Photoion-Fluorescence Coincidence (PEPIFCO) technique was developed as an upgrade of the PIFCO technique in order to detect photoelectrons as well as photoions and fluorescence, as the name suggests. New emissions from the Photoionisation of N_2, NO, CO, CO_2, CS_2, OCS, N_2O, SO_2 and CF_4 were discovered using this method. [61, 62, 129] The Photoelectron-Photoelectron-Fluorescence Coincidence (PEPEFCO) technique was developed as an upgrade to the PEPEPIPICO (described below). The PEPEFCO technique has been used to confirm the emissions from the CS_2 and N_2O dications that were seen using the PEPIFCO technique. [61, 62]

The Photoelectron-Photoion-Photoion Coincidence technique (PEPIPICO) records the coincidences between the pair of ions formed after dissociative double photoionisation. However, in contrast to the PIPICO technique, detection of one of the photoelectrons from the ionisation event is used as a time zero to give absolute flight times of the photoions. These absolute measurements of the ionic times of flight allow the individual masses of the photoions to be determined. This is in contrast to the earlier PIPICO experiments which only determine the mass difference between the ions. The fragmentation of various doubly charged molecules including CD_3CN^{2+}, toluene^{2+}, SO_2^{2+}, CH_4^{2+} and CS_2^{2+} has been studied. [98, 130-133] The Photoelectron-Photoelectron-Photoion-Photoion Coincidence (PEPEPIPICO) technique was developed as an upgrade of the PEPECO technique. So far the technique has been used to study CF_4, CS_2^{2+}, ICN, BrCN and N_2O dications. [61, 62, 134, 135]

1.3 Bimolecular reactivity of molecular dications

A bimolecular reaction involves the interaction of a pair of atoms or molecules resulting in the exchange of electrons or atoms. The result of the reaction will depend on the identity of the reactants and the collision energy of the system. However, investigations into the bimolecular reactivity of dications with neutrals have revealed three main types of reactions; electron transfer (dissociative and non-dissociative single or double electron transfer), energy transfer (collision induced charge separation and collision induced neutral loss) and finally bond-forming reactions. These three classes of reaction are described in the next section.

1.3.1 Electron transfer reactions

Single electron transfer involves the exchange of a single electron between the neutral species and the dication. Electron transfer reactions can be classed as either non-dissociative (equations (1.3) and (1.4)) or dissociative (equations (1.5) and (1.6)).

Non-dissociative electron transfer	$M_2^{2+} + X_2$	$\rightarrow$	$M_2^{+} + X_2^{+}$	(1.3)
Example [136]	$Ne^{2+} + Ar$	$\rightarrow$	$Ne^{+} + Ar^{+}$	(1.4)
Dissociative electron transfer	$M_2^{2+} + X_2$	$\rightarrow$	$M_2^{+} + X^{+} + X$	(1.5)
Example [137]	$N_2^{2+} + O_2$	$\rightarrow$	$N_2^{+} + O^{+} + O$	(1.6)

In a non-dissociative electron transfer (NDET) reaction the electron is transferred and the dication and neutral are converted into a pair of monocations with no subsequent fragmentation. In a dissociative electron transfer reaction an electron is again transferred from the neutral to the dication. However, at least one of the resulting monocations subsequently fragments so the reaction yields at least three products. Generally, dissociative electron transfer reactions occur because the electron transfer led to the formation of product ions in unstable electronic states which then subsequently fragment. However, there is evidence, from the PSCO experiment, that a pair of monocations accompanied by a neutral, which appear to be the typical products of a dissociative electron transfer reaction, can in fact be formed from a collision complex. [138] Chapter Three of this thesis presents representative PSCO data for a single non-dissociative electron transfer reaction and a dissociative single electron transfer reaction. Single electron transfer, particularly non-dissociative, is often the most abundant process in dication-neutral collision systems. This propensity of NDET was evident in the early investigations of dication-neutral reactions which often involved collisions of rare-gas

atoms, Ar, Kr and Xe, with dication partners such as CO^{2+} and CO_2^{2+}. [77, 139, 140, 141] This dominance of electron transfer is also is evident from the relative intensities of the reaction channels observed in the research for this thesis.

Double electron transfer (equations (1.7), (1.8), (1.9) and (1.10)) is believed to involve the either the simultaneous transfer of two electrons or two successive single electron transfers. Again, double electron transfer can be non-dissociative or dissociative.

Non-dissociative double electron transfer	$X^{2+} + Y$	$\rightarrow$	$X + Y^{2+}$	(1.7)
Example [142]	$^{13}CO^{2+} + Xe$	$\rightarrow$	$^{13}CO + Xe^{2+}$	(1.8)
Dissociative double electron transfer	$X^{2+} + Y_2$	$\rightarrow$	$X + Y^+ + Y^+$	(1.9)
Example (Chapter Four)	$N_2^{2+} + CO_2$	$\rightarrow$	$N_2 + CO^+ + O^+$	(1.10)

For electron transfer reactions, the PSCO experiment can derive detailed dynamical information about non-dissociative electron transfer, dissociative electron transfer and dissociative double electron transfer. However, because the PSCO experiment detects ion pairs we can not derive dynamical information for non-dissociative double electron transfer reactions because these reactions do not result in the formation a pair of product ions.

1.3.2 Energy transfer reactions - collision induced charge separation and collision induced neutral loss.

In a dication-neutral collision system there may be enough kinetic energy available to promote the dication to an excited vibrational or electronic level which decays to form a pair of monocations. Such dissociative processes are observed as collision induced charge separation (CICS) reactions:

Collision induced charge separation	$XY^{2+} + M$	$\rightarrow$	$X^+ + Y^+ + M$	(1.11)
Example [141]	$CO^{2+} + He$	$\rightarrow$	$C^+ + O^+ + He$	(1.12)

This example (1.12) of a CICS reaction is the most dominant channel in the reaction of CO^{2+} with He.

A second method of decay of a collisionally excited dication is via collision-induced neutral loss (CINL), where the dication dissociates but the double charge remains on one fragment, equations (1.13) and (1.14).

Collision induced neutral loss	$XY^{2+} + M$	$\rightarrow$	$X^{2+} + Y + M$	(1.13)
Example [143]	$CF_3^{2+} + H_2O$	$\rightarrow$	$CF_2^{2+} + F + H_2O$	(1.14)

CINL reactions are most common for reactions of perfluorinated dications such as the above example, (1.14). *Ab-initio* calculations show the structural geometry on CF_3^{2+} is C_{2v} with one long C-F bond. [144] The F atom involved in this long bond will be weakly bonded and hence easily lost. Dynamical information can not be obtained for CINL reactions using the PSCO technique since this dissociation process does not generate two ionic fragments.

1.3.3 Bond-forming reactions

A 'bond-forming' reaction is one which involves, as the name suggests, the formation of a chemical bond in the products that is not present in the reactants. Dication-neutral bond-forming chemical reactions usually produce a pair of singly charged ions, often accompanied by one or more neutral species, as shown by reaction (1.15). The mutual repulsion between the pair of positive products gives them a high kinetic energy. Hence, the products of dication reactions are commonly more energetic than the ionic products of monocation-neutral reactions.

Bond-forming reaction $XY^{2+} + M_2 \rightarrow XM^+ + M^+ + Y$ (1.15)

As previously mentioned, the first dication-neutral bond-forming reaction was observed by Chatterjee and Johnson in the late 1980s (1.1). [21]

First observed bond-forming reaction: $O_2^{2+} + NO \rightarrow NO_2^+ + O^+$ (1.1)

Some of the earliest observations of dication-neutral bond-forming reactions by Price *et al* in the early 1990s involved the reactions of species such as CO_2^{2+}, CF_2^{2+} and OCS^{2+} with simple neutral species such as D_2 to form X-D bonds (1.16). [145]

Early observation example $OCS^{2+} + D_2 \rightarrow DS^+ + [D + O + N]^+$ (1.16)

Further detailed studies of the reactions between dications and H_2/D_2 have shown that these proton transfer bond-forming reactions can in fact dominate the reaction's yield for example (1.17). [146]

Proton transfer bond-forming example $CHBr^{2+} + H_2 \rightarrow CBr^+ + H_3^+$ (1.17)

The bond-forming reactions of CF_n^{2+} have been studied intensively. [19, 143, 147-152] These reactions often appear to involve negative ion transfer from the neutral to the dication, (1.18) and (1.19).

'Negative ion transfer' CF_n^{2+} reaction $CF_n^{2+} + M_2 \rightarrow MCF_n^+ + M^+$ (1.18)

Example [19] $CF_2^{2+} + H_2 \rightarrow HCF_2^+ + H^+$ (1.19)

In fact, the actual mechanism of these bond-forming reactions does not involve anion transfer. Studies by Herman *et al* using angularly resolved detection showed the bond-forming products in reaction (1.19) were scattered over a larger range of angles than the products of the accompanying charge transfer reactions. Similar behaviour was also observed for the bonding forming reactions of CO_2^{2+} with D_2 by Herman *et al.* This behaviour was linked with the decay of a collision complex with a finite lifetime. [19, 153]

Several CF_n^{2+} reactions were subsequently studied at University College London, experimentally using a crossed beam method by Tafadar *et al*, the PSCO by Harper *et al*, and computationally by Lambert *et al.* [147, 150, 152] Examples of some of the reactions studied by this group are shown below, (1.20), (1.21) and (1.22).

Crossed beam method example [147]	$CF_3^{2+} + HD$	$\rightarrow$	$HCF_2^+ + D^+ + F$	(1.20)
		$\rightarrow$	$DCF_2^+ + H^+ + F$	
PSCO example [152]	$CF_2^{2+} + H_2O$	$\rightarrow$	$HCF_2^+ + H^+ + O$	(1.21)
Computational example [150]	$CF_2^{2+} + H_2O$	$\rightarrow$	$OCF^+ + HF + H^+$	(1.22)

The studies by Tafadar *et al* of the bond-forming reactions of CF_3^{2+} (1.20) and CF_2^{2+} (as well as CO_2^{2+}), used HD as the neutral reactant, primarily to determine if there was an intramolecular isotope effect. In the CF_3^{2+} + HD system, the reaction to form XCF_2^+ (X = H or D) exhibited a strong intramolecular isotope effect favouring the formation of DCF_2^+, as did the reaction to form DCF_2^+ in the CF_2^{2+} + HD system. In the CO_2^{2+} + HD system, the reaction to form XCO^+ (X = H or D) also exhibited a strong intramolecular isotope effect favouring the formation of DCO^+. Initially this preference towards bond-forming with the D was attributed to symmetric polarisation of HD, which, when associated with the non-central centre of mass of the molecule, resulted in a closer approach of D to the reactant dication. However this explanation was subsequently rejected when a bond-forming channel to form XF^+ was observed in the CF_3^{2+} + HD system, showing no intramolecular isotope effect. It appeared that in fact a more likely explanation was that the reactants formed a collision complex that had time to rearrange before dissociation. Harper *et al* used the PSCO to derive angular scattering distributions of the bond-forming reactions of the type (1.21) and (1.22). The products of these bond-forming reactions studied by Harper *et al* were symmetrically scattered over the range of scattering angles. This symmetrical scattering confirmed that the reaction mechanism involved a collision complex with a lifetime at least comparable with its rotational period. Therefore, to summarise, these studies showed that the CF_n^{2+} bond-forming reactions are often produced via the formation of a collision complex which subsequently undergoes

charge separation with the molecular ion then rearranging, and possibly dissociating, to yield the bond-forming product.

An additional type of dication-neutral bond-forming reaction yields a doubly charged product, as shown in equations (1.23), (1.24) and (1.25). [26, 154]

Dicationic product reaction	$XY^{2+} + M$	$\rightarrow$	$MX^{2+} + Y$	(1.23)
Examples	$CO^{2+} + Ar$	$\rightarrow$	$ArC^{2+} + O$	(1.24)
	$C_7H_6^{2+} + C_2H_2$		$C_9H_6^{2+} + H_2$	(1.25)

Bassi *et al* have reported the detection of several reactions of the type (1.23) in their efforts to study doubly charged molecular ions containing rare gas atoms. Bassi *et al* detected ArC^{2+} from the reactions of Ar^{2+} with CO and CO_2 as well as ArN^{2+} from the reaction of Ar^{2+} with N_2 and ArO^{2+} from the reaction of Ar^{2+} with O_2. Bassi *et al* measure the integral cross-sections of these reactions as a function of collision energy using a Guided Ion Beam technique which is discussed in section 1.4.1.3. The cross sections for these reactions peak in the region of 2 to 20 eV. [154-157] Burnside *et al* detected the product ArS^{2+} from the reaction of SF^{2+} with Ar. [158] The reaction mechanism proposed involved the formation of a collision complex, $ArSF^{2+}$, and consideration of the energetics showed it would be more unlikely that the $ArSF^{2+}$ would decompose to form monocation bond-forming products than the observed ArS^{2+} product. Roithová *et al* also detected bond-forming reactions that maintain the dication charge with larger organic molecules such as that shown in equation (1.25). These reactions are proposed as a route for the gas-phase synthesis of polyaromatic hydrocarbons (PAH) in the interstellar medium. [26]

1.4 Probing dication-neutral reactions

The following section discusses some of the experimental methods used to study the reactions of dications with neutrals. The Landau-Zener 'reaction window' theory used to account for dication-neutral electron transfer reactions is also presented.

1.4.1 Experimental techniques

Initial experiments to study dication reactivity were carried out on conventional or modified mass spectrometers. However, for more advanced studies of dication-neutral reactions it was necessary to develop dedicated instruments which often operated at lower collision energies. These low-energy methods provide a much greater opportunity to

observe chemical bond-forming reactions as well as charge transfer reactions. The following sections discuss these methods of probing dication-neutral reactions.

1.4.1.1 Crossed beam experiments

There are several variations of the "crossed beam experiment". In general, the reactant ions are formed by electron ionisation of an appropriate precursor gas, extracted at low (typically ~100 V) acceleration potentials, and mass analysed to form a dication beam. The dications then interact with the neutral of interest and the products are extracted and analysed. Several reactions have been studied using this technique including the reactions of CF^{2+}, CF_2^{2+}, CF_3^{2+}, OCS^{2+}, CO_2^{2+}, CO^{2+}, SF^{2+} with rare gases, CF_2^{2+} with NH_3, H_2O and H_2S, CF_3^{2+} with HD, H_2 and D_2 and Ar^{2+} with NH_3. [20, 141-143, 147, 149-151, 158-163] In some crossed beam experiments the products can also be angularly resolved before detection.

The crossed beam apparatus used by the Prague group allows angularly resolved studies at low collision energy that give information on the dynamics of dication collision systems. [19] The experiment employs standard electron ionisation in a low pressure ion source. The ions are then extracted, mass analyzed, and decelerated to the required energy. The dication beam is crossed at right angles with a beam of the neutral reactant species which emerges from a multi-channel jet. Reactant and product ions pass through a detection slit into a retarding potential energy analyzer, they are then accelerated and focused into another mass spectrometer, mass analyzed, and detected. Angular distributions are obtained by rotating the two beams about the scattering centre. A relatively wide range of dication-neutral reactions has been studied using this angularly resolved technique including $C_4H_3^{2+}$ with Kr, Xe, H_2, N_2, NO, NH_3, C_2H_2 and CH_4, CF_2^{2+} with Ar, Ne and D_2, and CO_2^{2+} with D_2, Ar and Ne. [19, 49, 140, 153, 164-167]

1.4.1.2 Guided Ion Beam experiments

Guided ion beam experiments typically consist of an ion source, some form of mass selection, a collision region, commonly constrained by an octopole to prevent the losses of ions with significant transverse velocities, and finally a detection mass spectrometer to count and identify the product ions. In the guided ion beam experiment used by Bassi *et al* in Trento, the ions are produced by electron bombardment of the neutral gas and are extracted and mass selected by a magnet mass spectrometer. The doubly charged ions are then injected into a radio-frequency octopole ion guide surrounded by the reaction cell

where the neutral reactant gas is introduced at pressures below 5×10^{-5} mbar. Changing the potential of the octopole changes the collision energy. The reactant and product ions are collected and guided to a quadrupole mass spectrometer. An electron multiplier is then used to detect the reactants and products. The integral cross sections can then be determined for the reactions over the range of collision energies studied and hence the effect of the collision energy on the reaction cross section can be successfully probed. This guided ion beam technique had been used to study the reaction of Ar^{2+} with O_2, CO^{2+} with Ar, Ar^{2+} with N_2. [154-157]

The CERISES (Collision Et Reaction d'Ions Selectionnares par Electrons de Seuil) guided ion beam experiment based in Paris, has played a particularly important role in the study of dication-neutral reactions of relevance to planetary ionospheres. CERISES was used to provide experimental information for the recent study modelling ionospherically relevant dications as discussed in section 1.1.2. The ions are produced by Photoionisation using synchrotron radiation and are extracted into a quadrupole-octopole-quadrupole arrangement. The dications are mass selected in the first quadrupole. The neutral gas is injected into the octopole and the dication- neutral reaction take place there. Finally the product and remaining parent ions are mass selected by the second quadrupole and then detected by a multichannel plate detector. CERISES has been used to studied the reactions of N_2^{2+} with O_2, CD_4, Ar and C_2D_4, CO_2^{2+} with CO_2 and CO and $CHCl^{2+}$ with Ar and D_2. [50, 168, 169]

The Berlin guided ion beam experiment consists of a multifunctional ion source, quadrupole mass filter, an ion flow tube and a quadrupole-octopole-quadrupole unit. The ions can be produced by electron ionisation, chemical ionisation or electrospray ionisation. The ions are then mass analysed or mass selected using the first quadrupole with a detector at the front of the flow tube. At the end of the flow tube a portion of the ions pass through a sampling disk. The ions extracted from the flow tube are directed towards the second quadrupole mass analyser, into the octopole collision cell and through the third quadrupole. A variety of dication-neutral systems have been studied using the Berlin experiment including the reactions of $CHBr^{2+}$ with H_2, CHX^{2+} (X=F, Cl, Br, and I) with Ne, Ar, Kr, Xe, N_2, O_2, CO, H_2O, and HCl, and $C_4H_3^{2+}$ with Kr, Xe, H_2, N_2, NO, NH_3, C_2H_2, and CH_4. [170-172]

1.4.2 Theoretical models of dication-neutral reactions

Landau-Zener Reaction Window (LZ-RW) theory has been used to successfully rationalise and theoretically model the electron-transfer reactions between dications and neutrals. [58, 142, 160] The LZ-RW theory is an extension of the Landau-Zener theory which was originally developed to rationalise the changing of potential energy curves in atom-atom collisions. [173, 174] By generalizing the Landau-Zener theory, and introducing some approximations, the electron transfer reaction of dication-neutral reaction systems can also be modelled; hence the LZ-RW theory has now been widely used for this purpose.

The LZ-RW theory allows the calculation of the probability of electron transfer allowing a collision system to move between a reactant potential and a product potential. A critical aspect of the LZ-RW theory is that the reactant and product potentials must cross. The transfer between the reactant and product potential curves can only occur in the region of the "crossing radius" r_c where they intersect, Figure 1.9.

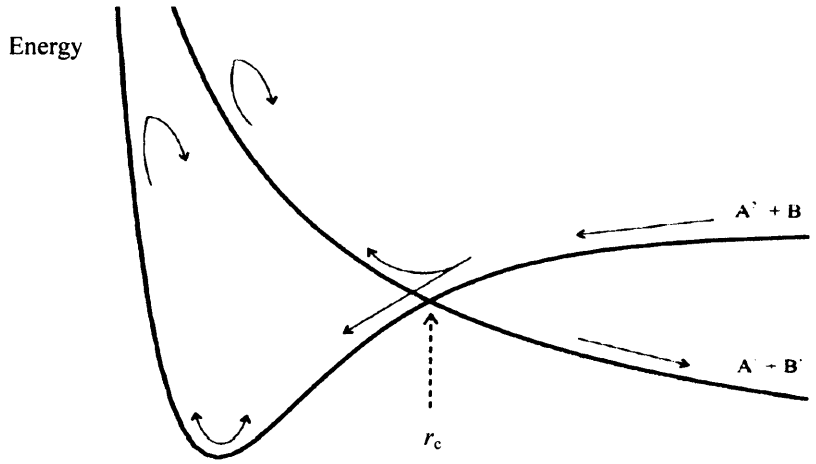

Figure 1.9 A potential energy surface of a dication-neutral reaction system with attractive reactant and repulsive product potential surfaces showing the "crossing radius" r_c where they intersect.

For a reaction system composed of a reactant channel and a product channel, the probability, P, that the reaction will occur is given by;

$$P = 2\delta\,(1-\delta) \qquad (1.26)$$

where δ is the probability that the collision system remains on the diabatic curve through the crossing. δ is a function of the electronic coupling matrix element between the two states, $H_{12}{}^2$, which can be determined from the energetics of the reactants and products,

the difference in the gradient of the slopes of the potential energy curves at the curve crossing, $|V_1'-V_2'|$, and the relative velocity of the two species, v_b;

$$\delta = \exp((-\pi |H_{12}|^2) / (2\hbar |V_1'-V_2'| v_b)) \quad (1.27)$$

Electron transfer is modelled as an avoided crossing between the prototypical reactant and product potential energy curves as shown in Figure 1.9. For dication electron transfer reactions the relative energies and shapes of the potential energy curves have a predictable form. The potential of the attractive reactant channel, $V(M^{2+} + N)$, can be modelled at significant interspecies separations using the polarization attraction of the reactants (Equation (1.28)). The repulsive product channel, $V(M^+ + N^+)$, can be modelled using the Coulombic law (Equation (1.29));

$$V(M^{2+} + N) = -Z^2e^2\alpha/2r^4 + \Delta E \quad (1.28)$$
$$V(M^+ + N^+) = e^2/r \quad (1.29)$$

where Z is the charge on the reactant ion (therefore $Z = 2$ for a dication), α is the polarisation of the neutral species and ΔE is the sum of the reaction exothermicity. If the reaction is to proceed, it will occur at the intersection of the crossings of the potentials, where $V(M^{2+} + N) = V(M^+ + N^+)$ but only if these potentials cross at an appropriate internuclear separation. By solving these equations for r where $V(M^{2+} + N) = V(M^+ + N^+)$, the curve crossing radius, r_c, can be determined. The value of r_c is linked to the probability of a successful reaction because $|H_{12}|^2$, featured in equation (1.27), is determined using the ionisation energy of the products A and B, I, and r_c; [175]

$$|H_{12}|^2 = 1.0(I_AI_B)(r_c^*)^2\exp(-1.72r_c^*) \quad (1.30)$$

where r_c^* is;

$$r_c^* = ((I_A^{1/2}+IB^{1/2}) / 2^{1/2})r_c \quad (1.31)$$

These functions predict that as r_c increases, $|H_{12}|^2$ decreases exponentially due to the increased distance the electron needs to tunnel from one atom to the other. When r_c increases from approximately 2 to 6 Å, the character of the avoided crossing switches. At interspecies separations larger than 6 Å, reactions are unlikely mainly because the distance between the species is too large for electron transfer; hence the interaction between the two species is very low. Here $\delta = 1$, indicating little interaction, and so $P = 0$. At small interspecies separations, lower than 2 Å, reactions are unlikely because the reactants interact too strongly and so the electron would transfer as the reactants approach and would transfer back as the products depart from each other. Here $\delta = 0$, indicating strong coupling, and hence again $P = 0$. Therefore it is between these limits of 'too far'

and 'too close', where these two types of unfavourable conditions for electron transfer switch. At this intermediate coupling peaking, $\delta = 0.5$, the probability of a reaction is highest, the "reaction window". The reaction probability may approach 50 % in the reaction window, where δ is neither too small (at very small interspecies separations) nor too large (at very large interspecies separations) for a successful electron transfer reaction. LZ-RW theory has shown that a successful crossing from the reactant potential to the product potential is most likely to occur at an interspecies separation of 2 to 6 Å, (the reaction window). [142, 176] In summary, the dication-neutral systems can be characterised by the avoided crossings of the reactant and product potentials. The internuclear separation at the intersection of the reactant and product potentials is used to determine the probability of an electron transfer reaction.

Within a collision system there may be many different curve intersections, each corresponding to the formation of different product electronic states, as shown in Figure 1.10. The dotted line in Figure 1.10 shows the electron transfer cross section, σ, which is at its maximum in the reaction window, encompassing the asymptotes of several different product channels.

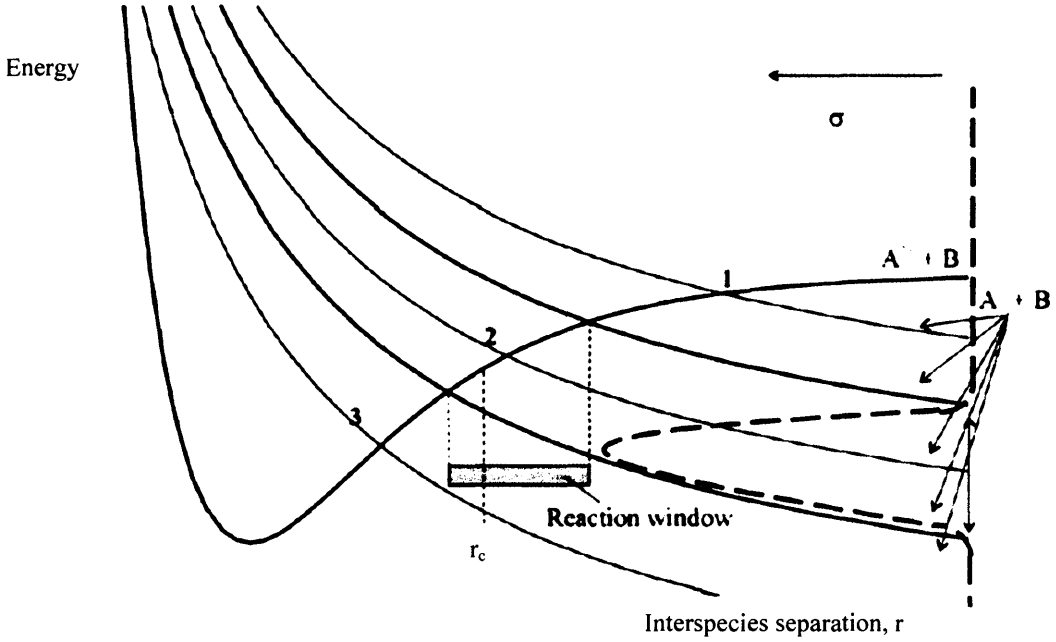

Figure 1.10 A potential energy surface showing the reaction window for a dication-neutral reaction.

The accessibility of different product asymptotes shown in Figure 1.10 explains the occurrence of both dissociative and non-dissociative electron transfer reactions. If the products are formed in stable states the reaction will be a non-dissociative electron

transfer. However, if one or more of the products are formed in unstable electronic states, these unstable nascent product states will dissociate, so the reaction will involve dissociative electron transfer. The LZ-RW theory has been used to rationalise the occurrence of non-dissociative electron transfer reactions verses dissociative electron transfer reactions using rare gases as the neutral reagent. Generally, as the ionisation potential of the neutral rare gas reagent decreases, the crossing radii for the population of stable lower energy product states moves out of the reaction window, and the crossing radii for the population of dissociative higher energy product states moves into the reaction window.

A general model of the potential surfaces involved in a bond-forming dication reaction has been developed by Herman *et al.* [19, 58] This model can explain many of the features of dication-neutral collisions, including bond-forming reactions. A schematic diagram used to explain the model is shown in Figure 1.11.

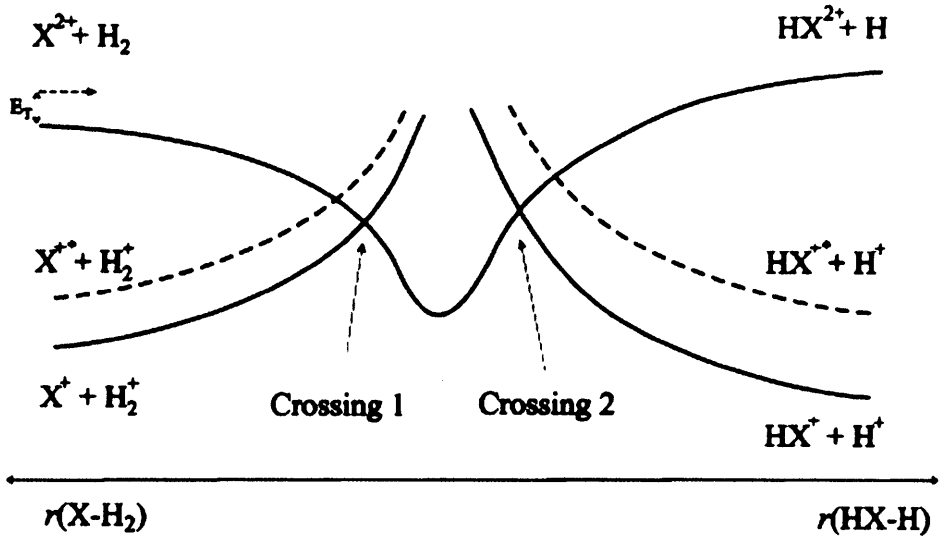

Figure 1.11 Schematic potential energy curve diagram to explain the interacting potential energy surfaces of bond-forming reactions from dication-neutral collisions. r is the inter species separation. [19, 58]

Figure 1.11 shows that the model distinguishes two regions of the potential energy surface. On the left, the neutral and dication approach each other and can undergo simple electron transfer, as we have seen above, to form a pair of monocations with the same connectivity as the reactants. On the right hand side of the diagram, we consider the separation of the "re-arranged species", the products of the reaction. As these species separate there is the possibility of electron transfer between them (at a curve crossing), so the products can be a pair of monocations or a dication and a neutral. How the collision system negotiates these different crossings determines which products are observed from

the interaction. As the dication and neutral approach at the first crossing (Figure 1.11, crossing one), there is a possibility of simple electron transfer occurring resulting in repulsive singly charged products, as in the 'LZ-RW' model in Figure 1.9. If an electron is not transferred, the dication and neutral can interact closely to create and break bonds in a collision complex. If no reaction occurs, the complex is likely to dissociate back to the reactants, but if a reaction does occur, the collision complex will dissociate along a new reactive co-ordinate. Along this reactive co-ordinate a new dication may be formed with a neutral, or, the system may reach the potential corresponding to two product monocations (crossing two). This model shows there is competition between electron transfer and formation of a collision complex. This explains why electron transfer is often the dominant process in dication neutral collisions, since for new chemical bonds to form collisions systems always have to negotiate the curve crossings leading to simple electron transfer.

1.5 Summary

We have thus introduced the topic of dication-neutral reactions. Doubly charged ions have been predicted in many energised environments, and the work on modelling dications in planetary ionospheres has been discussed here. The properties of dications and various methods to form and probe dications, have been explained, as well as the reactivity of dications with neutrals and various techniques used to probe these reactions. In the next Chapter, the experimental method used in this thesis to further the knowledge of dication-neutral bond-forming reaction is described.

1.6 References

[1] Conrad, R, 1930, Phys. Z., 31, 888.
[2] Price, S. D., 2003, Physical Chemistry Chemical Physics, 5, 9, 1717.
[3] Vaughan, A., 1931, Physical Review, 38, 1687.
[4] Hagstrum, H. D. and Tate, J. T., 1941, Physical Review, 59, 354.
[5] Friedlander, E., Kallman, H., Lasereff, W., and Rosen, B., 1932, Z. Phys, 76, 70.
[6] Pauling, L, 1933, Journal of Chemical Physics, 1, 56.
[7] Griffiths, I. W., 1997, Rapid Communications in Mass Spectrometry, 11, 1, 3.
[8] Dawber, G., Mcconkey, A. G., Avaldi, L., Macdonald, M. A., King, G. C., and Hall, R. I., 1994, Journal of Physics B-Atomic Molecular and Optical Physics, 27, 11, 2191.
[9] Eland, J. H. D., 2003, Chemical Physics, 294, 2, 171.
[10] Moddeman, W. E., Carlson, T. A., Krause, M. O., Pullen, B. P., Bull, W. E., and Schweitz, G. K., 1971, Journal of Chemical Physics, 55, 5, 2317.
[11] Wetmore, R. W. and Boyd, R. K., 1986, Journal of Physical Chemistry, 90, 22, 5540.
[12] Vekey, K., Brenton, A. G., and Beynon, J. H., 1986, Journal of Physical Chemistry, 90, 16, 3569.
[13] Mathur, D., Kingston, R. G., Harris, F. M., Brenton, A. G., and Beynon, J. H., 1987, Journal of Physics B-Atomic Molecular and Optical Physics, 20, 8, 1811.
[14] Pedersen, J. O. K. and Hvelplund, P., 1987, Journal of Physics B-Atomic Molecular and Optical Physics, 20, 10, L317.
[15] Herman, Z., Jonathan, P., Brenton, A. G., and Beynon, J. H., 1987, Chemical Physics Letters, 141, 5, 433.
[16] Reid, C. J., Harris, F. M., and Beynon, J. H., 1988, International Journal of Mass Spectrometry and Ion Processes, 82, 1-2, 151.
[17] Reid, C. J., Ballantine, J. A., and Harris, F. M., 1989, International Journal of Mass Spectrometry and Ion Processes, 93, 1, 23.
[18] Hu, W. P., Harper, S. M., and Price, S. D., 2002, Measurement Science & Technology, 13, 10, 1512.
[19] Herman, Z., Zabka, J., Dolejsek, Z., and Farnik, M., 1999, International Journal of Mass Spectrometry, 192, 191.
[20] Newson, K. A., Tafadar, N., and Price, S. D., 1998, Journal of the Chemical Society-Faraday Transactions, 94, 18, 2735.
[21] Chatterjee, B. K. and Johnsen, R., 1989, Journal of Chemical Physics, 91, 2, 1378.
[22] Witasse, O., Dutuit, O., Lilensten, J., Thissen, R., Zabka, J., Alcaraz, C., Blelly, P. L., Bougher, S. W., Engel, S., Andersen, L. H., and Seiersen, K., 2002, Geophysical Research Letters, 29, 8.
[23] Leach, S., 1986, Journal of Electron Spectroscopy and Related Phenomena, 41, 3-4, 427.
[24] Mathur, D., 2004, Physics Reports-Review Section of Physics Letters, 391, 1-2, 1..
[25] Allamandola, L. J., Tielens, A. G. G. M., and Barker, J. R., 1985, Astrophysical Journal, 290, 1, L25.
[26] Roithova, J. and Schroder, D., 2006, Journal of the American Chemical Society, 128, 13, 4208.
[27] Rosi, M., Bauschlicher, C. W., and Bakes, E. L. O., 2004, Astrophysical Journal, 609, 2, 1192.
[28] Nicolaides, C. A., 1989, Chemical Physics Letters, 161, 6, 547.
[29] Taylor, P. R. and Partridge, H., 1987, Journal of Physical Chemistry, 91, 24, 6148.
[30] Calandra, P., O'Connor, C. S. S., and Price, S. D., 2000, Journal of Chemical Physics, 112, 24, 10821.
[31] Love, N. A. and Price, S. D., 2004, Physical Chemistry Chemical Physics, 6, 19, 4558.
[32] Straub, H. C., Lindsay, B. G., Smith, K. A., and Stebbings, R. F., 1996, Journal of Chemical Physics, 105, 10, 4015.
[33] Lesech, C., 1992, Chemical Physics Letters, 200, 4, 369.
[34] Vincze, A., Yinon, J., Peres, T., and Lifshitz, C., 1999, International Journal of Mass Spectrometry, 192, 99.
[35] Schunk, R. W and Nagy, F. N., 2000, Ionospheres: Physics, Plasma physics and Chemistry., Cambridge Atmospheric and Space Science, Ed. Dessler, A.J; Houghton, J.T; Rycroft, M.J.
[36] Simon, C., Lilensten, J., Dutuit, O., Thissen, R., Witasse, O., Alcaraz, C., and Soldi-Lose, H., 2005, Annales Geophysicae, 23, 3, 781.
[37] Lilensten, J., Witasse, O., Simon, C., Solidi-Lose, H., Dutuit, O., Thissen, R., and Alcaraz, C., 2005, Geophysical Research Letters, 32, 3.
[38] Gronoff, G., Lilensten, J., Simon, C., Witasse, O., Thissen, R., Dutuit, O., and Alcaraz, C., 2007, Astronomy & Astrophysics, 465, 2, 641.
[39] Hoffman, J. H., Hanson, W. B., Lippinco, C. R., and Ferguson, E. E., 1973, Radio Science, 8, 4, 315.
[40] Prasad, S. S. and Furman, D. R., 1975, Journal of Geophysical Research, 80, 10, 1360.
[41] Breig, E. L., Torr, M. R., Torr, D. G., Hanson, W. B., Hoffman, J. H., Walker, J. C. G., and Nier, A. O., 1977, Journal of Geophysical Research-Space Physics, 82, 7, 1008.

[42] Breig, E. L., Torr, M. R., and Kayser, D. C., 1982, Journal of Geophysical Research-Space Physics, 87, NA9, 7653.
[43] Chappell, C. R., Olsen, R. C., Green, J. L., Johnson, J. F. E., and Waite, J. H., 1982, Geophysical Research Letters, 9, 9, 937.
[44] Carroll, P. K., 1958, Canadian Journal of Physics, 36, 11, 1585.
[45] Hellner, L., Besnard, M. J., Dujardin, G., and Malinovich, Y., 1988, Chemical Physics, 119, 2-3, 391.
[46] Avakyan, S. V., 1998, Journal of Optical Technology, 65, 11, 870.
[47] Avakyan, S. V., 2001, Physics and Chemistry of the Earth Part C-Solar-Terrestial and Planetary Science, 26, 4, 259.
[48] Mathur, D., Andersen, L. H., Hvelplund, P., Kella, D., and Safvan, C. P., 1995, Journal of Physics B-Atomic Molecular and Optical Physics, 28, 15, 3415.
[49] Mrazek, L., Zabka, J., Dolejsek, Z., and Herman, Z., 2003, Collection of Czechoslovak Chemical Communications, 68, 1, 178.
[50] Franceschi, P., Thissen, R., Zabka, J., Roithova, J., Herman, Z., and Dutuit, O., 2003, International Journal of Mass Spectrometry, 228, 2-3, 507.
[51] Niemann, H. B., Harpold, D. N., Feng, S., Kasprzak, W. T., Way, S. H., Atreya, S. K., Block, B., Carignan, G. R., Donahue, T. M., Nagy, A. F., Bougher, S. W., Hunten, D. M., Owen, T. C., Bauer, S. J., Hayakawa, H. J., Mukai, T., Miura, Y. N., and Sugiura, N., 1998, Earth Planets and Space, 50, 9, 785.
[52] Rodrigo, R., Garciaalvarez, E., Lopezgonzalez, M. J., and Lopezmoreno, J. J., 1990, Journal of Geophysical Research-Solid Earth and Planets, 95, B9, 14795.
[53] Krasnopolsky, V. A., Bowyer, S., Chakrabarti, S., Gladstone, G. R., and Mcdonald, J. S., 1994, Icarus, 109, 2, 337.
[54] Neir, A. O, 1977, Journal of Geophysical Research, 82, 4341.
[55] Hanson, W. B., 1977, Journal of Geophysical Research, 82, 4351.
[56] Carroll, P. K., 1958, Canadian Journal of Physics, 36, 11, 1585.
[57] Price, S. D., 1997, Journal of the Chemical Society-Faraday Transactions, 93, 15, 2451.
[58] Price, S. D., 2007, International Journal of Mass Spectrometry, 260, 1, 1.
[59] Cossart, D., Launay, F., Robbe, J. M., and Gandara, G., 1985, Journal of Molecular Spectroscopy, 113, 1, 142.
[60] Leach, S., Devoret, M., and Eland, J. H. D., 1978, Chemical Physics, 33, 1, 113.
[61] Taylor, S., Eland, J. H. D., and Hochlaf, M., 2006, Journal of Chemical Physics, 124, 20.
[62] Taylor, S., Eland, J. H. D., and Hochlaf, M., 2006, Chemical Physics, 330, 1-2, 16.
[63] Peng, J. P., Moskovets, E. V., and Gellene, G. I., 1997, Journal of the American Society for Mass Spectrometry, 8, 12, 1262.
[64] Roithova, J., Milko.P, Ricketts, C. L., Schroder, D., Dekoj, V., and Belohradsky, M., 2007, Journal of American Chemical Society, In Press.
[65] Besnard, M. J., Hellner, L., Dujardin, G., and Winkoun, D., 1988, Journal of Chemical Physics, 88, 3, 1732.
[66] Roithova, J., Zabka, J., Ascenzi, D., Franceschi, P., Ricketts, C. L., and Schroder, D., 2006, Chemical Physics Letters, 423, 1-3, 254.
[67] Straub, H. C., Renault, P., Lindsay, B. G., Smith, K. A., and Stebbings, R. F., 1996, Physical Review A, 54, 3, 2146.
[68] Harper, S., Calandra, P., and Price, S. D., 2001, Physical Chemistry Chemical Physics, 3, 5, 741.
[69] Love, N. A. and Price, S. D., 2004, International Journal of Mass Spectrometry, 233, 1-3, 145.
[70] Dorman, F. H. and Morrison, J. D., 1961, Journal of Chemical Physics, 35, 2, 575.
[71] Dorman, F. H. and Morrison, J. D., 1963, Journal of Chemical Physics, 39, 7, 1906.
[72] Fainelli, E., Maracci, F., Platania, R., and Avaldi, L., 1998, Journal of Electron Spectroscopy and Related Phenomena, 87, 3, 169.
[73] Fainelli, E., Maracci, F., Platania, R., and Avaldi, L., 2001, Journal of Electron Spectroscopy and Related Phenomena, 119, 1, 81.
[74] Moddeman, W. E., Carlson, T. A., Krause, M. O., Pullen, B. P., Bull, W. E., and Schweitz, G. K., 1971, Journal of Chemical Physics, 55, 5, 2317.
[75] Brenton, A. G., 1995, Journal of Mass Spectrometry, 30, 5, 657.
[76] Brenton, A. G., 2000, International Journal of Mass Spectrometry, 200, 1-3, 403.
[77] Hamdan, M. and Brenton, A. G., 1989, Journal of Physics B-Atomic Molecular and Optical Physics, 22, 1, L9.
[78] Appell, J., Durup, J., Fehsenfe, F. C., and Fournier, P., 1973, Journal of Physics B-Atomic Molecular and Optical Physics, 6, 1, 197.
[79] Furuhashi, O., Kinugawa, T., Masuda, S., Yamada, C., and Ohtani, S., 2001, Chemical Physics Letters, 337, 1-3, 97.
[80] Furuhashi, O., Kinugawa, T., Masuda, S., Yamada, C., and Ohtani, S., 2001, Chemical Physics Letters, 342, 5-6, 625.

[81] Furuhashi, O., Kinugawa, T., Hirayama, T., Koizumi, T., Yamada, C., and Ohtani, S., 2003, Chemical Physics, 295, 2, 185.
[82] Furuhashi, O., Kinugawa, T., Hirayama, T., Koizumi, T., Yamada, C., and Ohtani, S., 2004, Physical Review A, 70, 5.
[83] Griffiths, I. W., Parry, D. E., and Harris, F. M., 1998, Chemical Physics, 238, 1, 21.
[84] Griffiths, I. W., Parry, D. E., and Harris, F. M., 1999, International Journal of Mass Spectrometry, 187, 651.
[85] Cossart, D. and Launay, F., 1985, Journal of Molecular Spectroscopy, 113, 1, 159.
[86] Cossart, D. and Cossartmagos, C., 1991, Journal of Molecular Spectroscopy, 147, 2, 471.
[87] Cox, S. G., Critchley, A. D. J., Kreynin, P. S., Mcnab, I. R., Shiell, R. C., and Smith, F. E., 2003, Physical Chemistry Chemical Physics, 5, 4, 663.
[88] Cosby, P. C., Moller, R., and Helm, H., 1983, Physical Review A, 28, 2, 766.
[89] Larsson, M., Sundstrom, G., Brostrom, L., and Mannervik, S., 1992, Journal of Chemical Physics, 97, 3, 1750.
[90] Martin, P. A., Bennett, F. R., and Maier, J. P., 1994, Journal of Chemical Physics, 100, 7, 4766.
[91] Masters, T. E. and Sarre, P. J., 1990, Journal of the Chemical Society-Faraday Transactions, 86, 11, 2005.
[92] Sundstrom, G., Carlson, M., Larsson, M., and Brostrom, L., 1994, Chemical Physics Letters, 218, 1-2, 17.
[93] Mullin, A. S., Szaflarski, D. M., Yokoyama, K., Gerber, G., and Lineberger, W. C., 1992, Journal of Chemical Physics, 96, 5, 3636.
[94] Szaflarski, D. M., Mullin, A. S., Yokoyama, K., Ashfold, M. N. R., and Lineberger, W. C., 1991, Journal of Physical Chemistry, 95, 6, 2122.
[95] Pilcher-Clayton, A. and Eland, J. H. D., 2005, Journal of Electron Spectroscopy and Related Phenomena, 142, 3, 313.
[96] Edvardsson, D., Danielsson, A., Karlsson, L., and Eland, J. H. D., 2006, Chemical Physics, 324, 2-3, 674.
[97] Eland, J. H. D., 2006, Chemical Physics, 323, 2-3, 391.
[98] Molloy, R. D. and Eland, J. H. D., 2006, Chemical Physics Letters, 421, 1-3, 31.
[99] Eland, J. H. D., 2005, Electron and Photon Impact Ionization and Related Topics 2004, 183, 115.
[100] Eland, J. H. D., Hochlaf, M., King, G. C., Kreynin, P. S., Leroy, R. J., Mcnab, I. R., and Robbe, J. M., 2004, Journal of Physics B-Atomic Molecular and Optical Physics, 37, 15, 3197.
[101] Kinugawa, T., Lablanquie, P., Penent, F., Palaudoux, J., and Eland, J. H. D., 2004, Journal of Electron Spectroscopy and Related Phenomena, 141, 2-3, 143.
[102] Slattery, A. E., Field, T. A., Ahmad, M., Hall, R. I., Lambourne, J., Penent, F., Lablanquie, P., and Eland, J. H. D., 2005, Journal of Chemical Physics, 122, 8.
[103] Hochlaf, M. and Eland, J. H. D., 2004, Journal of Chemical Physics, 120, 14, 6449.
[104] Ahmad, M., Lablanquie, P., Penent, F., Lambourne, J. G., Hall, R. I., and Eland, D., 2006, Journal of Physics B-Atomic Molecular and Optical Physics, 39, 17, 3599.
[105] Dawber, G., Mcconkey, A. G., Avaldi, L., Macdonald, M. A., King, G. C., and Hall, R. I., 1994, Journal of Physics B-Atomic Molecular and Optical Physics, 27, 11, 2191.
[106] Hall, R. I., Mcconkey, A., Avaldi, L., Macdonald, M. A., and King, G. C., 1992, Journal of Physics B-Atomic Molecular and Optical Physics, 25, 2, 411.
[107] Hochlaf, M., Hall, R. I., Penent, F., Kjeldsen, H., Lablanquie, P., Lavollee, M., and Eland, J. H. D., 1996, Chemical Physics, 207, 1, 159.
[108] Hochlaf, M., Hall, R. I., Penent, F., Eland, J. H. D., and Lablanquie, P., 1998, Chemical Physics, 234, 1-3, 249.
[109] Yencha, A. J., Juarez, A. M., Lee, S. P., King, G. C., Bennett, F. R., Kemp, F., and Mcnab, I. R., 2004, Chemical Physics, 303, 1-2, 179.
[110] Krassig, B. and Schmidt, V., 1992, Journal of Physics B-Atomic Molecular and Optical Physics, 25, 14, L327.
[111] Newson, K. A., Luc, S. M., Price, S. D., and Mason, N. J., 1995, International Journal of Mass Spectrometry and Ion Processes, 148, 3, 203.
[112] O'Connor, C. S. and Price, S. D., 1999, International Journal of Mass Spectrometry, 184, 1, 11.
[113] Oconnor, C. S. S., Jones, N. C., ONeale, K., and Price, S. D., 1996, International Journal of Mass Spectrometry and Ion Processes, 154, 3, 203.
[114] Lundqvist, M., Baltzer, P., Edvardsson, D., Karlsson, L., and Wannberg, B., 1995, Physical Review Letters, 75, 6, 1058.
[115] Lundqvist, M., Edvardsson, D., Baltzer, P., Larsson, M., and Wannberg, B., 1996, Journal of Physics B-Atomic Molecular and Optical Physics, 29, 3, 499.
[116] Lundqvist, M., Edvardsson, D., Baltzer, P., and Wannberg, B., 1996, Journal of Physics B-Atomic Molecular and Optical Physics, 29, 8, 1489.

[117] Edvardsson, D., Lundqvist, M., Baltzer, P., Wannberg, B., and Lunell, S., 1996, Chemical Physics Letters, 256, 3, 341.
[118] Masuoka, T., 1994, Journal of Chemical Physics, 100, 9, 6422.
[119] Masuoka, T., 1994, Journal of Chemical Physics, 101, 1, 322.
[120] Winkoun, D. and Dujardin, G., 1986, Zeitschrift fur Physik D-Atoms Molecules and Clusters, 4, 1, 57.
[121] Masuoka, T., Koyano, I., and Saito, N., 1992, Journal of Chemical Physics, 97, 4, 2392.
[122] Ibuki, T., Imamura, T., Koyano, I., Masuoka, T., and Brion, C. E., 1993, Journal of Chemical Physics, 98, 4, 2908.
[123] Masuoka, T., Okaji, A., and Kobayashi, A., 2002, International Journal of Mass Spectrometry, 218, 1, 11.
[124] Feng, R. F., Cavell, R. G., and Hitchcock, A. P., 2005, Journal of Electron Spectroscopy and Related Phenomena, 144, 231.
[125] Dujardin, G., Hellner, L., Winkoun, D., and Besnard, M. J., 1986, Chemical Physics, 105, 1-2, 291.
[126] Masuoka, T., 1999, Journal of Electron Spectroscopy and Related Phenomena, 103, 53.
[127] Field, T. and Eland, J. H. D., 1992, Chemical Physics Letters, 197, 6, 542.
[128] Field, T. A. and Eland, J. H. D., 1993, Chemical Physics Letters, 211, 4-5, 436.
[129] Taylor, S. and Eland, J. H. D., 2005, Chemical Physics, 315, 1-2, 8.
[130] Hatherly, P. A., Stankiewicz, M., Frasinski, L. J., Codling, K., and Macdonald, M. A., 1989, Chemical Physics Letters, 159, 4, 355.
[131] Field, T. A. and Eland, J. H. D., 1999, Chemical Physics Letters, 303, 1-2, 144.
[132] Feng, R. F., Cavell, R. G., and Hitchcock, A. P., 2005, Journal of Electron Spectroscopy and Related Phenomena, 144, 231.
[133] Harada, C., Tada, S., Yamamoto, K., Senba, Y., Yoshida, H., Hiraya, A., Wada, S., Tanaka, K., and Tabayashi, K., 2006, Radiation Physics and Chemistry, 75, 11, 2085.
[134] Feifel, R., Eland, J. H. D., Storchi, L., and Tarantelli, F., 2006, Journal of Chemical Physics, 125, 19,
[135] Eland, J. H. D. and Feifel, R., 2006, Chemical Physics, 327, 1, 85.
[136] Harper, S. M., Hu, W. P., and Price, S. D., 2002, Journal of Physics B-Atomic Molecular and Optical Physics, 35, 21, 4409.
[137] Ricketts, C. L., Harper, S. M., Hu, S. W. P., and Price, S. D., 2005, Journal of Chemical Physics, 123, 13, 124322-1.
[138] Harper, S. M., Hu, S. W. P., and Price, S. D., 2004, Journal of Chemical Physics, 120, 16, 7245.
[139] Agee, J. H., Wilcox, J. B., Abbey, L. E., and Moran, T. F., 1981, Chemical Physics, 61, 1-2, 171.
[140] Herman, Z., Jonathan, P., Brenton, A. G., and Beynon, J. H., 1987, Chemical Physics Letters, 141, 5, 433.
[141] Price, S. D., Rogers, S. A., and Leone, S. R., 1993, Journal of Chemical Physics, 98, 12, 9455.
[142] Rogers, S. A., Price, S. D., and Leone, S. R., 1993, Journal of Chemical Physics, 98, 1, 280.
[143] Kearney, D. and Price, S. D., 2003, Physical Chemistry Chemical Physics, 5, 8, 1575.
[144] Kaltsoyannis, N. and Price, S. D., 1999, Chemical Physics Letters, 313, 3-4, 679.
[145] Price, S. D., Manning, M., and Leone, S. R., 1994, Journal of the American Chemical Society, 116, 19, 8673.
[146] Roithova, J., Zabka, J., Herman, Z., Thissen, R., Schroder, D., and Schwarz, H., 2006, Journal of Physical Chemistry A, 110, 20, 6447.
[147] Tafadar, N. and Price, S. D., 2003, International Journal of Mass Spectrometry, 223, 1-3, 547.
[148] Newson, K. A., Tafadar, N., and Price, S. D., 1998, Journal of the Chemical Society-Faraday Transactions, 94, 18, 2735.
[149] Newson, K. A. and Price, S. D., 1998, Chemical Physics Letters, 294, 1-3, 223.
[150] Lambert, N., Kaltsoyannis, N., and Price, S. D., 2003, Journal of Chemical Physics, 119, 3, 1421.
[151] Lambert, N., Kaltsoyannis, N., Price, S. D., Zabka, J., and Herman, Z., 2006, Journal of Physical Chemistry A, 110, 9, 2898.
[152] Harper, S. M., Hu, S. W. P., and Price, S. D., 2004, Journal of Chemical Physics, 121, 8, 3507.
[153] Mrazek, L., Zabka, J., Dolejsek, Z., Hrusak, J., and Herman, Z., 2000, Journal of Physical Chemistry A, 104, 31, 7294.
[154] Lu, W. Y., Tosi, P., and Bassi, D., 2000, Journal of Chemical Physics, 112, 10, 4648.
[155] Tosi, P., Correale, R., Lu, W. L., Falcinelli, S., and Bassi, D., 1999, Physical Review Letters, 82, 2, 450.
[156] Tosi, P., Lu, W. Y., Correale, R., and Bassi, D., 1999, Chemical Physics Letters, 310, 1-2, 180.
[157] Ascenzi, D., Franceschi, P., Tosi, P., Bassi, D., Kaczorowska, M., and Harvey, J. N., 2003, Journal of Chemical Physics, 118, 5, 2159.
[158] Burnside, P. W. and Price, S. D., 2006, International Journal of Mass Spectrometry, 249, 279.
[159] Lambert, N., Kearney, D., Kaltsoyannis, N., and Price, S. D., 2004, Journal of the American Chemical Society, 126, 11, 3658.
[160] Manning, M., Price, S. D., and Leone, S. R., 1993, Journal of Chemical Physics, 99, 11, 8695.

[161] Newson, K. A. and Price, S. D., 1997, Chemical Physics Letters, 269, 1-2, 93.
[162] Tafadar, N., Kaltsoyannis, N., and Price, S. D., 1999, International Journal of Mass Spectrometry, 192, 205.
[163] Tafadar, N., Kearney, D., and Price, S. D., 2001, Journal of Chemical Physics, 115, 19, 8819.
[164] Herman, Z., 1996, International Reviews in Physical Chemistry, 15, 1, 299.
[165] Jasik, J., Roithova, J., Zabka, J., Thissen, R., Ipolyi, I., and Herman, Z., 2006, International Journal of Mass Spectrometry, 255, 150.
[166] Roithova, J., Zabka, J., Hrusak, J., Thissen, R., and Herman, Z., 2003, Journal of Physical Chemistry A, 107, 38, 7347.
[167] Roithova, J., Zabka, J., Thissen, R., and Herman, Z., 2003, Physical Chemistry Chemical Physics, 5, 14, 2988.
[168] Dutuit, O., Thissen, R., and Soldi-Lose, H., 2005, -Unpublished.
[169] Roithova, J., Thissen, R., Zabka, J., Franceschi, P., Dutuit, O., and Herman, Z., 2003, International Journal of Mass Spectrometry, 228, 2-3, 487.
[170] Roithova, J., Herman, Z., Schroder, D., and Schwarz, H., 2006, Chemistry-A European Journal, 12, 9, 2465.
[171] Roithova, J., Zabka, J., Herman, Z., Thissen, R., Schroder, D., and Schwarz, H., 2006, Journal of Physical Chemistry A, 110, 20, 6447.
[172] Jasik, J., Roithova, J., Zabka, J., Thissen, R., Ipolyi, I., and Herman, Z., 2006, International Journal of Mass Spectrometry, 255, 150.
[173] Zener, C., 1932, Proceedings of the Royal Society of London Series A, 137, 696.
[174] Landau, L, 1932, Phys Z Sowjetunion, 2, 26.
[175] Olson, R. E., Smith, F. T., and Bauer, E., 1971, Applied Optics, 10, 8, 1848.
[176] Manning, M., Price, S. D., and Leone, S. R., 1993, Journal of Chemical Physics, 99, 11, 8695.

Chapter 2 Experimental Arrangement and Data Processing

2.1 Experimental overview

This chapter will give a detailed description of the PSCO experimental arrangement and the process associated with transforming the raw data into scattering diagrams. The apparatus has been developed as a general technique to study the dynamics and energetics of gas-phase dication-molecule reactions. A time-of-flight mass spectrometer (*TOF-MS*) coupled with a position sensitive detector (PSD) is used to collect in coincidence, on an event by event basis, pairs of singly-charged product ions formed by dication-neutral reactions. [1, 2] This chapter will show how these data are recorded and subsequently processed in order to yield detailed information about the dynamics of dication reactions. However, first a brief overview of the whole experiment is presented, and a general schematic of the experimental apparatus is shown in Figure 2.1.

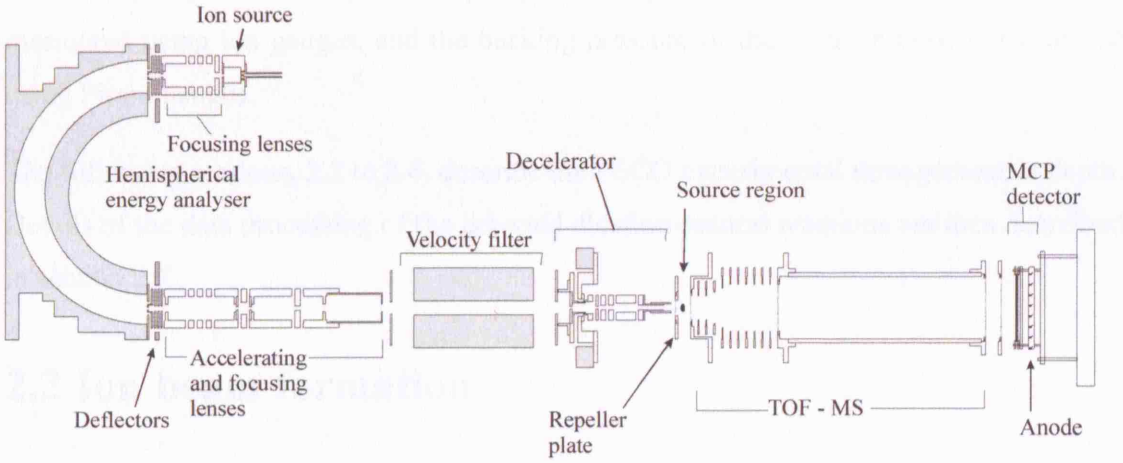

Figure 2.1 The PSCO experimental arrangement.

The reactant ions are generated via electron ionisation (EI) of the appropriate precursor gas in the ion source. These reactant ions, as well as other singly and doubly charged ions, are extracted and pass through the hemispherical energy analyser. Here the ions are energy selected. The ion beam is pulsed by deflectors at the exit of the energy analyser, creating packets of dications. The packets of dications then pass through a series of focusing and accelerating lenses, which are tuned to optimise the shape and size of the beam. A commercial velocity filter then selects the dications from the packets of ions, and the resulting dication pulses are decelerated to an appropriate collision energy, a few

electron volts (eV), using a commercial decelerator. The dication pulses interact with the neutral gas at the source region of the *TOF-MS*. After the interaction of the dications and neutral gas, a positive voltage is applied to the repeller plate and the product ions, and any unreacted dications, are extracted and accelerated into the field free drift tube of the *TOF-MS*. The ions impact upon the PSD at the end of the *TOF-MS* drift tube. The PSD consists of a pair of multi channel plates (MCPs) ahead of two wire wound anodes of known length. The electron cascade from the MCP impacts on the anodes and this signal propagates along both wires to each of their ends. The flight time and the arrival time of the signal at the end of each of the wire anodes are recorded for each of the detected ions. Hence, the position of the ion, and subsequently the velocity vectors for each of the ions can be derived.

An important requirement for the PSCO technique is that the dication-neutral reactions must occur under single collision conditions. In order to attain single collision conditions, the experiment must operate under high vacuum conditions. Therefore the experiment is constructed to yield a base pressure of 10^{-7} Torr. The apparatus described above is enclosed in three stainless steel chambers each pumped by water cooled diffusion pumps backed by rotary pumps. The pressure in each of the chambers is monitored using ion gauges, and the backing pressure of the rotary pumps is monitored using Pirani gauges.

The following sections, 2.2 to 2.6, describe the PSCO experimental arrangement in depth. Details of the data processing of the detected dication-neutral reactions are then described in section 2.7.

2.2 Ion beam formation

The reactant doubly charged ions, as well as other singly and doubly charged ions, are generated via EI, in the ion source. The ionisation occurs in the ion source block which is kept at a low positive voltage, normally between 2 and 10 volts. The voltage of the source block defines the "rest potential" of the reactant ions. The ions are extracted from the source block and pass through a hemispherical energy analyser in order to energy filter the ion beam to a restricted energy spread.

2.2.1 Ion production by electron ionisation (EI)

Ions, both singly and multiply charged, are formed in the source block from the neutral precursor gas using EI. [3-5] Figure 2.2 shows a schematic of the EI source.

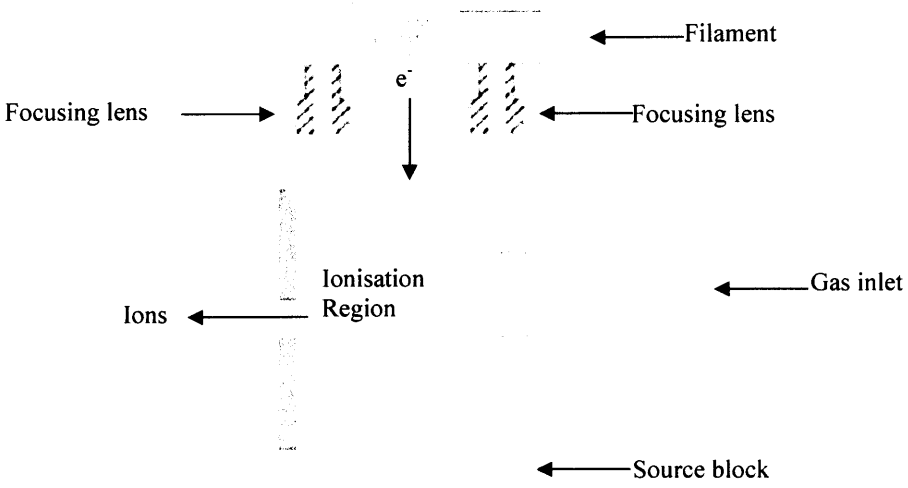

Figure 2.2 A schematic of the EI source.

The electrons which induce ionisation are produced from a custom made filament by thermionic emission. By applying a negatively charged voltage to the shield behind the filament, and appropriately biasing the filament with respect to the source block, the electrons are accelerated into the chamber in the source block to interact with the precursor gas. A variety of singly and multiply charged ions will be produced from these electron-molecule interactions, including fragment ions, depending on the precursor gas. The bias voltage of the filament is usually set to yield 100-200 eV electrons, and the precise value is optimized to maximize the yield of the desired dication.

2.2.1.1 Filament material

Tungsten filaments are used for producing ions from N_2 and CO_2. Tungsten filaments are classically the most common type of filaments used for EI because tungsten has a high strength and known resistance to chemical attack. When tungsten filaments are used with gases such as N_2 and CO_2, the lifetime of the filament is of the order of several months of continuous use. However, at the high operation temperatures of the filaments, oxygen, as well as other gases including nitric oxide, can cause the tungsten to degrade rapidly. The oxygen is believed to react with the tungsten to produce a tungsten oxide which is evident

from a yellow residue that is found to coat the filament upon its removal. Upon production of the tungsten oxide the filament wire is eroded and eventually fails. As little as five days of continuous use with oxygen can destroy the tungsten filament. Therefore, to study reactions of O_2^{2+}, custom made yttrium coated filaments were used for producing ions from O_2. These filaments are highly resistant to attack from oxygen and successful in production of O_2^{2+} ions. The filaments also exhibit the same performance level for the production of N_2^{2+} and CO_2^{2+} as the tungsten filaments.

2.2.1.2 Advantages and disadvantages of EI

The main advantages of EI over other ionisation techniques are that EI is one of the most simple, cheap and robust ways to make ions. One disadvantage is that at the electron energies we use (usually between 150 to 250 eV), it is hard to make significant quantities of atomic dications such as N^{2+}, C^{2+} or O^{2+}.

In the results presented in this thesis, other ions produced by the simple, indiscriminate EI in addition to the relevant dication, present no interference problems. This is partly because a velocity filter is used to select only the dication of interest and partly because many of the other ions formed in the source will be monocations which will not react to produce two charged species, and so will not be collected. However, interference could present a problem if the masses of the ions were close. For example, when studying $C_2H_2^{2+}$ (m/z=13), if C_2H^{2+} (m/z=12.5) were also produced, they would lie very close in the mass spectrum. In this case, the velocity filter would only be able to remove some of the C_2H^{2+}, and therefore some would go on to react in the source region and then these reactions would also be present in the coincidence spectrum.

The main disadvantage of the use of electron ionisation for dication generation is that is does not offer the state selectively that some other techniques can provide. [6] In principle, in electron ionisation, any dication states with an ionisation energy less than the electron energy can be populated. As will be seen below, the population of more than one reactant state leads to broadening in the exothermicity spectra we derive for all of the reactions we observe. However, the lifetime of the dication states themselves do provide some sort of "internal" state selectivity, as only dication states which can survive to reach the interaction region will undergo collisions. As will be seen in the results chapters, the exothermicity spectra derived from our PSCO data frequently do not show any resolved structure. Yet for the atomic electron transfer reaction, the resolution of the exothermicity spectra is clearly sufficient to resolve states 0.3 eV apart. [7, 8] The fact that

EI populates multiple vibrational levels of the target dications, as well as several possible electronic states, means that the exothermicity of the reactions of all these dication states is convoluted in the experimental exothermicity spectrum. As a result, in many cases, there are no clearly resolved signals.

2.2.2 Ion extraction

Figure 2.3 shows a schematic of the source block, the lens and deflectors, which are all situated before the hemispherical energy analyser.

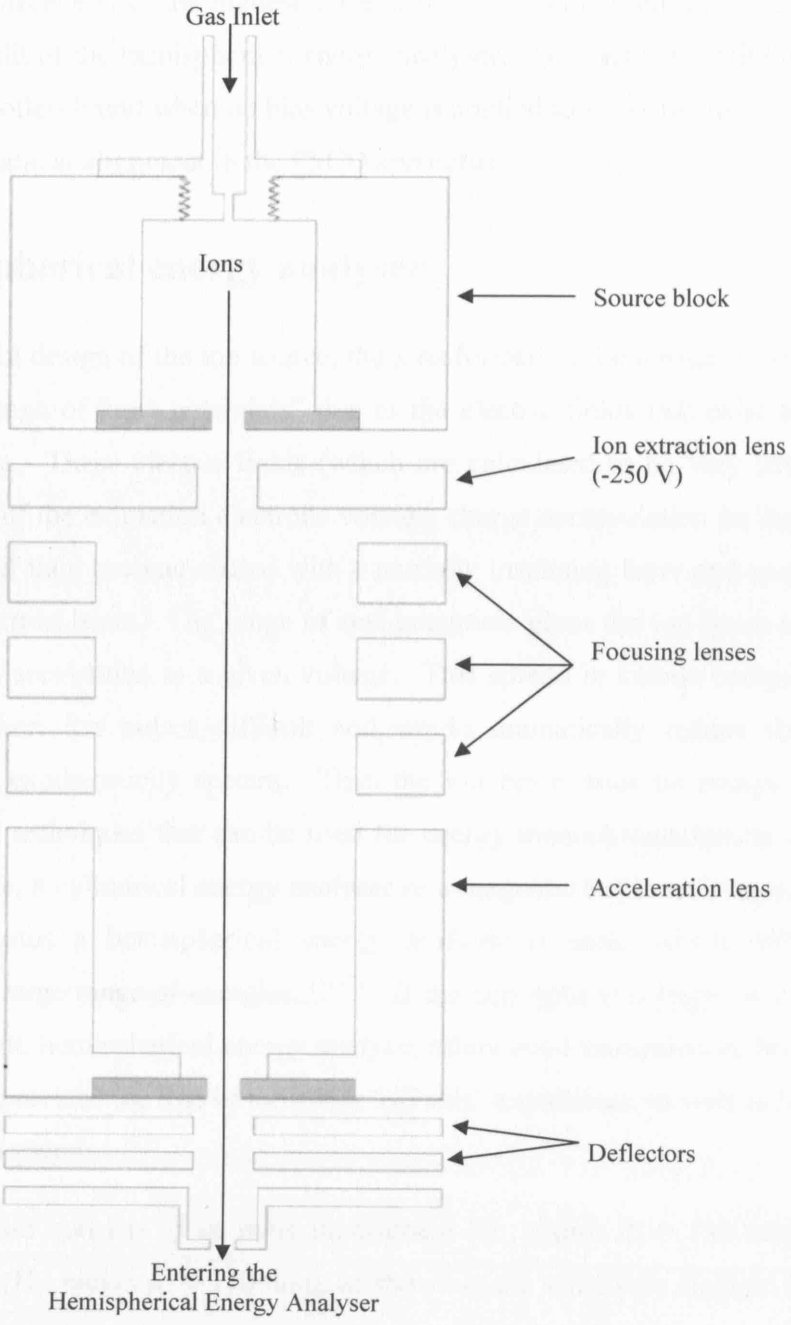

Figure 2.3 The path of the ions from the EI source to the energy analyser.

All ions produced in the EI source, both singly and doubly charged, are extracted from the ionisation region by a -250 V negatively charged electrode (Figure 2.3). The ions are then guided by three focusing lenses. These lenses are tuned, by measuring the current on the entrance slits of the hemispherical energy analyser, to achieve the maximum transmission of ions into the hemisphere. If necessary, minor alignment changes to the beam trajectory can be made by applying small voltages to the sets of deflectors, horizontal and vertical, in front of the entrance slit to the hemispherical energy analyser. The best alignment of the beam will correlate with the best transmission of the ions through the hemispherical energy analyser. Hence the optimum voltage on the entrance deflectors will correlate with the highest current, or close to the highest, measured at or beyond the exit slit of the hemispherical energy analyser. The fact that optimum current on the exit slit is often found when no bias voltage is applied to the deflectors is testament to the good mechanical alignment in the PSCO apparatus.

2.2.3 Hemispherical energy analyser

Despite the careful design of the ion source, the ions formed in the ionisation volume are created with a range of "rest potentials" due to the electric fields that exist across the ionisation volume. These electric fields (which are calculated to be very small) arise from penetration of the extraction electrode voltage, charge accumulation on the walls of the source block if they become coated with a partially insulating layer and on the space charge of the electron beam. The range of rest potentials gives the ion beam an energy spread when it is accelerated to a given voltage. This spread in kinetic energies would make forming short ion pulses difficult and would dramatically reduce the energy resolution in the exothermicity spectra. Thus the ion beam must be energy selected. There are several techniques that can be used for energy monochromatization of an ion beam, for example, a cylindrical energy analyser or a magnetic bottle technique. [9, 10] In the PSCO apparatus a hemispherical energy analyser is used, which offers good resolution over a large range of energies. [11-13] If the hemisphere is large, as it is in the PSCO arrangement, hemispherical energy analysis offers good transmission, because the double focussing prevents the loss of ions with 'off axis' trajectories, as well as helping to improve the beam shape.

The energy analyser consists of an inner hemisphere (H_1, radius R_1 = 130 mm) and an outer hemisphere (H_2, radius R_2 = 170 mm), as shown in the schematic diagram in Figure 2.4.

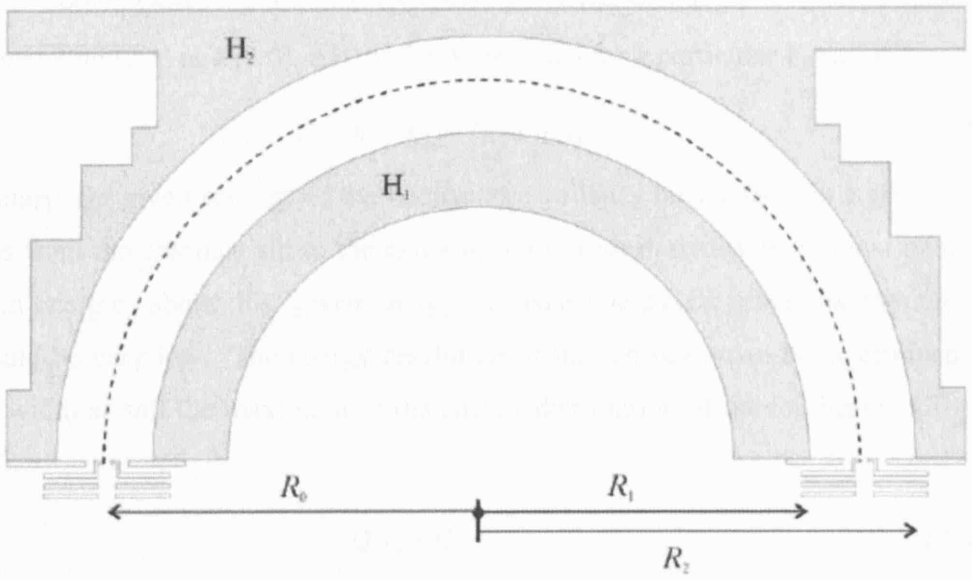

Figure 2.4 A schematic of the hemispherical energy analyser.

The ions are directed into the analyser, entering at the mean radius (2.1) of the two hemispheres (mean radius R_0 = 150 mm).

$$R_0 = (R_1 + R_2) / 2 \tag{2.1}$$

By applying voltages to the inner and outer hemispheres the ions will be deflected through 180° along an arc through the hemisphere. This arc is defined in part by R_0 and in part by the 'pass voltage', V_0, determined by the voltages, V_{outer} and V_{inner}, applied to the outer and inner hemispheres. At a particular V_0, only ions of a particular kinetic energy will pass through the hemisphere and ions of all other kinetic energies will be deflected and hence will not reach the exit of the hemisphere. Ions are formed effectively at rest in the source block at a voltage T, and are then accelerated by a potential V_r to the pass energy of the analyser.

$$V_0 = T - V_r \tag{2.2}$$

Therefore, the potentials of the outer and inner hemispheres, for particular values of V_0, T and V_r, can be calculated from (2.3) and (2.4):

$$V_{outer} = -V_0 [(2R_0 / R_2)-1] + T \tag{2.3}$$
$$V_{inner} = -V_0 [(2R_0 / R_1)-1] + T \tag{2.4}$$

The potential difference, ΔV, between the two hemispheres when ions of a particular T travel through the hemisphere at V_0 can be determined from (2.5):

$$\Delta V = V_{outer} - V_{inner} \tag{2.5}$$

$V_{outer} - V_{inner}$ can be determined from (2.3) and (2.4):

$$\Delta V = V_{outer} - V_{inner} = V_0 [(2R_0 / R_1)-1] - V_0 [(2R_0 / R_2)-1] \quad (2.6)$$

Therefore using (2.1) and (2.6), ΔV can be determined for a particular V_0 (2.7):

$$\Delta V = V_0 [(R_2 / R_1) - (R_1 / R_2)] \quad (2.7)$$

In summary, for given settings of the hemisphere voltages only ions with a given energy can pass from the entrance slit to the exit slit. Of course in reality there must be a small spread in energies about this 'given energy', or pass energy E_0, otherwise the ion count rate would be very low. The energy resolution of the ion beam can be determined from the full width at half the maximum of the energy distribution of the ion beam, $\Delta E_{1/2}$, and E_0, (2.8).

$$\Delta E_{1/2} / E_0 \quad (2.8)$$

The value of E_0 is set manually in the PSCO experiment to satisfy the lowest possible value of $\Delta E_{1/2}$ with a good ion count rate. A good count rate is typically between 500 and 4000 ions/second depending on the precursor gas. Typically, E_0 is always set to 4 eV where the conditions of low $\Delta E_{1/2}$ and reasonable ion count rate are met. The theoretical energy resolution of the PSCO hemispherical energy analyser is 1.1 % of E_0. However, this theoretical energy resolution assumes a negligible angular spread of the ions entering the hemisphere. In the PSCO experiment the ions entering the hemisphere have an angular spread of approximately 10°, hence the typical energy resolution is closer to 4.5 %. [14] The energy resolution could be improved by reducing the size of the pre-hemisphere lens apertures; however this would significantly lower the ion transmission which is unnecessary given that the performance of the hemisphere in the current arrangement is more than satisfactory.

After the exit of the hemispherical energy analyser there are more deflectors - horizontal and vertical, similar to those at the entrance of the hemisphere. These deflectors, like the entrance deflectors, can be used to adjust the beam trajectory. However the main function of the horizontal pair of deflectors is to 'pulse' the ion beam, as is discussed in section 2.3.

2.3 Pulsed beam

Upon leaving the hemispherical energy analyser the beam is 'pulsed' by applying triangular voltage waveforms to the pair of horizontal deflectors following the exit slit. Before describing how the beam is pulsed we will first consider the advantages of using a pulsed beam over a continuous beam.

2.3.1 Advantages of using ion pulses over a continuous beam

The main advantage of pulsing the beam is that the noise in the mass spectrum, and hence coincidence spectrum, is dramatically reduced. When mass spectra of a continuous dication beam are recorded, a marked "background" signal is readily apparent before the dication peak. The background signal from the continuous beam before the dication peak would swamp any signals from products lighter than the dication. This significant ion signal before the dication peak is due to the detection of dications from the beam which were beyond the source region of the *TOF* drift tube when the repeller plate was pulsed. These ions, which were in the acceleration region, or drift tube, will therefore have a shorter *TOF* than the dications in the source region due to the reduced distance to the detector, and are hence detected as signals "before" the dication peak. When using pulses of dications, as opposed to a continuous beam, the voltage is applied to the repeller plate when the dications are in the centre of the source region. Hence, very few ions will have travelled as far as the acceleration region or drift tube by the time of the repeller plate pulse, and the previous ion pulse will have already reached the detector. This dramatic reduction of ions outside the source region also means there is a reduction of reactions outside the source region, hence, the noise around the reaction peaks in the coincidence spectrum is also reduced. Further details on the noise, or 'tails', around the reaction peaks in the coincidence spectra are given in Chapter Three.

Employing a pulsed beam also improves the angular and energy resolution in the ionic velocities derived from the PSCO spectral data. When a 'continuous' beam is used the *TOF* source region is completely filled with ions, where as when a 'pulsed' beam is used, there is only the restricted range of ion positions occupied by ions in the *TOF* source region. Therefore the point of interaction between the two reactants is more localised, which minimises both the spread in the flight times recorded in the *TOF* mass spectra and the uncertainty in the position of the reactive events.

2.3.2 Creating the pulsed beam

As previously mentioned, the beam is 'pulsed' by applying voltage waveforms to the pair of horizontal deflectors which are situated after the exit slit of the hemispherical energy analyser. In order that the ion packets, created by the pulsing process described in this section, do not degrade as they progress further though the subsequent ion optics, it is important that the ions making up the beam are as restricted in energy spread as possible.

This is why the pulsing of the beam is performed after the energy selection by the hemispherical energy analyser.

The voltage waveforms applied at each of the deflectors are oscillating triangular voltage waveforms which are 180° out of phase. The two waveforms are centred on the beam potential. The triangular waveform is generated by a commercial function generator, and then passed onto a custom designed unit, which creates the two identical, but 180° out of phase, waveforms. Figure 2.5 shows a schematic by Hu *et al* of the timing chain involved in producing the dication pulses. [7] The timing also involves the pulsing of the repeller plate, so that the ion pulses can reach the centre of the reaction region before extraction into the drift tube.

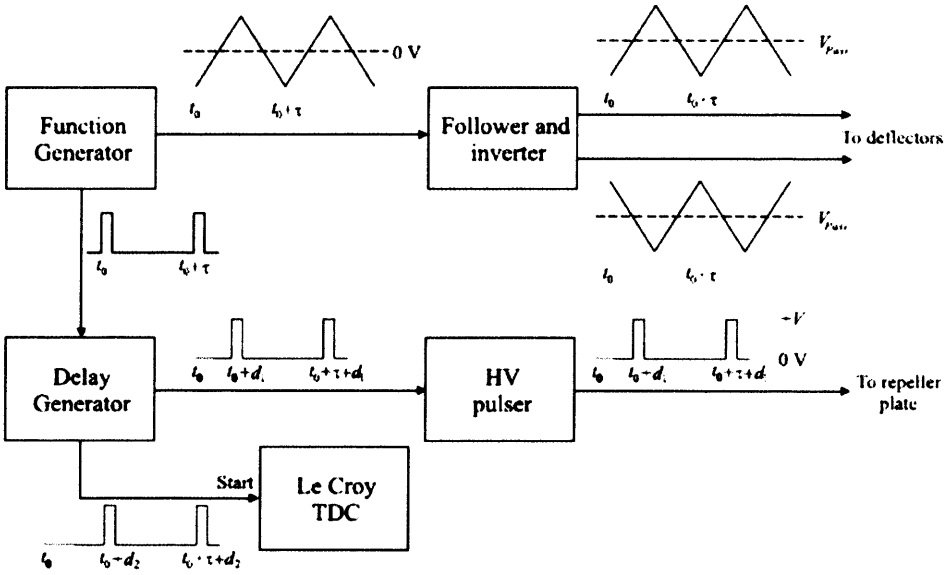

Figure 2.5 A schematic of the timing chain involved in pulsing the deflectors as well as the repeller plate. [7]

The application of these voltages to the two electrodes in the defector pair sweeps the ions from one side of the central path to the other and back, across the aperture which follows the deflectors. A pulse of ions is therefore generated because the ions can only pass through the aperture when the deflector voltages are close to the beam potential. The duration of the ion pulse generated depends upon the magnitude of the peak voltage of the triangular waveforms and the frequency of their oscillation. The next section details how the length of the ion pulses is optimised.

2.3.3 Monitoring the quality of the dication pulses

When pulsing the ion beam, it is desirable to create temporally "short" ion pulses thereby optimising the advantages of using a pulsed beam which are discussed in the previous

section (section 2.3.2). In order to monitor the ion pulses, the repeller plate is not pulsed, and the dication pulses can fly freely through the PSCO to the PSD. Thus the temporal duration of the ion pulses can be recorded by monitoring the ions' arrival time distribution at the PSD. Optimized pulse durations are typically 0.5 μs to 2 μs duration, and can be adjusted by altering the peak-to-peak amplitude, frequency and mean voltage of the waveform applied to the deflectors.

In normal operation the function generator used to create the waveforms triggers a delay generator, which controls the application of the voltage to the repeller plate. The delay between the reference point of the pulse to the deflectors and the application of the voltage to the repeller plate is adjustable, so that dication pulse is in the centre of the source region when the repeller plate voltage is applied. The correct delay can be found by altering the delay until the dication peak appears symmetrical in the *TOF* mass spectrum. If the repeller plate pulse is "too early" the dication peak tails to longer flight times. If the repeller plate pulse is "too late" the dication peak tails to shorter flight times. Figure 2.6 shows a typical PSCO *TOF* spectrum with a magnified inset to show the desired symmetry of the "pedestal" of the dication peak. This pedestal clearly shows the above tailing when the repeller plate is not pulsed with the correct phase relationship to the pulsing of the deflectors.

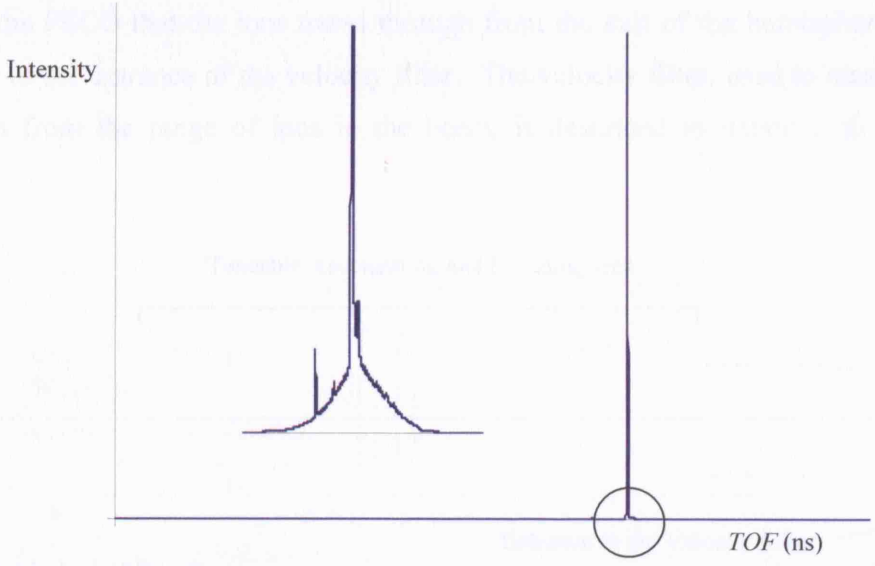

Figure 2.6 An example of a *TOF* mass spectrum with an inset showing the desired symmetrical nature of dication peak. The very small peak observed in the inset, at a slight shorter *TOF* than the dication (Ar^{2+}), is a very small background level of H_2O^+ impurity.

It is imperative to ensure that pulsing the dication beam does not in any way perturb or broaden the energy distribution of the ions. As previously mentioned, the ideal pulses are

created by rapidly changing the deflector voltages. However, if the deflectors are pulsed too fast (>50 kHz) the rest potential of the ions can be shifted, as the ions do not have enough time to respond to the changing deflector voltages; when the rate of change of the deflector voltages is so fast that it is of the order of the ion transit time across the deflector region. Since the *TOF* of the dication in the *TOF* mass spectra is a sensitive probe of the energy of the dications in the source region of the *TOF-MS* that we continually monitor when setting up the pulsing, the *TOF* of the dications from the pulsed beam is identical to that from a continuous ion beam. Thus it is possible to ensure the shortest dication pulses are created without creating pulses that are so short that the ion energy is perturbed.

2.4 Acceleration and focusing of the beam

After leaving the hemispherical energy analyser, and passing through the deflectors, the ions are accelerated and focused by a series of electrostatic lenses until they reach the velocity filter. The voltages on these lenses can be individually tuned to optimise the dication beam quality and alignment. This tuning is achieved by monitoring the ion counts and the shape of the unreacted dication beam on the PSD. The optimum beam shape is found by tuning under continuous beam conditions, and normally when the ions are pulsed the beam is further improved. Figure 2.7 shows a schematic diagram of the area of the PSCO that the ions travel through from the exit of the hemispherical energy analyser to the entrance of the velocity filter. The velocity filter, used to mass select the dications from the range of ions in the beam, is described in detail in the following section.

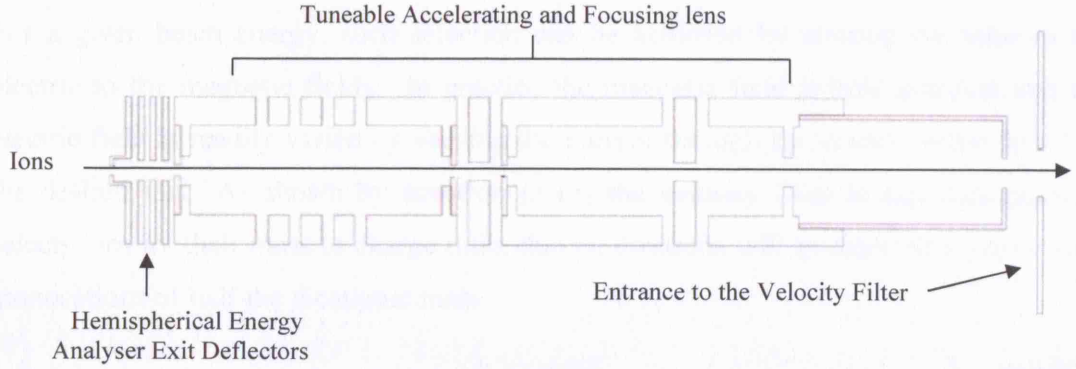

Figure 2.7 A schematic of the path of the ions from exit of the hemispherical energy analyser to the velocity filter.

2.5 Velocity filter

After exiting the hemispherical energy analyser and the subsequent acceleration and focusing lenses, a commercial velocity filter is used to mass select the dications from the packets of ions. The velocity filter consists of an electro-magnet and a pair of electrostatic deflection plates. This arrangement can be used to generate perpendicular electric and magnetic fields. The filter can be set to transmit ions with a certain velocity by adjusting the electric field equation (2.9), relative to the magnetic field equation (2.10);

$$F_E = Ez \tag{2.9}$$
$$F_B = Bzv \tag{2.10}$$

where F_E is the electrostatic force, F_B is the magnetic force, E is the electric field strength, B is the magnetic field strength, z is the charge of the ion and v is the velocity of the ion (2.11) and (2.12). For ions accelerated to a beam potential V_0 we have:

$$V_0 = (\tfrac{1}{2}mv^2)/\, z \tag{2.11}$$
$$v = (2zV_0/m)^{\frac{1}{2}} \tag{2.12}$$

When F_E and F_B are equal, (2.13), then only ions of a particular velocity, v_1, can pass through the velocity filter while all others, with a velocity greater or smaller than v_1, are deflected.

$$Bzv = Ez \tag{2.13}$$

As the ions have already been energy selected, V_0 is the same for all ions. Therefore, selecting a particular velocity will effectively select a particular mass, (2.6).

$$(2zV_0/m)^{\frac{1}{2}} = E/B \tag{2.14}$$

For a given beam energy, such selection can be achieved by altering the ratio of the electric to the magnetic fields. In practice the magnetic field is held constant and the electric field is readily varied by varying the current through the electric plates to select the desired ion. As shown by equation (2.15) the velocity filter in this configuration selects ions by their mass to charge ratio, that is, dications will be selected together with monocations of half the dicationic mass.

$$m / z = 2V_0 / (E/B)^2 \tag{2.15}$$

However, in the PSCO technique these monocations do not cause problems as any subsequent monocationic reactions will not result in the formation of two singly charged species, and hence the dication-neutral reactions are easily identified. The mass

resolution achieved by using an appropriate beam potential, is sufficient to select mainly just the dication in of interest, although very low traces of isotopes may be visible in the mass spectra. However, these isotope traces are so weak that it is rare to see any reaction interference in the coincidence spectra. [15]

2.6 Decelerator

After leaving the velocity filter the dications are decelerated to an appropriate collision energy, typically a few electron Volts, in the lab frame. Such low collision energies are employed because dication-neutral bond forming reactions have been shown to be more likely to occur at low collision energies. [16] A commercial system of ion optics is used for this deceleration and is shown in Figure 2.8. The ion optics are labelled 1 to 8 in the diagram and discussed following the figure.

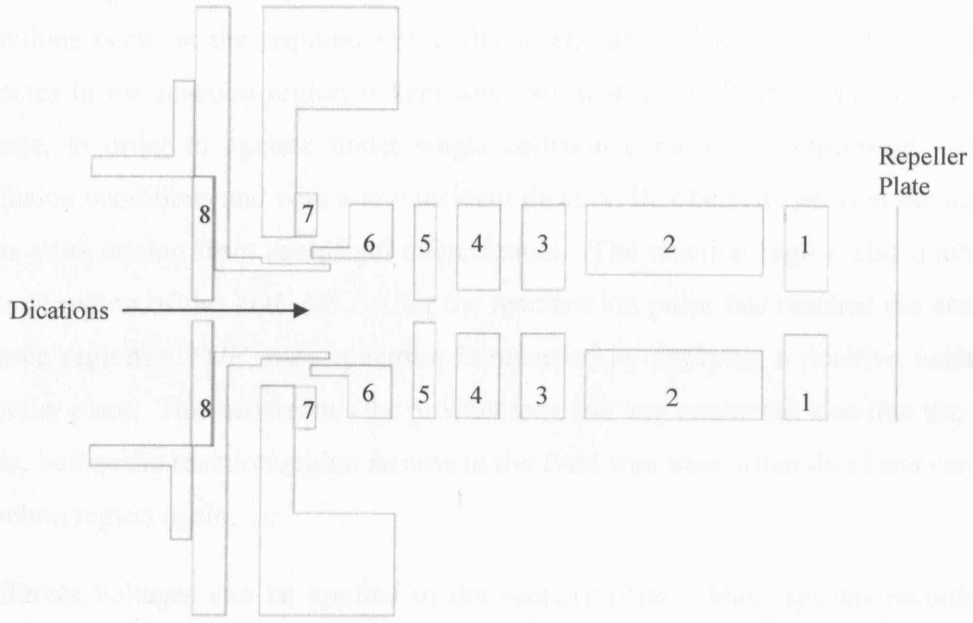

Figure 2.8 A schematic of the decelerator with the ion optics labelled 1 to 8.

The first two ion optics that the dications pass through, 8 and 7, are typically held at the beam potential upon leaving the velocity filter of -250 V. However voltages as low as -40 V may be applied to optic 8 if it helps with the beam focusing. The next three optics, 6, 5 and 4, are used to decelerate the beam. Typically 5 and 6 may be held close to -250 V while 4 will be held at an 'intermediate' potential of approximately -150 V. The final three optics; 3, 2 and 1, are used to refocus the dication beam, to ensure there is little divergence in the ions' trajectory as they enter the reaction region. 3, 2 and 1 are in fact used as an 'Einzel' focusing lens, which means that 3 and 1 are held close to 0 V, while 2

is varied to find the best focus. Typically, optic 2 will be held at approximately -15 V. The optimisation of the decelerator is achieved again by observing changes in the ion counts and the shape and centring of the un-reacted dication beam on the PSD. As previously mentioned, such tuning is first performed under continuous beam conditions, and when the ions are pulsed the quality of the beam is further improved. The next section will describe the reaction region where the dications interact with the neutral reagent.

2.7 Reaction region

Following the deceleration, the dication pulses enter the reaction region through a mesh covered aperture in the repeller plate. In the reaction region the dications interact with an effusive jet of the neutral gas and the bimolecular reactions of interest occur. The reaction region is initially maintained in a field-free state to ensure the dication neutral reactions occur at the required low collision energies. The gas pressure of the neutral species in the reaction region is kept low, below 4 x 10^{-6} Torr as monitored by an ion gauge, in order to operate under single collision conditions. Operating under single collision conditions and with a low incident dication flux helps to prevent the detection of ions pairs arising from accidental coincidences. The reaction region also doubles as the source region of the *TOF-MS*. After the reactant ion pulse has reached the centre of the source region, a *TOF* mass spectrum is recorded by applying a positive voltage to the repeller plate. This accelerates the product ions and any unreacted ions into the *TOF* drift tube, before the reaction region returns to the field free state when dications can enter the reaction region again.

Different voltages can be applied to the repeller plate. Mass spectra recorded with a "high" voltage on the repeller plate, usually 300 V, result in short enough ionic times of flight to gather the full angular scattering from the dication reactions. Mass spectra recorded with lower voltages on the repeller plate, such as 100 V or 50 V, result in longer ionic times of flights, and better energy resolution. However, at lower repeller plate voltages, ions with significant sideways velocities are not detected as they fly beyond the detector radius and thus incomplete angular distributions are recorded.

2.8 Time-Of-Flight Mass spectrometry

As previously mentioned, the reaction region also doubles as the source region of the *TOF-MS*. Following the acceleration of the ions out of the reaction/source region by the application of a voltage to the repeller plate, the ions pass into a second acceleration field and then into a field free drift tube before a final acceleration onto the PSD for detection.

The basis of *TOF* mass spectrometry is that when ions are all accelerated to the same energy, the velocity of the ion is depends on its mass. Hence, given that the ions of different masses take different lengths of time to travel the length of a given path, by recording the *TOF* of an ion its mass can be derived. Figure 2.9 shows a schematic of a simple "two-field" *TOF-MS*.

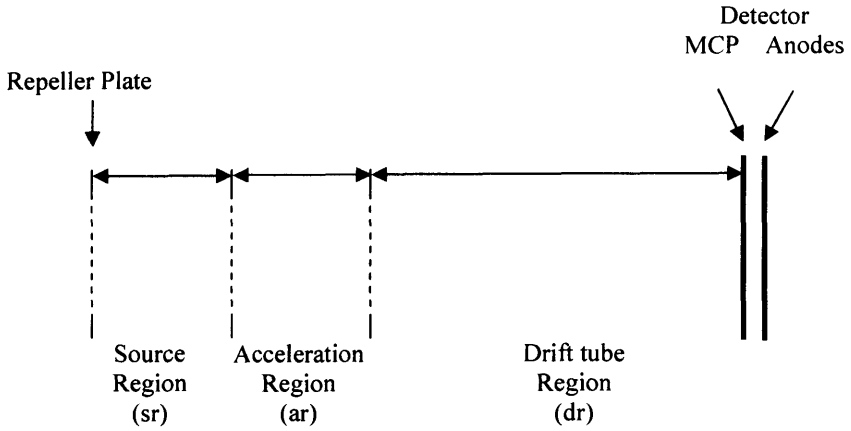

Figure 2.9 A schematic of a typical two field *TOF-MS*.

The *TOF* of an ion is composed of the sum of the *TOF*s (t) of the ion in each region, (t) (2.16);

$$TOF = t_{(sr)} + t_{(ar)} + t_{(dr)} \qquad (2.16)$$

By using Newtonian mechanics to determine 't' for each region, the Wiley – McLaren *TOF* derivation (see Appendix A.1 for full details) shows the time of flight is proportional to the square root of the mass to charge ratio (2.17); [17]

$$TOF = c\sqrt{(m/z)} \qquad (2.17)$$

Of course, in practice, not all the ions are accelerated to the same final potential due to the variations in positions of ions in the source region when the repeller plate is pulsed. Ions extracted from the source region closer to the repeller plate, Ion_a, have further to travel to the detector than ions extracted from the source region closer to the acceleration region,

Ion$_b$. However *Ion*$_a$ will be accelerated to a greater potential at the end of the source field than *Ion*$_b$. Therefore *Ion*$_a$ may in fact over take *Ion*$_b$ before detection. This will result in a variation in the *TOF* of ions of the same mass with source position, making it hard to resolve ions of a similar mass. However, in 1955 Wiley and McLaren discovered that by applying a certain set of electric fields in a two-field *TOF-MS* the variation of ionic *TOF*s with source position could be dramatically reduced. [17] Indeed, in principle, about the centre of the source the ionic *TOF* no longer depends on the ions initial position in space (to first order). This property is known as 'first order' space focusing. First order space focusing therefore controls the point where *Ion*$_a$ catches *Ion*$_b$, as described above.

Wiley and MCLaren derived their focus condition by writing an expression for the *TOF* in terms of the ion's position, as shown in Appendix A.1. Wiley and McLaren then analytically derived the relationships between the lengths of the various regions of the spectrometer and the voltages applied for the first differential of *TOF* with source position to be zero; hence the name 'first order focusing'.

First order focusing is very successful and still used in many *TOF* spectrometers today. However, in 1993 Eland discovered through numerical simulations that in fact further improvements could be made to improve the space focusing characteristics. [18] By constraining the geometry and the fields so that both the first and second derivatives of *TOF* with source position were equal zero, Eland obtained improved 'second order focusing' designs. To achieve this higher order focus, the voltages required for the electric fields in many of the existing first order designs were impractical. Therefore in order to achieve second order focusing with realistic electric fields, experimental geometries (the length of the source, acceleration and drift regions) had to be changed. The main differences in general experimental design between first and second order focusing experiments is that a longer acceleration region is required to achieve second order focussing with practical voltages. Since the PSCO apparatus was designed after the discovery of second order focussing, and that an independence of the *TOF* on source position is key to extracting the velocities of the ions from their *TOF*s, the *TOF-MS* employed in this thesis was constructed to achieve second order focusing. In the PSCO experiment the reaction region (also source region), the acceleration region and the drift tube are 1.6 cm, 11 cm and 27.5 cm long respectively. The long length of the acceleration region requires the use of guard rings, held at appropriate voltages, to maintain field uniformity. Typically we have an acceleration voltage of -1910 V when using a 300 V repeller plate pulse. These voltage conditions produce ion peaks with

approximately 3 ns half widths. Approximately -350 V is applied to the drift tube when using a 50 V repeller plate, where the half widths of the peaks are slightly wider at about 8 ns. In the PSCO experiment the *TOF-MS* are recorded using a Position Sensitive Detector (PSD) which is described in the next section.

2.9 Position Sensitive Multi-Channel Plate Detector

The Position Sensitive Detector (PSD), as shown in Figure 2.10, is a commercial device consisting of a pair of multi-channel plates (MCPs) ahead of two, perpendicularly wound, wire anodes of known lengths. [19-21]

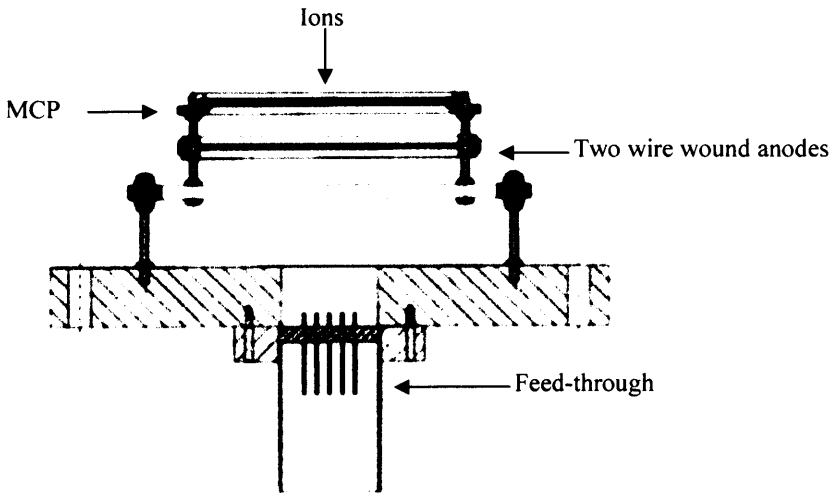

Figure 2.10 A schematic of the PSD.

The wire wound anodes are wound perpendicularly to each other. One anode is used for the determination of the position in the x direction and one for the y direction as shown schematically in Figure 2.11.

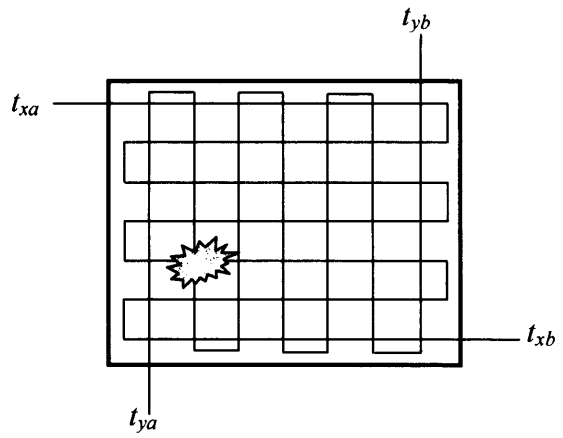

Figure 2.11 A schematic of the wire wound anodes showing the four end which translate to four times *txa*(i), *txb*(i), *tya*(i), *txb*(i).

Using the MCP and dual wire wound anodes means positional information and the arrival time of each ion can be determined. When an ion hits the MCP, the MCP generates a cascade of electrons that hits the wires of the delay line anode. The charge pulse from the MCP propagates along each wire to its ends, and the signals from both the ends of the two wires are passed as stop pulses to the timing circuitry. This methodology results in four times [$t_{xa}(i)$, $t_{xb}(i)$, $t_{ya}(i)$, $t_{xb}(i)$] for each ion in the pair (i=1, 2), measured relative to the pulsing of the repeller plate. As shown in more detail below (section 2.11.2.2), by detecting the arrival time of the charge pulse at both ends of each signal wire and then calculating the difference between the arrival times, the position of the ion's arrival can be determined. The *TOF* of each ion in the pair $t_{expt}(i)$ is recorded by detecting the voltage spike on the MCP supply when an ion is multiplied. Hence, there are five times recorded for each ion arrival, four times from the wire anodes and one from the MCP conversion signal, and so ten times for each ion pair we detect.

Each of the two arrays of wire wound anodes consists of two wires; one wire as a signal collection wire and one as a reference wire. The signal wires are approximately 70 V more positively charged than the reference wires to ensure that the electron cascade is mainly collected on the signal collection wire. The detection set up has a 'multi-hit' capability which means two ion arrivals within less than 32 nanoseconds of each other can be detected. The value of 32 ns is due the the dead time of the discriminator limits the minimum time difference between detectable signals on a given signal channel. During an experimental run the ten times associated with each pair event detected are stored for off-line processing.

2.10 Signal processing and data collection

A six channel amplifier is used to process the signals from the PSD. One channel is used to process the timing signal from the front of the MCP and a second channel is used to process the timing signal from the back of the MCP (although this channel is not actually needed in the PSCO arrangement). Four channels are used to amplify the signal from the four ends of the delay wires. Each channel has an adjustable threshold set to ensure the real signal is discriminated from the electronic noise. This amplifier is in fact a differential amplifier, therefore the signal is actually determined from the difference between the voltages applied at end of the wires and hence noise can be eliminated.

These ion signals are then passed to 5 of the stop channels of a LeCroy 3377 time-to-digital converter (TDC). The delay generator that controls when the voltage is applied to the repeller plate also starts the TDC after a suitable delay (400 ns) to avoid the detection of RF noise from the pulsing of the repeller plate. The resulting 5 times for a single ion arrival, or 10 times for an ion pair detection, are then passed as an "event" to a memory unit (LeCroy 2367) for storage. This transfer is via a fast encoding and readout analogue (FERA) interface. Events are accumulated in the memory unit until it is full (512 kB), at which point the data is transferred to the data collection program on the PC. When the data has been transferred to the PC, the memory unit is then cleared to begin collecting data again. Events involving detection of a single ion are just added to a "singles" mass spectrum stored on the PC, a histogram of counts against flight time. The 10 times making up the "pair" events are simply added to a list of pair events. Thus the critical data set is a list of sets of 10 'times' for each pair event detected. This dataset is then processed off line using the PC as discussed in section 2.11.1. The computer program on the PC is also used to set, and alter, the voltages on lenses before the hemispherical energy analyser, the deflectors and the voltages on the hemispherical energy analyser.

2.11 Data Processing

Once the raw data from the PSCO experiment is stored, it is initially complied into a 'coincidence spectrum'. It is then processed to determine the reaction dynamics and energetics for two and three-body reactions.

2.11.1 Coincidence spectrum

The initial step in the off-line processing is the construction of a two dimensional coincidence ('pairs') spectrum - a histogram of the flight time of $t_{expt}(1)$ against $t_{expt}(2)$ – for all the pairs detected. [2, 22-24] The coincidence spectrum is discussed in detail in Chapter Three so only a brief introduction to it is given here. In the coincidence spectrum the *TOF* of the heavier ion in the pair is plotted along the x axis and the *TOF* of the lighter ion along the y axis for each ion pair detected. Individual reaction channels appear as peaks allowing immediate identification of both product ions formed in the reaction as shown in the basic schematic in Figure 2.12.

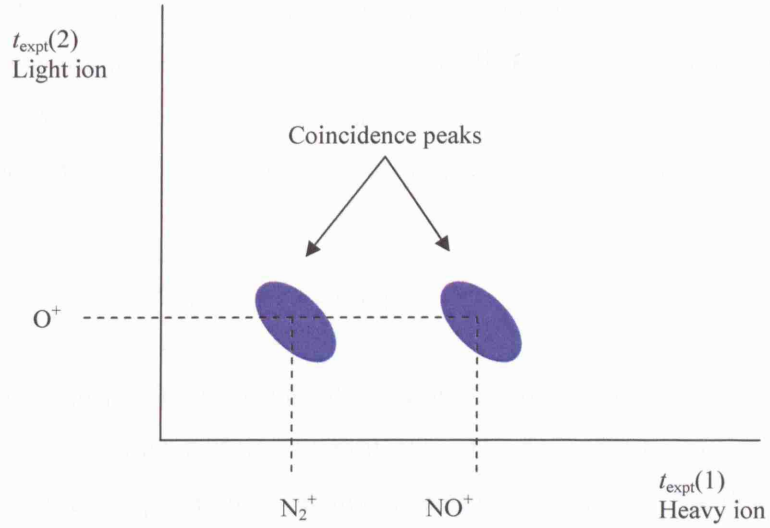

Figure 2.12 A basic schematic showing a section of a coincidence spectrum with two example reactions pairs.

The analysis computer programme then allows the user to select a particular coincidence peak, and the individual events detected for that reaction channel can then be processed to yield the dynamics. This subset of the data set, again, consists of a list of the 10 times recorded for each of the individual ion pairs making up that particular peak.

2.11.2 Determining the laboratory frame velocity

To derive the details of the reaction dynamics and kinematics for each selected channel we need to determine the x, y and z velocity components for both product ions in the Laboratory (LAB) frame. These then need to be converted to the Centre-Of-Mass (COM) frame for ease of interpretation.

2.11.2.1 The Laboratory frame (LAB)

The LAB frame is a frame of reference whereby the movement of the ions can be described relative to their surroundings. In the PSCO experiment the LAB frame describes the movement of the ions relative to the axes of the PSCO instrument.

2.11.2.2 Deriving the LAB frame x , y and z velocity components of an ion

To derive the x and y velocity components of a product ion $v_x(i)$ and $v_y(i)$ (the components perpendicular to the axis of the *TOF-MS* in the LAB frame) we need to know the position

of the ion's arrival at the PSD. These positions $x(i)$ and $y(i)$, are measured relative to the centre of the detector, and are determined from the difference between the times of arrival of the charge pulse at the ends of each delay line via equations (2.18) and (2.19), together with the calibrated relationship between position and time (1.96 ns mm^{-1}) for the delay lines.

$$x(i) = [t_{xa}(i) - t_{xb}(i)] / 1.96 \quad (2.18)$$
$$y(i) = [t_{ya}(i) - t_{yb}(i)] / 1.96 \quad (2.19)$$

To determine $v_x(i)$ and $v_y(i)$, we also need to know the position (x_0, y_0) of the region where the dication pulses interact with the neutral gas. The co-ordinates x_0 and y_0 are readily determined from the x, y position of the unreacted dication beam at the detector. We also require the total flight time of the ion from the reaction region to the detector. This total flight time is $t_{expt}(i)$ plus the electronic delay c between the pulsing of the repeller and the start of data collection, where c can be determined by calibration of the mass spectrum. Hence we have:

$$v_x(i) = (x(i) - x_0) / (t_{expt}(i) + c) \quad (2.20)$$
$$v_y(i) = (y(i) - y_0) / (t_{expt}(i) + c) \quad (2.21)$$

The z velocity component for each product ion $v_z(i)$ is determined from the deviation of $t_{expt}(i)$ from the flight time of an ion of the same mass but with zero initial kinetic energy t_0, using the Wiley-McLaren "braking time" relationship. Again, the appropriate value of t_0 can be determined by calibration of the mass spectrum. In equation (2.22), e is the charge on an electron, Z is the charge number of the ion and F is the electric field strength in the source region determined via a calibration experiment.

$$v_z(i) = -(t_{expt}(i) - t_0(i))eZF / m(i) \quad (2.22)$$

Using the above procedure we can derive the LAB frame velocity vectors $v(i)=(v_x,v_y,v_z)$ of both ions (i=1,2) detected in every pair event of interest.

2.11.3 Determining the Centre of Mass frame velocity

The dynamics of the reaction under study is most clearly revealed when the ionic velocities are presented in the Centre of Mass (COM) frame. [2, 25-27]

2.11.3.1 The Centre of Mass frame

The COM frame of reference is used to describe the movement of the reactants and products relative to the centre of mass of the collision system. Therefore, when

interpreting the movement of the reactants and products in the centre of mass frame, the centre of mass is effectively 'stationary', throughout the collision. Hence when using the COM frame, the momentum of the system is zero and reaction is considered without the complication of momentum. Therefore in the COM frame we can view solely the angular velocities of the products relative to each other, or the velocity of the products relative to the direction of the velocity of the COM in the LAB frame, which in the PSCO experiment is very similar to the direction of the COM velocity of the dication.

2.11.3.2 Deriving the velocity of the COM

Converting the pairs of the LAB velocity vectors, $v(i)$, to pairs of velocity vectors, $w(i)$, in the COM frame requires the velocity of the COM of the collision system, v_c in the LAB frame. Two methods can be used to calculate v_c. In the first method v_c is determined from the velocity of the dication in the LAB frame v_{di}, and the mass of the dication and neutral:

$$v_c = m_{di}v_{di} / (m_{di} + m_{nu}) \qquad (2.23)$$

The velocity of the dication is determined using the energy of the dication, which is known from the voltages used to guide the ions through the hemispherical energy analyser. Here we assume the dication beam is directed exactly along the z-axis, a reasonable assumption given the quality of the PSCO ion beams, and that the velocity of the dication is much larger than that of the effusive neutral molecule, again, a good assumption at the collision energies employed in the PSCO experiment. The above procedure gives us an average value of v_c for a given experiment. The second method for determining v_c is applicable for a two-body reaction. For this class of reactions, v_c can be determined from the product velocities for each individual event detected:

$$v_c = (m(1)v(1) + m(2)v(2)) / (m(1) + m(2)) \qquad (2.24)$$

For two-body reactions these two methods for determining v_c provide values in excellent agreement.

2.11.3.3 Converting from LAB frame to COM frame

Once a value of v_c has been determined we can convert the product velocities in the LAB frame to the COM frame:

$$W(i) = v(i) - v_c \qquad (2.25)$$

Hence we attain the COM velocity vectors for each of the ion products for every reactive event detected. The Newton diagram in Figure 2.13 shows this conversion from the LAB to the COM frame. [25]

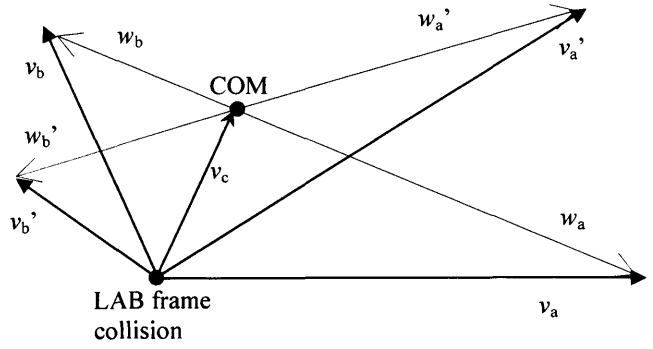

Figure 2.13 A Newton velocity vector diagram to show the relationship between the LAB and the COM velocities where v_a and v_b are the reactant LAB frame velocities, w_a and w_b are the reactant COM frame velocities, v_a' and v_b' are the product LAB frame velocities and w_a' and w_b' are the product COM frame velocities. [25]

2.11.3.4 Determining the COM frame velocity of a third body

Since the PSCO technique detects both ions formed in the dication neutral reaction, if the reaction of interest involves the formation of a third, undetected, neutral species its velocity can be determined simply via conservation of momentum in the COM frame:

$$w(3) = - [m(1)w(1) + m(2)\, w(2)]/\, m(3) \qquad (2.26)$$

Hence the COM velocity vectors for all reaction products for each reactive event detected are obtained for two and three-body reactions. Full dynamics and energetics can then be determined for any two or three-body reactions. This offers a significant advantage over conventional techniques where only one ionic product at a time can be detected.

2.11.4 Angular scattering

To reveal the dynamics of the reaction we must examine the correlations between the velocity vectors for each of the reaction products. The angular scattering is represented using polar histograms, more commonly known as scattering diagrams.

2.11.4.1 Angular scattering with respect to v_c

An initial probe of the correlations between the product velocities is to examine the scattering of these velocities in the COM frame with respect to the direction of v_c. Note that the direction of v_c is effectively the same as the direction of the LAB and COM velocity of the reactant dication, $\omega(N_2^{2+})$. A scattering diagram with respect to v_c is constructed using the magnitude of $w(i)$ as the radial coordinate, and the angle φ of $w(i)$ with respect to v_c as the angular co-ordinate. The angle φ is determined from the dot product of $w(i)$ with v_c. Since $0° \leq \varphi \leq 180°$, the scattering data for one product can be plotted in the upper half of the scattering diagram, whilst the data for a second product can be plotted in the lower half. This is shown by the example scattering diagram in Figure 2.14 of the products of the reaction of N_2^{2+} with NO, where N_2^+ is plotted in the upper half of the diagram and O^+ is plotted in the lower half of the diagram.

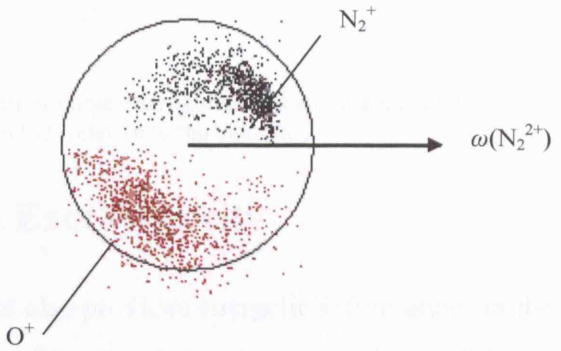

Figure 2.14 An example scattering diagram, showing the velocity of N_2^+ and O^+ relative to the velocity of the dication in the COM frame, $\omega(N_2^{2+})$.

2.11.4.2 Angular scattering with respect to a third product

Internal frame scattering diagrams can be constructed to show the scattering of any two products relative to the third product. Internal frame scattering diagrams are again polar histograms. These use the magnitude of the velocity of a given ion, for example $w(1)$, as the radial co-ordinate, and the angle θ between $w(1)$ and $w(2)$, if ion 2 is to be the reference ion, as the angular co-ordinate. Again, θ can be determined from the dot product of $w(1)$ with $w(2)$. As with the regular scattering diagram, since $0° \leq \theta \leq 180°$, the internal frame scattering data for ion 1 with respect to ion 2 can be plotted in the upper half of the diagram, and the data for ion 3 with respect to ion 2 can be displayed in the lower half. The velocity of any of the three products can be used as the reference velocity for an internal frame scattering diagram. For a two-body reaction the angle between the

velocities of the two ionic products will always be 180° due to conservation of momentum. However, for three-body reactions the scattering of two of the products relative to the third product - the internal frame scattering - is a very powerful probe of the reaction mechanism. For example, one of the reaction channels detected following the collisions of N_2^{2+} with NO forms three products; N_2^+, O^+ and N. These three reaction products are shown together in the example internal frame scattering diagram in Figure 2.15.

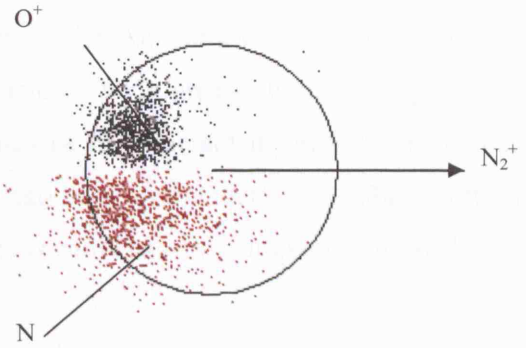

Figure 2.15 An example internal frame scattering diagram, showing the velocity of N and O^+ relative to the velocity N_2^+.

2.11.5 Reaction Exothermicity

The PSCO experiment also provides energetic information on the reactive events that are detected. In principle, if the translational energy release of the reaction, T, is known, and the centre of mass collision energy is also known, E_c, we can determine the translational exothermicity of the reactive event ΔE. The exothermicity (ΔE) for each reactive event can therefore be expressed in terms of T and E_c.

$$\Delta E = E_{\text{products}} - E_{\text{reactants}} = T - E_c \qquad (2.27)$$

For a two-body reaction, the kinetic energy release of the reaction in the COM frame (T) can be determined from the reduced mass of the products, μ_p, and the magnitudes of the lab velocity vectors;

$$T = \tfrac{1}{2}\,\mu_p\,[(v_x(1) - v_x(2))^2 + (v_y(1) - v_y(2))^2 + (v_z(1) - v_z(2))^2] \qquad (2.28)$$

The COM collision energy, E_c, is determined by two methods. The first method uses the dication velocity, s_d, (the velocity of the neutral is not considered because it is assumed to be negligible) and the reduced mass of the reactants, μ_r as seen in equation (2.29). The second method can be used for a two-body product reaction by using the velocity of the

COM of the collision system in the LAB frame, v_c, and the reduced mass of the products, μ_p, as seen in equation (2.30).

$$E_c = \tfrac{1}{2}\,\mu_r\, s_d^{\,2} \qquad (2.29)$$

$$E_c = \tfrac{1}{2}\,\mu_p\, v_c^{\,2} \qquad (2.30)$$

The kinetic energy release of the reaction in the COM frame can also be determined for three-body product reactions, where there are two ions and a third neutral species, by using the COM velocities;

$$T = \tfrac{1}{2}\,[m(1)w(1)^2 + m(2)w(2)^2 + m(3)w(3)^2] \qquad (2.31)$$

Therefore, a histogram of the ΔE values for the reactive events detected for a given channel can be constructed. Such an exothermicity spectrum may be used to provide information on the states of the reactant dication present in the beam and the product states populated in dication-neutral reactions. The exothermicity spectrum for the reaction of Ar^{2+} with He is shown as an example in Figure 2.16.

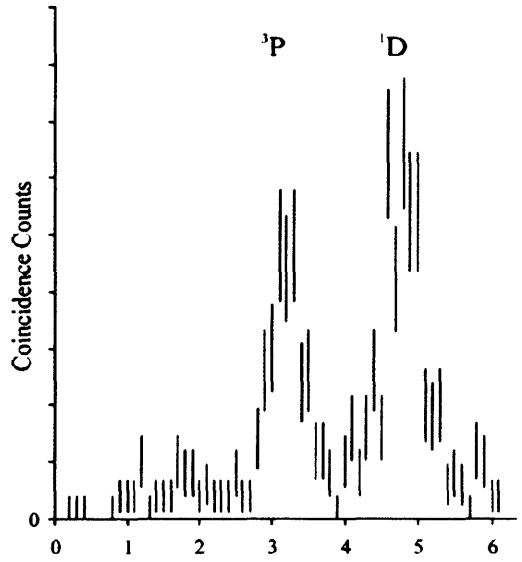

Figure 2.16 The exothermicity spectrum for the reaction of Ar^{2+} with He shows the reactions of Ar^{2+} in the ^3P and ^1D states to form Ar^+ (^2P) and He^+ (^2S). [7]

2.12 Summary

This Chapter has explained the PSCO experiment which is used to detect pairs of ions in coincidence, resulting from dication-neutral reactions using Position Sensitive Detection with Time-Of-Flight Mass Spectrometry. Hence the data detected can be used not only to discover the reactivity of these dication-neutral interactions, but also to reveal detailed information about the individual reaction channel mechanisms and energetics.

2.13 References

[1] Harper, S. M., Hu, W. P., and Price, S. D., 2002, Journal of Physics B-Atomic Molecular and Optical Physics, 35, 21, 4409.
[2] Ricketts, C. L., Harper, S. M., Hu, S. W. P., and Price, S. D., 2005, Journal of Chemical Physics, 123, 13, 124322-1.
[3] Burnside, P. W. and Price, S. D., 2006, International Journal of Mass Spectrometry, 249, 279-288.
[4] Roithova, J., Zabka, J., Herman, Z., Thissen, R., Schroder, D., and Schwarz, H., 2006, Journal of Physical Chemistry A, 110, 20, 6447.
[5] Straub, H. C., Lindsay, B. G., Smith, K. A., and Stebbings, R. F., 1996, Journal of Chemical Physics, 105, 10, 4015.
[6] Dutuit, O., Alcaraz, C., Gerlich, D., Guyon, P. M., Hepburn, J., MetayerZeitoun, C., Ozenne, J. B., Schweizer, M., and Weng, T., 1996, Chemical Physics, 209, 2-3, 177.
[7] Hu, W. P., Harper, S. M., and Price, S. D., 2002, Measurement Science & Technology, 13, 10, 1512.
[8] Harper, S. M., Hu, S. W. P., and Price, S. D., 2004, Journal of Chemical Physics, 120, 16, 7245.
[9] Hall, R. I., Mcconkey, A., Ellis, K., Dawber, G., Avaldi, L., Macdonald, M. A., and King, G. C., 1992, Measurement Science & Technology, 3, 3, 316.
[10] Penent, F., Lablanquie, P., Hall, R. I., Palaudoux, J., Ito, K., Hikosaka, Y., Aoto, T., and Eland, J. H. D., 2005, Journal of Electron Spectroscopy and Related Phenomena, 144, 7.
[11] Jost, K., 1979, Journal of Physics E-Scientific Instruments, 12, 10, 1001.
[12] Parr, A. C., Southworth, S. H., Dehmer, J. L., and Holland, D. M. P., 1984, Nuclear Instruments & Methods in Physics Research Section A-Accelerators Spectrometers Detectors and Associated Equipment, 222, 1-2, 221.
[13] Price, S. D. and Eland, J. H. D., 1992, Measurement Science & Technology, 3, 3, 306.
[14] Ovrebo, G. K. and Erskine, J. L., 1981, Journal of Electron Spectroscopy and Related Phenomena, 24, 2, 189.
[15] Wahlin, L., 1964, Nuclear Instruments & Methods, 27, 1, 55.
[16] Price, S. D., 2003, Physical Chemistry Chemical Physics, 5, 9, 1717.
[17] Wiley, W. C. and Mclaren, I. H., 1955, Review of Scientific Instruments, 26, 12, 1150.
[18] Eland, J. H. D., 1993, Measurement Science & Technology, 4, 12, 1522.
[19] Ali, I., Dorner, R., Jagutzki, O., Nuttgens, S., Mergel, V., Spielberger, L., Khayyat, K., Vogt, T., Brauning, H., Ullmann, K., Moshammer, R., Ullrich, J., Hagmann, S., Groeneveld, K. O., Cocke, C. L., and Schmidt-Bocking, H., 1999, Nuclear Instruments & Methods in Physics Research Section B-Beam Interactions with Materials and Atoms, 149, 4, 490.
[20] Oelsner, A., Schmidt, O., Schicketanz, M., Klais, M., Schonhense, G., Mergel, V., Jagutzki, O., and Schmidt-Bocking, H., 2001, Review of Scientific Instruments, 72, 10, 3968.
[21] Hsieh, S. and Eland, J. H. D., 1995, Rapid Communications in Mass Spectrometry, 9, 13, 1261.
[22] Eland, J. H. D., 1987, Molecular Physics, 61, 3, 725.
[23] Eland, J. H. D. and Pearson, A. H., 1990, Measurement Science & Technology, 1, 1, 36.
[24] Love, N. A. and Price, S. D., 2004, International Journal of Mass Spectrometry, 233, 1-3, 145.
[25] Levine, R. D. and Bernstein, R. B, 1987, Molecular Reaction Dynamics and Chemical Reactivity (New York: Oxford University Press),
[26] Harper, S. M., Hu, S. W. P., and Price, S. D., 2004, Journal of Chemical Physics, 121, 8, 3507.
[27] Mrazek, L., Zabka, J., Dolejsek, Z., Hrusak, J., and Herman, Z., 2000, Journal of Physical Chemistry A, 104, 31, 7294.

Chapter 3 Introduction to the Nitrogen Dication and the PSCO spectra

3.1 Introduction

The importance of doubly charged ions in the terrestrial ionosphere was first proposed in 1975, but generally the significance of dications, and the processes they are involved in, have been assumed to be negligible in planetary atmospheres.[1] However, ionisation cross section measurements have shown that doubly charged ions can represent up to approximately 40 % of the total ionisation process, such as the formation of Cl^{2+} in the electron ionisation of HCl.[2] In addition, some dications, such as N_2^{2+}, have been shown to possess very stable electronic states (which will be discussed later in the Chapter).[3] Hence dications and their reactions may have more significance in planetary ionospheres than initially thought. The molecular nitrogen dication (N_2^{2+}) has been predicted to be present in the terrestrial ionosphere, and so Chapters Four to Six of this thesis discuss the reactions of N_2^{2+}.[4] This Chapter acts as the general introduction to N_2^{2+} and the previous work on the reactions of neutrals with N_2^{2+}, while also explaining some of the features observed in the PSCO spectra, such as reaction 'tails' and false coincidence strips.

3.1.1 N_2^{2+} in ionospheres

As discussed in Chapter One, computational predictions have recently been made of the concentrations of the relevant doubly charged ions in the ionospheres of Earth, Mars and the moon of Saturn, Titan. Generally these computational predictions renewed the ionospheric interest in dications and their reactions with neutrals, providing further evidence that dications, and processes involving dications, may have more significance than previously thought in the upper atmospheres of planets. N_2^{2+} is of particular interest because of the high abundance of nitrogen in the atmosphere of Earth, as well as in other atmospheres such as that of Titan. The modelling of N_2^{2+} in the terrestrial ionosphere shows that N_2^{2+} will be removed both by dissociative recombination with electrons and by collisions with the abundant neutral species N_2, O_2 and O. The modelling of the N_2^{2+} ions in the ionosphere of Titan suggests the N_2^{2+} ions are removed by dissociative recombination with thermal electrons and by reactions with neutral species. The

atmosphere of Titan is very nitrogen rich but also contains hydrogen, argon and hydrocarbons, such as CH_4 and C_2H_2.[4, 5]

3.1.2 The N_2^{2+} Chapters

As mentioned above, Chapters Four to Six discuss reactions of molecular nitrogen dication (N_2^{2+}). Initially we studied the potentially terrestrially significant reactions of N_2^{2+} and O_2 using PSCO spectroscopy coupled with Time-Of-Flight Mass Spectrometry (*TOF-MS*). Then in order to obtain an overall mechanistic picture of the reactivity of N_2^{2+} with neutrals we have also studied the reactions of N_2^{2+} with gases of lower abundance in the ionosphere of Earth and Titan (Ne, NO, CO_2, H_2O, Ar, CH_4, H_2, and C_2H_2) using the PSCO technique. The reactions of N_2^{2+} with lower abundance neutrals are unlikely to be significant in the ionosphere although only modelling can really confirm this assumption. The PSCO technique was used to detect the pairs of singly charged ions resulting from the dication-neutral reactions, on an event by event basis, in coincidence. The velocity vectors for each of the product ions were then extracted, and the magnitude and orientation of these velocity vectors used to give a detailed insight into the dynamics of the reaction channels.[6]

A vast amount of chemistry has been observed in this survey of the reactions of N_2^{2+} with neutrals; many non-dissociative electron transfer, dissociative electron transfer, dissociative double electron transfer and bond-forming reactions have been detected. As previously mentioned, the Landau-Zener reaction window model has been used extensively in the literature to successfully rationalise electron transfer reactions, therefore this thesis concentrates on the bond-forming reactions observed between dications and neutrals.[7-10] These bond-forming channels are often weak, compared to electron transfer reactions. Although there are cases where the bond-forming channels are the dominant reactive channel; for example Roithová *et al* have shown that a bond-forming protonation channel, which formed CBr^+ and H_3^+, is the most dominant channel in the reaction of $CHBr^{2+}$ with H_2.[11] More background information on dication-neutral bond-forming channels has been presented in Chapter One. Despite the weak nature of dication-neutral bond-forming channels, the unusual reaction mechanisms of these channels mean they are of both fundamental and ionospheric interest. The energetic nature of the reactant dications can lead to differences in the reactivity compared to analogous monocation-neutral reactions. While there are few direct comparative studies of dication-neutral reactions with analogous monocation-neutral reactions there are some

examples such as that of Bassi *et al* who comparatively studied the bond-forming reaction of Ar^+ with N_2, (3.1), and the bond-forming reaction of Ar^{2+} with N_2, (3.2);

$$Ar^+ + N_2 \rightarrow ArN^+ + N \quad (3.1)$$
$$Ar^{2+} + N_2 \rightarrow ArN^{2+} + N \quad (3.2)$$

Bassi *et al* found that the cross-sections of these reactions varied differently, as a function of collision energy, when the reactions were studied over a range of collision energies.[12, 13] The cross-section of reaction (3.1) increased between 5 and 20 eV collision energy, then slowly decreased over tens of eV. The cross section of reaction (3.2) increased between 1 and 10 eV collision energy but then rapidly decreased between 10 eV to 11 eV. However, when a dication reacts to form two monocations we see the fundamental differences compared to monocation-neutral reactions.[14] When a dication reacts to form two monocationic products, the monocations will be translationally energetic because of the Coulombic repulsion of the two like-charged products. Hence the products of dication-neutral reactions are far more energetic than the monocation and neutral products of a monocation-neutral reaction. This energetic nature of the dication-neutral reaction products also means they may go on to overcome reaction barriers with other species, for example in the ionosphere there may be reaction barriers which the products of monocation-neutral reactions can not surmount.

The results presented in Chapters Five and Six, concentrate on the bond-forming reactions of N_2^{2+} with atmospherically relevant neutral gases (Appendix B presents some bond-forming reactions of CO_2^{2+} and O_2^{2+}). All the reactions of N_2^{2+} studied using the PSCO experiment have been run at relatively low collision energies (between approximately 4 eV and 14 eV in the COM frame), primarily to optimise the probability of detecting these bond-forming reactions. However, generally the electron transfer reactions, in particular non-dissociative electron transfer reactions, tend to be the strongest product channels in the reactions of dications and neutrals, even at the lowest collision energies probed by the PSCO experiment. In fact non-dissociative and dissociative electron transfer reactions are observed in almost every dication-neutral reaction investigated for this thesis. Therefore, for completeness, and despite the previous attention to these processes, electron transfer reactions are briefly discussed in Chapter Four.

3.1.2.1 Chapter Four - N_2^{2+} with Ne and NO (non-dissociative and dissociative electron transfer reactions)

Chapter Four describes the PSCO data gathered as part of this thesis for the non-dissociative electron transfer reaction of Ne with N_2^{2+} and a dissociative electron transfer reaction between NO with N_2^{2+}. The Landau-Zener model has also been used in Chapter Four to probe the electronic state selectivity of the non-dissociative single electron transfer reaction between Ne and N_2^{2+}. Details of the Landau-Zener theory are given in Chapter One and a brief summary of the theory Chapter Four.

3.1.2.2 Chapter Five - N_2^{2+} with O_2, CO_2 and H_2O (bond-forming reactions)

The bond-forming reactions of O_2, CO_2 and H_2O with N_2^{2+} are discussed in Chapter Five. These reactions have been grouped together because of similarities in reaction mechanism. Specifically, most of the bond-forming channels described in Chapter Five involve the decay of a collision complex via neutral loss. These reactions may be of relevance to the ionosphere of Earth.

3.1.2.3 Chapter Six - N_2^{2+} with Ar, CH_4, H_2 and C_2H_2 (bond-forming reactions)

The bond-forming reactions of Ar, CH_4, H_2 and C_2H_2 with N_2^{2+} are discussed in Chapter Six. These reactions have been grouped together because of the scattering diagrams show evidence of very fast, reaction mechanisms which do not involve a long-lived collision complex. The reactions of N_2^{2+} with the neutrals Ar, CH_4 and H_2 may be of relevance to the Earth's atmosphere and the reactions of N_2^{2+} with the neutrals Ar, CH_4, H_2 and C_2H_2 may be relevant to the atmosphere of Titan.

3.1.3 Isolated nitrogen dications (N_2^{2+})

Partly because of the abundance of N_2 in the Earth's atmosphere, N_2^{2+} is one of the most thoroughly investigated dications. Although there have been a small number of previous studies of the reactivity of N_2^{2+} with neutral gases (see the following section, 3.1.4, for a discussion of previous studies of the reactivity of N_2^{2+} with neutral gases), previous investigations of N_2^{2+} often concentrated on probing the isolated N_2^{2+} dication. In particular, the previous investigations have concentrated on the determination of the electronic, vibrational and rotational energy levels of N_2^{2+}. There have also been some studies to determine the lifetime of N_2^{2+}; an important consideration since the dication must live for long enough to encounter another species if the dication is to react, particularly in the ionosphere.

The electronic, vibrational and rotational energy states of N_2^{2+} have been studied using a range of experimental techniques, as listed in Table 3.1, and theoretical methods. Some of these experimental methods in Table 3.1 are briefly described in Chapter One.

Method	Key conclusions by researchers, regarding the electronic and vibrational states of the N_2^{2+} dication.
Threshold Electron Ionisation	The early work of Dorman *et al* (1963) and Mark (1975) determined the double ionisation energy of N_2^{2+}, finding values of 42.7±0.1 eV and 42.9±0.3 eV respectively.[15, 16] Dorman *et al* also found an excited state of N_2^{2+} at 43.8±0.1 eV. Agee *et al* (1981) also determined a double ionisation enegy for N_2^{2+} of 42.7±0.5 eV.[17]
Auger Spectroscopy	Moddeman *et al* identified seven electronic states of N_2^{2+} in an Auger spectrum using electron ionisation and determined the double ionisation energy as 42.9 eV in 1971.[18]
Translational Energy Spectroscopy	Appell *et al* measured a double ionisation of N_2^{2+} at 43.1±0.5 eV and also detected an excited state at 45.2±0.5 eV in 1973.[19] Hamdan *et al* (1989) and Koslowski *et al* (1991) measured the ionisation energies, and assigned, three of lowest lying states of N_2^{2+}.[20, 21]
Kinetic Energy Release Spectroscopy	Boyer *et al* (1989), Yousif *et al* (1990), Vancura *et al* (1994) and Cho *et al* (1995) studied the kinetic release in the dissociation of the N_2^{2+} dication and Yousif *et al* also observed seven electronic states of N_2^{2+} some of which they assigned.[22-25] Lundqvist *et al* used Doppler-Free Kinetic Energy Release Spectroscopy to vibrationally resolve the $^1\Pi_u$, $^3\Pi_g$ and $^1\Sigma_u^+$ electronic states in 1996.[26]
Optical Fluorescence Spectroscopy	Carroll was the first to observe fluorescence from the N_2^{2+} ion in 1958, tentatively assigning the band to the $^1\Sigma_u^+$-$X^1\Sigma_g^+$ transition.[27] Cossart *et al* confirmed this assignment and observed two other weaker bands in 1985.[28-30]
Laser Ion Photo-fragment Spectroscopy	Masters *et al* (1990), Larsson *et al* (1992), Cosby *et al* (1993), Sundstrom *et al* (1994) and Martin *et al* (1994), all studied the N_2^{2+} $^1\Pi_u$–$X^1\Sigma_g^+$ transition, obtaining increasingly more resolved rovibrational photopredissociation spectra of the transition.[31-35] Szaflarski *et al* (1991) and Mullin *et al* (1992) assigned and obtained a vibrationally resolved photofragment spectrum of the transitions between the $^3\Pi_g$–$^3\Sigma_u^+$.[36, 37]
Threshold Photo-electrons Coincidence Spectroscopy	Hall *et al* recorded a spectrum of N_2^{2+} with vibrational structure of three electronic states which were assigned as $X^1\Sigma_g^+$, $^3\Pi_u$ or $^3\Sigma_g^-$ and possibly $^3\Sigma_u^+$ in 1992. They also determined a double ionisation threshold of 43.00±0.03 eV.[38] Dawber *et al* then improved this to find a double ionisation threshold of 43.001±0.010 eV and vibrationally resolved the $X^1\Sigma_g^+$, $^3\Pi_u$, $^1\Pi_u$ electronic states and the tentatively assigned $^1\Sigma_u^+$electronic state in 1994.[39] Hochlaf *et al* vibrationally resolved the $X^1\Sigma_g^+$, $^3\Pi_u$ and $^3\Sigma_g^-$ electronic states and found a double ionisation threshold of 43.004±0.005 eV in 1996.[40]
Other coincidence methods	Besnard *et al* used the Photoion - Photoion coincidence technique to observe and determine the ionisation energies of six electronic states of N_2^{2+} which they tentatively assigned as the $^1\Pi_u$, $^3\Sigma_g^-$, $^1\Delta_g$, $^1\Sigma_g^+$, $^1\Pi_g$ and $^3\Delta_u$ electronic states in 1988.[41] Hellner *et al* used Photoion -Photon of Fluorescence Coincidence Spectroscopy to identify the $^1\Sigma_u^+$-$^1\Sigma_g^+$ transition in 1988.[42] Krässig *et al* observed vibrational levels of the lowest lying electronic states of N_2^{2+} using Double Zero Kinetic Energy Electron Coincidence Spectroscopy in 1992.[43] Most recently, in 2006, Ahmad *et al* used the *TOF* Photoelectron - Photoelectron Coincidence method together with Threshold Photoelectron Coincidence Spectroscopy to observe and determine the ionisation energies of the $X^1\Sigma_g^+$, $^3\Pi_u$, $^3\Sigma_g^-$,$^1\Pi_u$, $^1\Delta_g$, $^3\Sigma_u^+$, $^3\Pi_g$, $^1\Pi_g$, $^1\Sigma_u^+$, and $^3\Delta_u$ electronic states.[44]

Table 3.1 A review of the experimental methods used to study the N_2^{2+} dication with a brief description of the main feature of the work.

Reliable literature values of the energies of the N_2^{2+} electronic states, and even the dications vibrational states, are very important when interpreting the PSCO derived

exothermicity spectra. Table 3.2 shows the energies of the experimentally derived electronic states of N_2^{2+} taken from the literature. These values for the electronic states of N_2^{2+} are used later in Chapter Four, in combination with the reaction exothermicity spectra derived from the PSCO data, to determine the dominate electronic states involved in the reaction of N_2^{2+} with Ne to form N_2^+ with Ne^+. The energies of the electronic states for the reaction products, N_2^+ and Ne^+, are also taken from the literature. The energies of the electronic states of N_2^{2+}, shown in Table 3.2, are also used in the subsequent N_2^{2+} chapters when determining the dominant electronic states involved in the reactions of N_2^{2+} with other neutral species.

Electronic states of N_2^{2+}	Energy/eV	Reference
$X^1\Sigma_g^+$	43.0	[45]
$A^3\Sigma_g^-$	43.7	[40]
$a^3\Pi_u$	43.9	[45]
$C^3\Sigma_u^+$	44.5	[38]
$b^1\Pi_u$	45.0	[45]
$D^3\Pi_g$	46.4	[46]
$c^1\Pi_g$	46.5	[21]
$e^1\Sigma_u^+$	50.9	[45]

Table 3.2 The experimentally determined electronic states of N_2^{2+} relative to the ground state of N_2. These values are used when determining the reactant and product states from the PSCO exothermicity spectra.

Research on the form of the potential energy surface of N_2^{2+} commenced nearly forty years ago. Early work showed the $X^1\Sigma_g^+$, $A^3\Sigma_g^-$ and $a^3\Pi_u$ states to be nearly degenerate. The restricted nature of the theoretical work forty years ago meant that for some time there was a confusion in the identification of the ground state of N_2^{2+}. The work of Thulstrup and Andersen, Taylor and Cossart *et al* showed the ground state was the $^1\Sigma_g^+$ state, but the equally respected work of Wetmore and Boyd, Hurley and Stalherm *et al* showed a $^3\Pi_u$ ground state.[29, 47-51] However the ground state was subsequently confirmed as the $X^1\Sigma_g^+$ state by the theoretical work of Taylor and Partridge and Senekowitsch *et al.*[52, 53] Detailed experimental studies, such as those using the Time-Of-Flight Photoelectron-Photoelectron Coincidence (*TOF*-PEPECO) method by the Eland group as mentioned in Table 3.1, have now yielded vibrationally resolved spectra of many of the metastable electronic states of N_2^{2+}.[44]

When first detected, dications were viewed as unstable, short lived species, hence a second experimental focus, concerning isolated dications, is the measurement of the lifetimes of these species. Some of the experimental methods for determining the lifetimes of dications such as Ion Translational Energy Spectrometry, Photoionisation

Coincidence techniques are briefly described in Chapter One. In the case of N_2^{2+}, Heavy-Ion Storage Rings have shown that N_2^{2+} ions can live for at least several seconds and, hence, can be considered stable against unimolecular dissociation. Generally the limiting factor in the Heavy-Ion Storage Ring measurements is the destruction rate of the dications via collisions with background gases. These lifetime measurements are therefore limited to the order of seconds.[3] Other methods have been used to measure the lifetime of specific vibrational dication states such as the High Frequency Deflection Technique used by Olsson *et al* to measure the much shorter, fluorescence lifetime of 6.0±0.5 ns for the v = 0 level of one of the excited electronic states of N_2^{2+}, $^1\Sigma_u^+$.[54]

Given the above discussion it is clear that the potential energy curves of N_2^{2+} have been relatively intensively studied. The studies conclude that the ground state of N_2^{2+} is the $X^1\Sigma_g^+$ state lying approximately 43.00 eV above the ground state of N_2. Also studies of the lifetime of N_2^{2+} show that N_2^{2+} can be considered stable with a lifetime of at least several seconds in the ground state. The following section discusses the previously studied reactions of N_2^{2+} with neutrals.

3.1.4 Previously studied reactions of N_2^{2+}

As mentioned before, the previous investigations of the reactions of N_2^{2+} with neutral gases have concentrated on electron transfer reactions. However there have also been some investigations of bond-forming reactions. In this Chapter the previously studied electron transfer reactions are described (section 3.1.4.1), followed by the previously studied bond-forming reactions of N_2^{2+} with neutrals (section 3.1.4.2). More specific details are given for the electron transfer reaction of N_2^{2+} with Ne since a study of this reaction, by the PSCO technique, is presented in Chapter Four.

3.1.4.1 Previously studied electron transfer reactions of N_2^{2+}

The reaction of N_2^{2+} with Ne has been previously studied by Hamdan *et al*, Koslowski *et al* and Kamber *et al*.[20, 21, 55] Koslowski *et al* studied the electron transfer reactions of N_2^{2+} with Ne at a collision energy of 400 eV. Koslowski *et al* propose that if the ionisation process proceeds via vertical transitions, assumed because the ionisation takes place on a short time scale compared to the relaxation time of the nuclei, the $X^1\Sigma_g^+$ and $c^3\Sigma_u^+$ states of N_2^{2+} will predominately be populated in low vibrational levels while the $a^3\Pi_u$, $A^3\Sigma_g^-$ and $b^1\Pi_u$ will be populated in highly excited vibrational states. Koslowski *et*

al state that since the $b^1\Pi_u$ state is known to predissociate in high vibrational levels it is ruled out as a reactant. They also state that the $A^3\Sigma_g^-$ state, as well as the high excited states, have vertical excitation energies that lie above the barriers of the respective potential curves at larger distances; so if populated they will dissociate immediately and hence were also ruled out as reacting states. Therefore Koslowski *et al* concluded that the majority of N_2^{2+} ions entering the collision region are the $X^1\Sigma_g^+$ ground state and the excited metastable states $a^3\Pi_u$ and $c^3\Sigma_u^+$. However they then also conclude that the $a^3\Pi_u$ electronic state, which is nearly degenerate with the $X^1\Sigma_g^+$ ground state in $v = 0$, does not react as readily as the ground state, $X^1\Sigma_g^+$, of N_2^{2+}. This is because they assume the electron transfer reaction proceeds via vertical transitions and the $a^3\Pi_u$ electronic state in high vibrational levels does not correlate with the measured spectra as well as the $X^1\Sigma_g^+$ electronic state in low vibrational levels.

Hamdan *et al* studied energy change spectra following the electron transfer reaction from Ne to $^{29}N_2^{2+}$ using a double-focusing translational energy spectrometer at a collision energy of 6 keV. They concluded the electron transfer channels for N_2^{2+} and Ne involve the $c^3\Sigma_u^+$ state and the ground electronic states of N_2^{2+}. Kamber *et al* studied state-selective, non-dissociative electron transfer reaction of N_2^{2+} with Ne at a collision energy of 28 eV using Ion Translational Energy Spectroscopy. Kamber *et al* found that in the electron transfer from Ne to N_2^{2+}, the N_2^{2+} $X^1\Sigma_g^+$, and $c^3\Sigma_u^+$ states participate. Therefore, to conclude, Hamdan *et al*, Koslowski *et al* and Kamber *et al* all find that the electron transfer reaction of N_2^{2+} with Ne involves the $c^3\Sigma_u^+$ electronic state and the ground electronic state, $X^1\Sigma_g^+$, of N_2^{2+}.

Other studies of the reactivity of N_2^{2+} include the studies of the reactions with D_2, He, Ar, N_2, CO_2 and H_2O. The reaction of N_2^{2+} with O_2 has been previously studied by Kamber *et al*; however, no mention is made of a bond-forming channel in their paper. The reaction of N_2^{2+} with Ar has been particularly well studied by several groups such as Dutuit *et al*, Kamber *et al*, Koslowski *et al*, Schulz *et al* and even a study in the 1960s by Savage *et al*.[21, 55-58] In the study of the reactions of N_2^{2+} with O_2, D_2, He, Ar and N_2 by Kamber *et al*, and a study of N_2^{2+} reactions with He and Ar by Koslowski *et al*, both propose the electron transfer reactions between the N_2^{2+} and neutral species all involve the $c^3\Sigma_u^+$ and $X^1\Sigma_g^+$ electronic states of N_2^{2+} as previously discussed. With the exception of the studies by Dutuit *et al* (See section 3.1.4.2), generally all these other studies of N_2^{2+} with neutrals concentrate on the electron transfer reactions, in some cases including the determination of the reaction cross-section, but there are no reports of bond-forming

channels. These experiments have also generally been carried out at collision energies in excess of 28 eV and up to the keV range, which is greater than the low collision energies, rarely exceeding 14 eV, used in the PSCO experiment.

3.1.4.2 Previously studied bond-forming reactions of N_2^{2+}

With regard to previous studies of bond-forming reactions of N_2^{2+}, this field was stimulated by the, as yet unpublished, work of Dutuit *et al.*[58] The formation of NO^+ from the reaction of N_2^{2+} with O_2 was first observed by Dutuit *et al* but the experimental technique used did not identify the ion paired with the NO^+ in the reaction. Hence this was an ideal system to study using the PSCO technique where the ion pair identity and the reaction mechanism could be determined. In a study of N_2^{2+} reactions with CD_4 by Dutuit *et al* several bond-forming products were observed including ND^+, ND_2^+, DCN^+ and D_2CN^+. In a study of the reactions of N_2^{2+} with C_2D_4, Dutuit *et al* also observed several bond-forming reactions with the detection of reaction products DCN^+, D_2CN^+ and D_3CN^+.

To conclude there has been a relatively high level of investigation of the reactions of N_2^{2+} with neutral gases. Important findings have been made; especially significant to this research is the conclusion that the dominant reacting states of N_2^{2+} are the $c^3\Sigma_u^+$ and the $X^1\Sigma_g^+$ electronic states. However, particularly with regards to the bond-forming reactions, there is still scope for considerably more study. There have been no previous experimental investigations of the reaction mechanisms of the bond-forming channels of N_2^{2+} with neutrals so Chapter Five and Six of this thesis concentrate on this aspect of the reactivity.

3.2 Experimental Features

However, as previously mentioned, this Chapter acts as the general introduction to N_2^{2+} and the previous work on the reactions of neutrals with N_2^{2+}, as well as discussing some of the PSCO experimental feature. Background information has been given on isolated N_2^{2+} ions in section 3.1.3, the previous work on the reactions of N_2^{2+} in section 3.1.4 and experimental features of the coincidence spectrum such as false coincidences and reaction peak 'tails' are explained in the subsequent sections.

3.2.1 Determination of Reaction Mechanisms

The mechanisms of the reactions detected in the pairs spectrum are inferred from the analysis of angular scattering diagrams derived from the PSCO data recorded with a repeller plate voltage of 300 V. At a repeller plate voltage of 300 V full angular distributions of the reaction products are recorded, whereas at lower repeller plate voltages the full angular scattering is not recorded. Figure 3.1 shows how at a repeller plate voltage of 300 V even the sideways scattered ions hit the detector, and full angular distributions are gathered. However, when using a repeller plate voltage of 50 V the sideways scattered ions are not detected but instead hit the wall of the drift tube, hence incomplete angular distributions are recorded.

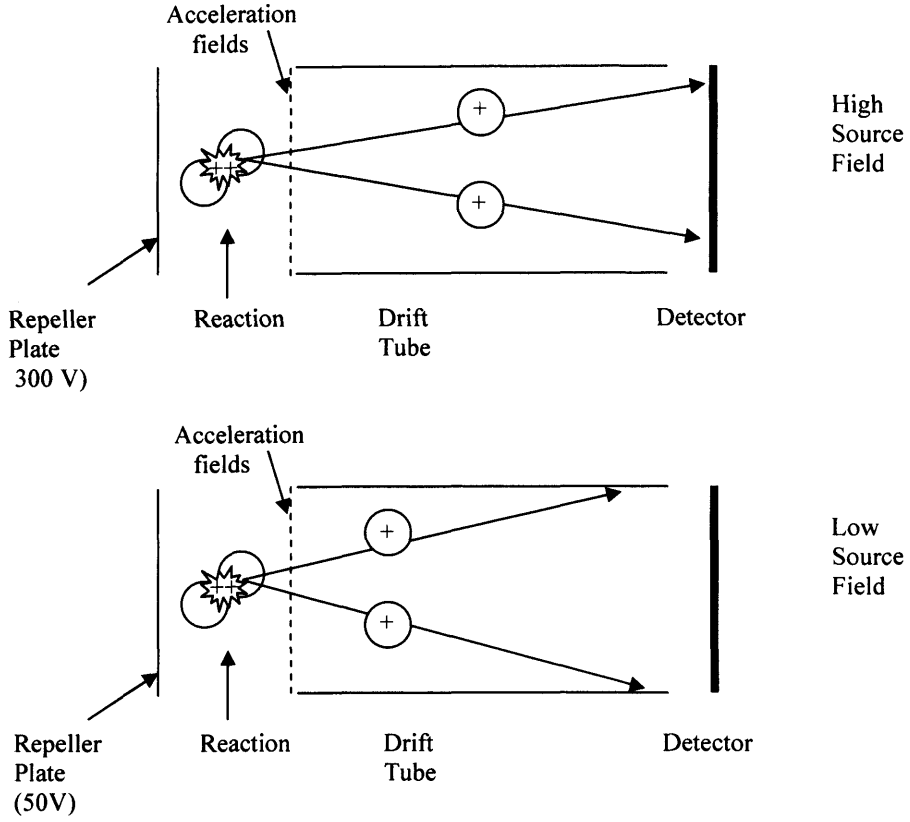

Figure 3.1 A schematic diagram to show the effect of the application of the repeller plate voltage on the detection of ions with sideways velocities at high and low repeller plate voltages. It is important to note that the trajectory of the ions in fact follows as parabola path as opposed to the simplified straight lines shown in this schematic.

The derivation of the angular scattering diagrams from the PSCO data has been described in detail in Chapter Two. However, to briefly reiterate, angular scattering diagrams are used as they are an informative way of representing the angular scattering of a particular reaction. Angular scattering diagrams are polar histograms where the radial co-ordinate

is the magnitude of the velocity of the ion in the COM frame and the angular co-ordinate is the angle between the ion and either the velocity of the dication in the Centre Of Mass, COM, frame ('angular scattering with respect to the velocity of the dication in the COM frame') or the velocity of a second product ('internal frame scattering diagrams'). The scattering of an ion is often termed 'forwards', 'backwards', 'sideways' or 'isotropic'. 'Forwards' scattering refers to product ions scattered in the same direction as that of the trajectory of their parent reactants relative to the COM. In the PSCO experiment the COM is always moving in the same direction as the dication pulses. So for example in the reaction of X^{2+} with Y, if the X^+ product ion continues to move in the same direction as the initial trajectory of the reactant X^{2+} relative to the COM, and the Y^+ product ion moves in the opposite direction to X^{2+} (in the direction of the Y) relative to the COM, the scattering, for both product ions, is termed 'forwards scattering'. Figure 3.2 shows a schematic of a scattering diagram where the products have been forwards scattered.

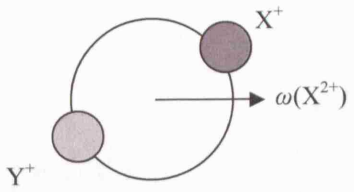

Figure 3.2 A schematic scattering diagram showing product ions, X^+ and Y^+, which are forwards scattered in the same directions as velocity of the dication in the COM frame, labelled $\omega(X^{2+})$.

If, for example in the reaction of X^{2+} with Y, the X^+ product ion moves in the opposite direction to the initial COM trajectory of the reactant X^{2+}, and the Y^+ product ion moves in the same direction to X^{2+} (opposite to Y) relative to the COM, the scattering, for the product ions, is termed 'backwards scattering', as shown by the schematic scattering diagram in Figure 3.3.

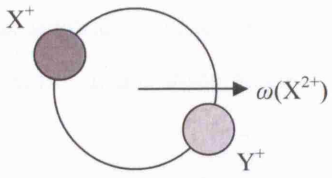

Figure 3.3 A schematic scattering diagram showing product ions, X^+ and Y^+, which are backwards scattered in the direction of velocity of the dication in the COM frame, labelled $\omega(X^{2+})$.

Obviously if forwards or backwards scattering is observed for one product in a 2-body product reaction, then the forwards and backwards scattering is mutually exclusive, due to

the conservation of momentum. However, 3-body reactions can involve both forwards and backwards scattering of products.

Ions scattered perpendicular to the velocity of the dication in the COM frame are termed 'sideways' scattered, while ions scattered uniformly over the entire range of solid angles are termed 'isotropic', shown schematically in Figure 3.4. However, due to the nature of the construction of the angular scattering diagrams, in reality it is difficult to distinguish visually between sideways and isotropic scattering since isotropic scattering will result in increased intensity in the sideways scattered region. It is possible to probe whether the ions are scattered uniformly over a range of angles, or not, but this does not form part of this research. Given that sideways scattering and isotropic scattering are likely to result from similar reaction mechanisms, such as those involving intermediate complexes with time to fully or partly rotate, we are more interested in whether the ions are scattered isotropically/sideways compared to forward/backwards scattering.

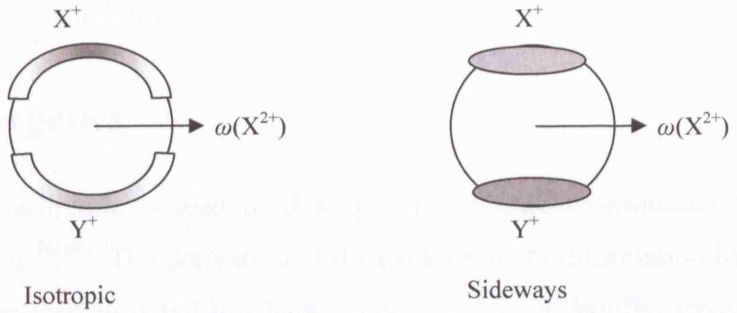

Figure 3.4 A schematic scattering diagram showing product ions, X^+ and Y^+, isotropically and sideways scattered with respect to the velocity of the dication in the COM frame, labelled $\omega(X^{2+})$.

The scattering angle between any ion and either, the velocity of the dication in the COM frame or the velocity of a second product, is always between 0° and 180°. So for example, as shown in Figure 3.5, two product ions, X^+, scattered at a specific angle, Θ, relative to the velocity of the second product Y^+, may have effectively travelled in different directions to each other, but at the same angle, Θ, to Y^+.

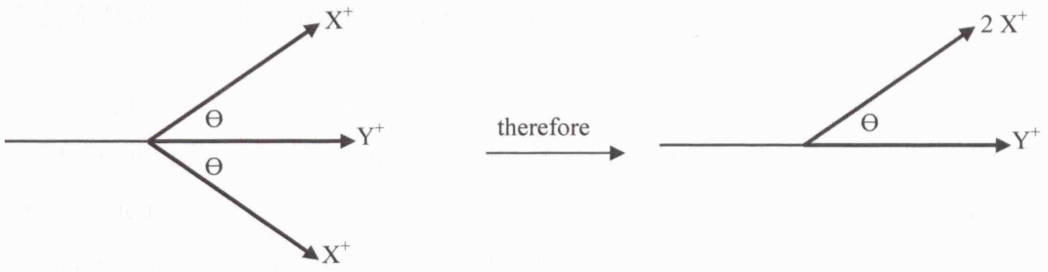

Figure 3.5 A schematic diagram to show how all the scattering information for one product can be plotted in one semicircle.

Figure 3.5 shows that despite the difference in direction is no difference in the angular scattering of these X^+ ions relative to the velocity of the second product, Y^+. Therefore in the 2-dimension plane the range of scattering angles from 0° to 180° covers the entire range of scattering angles of one product ion relative to a second product, or with respect to the velocity of the dication in the COM frame, in three- dimensional space. Hence when plotting this information in a scattering diagram it occupies one semicircle, and therefore in scattering diagrams one product can be plotted in the top half of the scattering diagram and a second product plotted in the lower half of the scattering diagram.

3.2.2 Energetics

The PSCO technique is also used to provide energetic information on the detected reactive events.[6, 60] The derivation of the exothermicity information from the PSCO data has been described in detail in Chapter Two. However, briefly, from the pairs data we derive a histogram of the values of the translational exothermicity, for each reactive event in a specific reactive channel. We can then use literature values of the heats of formation and relevant ionisation energies of the reactants and products to derive the literature exothermicities for the specific reaction. By comparing the experimental and literature exothermicity values, it is sometimes possible to draw conclusions about the electronic states of the products and reactants. Unlike the angular scattering diagrams, the exothermicity spectra with the best resolution are derived from data collected using a low repeller plate voltage. When assigning the electronic transitions of a reaction, we can also consider the spin selection rules to determine the conservation of spin angular momentum in the collision, and hence which transitions are 'allowed' or 'forbidden'. Forbidden transitions can still occur, but if many electronic transitions are assigned to the PSCO exothermicity spectra, it has been shown that the 'allowed' transitions contribute the most to the reaction intensity. [61]

3.2.3 False coincidence removal

The relative intensities of the different reactive channels observed in the pairs spectrum can be measured by comparing the numbers of counts in each coincidence peak. In the case of the reactions of N_2^{2+} with neutrals, some reaction channels form a N^+ product ion, the signals of which are contaminated by the false coincidences. False coincidences, and the measures taken to prevent their interference in the data analysis, will be explained in detail shortly. However, firstly Figure 3.6 shows a schematic of an example of a coincidence spectrum.

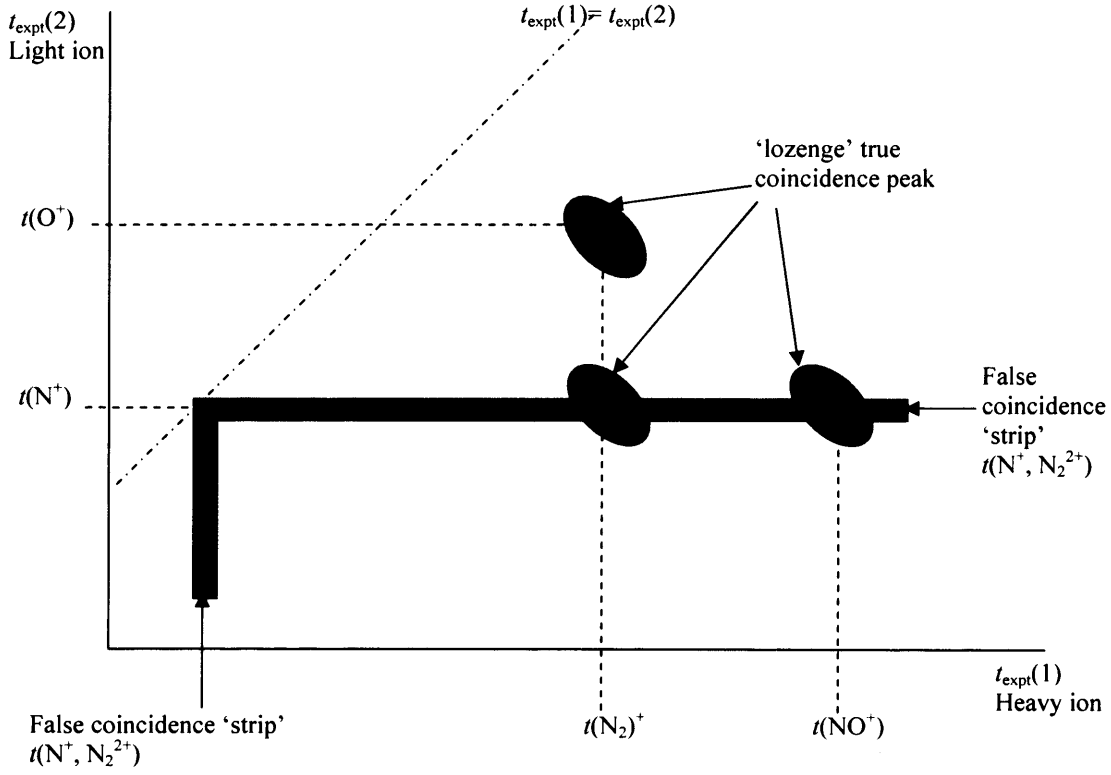

Figure 3.6 A schematic of an example of a coincidence 'pairs' spectrum showing the 'lozenge' shaped coincidence peaks, with false coincidence 'strips' running through two of the coincidence peaks. The schematic is based on the true coincidence spectrum of the reactions of N_2^{2+} with NO which will be discussed Chapter Four.

In Figure 3.6, two peaks, shown as N_2^+ paired with N^+ and the NO^+ paired with N^+, have a false coincidence 'strip' running through them while the other peak, shown as N_2^+ paired with O^+, is not contaminated by false coincidences. The width of the false coincidence strips is actually exaggerated as a visual aid in this schematic. As can be seen in the schematic Figure 3.6, the 'true' coincidence peaks form in a distinctive lozenge shape, which is due to the significant kinetic energy release in the reactions. The

false coincidences however, form strips of intensity which have a narrow width due to the small spread in the *TOF* of the ions from the ion pulses. Since the 'lozenge' shape spreads the true coincidence peaks away from the narrow strip of false coincidences, the true reaction peaks are readily visible in the pairs spectrum. An additional feature shown in this schematic coincidence spectrum is the dashed diagonal line where $t_{expt}(1) = t_{expt}(2)$. This is to demonstrate that no ions pairs are observed above this line because the heaviest ion of the ion pair is always plotted along the horizontal axis while the lightest ion of the pair is always plotted along the vertical axis of the spectrum. Hence, while an actual diagonal line is not observed in a true coincidence spectrum, the whole coincidence spectrum will in fact only form below the $t_{expt}(1) = t_{expt}(2)$ line.

False coincidences stem from the detection of an ion pair that does not originate from the same reactive event. The PSCO experiment runs at low dication fluxes, on average significantly less than one reactant dication per ion pulse, and with a neutral gas pressure which ensures single-collision conditions. Under these experimental constraints, the probability of recording a false coincidence involving the detection of the products of two different reactive events originating from two different dications in the same reactant ion pulse is negligible. Thus, the false coincidences are dominated by events where an unreacted ion in the ion pulse is detected in coincidence either with a random ion arrival or with one of the products of the reaction of an N_2^{2+} ion from the same pulse. The rate of such coincidences is significant in the N_2^{2+}/neutral collision system due to the reactant ion beam being composed of predominantly N^+ ions, together with a smaller but significant number of N_2^{2+} ions. Note, of course, that the monocations in the reactant ion beam cannot react to generate a genuine ion pair and so, other than the increased rate of false coincidences, these contaminant monocations do not complicate the interpretation of the pairs spectrum. Therefore in the case of N_2^{2+} false coincidences appear in the pairs spectrum as a vertical intensity strip where $t_{expt}(1)$ is the time of an ion with m/z=14 and as a horizontal intensity strip where $t_{expt}(2)$ is the time of an ion with m/z=14.

As previously mentioned, in a reaction with a N^+ ion the number of pairs in the peak will be elevated by the contamination of false coincidences, affecting the relative intensity analysis as well as the appearance of the scattering diagrams and exothermicity spectra. Therefore, before performing any further analysis, the contribution of false coincidences to the pairs in the coincidence peak, must be subtracted. The "false" N^+ ions appear as a sharp peak in the velocity distribution of the m/z=14 product so the false coincidences are easily identified, and removed from the dataset. All relative intensities of channels

involving an N^+ product, from a reaction of N_2^{2+}, are determined after this false coincidence subtraction. All angular scattering diagrams and reaction exothermicity histograms presented are also constructed from the data set after the false coincidences have been subtracted.

3.2.4 Coincidence spectrum tails

The most intense part of the coincidence spectrum is the 'true' reaction peak as seen in the real coincidence spectrum in Figure 3.7.

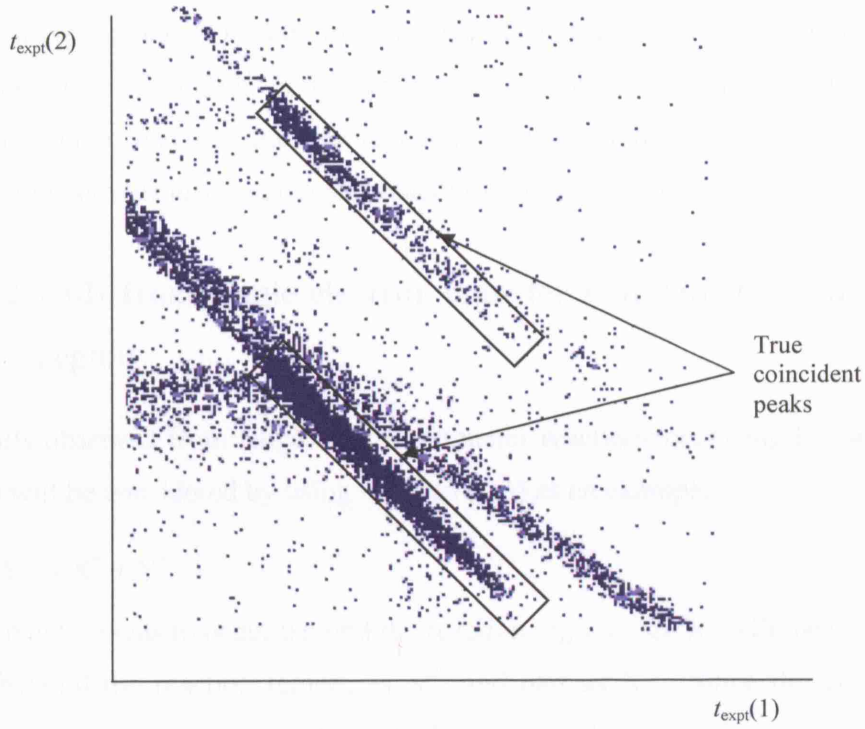

Figure 3.7 A real coincidence spectrum, from the collisions of N_2^{2+} with Ne, boxing the true reaction peaks and also showing the 'tails' leading from the reaction peaks.

However, 'tails' leading from the reaction peaks are also observed in the spectrum. Indeed, 'tails' can be seen in the coincidence spectra shown throughout this thesis. This section will explain the origins of the tails. First is it important to note that the 'spot' plots of the pairs spectra over emphasize the reaction peak tails. Once a pixel is filled with a 'spot' to denote the detection of a reaction pair, that 'spot' will visually appear no more intense despite the number of reaction pairs in that 'spot' region. Therefore the weak tails leading from the considerably more intense reaction peaks, visually appear to be more intense, over emphasized in the pairs spectrum, than their true intensity.

The true coincidence peak is formed from products formed near the centre of the reaction region just before they are extracted out of the reaction region by the application of voltage to the repeller plate. The tail leading from a particular peak is formed by the same reaction as the main peak but occurring under 'different' circumstances, hence the *TOF* of the ions is altered. The following sections will describe what these 'different circumstances' are and hence why these tails are present in the coincidence spectra. The final part of this section will then explain how the tails in the coincidence spectra can be reduced or eliminated by using a pulsed beam of dications instead of a continuous beam.

3.2.4.1 Coincidence spectrum tails - reactions beyond the reaction region

The first type of tail is formed by reactions of the dication pulses that occur beyond the reaction region of the *TOF* in the acceleration region. These types of tails are commonly seen for single electron transfer reactions, discussed in section 3.3.4.1.1, as well as dissociative double electron transfer reactions, discussed section 3.3.4.1.2.

3.2.4.2 Tails from single electron transfer reactions beyond the reaction region

The tails observed from single electron transfer reactions occurring beyond the reaction region will be considered by using reaction (3.3) as an example.

$$X^{2+} + Y \rightarrow X^{+} + Y^{+} \qquad (3.3)$$

If this reaction was to occur beyond the reaction region then X^+ will have spent part of its time, beyond the reaction region, as X^{2+} and part as X^+. Since the *TOF* of an ion is relative not just to the mass of an ion but in fact the *m/z* ratio, X^{2+} is faster than X^+. Therefore the X^+ formed beyond the reaction region will have a shorter *TOF* than X^+ formed in the reaction region. However if the reaction occurs beyond the reaction region, then Y is initially close to stationary and the Y^+ ion formed will not experience the field from the voltage application to the repeller plate to extract the ions into the drift tube. The Y^+ will then only be accelerated by the acceleration region voltages, hence the total voltage the Y^+ experiences is lower than the acceleration voltage experienced by the Y^+ formed in the reaction region - where the Y^+ experiences the repeller plate voltage in addition to the acceleration region voltages. Therefore the Y^+ formed outside the reaction region will be considerably less energetic than a Y^+ formed inside the reaction region. The further the reaction occurs from the reaction region the less the acceleration the Y^+

will experience from the acceleration region voltages and hence the longer the *TOF* will be compared to that *TOF* of a Y^+ formed in the reaction region.

By the above arguments, the difference between the *TOF*s of the products formed beyond the reaction region and the *TOF*s of the same products formed in the reaction region will increase, the further from the reaction region the reaction occurs. Hence the tails are observed as diagonal lines of intensity across the coincidence spectrum as labelled in Figure 3.8, leading to shorter *TOF* for the product ion starting life as the dication, and longer *TOF* for product ion starting life as the neutral.

As previously mentioned, the coincidence spectrum is formed by always plotting the shortest *TOF* on the vertical axis against the longest *TOF* on the horizontal axis. Therefore if the *TOF* of X^+, in the real reaction peak, is longer than the *TOF* of Y^+, the tail will form above the real peak. However the further the reaction occurs from the reaction region the longer the *TOF* of Y^+ becomes until eventually the *TOF* of Y^+ is longer than the *TOF* of X^+ and the tail forms diagonally below the real peak. This therefore means that the tails lead diagonally away from the real reaction peaks in one direction and are then reflected where $t_{expt}(1) = t_{expt}(2)$ to continue in the other direction. Of course if the *TOF* of X^+, in the real reaction peak, is shorter than the *TOF* of Y^+, the tail will only form below the real peak. These types of diagonal tails are commonly seen for single electron transfer reactions (both non-dissociative and dissociative).

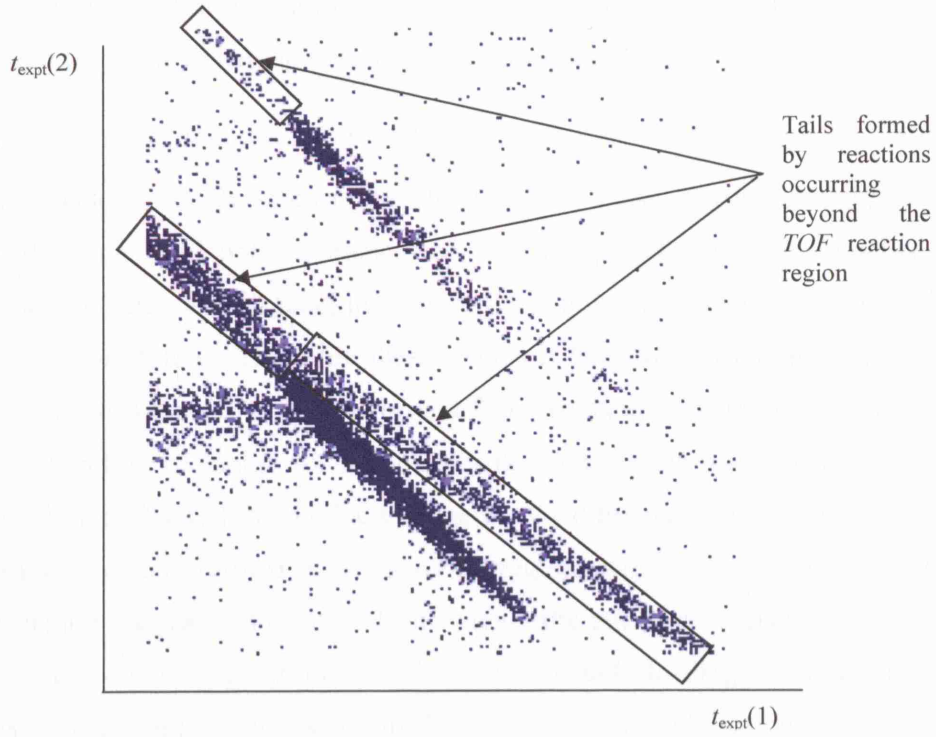

Figure 3.8 A real coincidence spectrum, from the collisions of N_2^{2+} with Ne, boxing the diagonal tails formed from reactions occurring beyond the *TOF* reaction region.

There is one exception to the diagonal tail formation observed for single electron transfer reactions. This exception occurs when the *TOF* of the product ion formed from the dication is the same as the *TOF* of the dication such as N_2^{2+} and N^+. Even if the reaction occurred beyond the reaction region, the *TOF* of the product ion formed from the dication would not be affected. However the *TOF* of the product ion formed from the neutral species would be affected. Technically this would manifest as a vertical or horizontal line where the product ion (such as N^+) formed from the dication (such as N_2^{2+}) has the same *TOF* but the product ion formed from the neutral has a longer *TOF*. However this line would occur along the line of false coincidences and therefore would not be easy to distinguish since reaction tails are weak compared to the false coincidences. These electron transfer reactions, when the *TOF* of the product ion formed from the dication is the same as the *TOF* of the dication, can then appear to have no tail.

3.2.4.3 Tails from dissociative double electron transfer reactions beyond the reaction region

Diagonal tails can also be observed for dissociative double electron transfer reactions. The products of dissociative double electron transfer are formed after double electron

transfer from the neutral to the dication, followed by dissociation of the initially neutral species into two singly charged ions such as in reaction (3.4).

$$X^{2+} + Y_2 \rightarrow X + Y_2^{2+} \text{ then } \rightarrow X + Y^+ + Y^+ \qquad (3.4)$$

When dissociative double electron transfer reactions occur beyond the reaction region, both product ions will not experience the voltage application to the repeller plate to extract the ions into the drift tube, instead they will only be accelerated by the voltages in the acceleration region. Therefore these ions will be less translationally energetic and hence slower than the product ions formed from a reaction in the reaction region. The *TOF* will therefore be longer for the ions formed outside the reaction region. Again the difference in the *TOF*s of the products formed beyond the reaction region, from the *TOF*s of the same products formed in the reaction region, will increase the further from the reaction region the reaction occurs. Hence again the tails are observed as diagonal lines across the coincidence spectrum but with both the tails leading to increasingly longer *TOF*s as seen in Figure 3.9. Since in this case the tail leads to longer *TOF*s for both product ions the tails only form above the true reaction peaks.

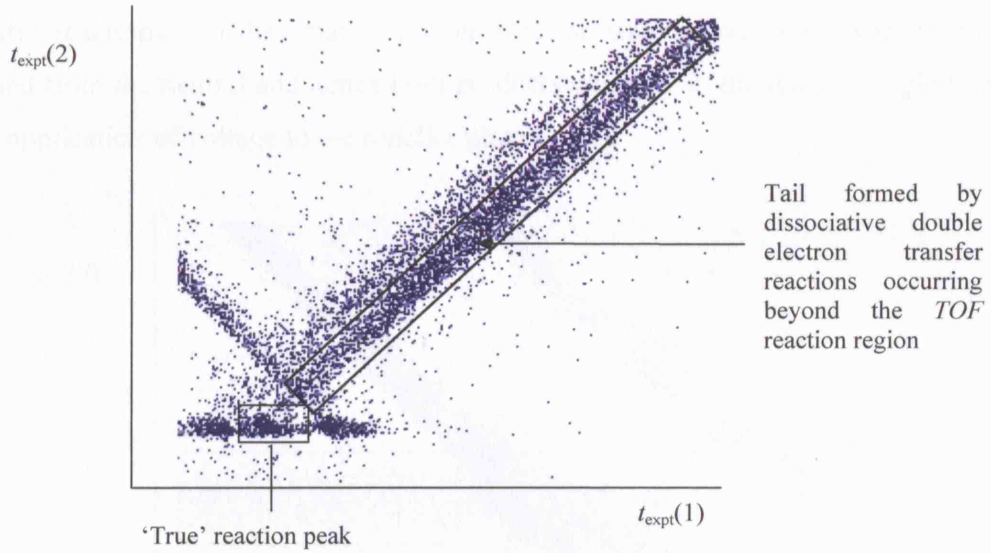

Figure 3.9 A section of a real coincidence spectrum, from the collisions of N_2^{2+} with C_2H_2, showing the diagonal tail formed above the true reaction peak (the boxed peak is H^+ paired with C_2H^+), leading to increasingly longer *TOF*s, formed by dissociative double electron transfer reactions occurring beyond the *TOF* reaction region.

3.2.4.4 Coincidence spectrum tails - reactions in the reaction region in between the applications of voltage to the repeller plate

The second type of tail forms when reactions occur in the reaction region but in between the application of the pulsed voltage to the repeller plate. Since the dication has significantly more energy than the neutral, the monocations formed from the dication parent will travel into the drift tube while the monocations formed from the neutral parent will remain in the reaction region until extracted into the drift tube by the next application of voltage to the repeller plate. Hence the monocations formed from the dication parent will have a shorter flight time, while the monocations formed from the neutral parent will have the expected flight time. Hence horizontal or vertical tails will form, leading to shorter *TOF* of the monocations formed from the dication parent but the same *TOF* of the monocations formed from the neutral parent. This type of tail is commonly seen for single electron transfer reactions.

Unlike the previous type of tail described, formed from reactions occurring beyond the reaction region, this type of tail will not be observed for dissociative double electron transfer reactions. In dissociative double electron transfer reactions both products are formed from the neutral and hence both products will stay in the reaction region until the next application of voltage to the repeller plate.

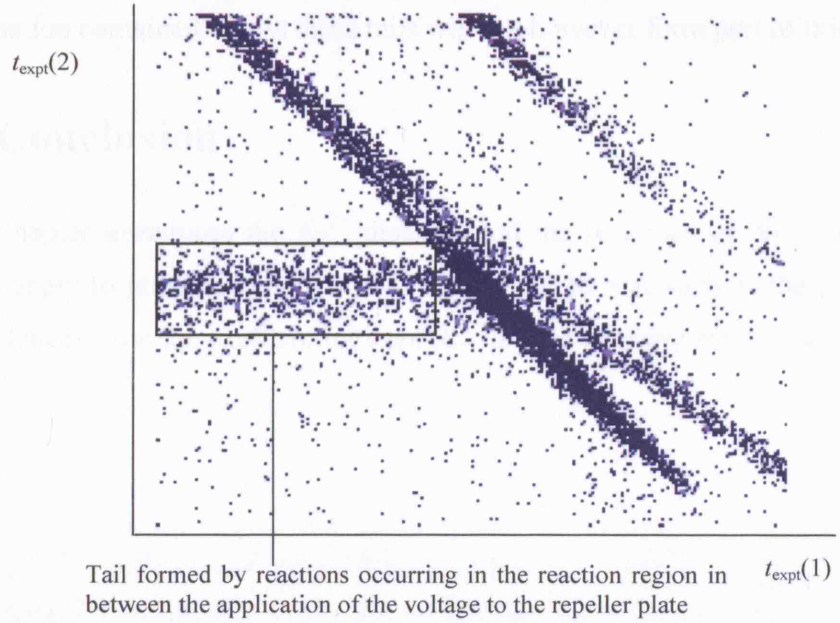

Figure 3.10 A real coincidence spectrum, from the collisions of N_2^{2+} with Ne, boxing the tail formed by reactions that occur in the reaction region but in between the applications of the voltage to the repeller plate, usually observed for single electron transfer reactions, dissociative or non-dissociative.

3.2.4.5 Reducing the tails

All types of tails can be significantly reduced by using a pulsed dication beam, although rarely fully eliminated. The advantages of using a pulsed beam over a continuous beam are described in Chapter Two, section 2.1.1. As previously described, pulsing the beam creates packets of dications which are extracted into the *TOF* drift tube (along with any reaction products) at the point when the dications packets are in the centre of the reaction region. Therefore, pulsing the beam means far fewer ions will have travelled as far as the acceleration region or drift tube when the voltage is applied to the repeller plate, than when using a continuous beam. Since the first type of tail is caused by reactions that occur beyond the reaction region, pulsing the beam reduces the tails. The other type of tail described, the tail formed by reactions occurring 'in between' voltage applications to the repeller plate, is often close to eliminated when using a pulsed beam. When the beam is pulsed there are very few ions in the reaction region in between the dication pulses and hence in between the applications of the voltage to the repeller plate.

Even though it is difficult to achieve a full elimination of all the tails, they do not interfere with the analysis of the coincidence spectrum as they are usually very weak compared to true reaction peaks and rarely run 'through' other reaction peaks. Interestingly these coincidence spectra tails actually contain a significant amount of information regarding the cross-section of the reaction at varying collision energy. Extracting and utilising the information contained within these tails will not however form part of this thesis.

3.3 Conclusion

This Chapter introduces the N_2^{2+} dication and the reactions of N_2^{2+}, specifying details which apply to reaction channels in Chapter Four to Six, such as the extraction of false coincidences from the exothermicity spectra in N^+ containing reaction channels.

3.4 References

[1] Prasad, S. S. and Furman, D. R., 1975, Journal of Geophysical Research, 80, 10, 1360.
[2] Harper, S., Calandra, P., and Price, S. D., 2001, Physical Chemistry Chemical Physics, 3, 5, 741.
[3] Mathur, D., Andersen, L. H., Hvelplund, P., Kella, D., and Safvan, C. P., 1995, Journal of Physics B-Atomic Molecular and Optical Physics, 28, 15, 3415.
[4] Simon, C., Lilensten, J., Dutuit, O., Thissen, R., Witasse, O., Alcaraz, C., and Soldi-Lose, H., 2005, Annales Geophysicae, 23, 3, 781.
[5] Lilensten, J., Witasse, O., Simon, C., Solidi-Lose, H., Dutuit, O., Thissen, R., and Alcaraz, C., 2005, Geophysical Research Letters, 32, 3.
[6] Hu, W. P., Harper, S. M., and Price, S. D., 2002, Measurement Science & Technology, 13, 10, 1512.
[7] Manning, M., Price, S. D., and Leone, S. R., 1993, Journal of Chemical Physics, 99, 11, 8695.
[8] Rogers, S. A., Price, S. D., and Leone, S. R., 1993, Journal of Chemical Physics, 98, 1, 280.
[9] Burnside, P. W. and Price, S. D., 2006, International Journal of Mass Spectrometry, 249, 279.
[10] Herman, Z., Zabka, J., Dolejsek, Z., and Farnik, M., 1999, International Journal of Mass Spectrometry, 192, 191.
[11] Roithova, J., Zabka, J., Herman, Z., Thissen, R., Schroder, D., and Schwarz, H., 2006, Journal of Physical Chemistry A, 110, 20, 6447.
[12] Tosi, P., Correale, R., Lu, W. L., Falcinelli, S., and Bassi, D., 1999, Physical Review Letters, 82, 2, 450.
[13] Tosi, P., Correale, R., Lu, W. Y., and Bassi, D., 1999, Journal of Chemical Physics, 110, 9, 4276.
[14] Price, S. D., 2003, Physical Chemistry Chemical Physics, 5, 9, 1717.
[15] Dorman, F. H. and Morrison, J. D., 1963, Journal of Chemical Physics, 39, 7, 1906.
[16] Mark, T. D., 1975, Journal of Chemical Physics, 63, 9, 3731.
[17] Agee, J. H., Wilcox, J. B., Abbey, L. E., and Moran, T. F., 1981, Chemical Physics, 61, 1-2, 171.
[18] Moddeman, W. E., Carlson, T. A., Krause, M. O., Pullen, B. P., Bull, W. E., and Schweitz, G. K., 1971, Journal of Chemical Physics, 55, 5, 2317.
[19] Appell, J., Durup, J., Fehsenfe, F. C., and Fournier, P., 1973, Journal of Physics B-Atomic Molecular and Optical Physics, 6, 1, 197.
[20] Hamdan, M. and Brenton, A. G., 1989, Journal of Physics B-Atomic Molecular and Optical Physics, 22, 1, L9.
[21] Koslowski, H. R., Lebius, H., Staemmler, V., Fink, R., Wiesemann, K., and Huber, B. A., 1991, Journal of Physics B-Atomic Molecular and Optical Physics, 24, 23, 5023.
[22] Boyer, K., Luk, T. S., Solem, J. C., and Rhodes, C. K., 1989, Physical Review A, 39, 3, 1186.
[23] Yousif, F. B., Lindsay, B. G., and Latimer, C. J., 1990, Journal of Physics B-Atomic Molecular and Optical Physics, 23, 3, 495.
[24] Vancura, J. and Kostroun, V. O., 1994, Physical Review A, 49, 1, 321.
[25] Cho, H. and Park, S. E., 1995, Physical Review A, 51, 2, 1687.
[26] Lundqvist, M., Edvardsson, D., Baltzer, P., and Wannberg, B., 1996, Journal of Physics B-Atomic Molecular and Optical Physics, 29, 8, 1489.
[27] Carroll, P. K., 1958, Canadian Journal of Physics, 36, 11, 1585.
[28] Cossart, D., Cossartmagos, C., and Launay, F., 1991, Journal of the Chemical Society-Faraday Transactions, 87, 16, 2525.
[29] Cossart, D., Launay, F., Robbe, J. M., and Gandara, G., 1985, Journal of Molecular Spectroscopy, 113, 1, 142.
[30] Cossart, D. and Launay, F., 1985, Journal of Molecular Spectroscopy, 113, 1, 159.
[31] Cosby, P. C., Moller, R., and Helm, H., 1983, Physical Review A, 28, 2, 766.
[32] Martin, P. A., Bennett, F. R., and Maier, J. P., 1994, Journal of Chemical Physics, 100, 7, 4766.
[33] Sundstrom, G., Carlson, M., Larsson, M., and Brostrom, L., 1994, Chemical Physics Letters, 218, 1-2, 17.
[34] Larsson, M., Sundstrom, G., Brostrom, L., and Mannervik, S., 1992, Journal of Chemical Physics, 97, 3, 1750.
[35] Masters, T. E. and Sarre, P. J., 1990, Journal of the Chemical Society-Faraday Transactions, 86, 11, 2005.
[36] Mullin, A. S., Szaflarski, D. M., Yokoyama, K., Gerber, G., and Lineberger, W. C., 1992, Journal of Chemical Physics, 96, 5, 3636.
[37] Szaflarski, D. M., Mullin, A. S., Yokoyama, K., Ashfold, M. N. R., and Lineberger, W. C., 1991, Journal of Physical Chemistry, 95, 6, 2122.
[38] Hall, R. I., Mcconkey, A., Avaldi, L., Macdonald, M. A., and King, G. C., 1992, Journal of Physics B-Atomic Molecular and Optical Physics, 25, 2, 411.

[39] Dawber, G., Mcconkey, A. G., Avaldi, L., Macdonald, M. A., King, G. C., and Hall, R. I., 1994, Journal of Physics B-Atomic Molecular and Optical Physics, 27, 11, 2191.
[40] Hochlaf, M., Hall, R. I., Penent, F., Kjeldsen, H., Lablanquie, P., Lavollee, M., and Eland, J. H. D., 1996, Chemical Physics, 207, 1, 159.
[41] Besnard, M. J., Hellner, L., Dujardin, G., and Winkoun, D., 1988, Journal of Chemical Physics, 88, 3, 1732.
[42] Hellner, L., Besnard, M. J., Dujardin, G., and Malinovich, Y., 1988, Chemical Physics, 119, 2-3, 391.
[43] Krassig, B. and Schmidt, V., 1992, Journal of Physics B-Atomic Molecular and Optical Physics, 25, 14, L327.
[44] Ahmad, M., Lablanquie, P., Penent, F., Lambourne, J. G., Hall, R. I., and Eland, D., 2006, Journal of Physics B-Atomic Molecular and Optical Physics, 39, 17, 3599.
[45] Dawber, G., Mcconkey, A. G., Avaldi, L., Macdonald, M. A., King, G. C., and Hall, R. I., 1994, Journal of Physics B-Atomic Molecular and Optical Physics, 27, 11, 2191.
[46] Mullin, A. S., Szaflarski, D. M., Yokoyama, K., Gerber, G., and Lineberger, W. C., 1992, Journal of Chemical Physics, 96, 5, 3636.
[47] Hurley, A. C., 1962, Journal of Molecular Spectroscopy, 9, 1, 18.
[48] Taylor, P. R., 1983, Molecular Physics, 49, 6, 1297.
[49] Thulstrup, E. W. and Andersen, A., 1975, Journal of Physics B-Atomic Molecular and Optical Physics, 8, 6, 965.
[50] Wetmore, R. W. and Boyd, R. K., 1986, Journal of Physical Chemistry, 90, 22, 5540.
[51] Stalherm, D., Cleff, B., Hillig, H., and Mehlhorn, W., 1969, Zeitschrift fur Naturforschung Part A-Astrophysik Physik und Physikalische Chemie, A 24, 11, 1728.
[52] Taylor, P. R. and Partridge, H., 1987, Journal of Physical Chemistry, 91, 24, 6148.
[53] Senekowitsch, J., Oneil, S., Knowles, P., and Werner, H. J., 1991, Journal of Physical Chemistry, 95, 6, 2125.
[54] Olsson, B. J., Kindvall, G., and Larsson, M., 1988, Journal of Chemical Physics, 88, 12, 7501.
[55] Kamber, E. Y., Akgungor, K., Safvan, C. P., and Mathur, D., 1996, Chemical Physics Letters, 258, 3-4, 336.
[56] Schulz, P. A., 1985, Journal of Chemical Physics, 83, 11, 5673.
[57] Savage, H. F. and Wittebor, F. C., 1968, Journal of Chemical Physics, 48, 4, 1872.
[58] Dutuit, O., Thissen, R., and Soldi-Lose, H., 2005, -Unpublished.
[59] Manning, M., Price, S. D., and Leone, S. R., 1993, Journal of Chemical Physics, 99, 11, 8695.
[60] Harper, S. M., Hu, W. P., and Price, S. D., 2002, Journal of Physics B-Atomic Molecular and Optical Physics, 35, 21, 4409.
[61] Schwarz, H., 2004, International Journal of Mass Spectrometry, 237, 1, 75.

Chapter 4 The reactions of the Nitrogen Dication Part I: Electron Transfer Reactions of N_2^{2+} with Ne and NO

4.1 Introduction

The results of the PSCO investigation of the reactions of N_2^{2+} with NO and Ne are presented in this Chapter. This Chapter will describe the observed experimental data for the non-dissociative electron transfer reaction of Ne with N_2^{2+} and a dissociative electron transfer reaction between NO with N_2^{2+}. The scattering diagrams for these reactions are typical for many of the non-dissociative and dissociative electron transfer reactions mentioned in this thesis. The Landau-Zener model has also been used in this Chapter to probe the electronic state selectivity of the non-dissociative single electron transfer reaction between Ne and N_2^{2+}.

The electron transfer reactions of dications with neutrals have been previously well studied experimentally as mentioned earlier in the thesis, and rationalised theoretically using the 'reaction window' approach based on the Landau-Zener theory.[1, 2] The Landau-Zener reaction window theory models an electron transfer as an avoided crossing between the interspecies potential energy surfaces of the reactants and products. These potential energy surfaces have a well known, predictable approximate form for dication-neutral electron transfer reactions and the relative energies are well known for most species. The reaction window theory explains how the probability of electron transfer in a dication-neutral reaction is dependent on the interspecies separations of the crossing of the reactant and product potential energy surfaces. If the potential energy surface of the dication-neutral crosses the product potential within the reaction window (2 to 6 Å interspecies separation) the reaction is likely to proceed. The relative energies of the species and the form of the potential energy curves are well known, the reactant channel is modelled using the polarization attraction of the reactants, the repulsive product channel is modelled using simple Coulomb repulsion, and hence the interspecies separation of the curve crossing can be determined. Hence the probability of electron transfer can be determined for a particular reaction exothermicity. The electronic states of the products formed from the electron transfer reaction of each of the electronic

reactant states of interest can then be inferred from the results. The Landau-Zener reaction window theory has been explained in more detail in Chapter One.

4.2 Experimental

Experimental detail on the PSCO methodology has been given in Chapter Two, together with details of the data processing and an introduction to N_2^{2+} and the PSCO spectra features has been give in Chapter Three. However specific details of the N_2^{2+} with Ne and N_2^{2+} with NO experiments performed are as follows. PSCO spectra were recorded for the reactions of N_2^{2+} with Ne at COM collision energies of 5.53 eV, 4.17 eV and 3.75 eV, with a repeller plate voltage of 300 V, 100 V and 50 V. The PSCO spectra for the reactions of N_2^{2+} with NO were collected and recorded with a 300 V repeller plate voltage, at a 7.24 eV COM collision energy. As discussed in Chapter Two, at the high repeller plate voltages (300 V) full angular scattering is recorded, while at the lower repeller plate voltages (50 V) better energy resolution is achieved. The data sets for each reaction system were processed to extract the relevant angular and energetic information. Landau-Zener reaction window calculations are also performed for the N_2^{2+} with Ne electron transfer reaction using a customised, pre-written program.

4.3 Results and discussion

Under the specific experimental conditions for the two collision systems (N_2^{2+} with Ne and N_2^{2+} with NO) discussed in this Chapter, no bond-forming channels were observed. However, in the majority of the collision systems studied in this thesis a non-dissociative electron transfer reaction and at least one dissociative electron transfer reaction is observed. The angular scattering for non-dissociative electron transfer reactions and dissociative electron transfer reactions is very similar in all the collision systems. In sections 4.3.1 and 4.3.2 the non-dissociative electron transfer reaction of N_2^{2+} with Ne and the dissociative electron transfer reaction of N_2^{2+} with NO are used to exemplify the angular scattering for these reaction types, as well as show how Landau-Zener analysis can be used to generally rationalize such non-dissociative electron transfer reactions. Details of the relative intensities of the different channels, the reaction energetics and the reaction mechanisms are discussed.

4.3.1 N_2^{2+} with Ne

The N_2^{2+} with Ne reaction was run under 'continuous' beam conditions on the PSCO experiment. That is, no pulse was applied to the deflectors to create a pulsed dication beam. As described in Chapter Two, when running under 'continuous' beam conditions there is significant 'noise' in the spectra at *TOF*s shorter than that of the dication. This 'noise' is the detection of ions, mainly dications (N_2^{2+} but also N^+ in this case) which were beyond the reaction region upon application of voltage to the repeller plate and therefore have a shorter *TOF* than the true *TOF* of the dication. In the collision system N_2^{2+} with Ne no true singly charged ion product can have a *TOF* less than that of an ion with m/z=14. Therefore it was not imperative to run the spectra with a pulsed beam. However for most of the subsequent collision systems discussed a pulsed beam was necessary since often it was evident that potentially one of the products could have a *TOF* less than that of an ion with m/z=14. Under the experimental conditions for the N_2^{2+} with Ne collision system, N^+ as a product could not be detected. Hence the only observable channel was the non-dissociative electron transfer reaction:

$$N_2^{2+} + Ne \rightarrow N_2^{+} + Ne^{+} \qquad (4.1)$$

The pairs spectrum in Figure 4.1 shows this non-dissociative electron transfer reaction. Three isotopic channels of this reaction can clearly be seen in Figure 4.1.

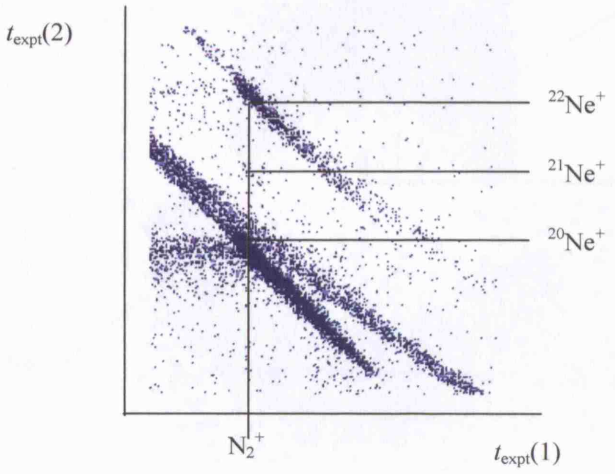

Figure 4.1 A coincidence pairs spectrum for the reaction of N_2^{2+} with Ne (4.1) at repeller plate voltage 300 V and E_{com} 4.58 eV, showing the reactions of the three isotopes, ^{20}Ne, ^{21}Ne, ^{22}Ne, and reaction peak 'tails'.

4.3.1.1 Relative intensities

Neon has three isotopes ^{20}Ne (90.5%), ^{21}Ne (0.3%) and ^{22}Ne (9.2%). In the pairs spectrum above the non-dissociative electron transfer channels with ^{20}Ne and ^{22}Ne are clearly observed. A trace of the non-dissociative electron transfer reaction with ^{21}Ne was also detected. The three channels, $N_2^+ + {}^{20}Ne^+$, $N_2^+ + {}^{21}Ne^+$, $N_2^+ + {}^{22}Ne^+$, are formed to the ratio of 264.6 : 1 : 27.6 which corresponds to (90.3 ± 1.5) % ($N_2^+ + {}^{20}Ne^+$), (0.3 ± 0.05) % ($N_2^+ + {}^{21}Ne^+$) and (9.4 ± 1.5) % ($N_2^+ + {}^{22}Ne^+$). Hence, the relative intensities of the three channels agree with the isotopic ratios.

4.3.1.2 Angular scattering

This section will show and explain the angular scattering of a non-dissociative electron transfer channel as an example for the other reaction systems studied in this thesis. The COM frame scattering diagram below was derived from the data of the non-dissociative electron transfer reaction of N_2^{2+} with ^{20}Ne. In the PSCO experiment the direction of the velocity of the COM in the LAB frame is very similar to the direction of the velocity of the dication in the COM frame. Hence the COM frame scattering diagrams are labelled relative to $\omega(N_2^{2+})$.

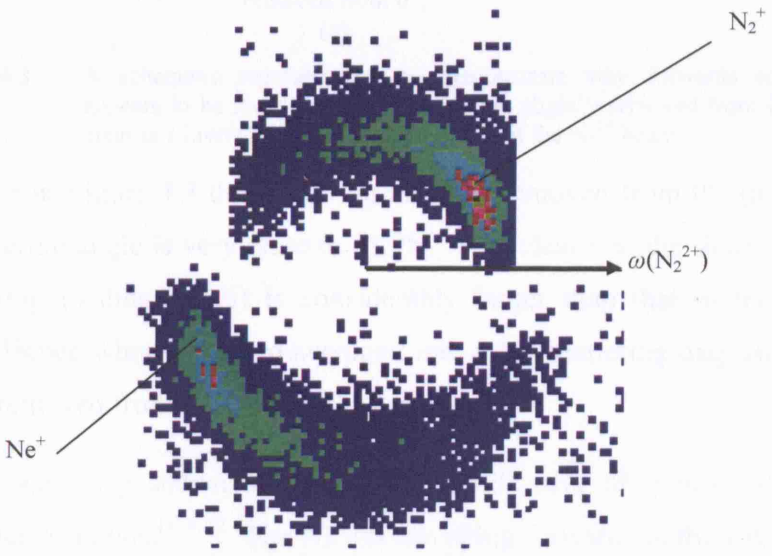

Figure 4.2 A scattering diagram product ions N_2^+ and Ne^+ (4.1) relative to the velocity of the dication in the COM frame, recorded at repeller plate voltage of 300 V and E_{com} 4.58 eV. Since the scattering angle for each ion lies between 0° and 180°, the N_2^+ ions are plotted in the top half and the Ne^+ ions in the lower half of the diagram.

The scattering diagram in Figure 4.2 shows that forward scattering dominates. That is N_2^+ and Ne^+ have mostly retained the initial COM directions of N_2^{2+} and Ne respectively. In forwards scattering the angle between the products and $\omega(N_2^{2+})$ would be 0°. However it is clear in Figure 4.2 that the scattering appears to be slightly removed from 0°. Scattering diagrams are 2D averages of a 3D system. At 0° to $\omega(N_2^{2+})$ there is only one possible direction in which the product can be scattered, where-as slightly off axis to $\omega(N_2^{2+})$ there are many possible directions through the azimuth around $\omega(N_2^{2+})$, in which the products could have been scattered. To further explain this phenomenon, both diagrams in Figure 4.3 schematically represent forwards scattering.

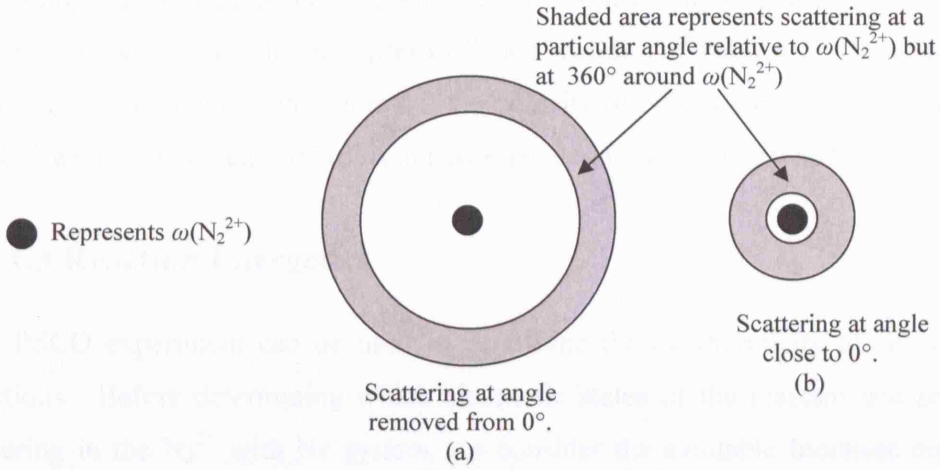

Figure 4.3 A schematic representation to demonstrate why forwards scattering appears to be more intensity at an angle slightly removed from 0°. The diagrams involve looking along the axis of the N_2^{2+} beam.

In one diagram in Figure 4.3 the scattering angle is removed from 0°, (a), while in the other the scattering angle is very close to 0°, (b). It is clear that the shaded area covered by the scattering in diagram (a) is considerably larger than that of the scattering in diagram (b). Hence when these are averaged into a 2D scattering diagram the intensity appears to be removed from 0° to $\omega(N_2^{2+})$.

The forwards scattering shown in Figure 4.2 is indicative of typical non-dissociative electron transfer reactions.[3, 4, 5] The N_2^{2+} is travelling forwards in the LAB frame while the Ne is close to stationary. Hence, in the COM frame the N_2^{2+} and Ne appear to be moving towards each other, as shown in the 'Before Collision' column of Table 4.1.

	Before Collision	After Collision (Forward Scattering)
Lab Frame	$N_2^{2+}\rightarrow$ Ne	$Ne^{+}\rightarrow$ $N_2^{+}\rightarrow$
COM Frame	$N_2^{2+}\rightarrow$ $\leftarrow$Ne	$\leftarrow Ne^{+}$ $N_2^{+}\rightarrow$

Table 4.1 The difference in the perceived directions of the reactants and products before and after the collision in the LAB and COM frames. It is important to note however that this is just a simplified schematic representation of the direction of travel, in reality very few reactions actually occur 'head on' as in the table.

As the N_2^{2+} travels past the Ne, an electron transfers from the Ne to the N_2^{2+}, forming Ne^{+} and N_2^{+}. Repulsion between these like-charged products pushes the N_2^{+} forward, continuing its original trajectory, and the Ne^{+} appears to be scattered in the opposite direction as N_2^{+}, as seen in the 'After Collision' column of Table 4.1. Hence in the COM frame scattering diagram in Figure 4.2 the velocity of N_2^{+}, is correlated with the velocity of N_2^{2+} while the velocity of Ne^{+} is anticorrelated with the velocity of N_2^{2+}.

4.3.1.3 Reaction Energetics

The PSCO experiment can be used to determine the exothermicity of dication-neutral reactions. Before determining which electronic states of the reactant and products are featuring in the N_2^{2+} with Ne system, we consider the available literature energetics to determine which electronic states are available and also review previous investigations of the N_2^{2+} with Ne system. Given that the reactant ionisation energies are known we can then use the Landau-Zener reaction window model to calculate the position of the reaction window in the collision system and, hence, the cross section of the electron transfer reaction at a given reaction exothermicities. By looking at the cross sections calculated for the different possible product channels, the product channels most likely to be present in the reaction system can be proposed. Subsequently, by comparing the literature information and the results of the Landau-Zener calculations with the experimentally derived PSCO data, we can determine the most likely electronic states interacting in the N_2^{2+} with Ne reaction.

4.3.1.4 Literature information of relevance to the N_2^{2+} and Ne reaction

As previously discussed, the reaction of N_2^{2+} with Ne has been investigated by Koslowski *et al*, Kamber *et al* and Hamdan *et al*. Table 4.2 shows the different electronic channels

proposed to feature in the N_2^{2+} with Ne electron transfer reaction by Koslowski *et al*, Kamber *et al* and Hamdan *et al*.

	Koslow-ski [6]	Kamber [7]	Hamdan [8]	ΔE (eV)
$N_2^{2+}(X^1\Sigma_g^+)+Ne(^1S)\rightarrow N_2^+(X^2\Sigma_g^+)+Ne^+(^2P_{3/2}, ^2P_{1/2})$	✓	✓	✓	5.9
$N_2^{2+}(X^1\Sigma_g^+)+Ne(^1S)\rightarrow N_2^+(A^2\Pi_{ui})+Ne^+(^2P_{3/2}, ^2P_{1/2})$	✓	✓	✓	4.7
$N_2^{2+}(X^1\Sigma_g^+)+Ne(^1S)\rightarrow N_2^+(B^2\Sigma_u)+Ne^+(^2P_{3/2}, ^2P_{1/2})$		✓		2.7
$N_2^{2+}(c^3\Sigma_u^+)+Ne(^1S)\rightarrow N_2^+(X^2\Sigma_g^+)+Ne^+(^2P_{3/2}, ^2P_{1/2})$			✓	7.4
$N_2^{2+}(c^3\Sigma_u^+)+Ne(^1S)\rightarrow N_2^+(A^2\Pi_u)+Ne^+(^2P_{3/2}, ^2P_{1/2})$	✓	✓		6.2
$N_2^{2+}(c^3\Sigma_u^+)+Ne(^1S)\rightarrow N_2^+(B^2\Sigma_u^+)+Ne^+(^2P_{3/2}, ^2P_{1/2})$		✓		4.2

Table 4.2 The electronic states proposed to feature in the N_2^{2+} with Ne electron transfer reaction by Koslowski *et al*, Kamber *et al* and Hamdan *et al*.[6, 7, 8] As previously mentioned there was originally a discrepancy in the assignment of the ground state of N_2^{2+}. Koslowski *et al* and Kamber *et al* denote the ground state as $X^1\Sigma_g^+$, while Hamdan *et al* denotes the ground state as $a^3\Pi_u$ as the ground state. The assignment of the $a^3\Pi_u$ state of N_2^{2+} as the ground state of N_2^{2+} by Hamdan *et al* is presumably due to these literature discrepancies in the labelling of the N_2^{2+} ground state. Since in fact the ground state of N_2^{2+} is the $X^1\Sigma_g^+$ state, the main electron transfer channels of N_2^{2+} and Ne seen by Hamdan *et al* actually involved the $c^3\Sigma_u^+$ electronic state and the ground electronic state, $X^1\Sigma_g^+$, of N_2^{2+}. Hence in this work $X^1\Sigma_g^+$ is shown in place of $a^3\Pi_u$ for the results of Hamdan *et al*.

It is important to consider the literature information not only to review the previous work on the N_2^{2+} with Ne electron transfer reactions but also to determine if any reactant or product electronic states can be ruled out of consideration. Experiments, reported in the literature, have determined the energies of a range of electronic states of N_2^{2+}, as discussed in Chapter Three. However, as previously mentioned and shown in Table 4.2, Koslowski *et al*, Kamber *et al* and Hamdan *et al* all conclude that the dominate reacting states of N_2^{2+} are $X^1\Sigma_g^+$ and $c^3\Sigma_u^+$.

The Ne reactant will be in its ground state, (^1S): this is expected for a neutral, thermal rare gas at room temperature. With regards to the product reactant states, Ne^+ is likely to only occupy the ground state, ($^2P_{3/2}$, $^2P_{1/2}$), as this system does not provide enough energy for Ne^+ to occupy the first excited state of Ne^+, ($^2S_{1/2}$), which is 26.9 eV above the ground state. Experiments, reported in the literature, have determined the energetics of the electronic states of N_2^+, as shown in Table 4.3. [9]

Electronic states of N_2^+	Energy/eV
$X^2\Sigma_g^+$	0
$A^2\Pi_{ui}$	1.1
$B^2\Sigma_u^+$	3.2
$a^4\Sigma_u^+$	3.2
$D^2\Pi_{gi}$	6.5
$C^2\Sigma_u^+$	8.0
$G^2\Sigma_g^+$	24.2

Table 4.3 The electronic states of N_2^+, quoted relative to the ground electronic state of N_2^+. [9]

Given the above information, in the subsequent consideration of the reaction exothermicity the only N_2^{2+} reactant states considered are the $X^1\Sigma_g^+$ and $c^3\Sigma_u^+$ states. Only the ground state of Ne and the ground state of Ne^+ are considered. All the possible states of N_2^+ shown in Table 4.3 are considered, with the exception of the $a^4\Sigma_u^+$ state since its existence has been questioned, and since it is degenerate with the N_2^+ state, $B^2\Sigma_u^+$. [9]

4.3.1.5 Landau-Zener reaction window calculations

The Landau-Zener reaction window (LZ-RW) model calculates the probability of an electron transfer reaction at a given reaction exothermicity.[1] Figure 4.4 shows the probability of electron transfer, as determined by the Landau-Zener theory, over the range of reaction exothermicities available to the N_2^{2+} with Ne collision system.

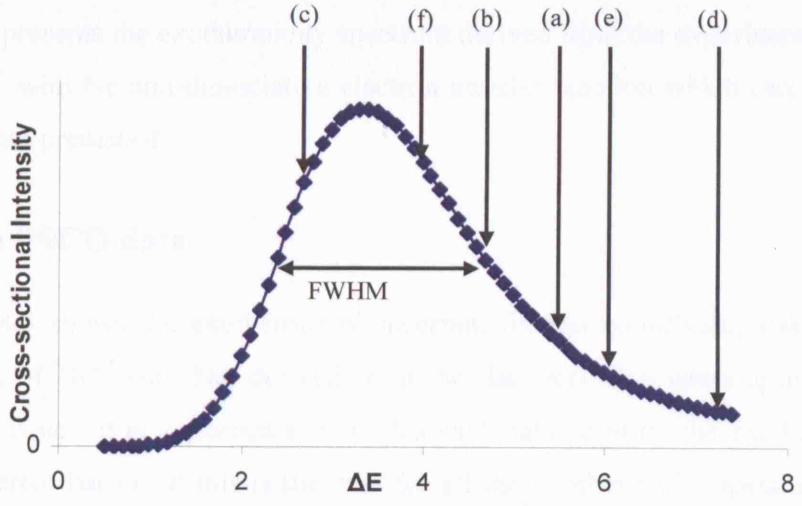

Figure 4.4 The calculated probability of electron transfer, as determined by the LZ-RW model, over the range of reaction exothermicities available to the N_2^{2+} with Ne collision system. The labels (a) to (f) cross reference with the exothermicity of the channels in Table 4.4.

According to the Landau-Zener reaction window calculations Figure 4.4, the highest probability of an electron transfer reaction is between the exothermicity of approximately

1.7 and 7.4 eV, with the dominant reaction window having a reaction exothermicity between approximately 2.3 to 4.9 eV, peaking at 3.3 eV. Table 4.4 shows the electronic states of the reactants and products for the N_2^{2+} with Ne electron transfer reaction as channels deduced from these Landau-Zener reaction window calculations. Each channel has been labelled (a) to (f) so the exothermicity of the channel can be cross referenced with the peak in the simulated PSCO exothermicity spectrum in Figure 4.4. The channels inside the Full Width, Half Maximum, FWHM, of the peak in the exothermicity spectrum should contribute the most to the reaction. Therefore the channels which have exothermicities outside the FWHM of the peak in the exothermicity spectrum, as labelled in Figure 4.4, are defined as 'minor' channels in Table 4.4.

		ΔE (eV)
$N_2^{2+}(X^1\Sigma_g^+) + Ne(^1S) \rightarrow N_2^+(X^2\Sigma_g^+) + Ne^+(^2P_{3/2}, ^2P_{1/2})$	(a)	5.9 minor
$N_2^{2+}(X^1\Sigma_g^+) + Ne(^1S) \rightarrow N_2^+(A^2\Pi_{ui}) + Ne^+(^2P_{3/2}, ^2P_{1/2})$	(b)	4.7
$N_2^{2+}(X^1\Sigma_g^+) + Ne(^1S) \rightarrow N_2^+(B^2\Sigma_u) + Ne^+(^2P_{3/2}, ^2P_{1/2})$	(c)	2.7
$N_2^{2+}(c^3\Sigma_u^+) + Ne(^1S) \rightarrow N_2^+(X^2\Sigma_g^+) + Ne^+(^2P_{3/2}, ^2P_{1/2})$	(d)	7.4 minor
$N_2^{2+}(c^3\Sigma_u^+) + Ne(^1S) \rightarrow N_2^+(A^2\Pi_u) + Ne^+(^2P_{3/2}, ^2P_{1/2})$	(e)	6.2 minor
$N_2^{2+}(c^3\Sigma_u^+) + Ne(^1S) \rightarrow N_2^+(B^2\Sigma_u^+) + Ne^+(^2P_{3/2}, ^2P_{1/2})$	(f)	4.2

Table 4.4 The reaction channels deduced from Landau-Zener calculations, labelled (a) to (f) in order to cross reference the channels with Figure 4.4.

The Landau-Zener calculations show that three channels, (b), (c) and (f), should provide the main contribution to the non-dissociative electron reaction of N_2^{2+} with Ne. The next section presents the exothermicity spectrum derived from the experimental PSCO data for the N_2^{2+} with Ne non-dissociative electron transfer reaction which can then be compared with these predictions.

4.3.1.6 PSCO data

Figure 4.5 shows the exothermicity spectrum for the non-dissociative electron transfer reaction of N_2^{2+} with Ne, derived from the data recorded when applying 50 V to the repeller plate. It is important to note that each data point on the exothermicity spectrum has an error bar on it; this is the case for all the exothermicity spectra displayed in this thesis.

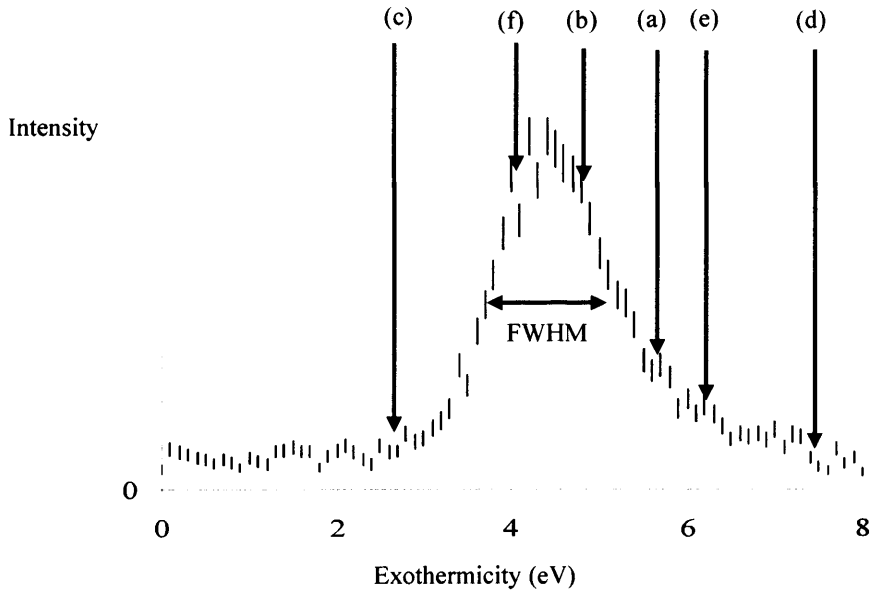

Figure 4.5 The exothermicity spectrum recorded when applying 50 V to the repeller plate for the N_2^{2+} with Ne electron transfer reaction. The different electronic channels of the reactions are denoted from (a) to (f). The channel referred to by each letter is defined in the following table, Table 4.5 as well as the previous table.

The vast majority of these reaction exothermicities lie between approximately 3 and 6 eV. However the main contributing channels will lie in the half height width of the peak which shows a spread of exothermicities between approximately between 3.5 and 5.3 eV with a maximum at approximately 4.4 eV. Table 4.5 shows the reactant and product electronic states for the N_2^{2+} with Ne system that correlate with the exothermicities recorded by the PSCO experiment. In Table 4.4 each channel has been labelled (a) to (f) so the exothermicity of the channel can be cross referenced with the peak in the PSCO exothermicity spectrum in Figure 4.5. However, the labels on the exothermicity spectra are only an indication of where the intensity related to the particular channels would be, if that channel were present in the reaction; again the channels inside the FWHM of the peak in the exothermicity spectrum are contributing the most to the reaction. Therefore the channels which feature outside the FWHM of the peak in the exothermicity spectrum, as labelled in Figure 4.5, are defined as very 'minor' channels in Table 4.5.

		ΔE (eV)
$N_2^{2+}(X^1\Sigma_g^+) + Ne(^1S) \rightarrow N_2^+(X^2\Sigma_g^+) + Ne^+(^2P_{3/2}, ^2P_{1/2})$	(a)	5.9 minor
$N_2^{2+}(X^1\Sigma_g^+) + Ne(^1S) \rightarrow N_2^+(A^2\Pi_{ui}) + Ne^+(^2P_{3/2}, ^2P_{1/2})$	(b)	4.7
$N_2^{2+}(X^1\Sigma_g^+) + Ne(^1S) \rightarrow N_2^+(B^2\Sigma_u) + Ne^+(^2P_{3/2}, ^2P_{1/2})$	(c)	2.7 minor
$N_2^{2+}(c^3\Sigma_u^+) + Ne(^1S) \rightarrow N_2^+(X^2\Sigma_g^+) + Ne^+(^2P_{3/2}, ^2P_{1/2})$	(d)	7.4 minor
$N_2^{2+}(c^3\Sigma_u^+) + Ne(^1S) \rightarrow N_2^+(A^2\Pi_u) + Ne^+(^2P_{3/2}, ^2P_{1/2})$	(e)	6.2 minor
$N_2^{2+}(c^3\Sigma_u^+) + Ne(^1S) \rightarrow N_2^+(B^2\Sigma_u^+) + Ne^+(^2P_{3/2}, ^2P_{1/2})$	(f)	4.2

Table 4.5 The reaction channels correlating with the PSCO data. The minor channels are those which are outside the FWHM region of the peak in the PSCO exothermicity spectrum.

Therefore, as seen in Table 4.5, the PSCO exothermicity spectrum can be explained by two main contributing electronic channels, channels (b) and (f). The fact that we only observe one peak, as opposed to a defined peak for each channel, in the exothermicity spectrum can be attributed to the population of a range of vibrational states of the N_2^{2+} reactant and the N_2^+ product which therefore overlap in energy. In purely atomic systems, such as Ar^{2+} with Ne, separate peaks for each channel can be observed in the PSCO exothermicity spectra.[4, 10] The next section summarises and compares the literature review, the Landau-Zener calculations and the PSCO experimental data for the reaction exothermicity of the N_2^{2+} with Ne reaction.

4.3.1.7 Exothermicity conclusions

The literature shows that the main reacting states of N_2^{2+} are $X^1\Sigma_g^+$ and $c^3\Sigma_u^+$ in the reaction of N_2^{2+} with Ne, and that it is not necessary to include the $a^4\Sigma_u^+$ state of N_2^+. Taking into account these considerations, the dominant reaction channels predicted by the Landau-Zener calculations and those observed experimentally in the PSCO data have been determined above. These reaction channels are shown in Table 4.6.

	Literature			Landau -Zener	PSCO Data	ΔE (eV)
	Koslo-wski [6]	Kam-ber [7]	Ham-dan [8]			
Collision Energy	400 eV	28 eV	6 keV			
$N_2^{2+}(X^1\Sigma_g^+)+Ne \rightarrow N_2^+(X^2\Sigma_g^+)+Ne^+$	✓		✓			5.9
$N_2^{2+}(X^1\Sigma_g^+)+Ne \rightarrow N_2^+(A^2\Pi_{ui})+Ne^+$	✓	✓	✓	✓	✓	4.7
$N_2^{2+}(X^1\Sigma_g^+)+Ne \rightarrow N_2^+(B^2\Sigma_u)+Ne^+$		✓		✓		2.7
$N_2^{2+}(c^3\Sigma_u^+)+Ne \rightarrow N_2^+(X^2\Sigma_g^+)+Ne^+$			✓			7.4
$N_2^{2+}(c^3\Sigma_u^+)+Ne \rightarrow N_2^+(B^2\Sigma_u^+)+Ne^+$		✓		✓	✓	4.2

Table 4.6 A summary of the major reaction channels for the N_2^{2+} with Ne electron transfer reaction in the literature, Landau-Zener calculations and the PSCO data.

Table 4.6 shows that for the N_2^{2+} with Ne electron transfer reaction the PSCO experimentally derived exothermicities agree with those observed in experiments in literature as well as with the Landau-Zener calculations. Certainly the exothermicities observed in the PSCO experiment can be explained using only the $X^1\Sigma_g^+$ and $c^3\Sigma_u^+$ electronic states of N_2^{2+}. Generally the previous studies of this reaction show that the product N_2^+ is formed in its ground state, $X^2\Sigma_g^+$ and its first and second excited states, $A^2\Pi_u$ and $B^2\Sigma_u^+$. However only the $A^2\Pi_u$ and $B^2\Sigma_u^+$ states of N_2^+ feature as major channels in the PSCO experiment and the Landau-Zener calculations. This can be attributed to the fact the PSCO operates at a lower collision energy than the experiments used in the previous studies and hence the PSCO experiment is more state selective as would be expected from reaction window theory at lower collision energies. Finally it is important to note that the Landau-Zener calculations show a significant electron transfer cross-section over a 'broad' range of reaction exothermicities, as do the PSCO exothermicity spectrum, for the non-dissociative electron transfer reaction of the N_2^{2+} with Ne, even though we have concluded there are only a small number of electronic channels contributing to the reaction exothermicity. The broad nature of the spectra is understandably due to the involvement of different vibrational states of the molecular species, N_2^{2+} and N_2^+.

In conclusion, a typical non-dissociative electron transfer reaction has been described, showing how the PSCO technique can be used to derive angular scattering diagrams as well as derive information regarding the reaction exothermicity. Of course a non-dissociative electron transfer reaction is only a two-body reaction. The angular scattering could therefore be determined simply detecting one product and using the conservation of momentum to determine the angular scattering of the second product. In contrast dissociative electron transfer reactions always have at least three reaction products, as do many bond-forming reactions, therefore detecting ion pairs using the PSCO technique is very useful for the determination of the angular scattering of three-body product reactions. The next section will describe a typical dissociative electron transfer reaction.

4.3.2 N_2^{2+} with NO

The PSCO experiment has been used to study the collisions of N_2^{2+} with NO. Four channels were observed in the coincidence spectrum: one non-dissociative electron transfer reaction, (4.2) and three dissociative electron transfer reactions, (4.3), (4.4) and (4.5).

$$N_2^{2+} + NO \rightarrow N_2^{+} + NO^{+} \quad (4.2)$$
$$N_2^{2+} + NO \rightarrow N_2^{+} + O^{+} + N \quad (4.3)$$
$$N_2^{2+} + NO \rightarrow N_2^{+} + N^{+} + O \quad (4.4)$$
$$N_2^{2+} + NO \rightarrow NO^{+} + N^{+} + N \quad (4.5)$$

A section of the coincidence spectrum is shown in Figure 4.6, showing the three dissociative electron transfer reactions: (4.3), (4.4) and (4.5).

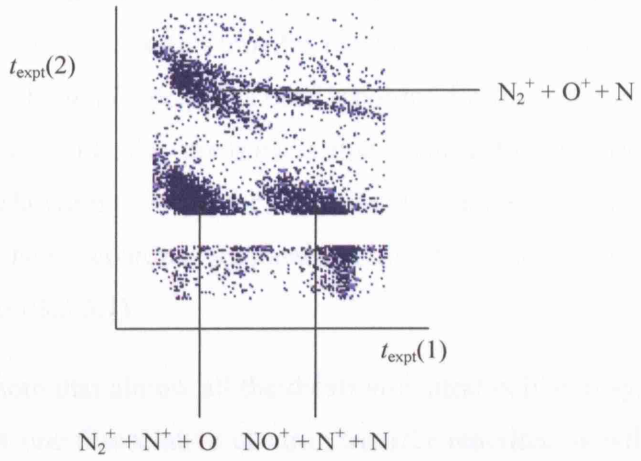

Figure 4.6 A section of a coincidence pairs spectrum for the reaction of N_2^{2+} with NO, showing the three dissociative charge transfer reactions, (4.3), (4.4) and (4.5). This pairs spectrum was recorded using a 300 V repeller plate, at a 7.24 eV COM collision energy.

The pairs spectrum has been collected using a pulsed beam but as can be seen in Figure 4.6, a horizontal section has been cut from the pairs collection where the false coincidences lie. In an early version of the pairs acquisition program, the total number of pairs collected in one coincidence spectrum was limited. This meant that if false coincidences were collected then the total number of pairs would rapidly be accumulated and only a small number of true reaction pairs would be collected. Therefore in order to allow long collection times for the true reactions, the omission of false coincidences was essential. Although this Chapter discusses the electron transfer reactions of dication-neutral reactions, generally this thesis concentrates on the bond-forming reactions in dication-neutral systems. When the omission of false coincidences from the pairs spectrum began to obstruct the data collection for the bond-forming reactions (for

example, those with a N^+ product), the program was significantly redeveloped to prevent the number of pairs from limiting the data collection. Hence, with the extension of the pairs collection, it was no longer necessary to omit the false coincidences from collection.

After the update in the data acquisition program, where necessary, the collection of coincidence spectra for reactions with bond-forming channels was repeated in order to collect the whole peak of a bond-forming reaction. With regards to the reaction channels observed following the collisions of N_2^{2+} with NO, the data collection of one of the dissociative electron transfer reactions (4.3) has not been obstructed by false coincidence cutting but the cutting of the false coincidences has obstructed the data collection for channels (4.4) and (4.5), which have a N^+ product. The omission of false coincidences makes analysis of the angular scattering and reaction exothermicity difficult, as a significant portion of the information has not been recorded. However this section only discusses one dissociative electron transfer reaction, as an example, $N_2^+ + O^+ + N$ (4.3), since the data from the whole peak has been recorded for this channel. The only issue the omission of false coincidences presents is that some estimates had to be made in the determination of relative intensities for channels (4.4) and (4.5). Given that only parts of the channels have been recorded, reasonable estimation was possible, as detailed in the next section (section 3.3.6.1).

It is important to note that almost all the dication-neutral collision systems studied in this thesis have at least one dissociative electron transfer reaction, as will become evident in the later Chapters. This significant occurrence of electron transfer reactions is not unexpected since electron transfer reactions have the highest probability of occurring in most dication-neutral collision systems. [11] Whether the electron transfer channel is dissociative or non-dissociative is dependent on the stability of the initial monocations formed after electron transfer.

Non-dissociative electron transfer

$$A_2^{2+} + B_2 \rightarrow A_2^+ \text{ (stable)} + B_2^+ \text{ (stable)} \rightarrow A_2^+ + B_2^+ \quad (4.6)$$

Dissociative electron transfer

$$A_2^{2+} + B_2 \rightarrow A_2^+ \text{ (stable)} + B_2^+ \text{ (unstable)} \rightarrow A_2^+ + B^+ + B \quad (4.7)$$
$$A_2^{2+} + B_2 \rightarrow A_2^+ \text{ (unstable)} + B_2^+ \text{ (stable)} \rightarrow A^+ + A + B_2^+ \quad (4.8)$$
$$A_2^{2+} + B_2 \rightarrow A_2^+ \text{ (unstable)} + B_2^+ \text{ (unstable)} \rightarrow A^+ + A + B^+ + B \quad (4.9)$$

If unstable species are formed they will dissociate and hence the channel is a dissociative electron transfer channel. As previously mentioned, in this collision system we observed

a non-dissociative electron transfer reaction and three dissociative electron transfer reactions. Two of the dissociative electron transfer reactions, (4.3) and (4.4), were of the type (4.7), where after electron transfer the $[NO]^+$ has dissociated, with the only difference being whether the charge remained on the O or the N;

$$A_2^{2+} + B_2 \rightarrow A_2^+ \text{ (stable)} + B_2^+ \text{ (unstable)} \rightarrow A_2^+ + B^+ + B \quad (4.7)$$
$$N_2^{2+} + NO \rightarrow N_2^+ + O^+ + N \quad (4.3)$$
$$N_2^{2+} + NO \rightarrow N_2^+ + N^+ + O \quad (4.4)$$

The remaining dissociative electron transfer reaction, (4.5), is of type (4.8) where the monocation product (N_2^+) formed from the parent dication (N_2^{2+}) after electron transfer has dissociated;

$$A_2^{2+} + B_2 \rightarrow A_2^+ \text{ (unstable)} + B_2^+ \text{ (stable)} \rightarrow A^+ + A + B_2^+ \quad (4.8)$$
$$N_2^{2+} + NO \rightarrow N^+ + N + NO^+ \quad (4.5)$$

The following section discusses the relative intensities of the four different channels observed in the N_2^{2+} with NO collision systems. The next section also explains how accurate estimates were made for the intensity of those peaks with an area of missing data due to false coincidence exclusion. Similar methodology is also used later to determine the relative intensities of other channels with missing data in the study of bond-forming reactions.

4.3.2.1 Relative intensities

Despite the omission of the false coincidences from reaction (4.4), the coincident peak shape and pairs intensity distribution of reactions (4.3) and (4.4) were observed to be very similar. In both coincidence peaks the intensity decreased as $t_{expt}(1)$ increased and $t_{expt}(2)$ decreased. Therefore the number of counts in the missing section of reaction peak (4.4) was accurately estimated by relatively scaling the number of counts in the same area of reaction peak (4.3) with the number of counts in the rest of the peaks as shown in Figure 4.7.

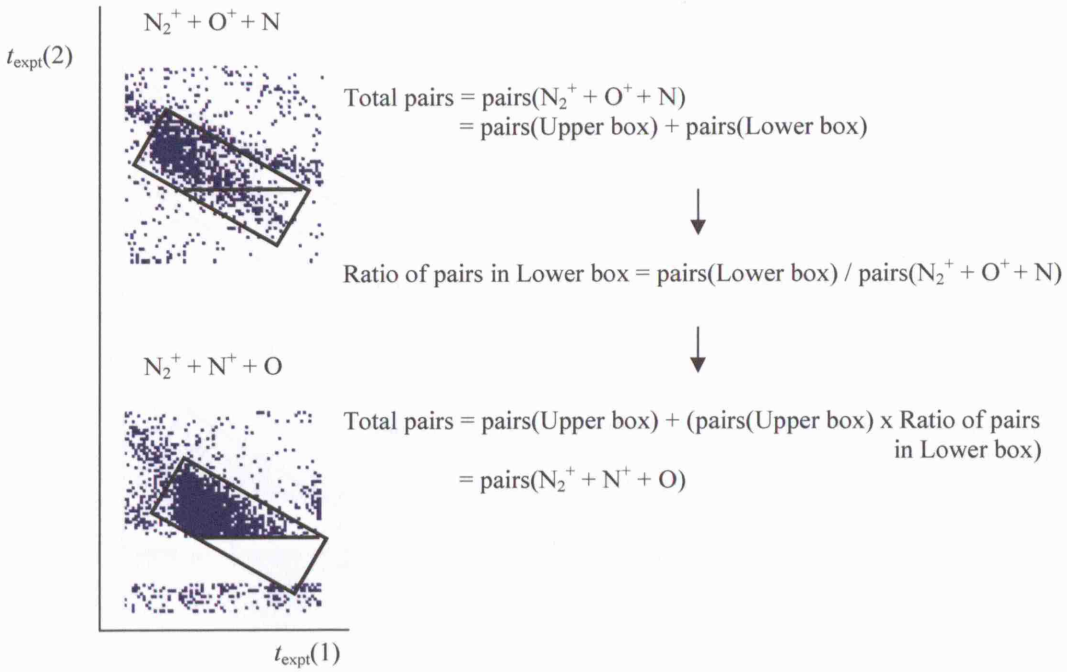

Figure 4.7 Estimating the total number of pairs in reaction (4.4) by estimating the number of pairs in the 'missing' section using a comparison with reaction (4.3).

The peak shape of reaction (4.5) is slightly different to that of the peaks of reactions (4.3) and (4.4). That is the intensity of pairs in reaction (4.5) appeared perhaps to be greater in the lower part of the peak as opposed to the upper part as seen in reaction peaks (4.3) and (4.4). The greater intensity in the lower half of the peak can not be attributed simply to the false coincidences as it extends beyond the area of the false coincidences. Therefore, if the intensity of the peak is estimated using the method described in Figure 4.7, the intensity would be underestimated. Hence, the number of counts in the missing area of reaction peak (4.5) is estimated using the method shown in Figure 4.8.

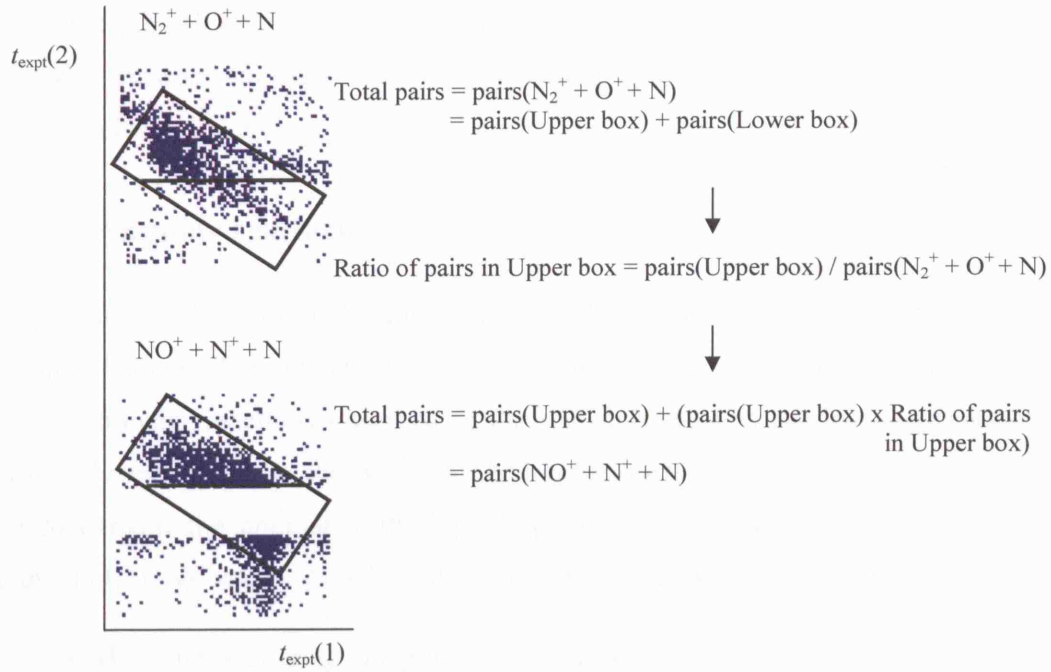

Figure 4.8 Estimating the total number of pairs in reaction (4.5) by estimating the number of pairs in the 'missing' section using a comparison with reaction (4.3).

The four channels observed in the reaction of N_2^{2+} with NO, $N_2^+ + NO^+$ (4.2), $N_2^+ + O^+ + N$ (4.3), $N_2^+ + N^+ + O$ (4.4) and $NO^+ + N^+ + N$ (4.5), were formed in the ratio 5.7 : 1 : 4.1(estimate) : 2.7(estimate). Therefore the non-dissociative electron transfer reaction, (4.2), was more intense than the dissociative electron transfer reactions (4.3), (4.4) and (4.5). Although the relatively intensities of the dissociative electron transfer reactions with an N^+ product, (4.4) and (4.5) were estimated it does appear that these reactions were more intense than the dissociative electron transfer reaction with an O^+ product, (4.3). As discussed in section 3.3.6, channel $NO^+ + N^+ + N$ (4.5) is accessed in a different way to channels $N_2^+ + O^+ + N$ (4.3) and $N_2^+ + N^+ + O$ (4.4) so it is not surprising that the relative intensities are different. However given the mechanistic similarity of reactions (4.3) and (4.4) it is particularly interesting that channel $N_2^+ + N^+ + O$ (4.4) is about four times as intense as channel $N_2^+ + O^+ + N$ (4.3). If we consider the dissociation of NO^+ to form ground state N^+ and O or N and O^+, the dissociation to form ground state N^+ and O is just slightly more exothermic than the dissociation of ground state NO^+ to form ground state N and O^+. Therefore the relative intensities are implying that the more exothermic channel is more favourable. However the difference in the relative formation of N and O^+ and N^+ and O from [NO^+] is most likely to be due to different electronic states of [NO^+] populated. The potential energy surfaces of NO^+ shows that population of the first excited of NO^+ should result in $N + O^+$. [12] However the next seven excited states of

NO^+, at least, dissociate to form $N^+ + O$. These states are energetically accessible and hence the population of these states explains the relative intensities observed. [12] The following section will discuss the angular scattering of the dissociative electron transfer reaction, channel (4.3).

4.3.2.2 Angular scattering

This section will show and explain the angular scattering of a dissociative electron transfer channel. The scattering diagrams shown are typical of those of the dissociative electron transfer reactions observed in the collision systems studied in this thesis. As previously mentioned in the N_2^{2+} with NO collision system, the appropriate reaction to use to explain the angular scattering of a dissociative electron transfer reaction was channel (4.3), $N_2^+ + O^+ + N$, where data from the whole peak has been recorded.

The COM frame scattering diagram in Figure 4.9 was derived from the data of the dissociative electron transfer reaction, (4.3), of N_2^{2+} with NO. Since in the PSCO experiment the direction of the COM is very similar to the direction of the dication in the COM frame, the COM frame scattering diagrams are labelled relative to $\omega(N_2^{2+})$.

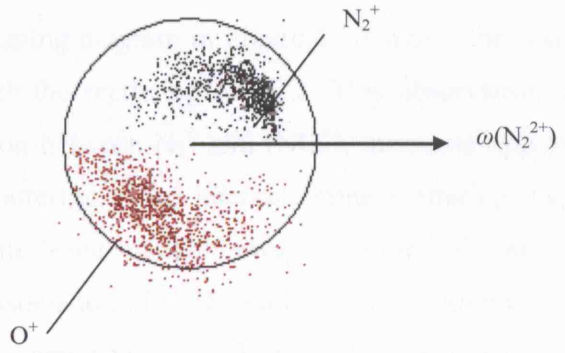

Figure 4.9 A scattering diagram, circle radius 1 cm μs^{-1}, showing N_2^+ and O^+ relative to the velocity of the dication in the COM frame, recorded at a 300 V repeller plate, with a 7.24 eV COM collision energy.

Figure 4.9 shows that forwards scattering of the ionic reaction products dominates, in the COM frame. Therefore N_2^+ has mostly retained the initial COM direction of N_2^{2+}, while O^+ is scattered in the opposite direction to N_2^{2+}. Although not shown in the figure, the N is also scattered in the opposite direction to N_2^{2+}. The forward scattering of all three products indicates that no complexation occurred during the reaction; therefore the reaction was a typical dissociative electron transfer reaction. The fact O^+ and N are both forward scattered, in the opposite direction to N_2^+, shows that the electron was transferred

from the NO to N_2^{2+}, with the $[NO^+]$ subsequently dissociating to O^+ and N as seen in mechanism (4.10).

$$N_2^{2+} + NO \rightarrow N_2^+ + [NO^+] \text{ then } [NO^+] \rightarrow N + O^+ \qquad (4.10)$$

The strong Coulomb repulsion between the two like charged species N_2^+ and $[NO^+]$ dominates the scattering. The internal frame scattering diagrams show whether the $[NO]^+$ dissociated inside or outside the field of the N_2^+. Figure 4.10 shows an internal frame scattering diagram, showing O^+ and N relative to N_2^+.

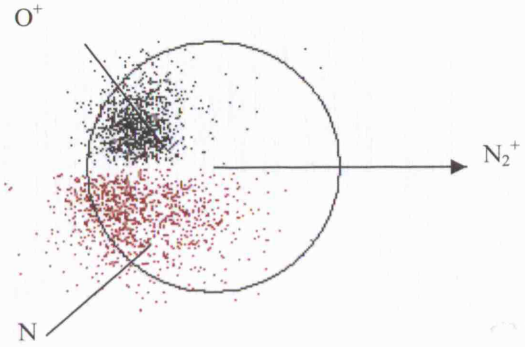

Figure 4.10 A scattering diagram, circle radius 1 cm μs^{-1}, showing N and O^+ relative to N_2^+ in the internal frame, recorded at a 300 V repeller plate, at a 7.24 eV COM collision energy.

The internal frame scattering diagram in Figure 4.10 shows the scattering of both N and O^+ is anticorrelated with the scattering of N_2^+. This observation is in accord with the initial Coulomb repulsion between N_2^+ and $[NO^+]$, momenta approximately 15 amu cm μs^{-1}, dominating the scattering. The internal frame scattering diagram in Figure 4.10 shows that the O^+ and the N are scattered away from the N_2^+ with very similar velocities as each other. If the dissociation of $[NO]^+$ had occurred within the field of N_2^+ then only the O^+ would have been accelerated away from the N_2^+ due to Coulomb repulsion. Hence a difference in the velocities of O^+ and N would have been observed in the internal frame scattering diagram. However it is clear that the velocity of O^+ and N are very similar implying that the dissociation of $[NO]^+$ to O^+ and N was relatively slow; occurring outside the field of the N_2^+ product, therefore both products retained the initial velocity of the $[NO]^+$, approximately 0.75 cm μs^{-1}, upon dissociation.

Therefore to conclude, the scattering seen in the COM and internal frame scattering diagrams in Figure 4.9 and Figure 4.10 is indicative of typical dissociative electron transfer reactions, in particular slow dissociative electron transfer reactions. The following section shows the exothermicity spectrum for this, (4.3), dissociative electron transfer reaction.

4.3.2.3 Reaction Energetics

The PSCO experiment was used to determine the exothermicity of the N_2^{2+} with NO reactions. Figure 4.11 shows the exothermicity spectrum for the dissociative electron transfer reaction, (4.3).

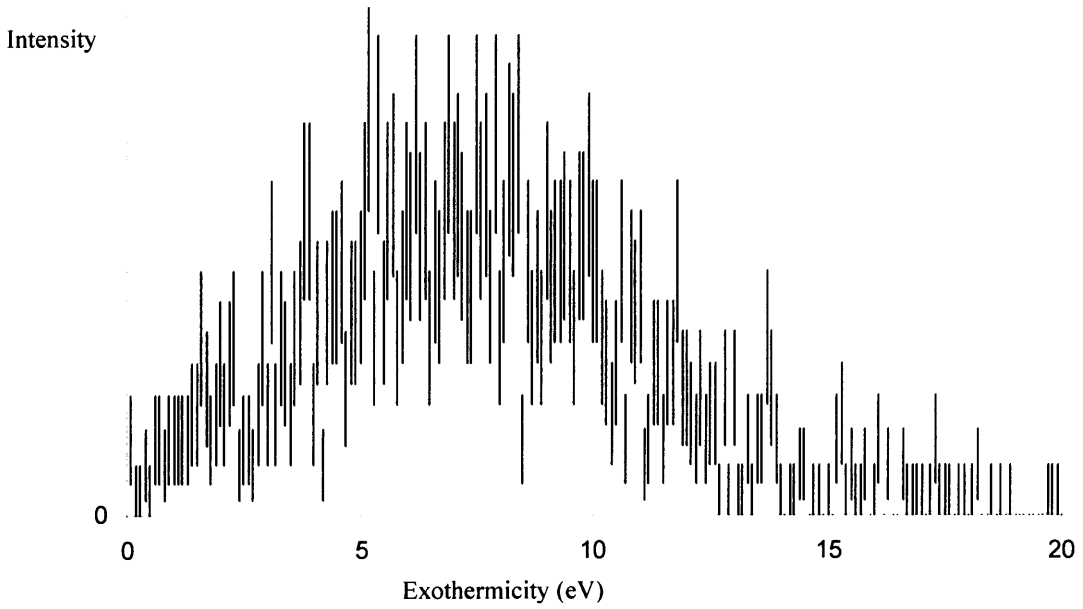

Figure 4.11 The exothermicity spectrum recorded when applying a 300 V to the repeller plate, derived from the data of the dissociative electron transfer reaction, (4.3).

Since no bond-forming reactions were observed in the reaction of N_2^{2+} with NO, the experiment was only performed with the application of a 300 V to the repeller plate. When applying a 300 V to the repeller plate, the resolution of the exothermicity spectrum is not optimal. Hence the exothermicity spectrum, for reaction (4.3), in Figure 4.11 is broad and unresolved. However some conclusions can be drawn. The exothermicity spectrum shows that all the reactions have an exothermicity between 0 and 13 eV, with the majority of the reactions having an exothermicity between 4 and 10 eV. The peak of the exothermicity spectrum is at approximately 7 eV. This peak at 7 eV agrees well with reaction (4.3) where all the reactants and products are in their ground states, which has a literature exothermicity of 7.3 eV.[9] The intensity observed below 7.3 eV can be attributed to the population of the product N_2^+ in excited vibrational or electronic states and/or the population of excited state O^+ and/or N. The intensity observed above 7.3 eV can only be attributed the population of excited vibrational or electronic states of the dication. A reaction of the $c^3\Sigma_u^+$ state of N_2^{2+} to form ground state products has a literature exothermicity of 8.8 eV.

4.4 Conclusion

Two reactions are discussed in this Chapter; the non-dissociative charge transfer reaction of N_2^{2+} with Ne and the dissociative charge transfer reaction of N_2^{2+} with NO. In these reaction systems, no bond-forming reactions were observed. Non-dissociative charge transfer reactions, which involve the simple transfer of an electron from the neutral to dication, and dissociative charge transfer reactions, which involve the transfer of an electron from the neutral to the dication followed by the subsequent dissociation of one of the monocations, are observed in most dication-neutral reaction systems.

4.5 References

[1] Rogers, S. A., Price, S. D., and Leone, S. R., 1993, Journal of Chemical Physics, 98, 1, 280.
[2] Manning, M., Price, S. D., and Leone, S. R., 1993, Journal of Chemical Physics, 99, 11, 8695.
[3] Herman, Z., Zabka, J., Dolejsek, Z., and Farnik, M., 1999, International Journal of Mass Spectrometry, 192, 191.
[4] Harper, S. M., Hu, W. P., and Price, S. D., 2002, Journal of Physics B-Atomic Molecular and Optical Physics, 35, 21, 4409.
[5] Hu, W. P., Harper, S. M., and Price, S. D., 2005, Molecular Physics, 103, 13, 1809.
[6] Koslowski, H. R., Lebius, H., Staemmler, V., Fink, R., Wiesemann, K., and Huber, B. A., 1991, Journal of Physics B-Atomic Molecular and Optical Physics, 24, 23, 5023.
[7] Hamdan, M. and Brenton, A. G., 1989, Journal of Physics B-Atomic Molecular and Optical Physics, 22, 1, L9.
[8] Kamber, E. Y., Akgungor, K., Safvan, C. P., and Mathur, D., 1996, Chemical Physics Letters, 258, 3-4, 336.
[9] NIST Chemistry WebBook, National Institute Of Standards and Technology, 2003, http://webbook.nist.gov.
[10] Hu, W. P., Harper, S. M., and Price, S. D., 2002, Measurement Science & Technology, 13, 10, 1512.
[11] Price, S. D., 2003, Physical Chemistry Chemical Physics, 5, 9, 1717.
[12] Albritton, D. L., Schmeltekopf, A. L., and Zare, R. N., 1979, Journal of Chemical Physics, 71, 8, 3271.

Chapter 5 The reactions of the Nitrogen Dication Part II: Bond-forming reactions of N_2^{2+} with O_2, CO_2 and H_2O

5.1 Introduction

The concentrations of N_2^{2+} dications have been predicted through modelling of the ionosphere of Earth and Titan. [1, 2] The N_2^{2+} dications predicted to be present in the terrestrial ionosphere are thought to be lost by dissociative recombination with electrons and by collisions with the abundant neutral species N_2, O_2 and O. We have therefore studied the reactive collisions of N_2^{2+} and O_2. In order to get an overall mechanistic picture of the reactivity of N_2^{2+} with neutrals we have also studied the reactions of N_2^{2+} with neutral gases of lower abundance in the terrestrial ionosphere such as CO_2 and H_2O (also see Chapter Four for the terrestrially relevant reactions of N_2^{2+} with Ne and NO and Chapter Six for the terrestrially relevant reactions of N_2^{2+} with CH_4, H_2 and Ar). A more detailed introduction to the ionosphere of Earth is given in Chapter One.

Since an introduction to N_2^{2+} and its reactions has been given in Chapter Three, this section will just give a brief overview of the previous work on the reactions of N_2^{2+} with O_2, CO_2 and H_2O which has been published. The electron transfer cross sections of N_2^{2+} with CO_2 and H_2O have been studied. [3] The reaction of N_2^{2+} with O_2 has been previously investigated by Kamber *et al*, but there is no mention of bond-forming channels in their paper. [4] Although unpublished as yet, the formation of NO^+ from the reaction of N_2^{2+} with O_2 was observed by Dutuit *et al.* [5] In this Chapter we discuss the reactions of N_2^{2+} with O_2, CO_2 and H_2O at relatively low collision energies (between 9 eV and 14 eV). These reactions have been grouped together as most of the proposed reaction mechanisms for the observed bond-forming channels are similar.

5.2 Experimental

Experimental details are given in Chapter Two, together with details of the data processing. [6] Specific details of the N_2^{2+} experiments with O_2, CO_2 and H_2O are as follows. The bimolecular reactions between N_2^{2+} and O_2 (section 4.3.1) have been studied at a range of COM collision energies (4.3, 5.0, 7.1, 7.5, 9.2 and 11.7 eV) with a

repeller plate voltage of 300 V to attain full angular scattering and at a COM collision energy of 4.4 eV with a lower repeller plate voltage of 100 V to try and achieve better energy resolution in the exothermicity spectra. The reaction of N_2^{2+} and CO_2 has been studied, at COM collision energies 4.5 eV and 7 eV, with a repeller plate voltage of 50 V and 300 V respectively. The PSCO spectra were recorded for the reactions of N_2^{2+} with H_2O at repeller plate 300 V with a 5.5 eV COM collision energy.

5.3 Results and discussion

In this Chapter, the bond-forming reactions of N_2^{2+} with O_2, CO_2 and H_2O are presented.[7] Details of the relative intensities of the different product formation channels, the reaction energetics and the reaction mechanisms derived from the PSCO experiments are discussed. The reaction energetics and reaction mechanisms are determined by analysis of the exothermicity spectra and the angular scattering diagrams derived from the PSCO data. For details of the derivation of the exothermicity spectrum and angular scattering diagrams from the PSCO data, see Chapter Two. As discussed in Chapter Three, in the reactions of N_2^{2+} with neutrals, some reaction channels have a N^+ product ion, hence the relevant coincidence peak lies in the same position as 'false coincidences'. These false coincidences stem from the coincident detection of an unreacted ion with either a random ion arrival or with one of the products of the reaction of an N_2^{2+} ion from the same pulse. Chapter Three details how the false coincidences are easily identified, and removed from the dataset before performing relative intensity analysis, or presenting angular scattering diagrams and reaction exothermicity histograms, for any reaction with an N^+ product ion.

A vast amount of chemistry has been observed in this survey of the reactions of N_2^{2+} with neutrals so only the bond-forming reactions are discussed in detail here, as other reaction types have been well rationalised previously (for some details on typical electron transfer reactions see Chapter Four, sections 4.3.1 and 4.3.2). Sections 4.3.1, 4.3.2 and 4.3.3 of this Chapter cover the bond-forming reactions of N_2^{2+} with O_2, CO_2 and H_2O respectively.

5.3.1 N_2^{2+} with O_2

The reaction of N_2^{2+} with O_2 has been published by Ricketts *et al.*[7] Five dominant bimolecular reactions can clearly be seen in the coincidence (pairs) spectra following

collisions of N_2^{2+} with O_2. The reactions observed are listed below and correspond to non-dissociative electron transfer, (5.1), dissociative electron transfer, (5.2) and (5.3), and two bond-forming channels, (5.4) and (5.5).

$$N_2^{2+} + O_2 \rightarrow N_2^{+} + O_2^{+} \quad (5.1)$$
$$N_2^{2+} + O_2 \rightarrow N_2^{+} + O^{+} + O \quad (5.2)$$
$$N_2^{2+} + O_2 \rightarrow O_2^{+} + N^{+} + N \quad (5.3)$$
$$N_2^{2+} + O_2 \rightarrow NO^{+} + O^{+} + N \quad (5.4)$$
$$N_2^{2+} + O_2 \rightarrow NO^{+} + N^{+} + O \quad (5.5)$$

A section of a typical coincidence spectrum, showing the two dissociative electron transfer reactions, (5.2) and (5.3), and the two bond-forming reactions, (5.4) and (5.5), is shown in Figure 5.1.

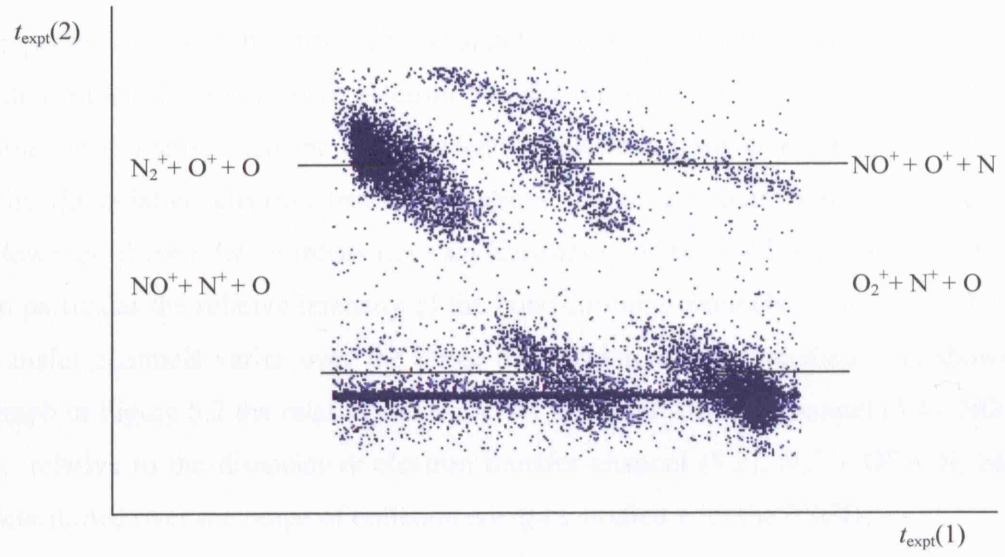

Figure 5.1 A section of the coincidence spectrum recorded following collisions of N_2^{2+} with O_2 at a COM collision energy 7.08 eV with a repeller plate voltage of 300 V. The horizontal line which runs through the reaction channels $NO^+ + N^+ + O$ and $O_2^+ + N^+ + O$ arises from false coincidences with unreacted ions in the dication beam as explained in Chapter Three, section 3.3.3. The origin of the 'tail' running from the channel $N_2^+ + O^+ + O$ arises from reactions outside the source region as described in Chapter Three, section 3.3.4.

The next section details the relative intensities of all the reactions following the collisions of N_2^{2+} with O_2, observed in the coincidence spectrum, at the range of low collision energies studied.

5.3.1.1 Relative intensities

The relative intensities of the different reactive channels observed in the pairs spectrum, can be measured by comparing the numbers of counts in each coincidence peak in the pairs spectrum. Section 4.3.1.2 discusses the angular scattering for the bond-forming reactions of N_2^{2+} with O_2; the angular scattering diagrams clearly reveal that these bond-forming reactions feature a high number of sideways scattered events. Hence the relative intensities are determined from the PSCO data recorded when using a 300 V repeller plate voltage where these sideways scattered events are recorded.

At the COM collision energy of 7.1 eV the non-dissociative electron transfer, dissociative electron transfer and bond-forming channels, reactions (5.1), (5.2), (5.3), (5.4) and (5.5), give relative intensities in an approximate ratio of 7 : 5 : 5 : 1 : 1 (to 0 decimal places) respectively. The bond-forming channels are approximately four to five times less intense than the dissociative electron transfer reactions and approximately five to seven times less intense than the non-dissociative electron transfer reaction at COM 7.1 eV. The dissociative electron transfer reactions are of approximately the same intensity. However, these relative intensities vary depending on the collision energy of the system. In particular the relative intensity of the bond-forming channels compared to the electron transfer channels varies over the range of collision energies studied. As shown by the graph in Figure 5.2 the relative intensities of the bond-forming channel (5.4), $NO^+ + O^+ + N$, relative to the dissociative electron transfer channel (5.2), $N_2^+ + O^+ + N$, have been determined over the range of collision energies studied with the PSCO.

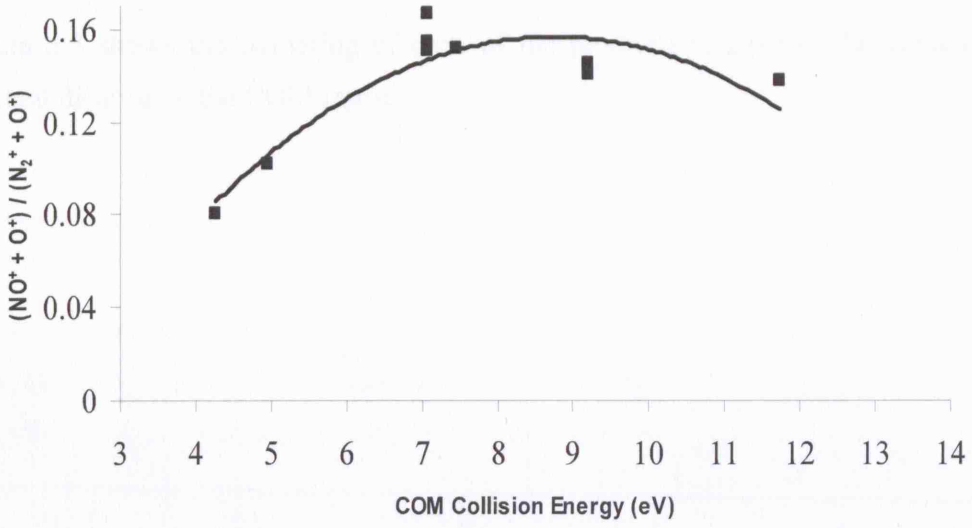

Figure 5.2 The intensity of reaction (5.4) against the intensity of reaction (5.2), as a function of the COM collision energy.

Even over the range of collision energies studied, there is a noticeable variation in the relative intensities of the channels. Certainly at the lowest collision energies studied, approximately 4 and 5 eV, the bond-forming channels become significantly weaker relative to the electron transfer reactions than at the higher collision energies studied. However at the highest COM collision energy studied of approximately 12 eV, there is a decrease in the intensity of the bond-forming channels compared to the dissociative electron transfer channels. Therefore the bond-forming channels are most intense, relative the electron transfer channels, at approximately 7 eV. Hence subsequently most of the collision systems are studied at approximately 7 eV in this thesis to optimise the intensity of the bond-forming channels. This study, of the effect of the collision energy on the relative intensity of the dication–neutral bond-forming channels, emphasises the necessity to determine accurate cross sections at a range of collision energies, to further study the effects of collision energy on these ionospherically relevant reactions. In the next section, section 4.3.1.2, the reaction mechanism of the bond-forming channels is derived from the angular scattering data.

5.3.1.2 Angular scattering

The mechanisms of the bond-forming reactions (5.4) and (5.5) detected in the pairs spectrum are derived from the analysis of angular scattering diagrams derived from the PSCO data recorded using a 300 V repeller plate in order to record full angular distributions of the reaction products.

5.3.1.2.1 The formation of $NO^+ + O^+ + N$

Figure 5.3 shows the scattering of each of the products relative to the velocity of the reactant dication in the COM frame.

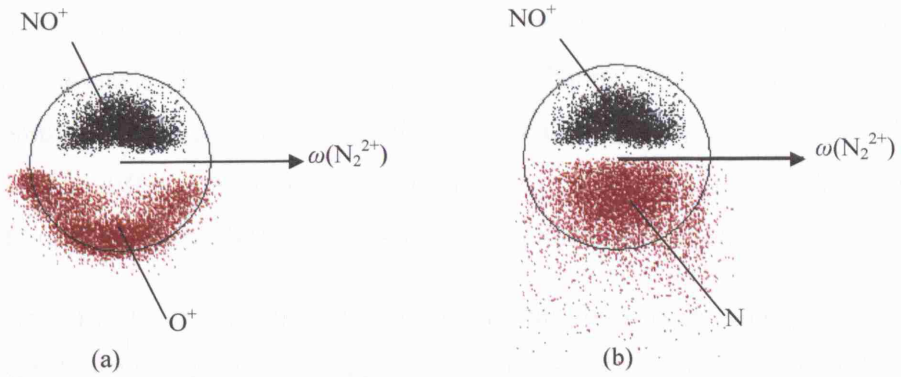

Figure 5.3 The scattering diagrams, circle radius 1.0 cm μs^{-1}, for (a) NO^+ and O^+ and (b) NO^+ and N with respect to the velocity of the reactant dication in the COM frame, recorded following collisions of N_2^{2+} with O_2 at 7.1 eV and with a 300 V repeller plate.

The scattering diagrams derived from the PSCO data for the formation of $NO^+ + O^+ + N$ (Figure 5.3) show that the products from this channel are predominantly sideways scattered, relative to N_2^{2+}, over a relatively large range of scattering angles. Such strong sideways scattering of all three products, as opposed to the forwards/backwards scattering observed for simple electron transfer reactions (see section 3.3.1), is a very strong indication that the products have been formed from the break-up of a collision complex: $[N_2O_2]^{2+}$. If a collision complex exists with a lifetime that is at least comparable with its own rotational period, the products of the decay of the complex will all be symmetrically scattered over a large range of angles in the COM frame.

The symmetrical features in the scattering diagrams of the product ions relative to N_2^{2+} confirm the products were formed from the decay of an initially 'long-lived' collision complex. If one of the products had been formed before the formation of the 'long-lived' complex, then we would expect to see a more defined scattering relationship between that product and the velocity of the centre of mass. However since all the products, NO^+, O^+ and N, are symmetrically scattered relative to the velocity of the dication in the COM frame, this initial long-lived collision complex must have involved all the products, $[N_2O_2]^{2+}$. There are two possible mechanisms by which the collision complex, $[N_2O_2]^{2+}$, could then decay; either by charge separation into two monocations, with one monocation subsequently dissociating, such as in (5.6) or (5.7), or by loss of a neutral species and with the resulting dication later dissociating such as (5.8).

$$[N_2O_2]^{2+} \rightarrow NO^+ + NO^+ \text{ then } NO^+ \rightarrow O^+ + N \quad (5.6)$$
$$[N_2O_2]^{2+} \rightarrow N_2O^+ + O^+ \text{ then } N_2O^+ \rightarrow NO^+ + N \quad (5.7)$$
$$[N_2O_2]^{2+} \rightarrow NO_2^{2+} + N \text{ then } NO_2^{2+} \rightarrow NO^+ + O^+ \quad (5.8)$$

If reactions mechanisms (5.6), (5.7) or (5.8) were operating to form the products of channel (5.4) the scattering diagrams relative to the velocity of the dication in the COM frame would obviously all be the same since all the channels proceed from a long-lived collision complex. However the internal frame scattering diagrams would all differ significantly. The differences in the internal frame scattering diagrams for these channels are demonstrated later through the use of schematic scattering diagrams.

If the mechanism (5.6) or (5.7) is operating, which involves initial charge separation of the complex, followed by neutral loss, then we would expect the velocity of the N atom to be correlated with that of the product ion formed in the last stage of the mechanism (O^+, (5.6), or NO^+, (5.7)), and anti-correlated with that of the product ion formed in the first stage of the mechanism (NO^+, (5.6), or O^+, (5.7)). The Coulomb repulsion between the two ions in the initial charge separating step would give the ions significant velocities in opposing directions. The subsequent dissociation of one of the ions would occur with an energy release significantly less than the initial Coulomb repulsion between the initial ion pair and hence the dissociated ion and neutral will move in the same direction with comparable velocities.

Since a lot of mechanistic information can be determined from the internal frame, we will now discuss what product scattering would be expected for the different possible mechanisms of decay of the collision complex. Figure 5.4 to Figure 5.6 show schematic diagrams of the internal frame scattering that would be observed if reaction mechanisms (5.6), (5.7) or (5.8) were operating to form the products NO^+, O^+ and N. In detail Figure 5.4 shows how if the collision complex, $[N_2O_2]^{2+}$, dissociates to yield NO^+ and NO^+, with one NO^+ further dissociating to form N and O^+, then in the internal frame the velocity of the N and O^+ will be correlated while the velocity of the NO^+ will be anti-correlated with the velocity of N and O^+.

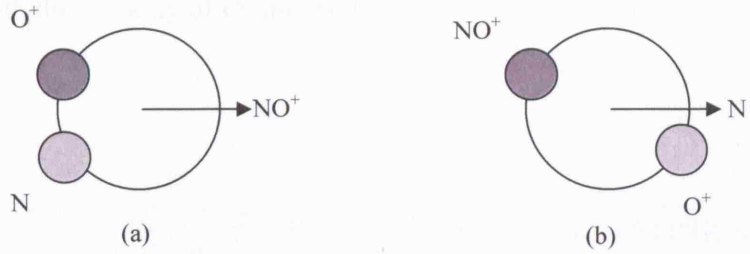

$$[N_2O_2]^{2+} \rightarrow NO^+ + NO^+ \text{ then } NO^+ \rightarrow O^+ + N \qquad (5.6)$$

Figure 5.4 A schematic of an internal frame scattering diagram for reaction mechanism (5.6), showing (a) O^+ and N relative to NO^+ and (b) NO^+ and O^+ relative to N.

Figure 5.5 shows how if the collision complex, $[N_2O_2]^{2+}$, dissociates to yield N_2O^+ and O^+, where the N_2O^+ further dissociates to form NO^+ and N, then in the internal frame the velocity of the N and NO^+ will be correlated while the velocity of the O^+ will be anti-correlated with the velocity of N and NO^+.

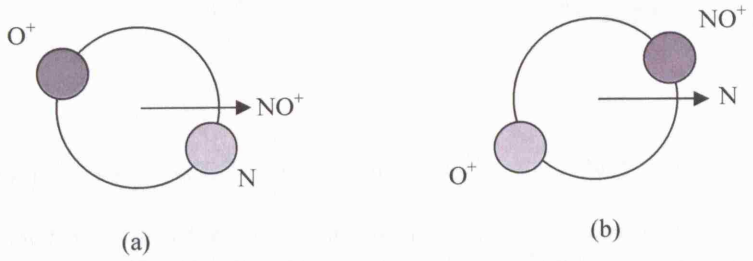

$$[N_2O_2]^{2+} \rightarrow N_2O^+ + O^+ \quad \text{then } N_2O^+ \rightarrow NO^+ + N \qquad (5.7)$$

Figure 5.5 A schematic of an internal frame scattering diagram for reaction mechanism (5.7) showing (a) O^+ and N relative to NO^+ and (b) NO^+ and O^+ relative to N.

Alternatively, the mechanism to form the products of channel (5.4) could involve initial neutral loss followed by charge separation, (5.8). The initial neutral loss will not occur with significant Coulomb repulsion hence the N atom will have a low velocity in the COM frame. Depending on the lifetime of the resulting NO_2^{2+} dication the velocity of the N may have little correlation with the velocity of either of the charged species. If the NO_2^{2+} dication lives for a time at least comparable with its rotational period before it dissociates, the velocity of the N atom will have no correlation with the velocities of either of the ionic products.

Figure 5.6 shows how if the collision complex, $[N_2O_2]^{2+}$, dissociates to yield $[NO_2^+]$ and N, where the $[NO_2^+]$ further dissociates to form NO^+ and O^+, then in the internal frame the velocity of the O^+ and NO^+ will be correlated while the velocity of the N will show no correlation with the velocity of O^+ and NO^+.

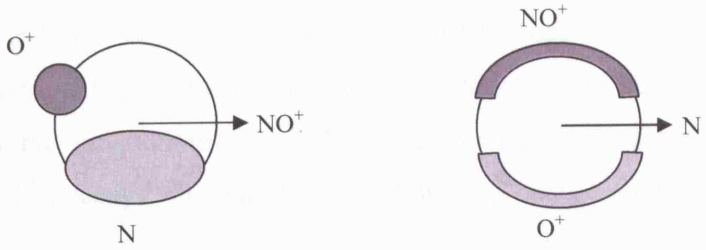

$$[N_2O_2]^{2+} \rightarrow NO_2^{2+} + N \quad \text{then } NO_2^{2+} \rightarrow NO^+ + O^+ \qquad (5.8)$$

Figure 5.6 A schematic of an internal frame scattering diagram for reaction mechanism (5.8) showing (a) O^+ and N relative to NO^+ and (b) NO^+ and O^+ relative to N. There may also be some observed displacement of the centre of the circularly formed scattering however this is not shown in these simplified schematic diagrams.

The internal frame scattering diagram presented in Figure 5.7 (a) shows that there is an anti-correlation between the velocities of the charged products NO^+ and O^+; the O^+ ion is scattered strongly in the opposite direction to the NO^+ product. Figure 5.7 (b), however, shows that the velocity of the N atoms is not strongly correlated with either of the velocities of the charged products. The scattering diagrams derived from the PSCO data, shown in Figure 5.7, are clearly most similar to the schematic scattering diagrams shown in Figure 5.6 and hence show that reaction mechanism (5.8) is the most likely reaction mechanism for the formation of the NO^+, O^+ and N from N_2^{2+} and O_2.

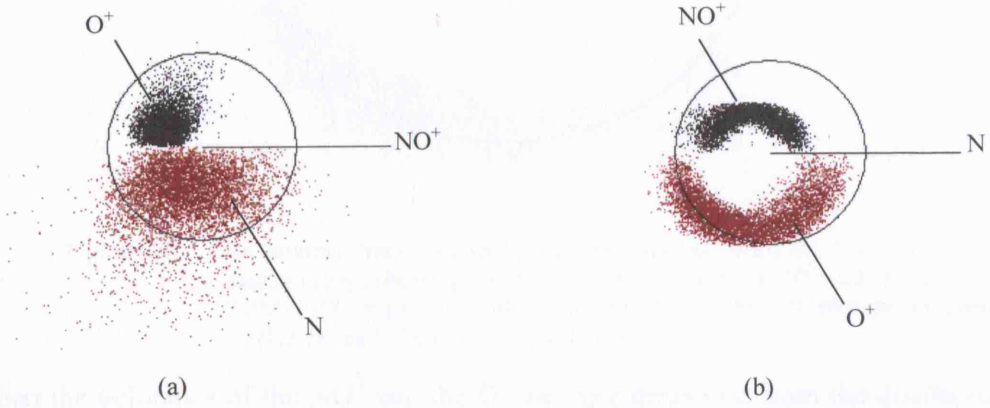

Figure 5.7 The internal frame scattering diagrams, circle radius 1.0 cm μs^{-1}, derived from the PSCO data for reaction (5.4), showing (a) O^+ and N relative to NO^+ and (b) NO^+ and O^+ relative to N.

Since the internal frame scattering diagrams show the N has no velocity correlation with either of the charged species, they therefore show that N was formed first and that the

subsequent $[NO_2^{2+}]$ ion has a lifetime at least comparable with its rotational period. The formation of the product ions from the decay of $[NO_2^{2+}]$ is confirmed by the mutual anti-correlation of the ion velocities in the internal frame (Figure 5.7 (a)). The internal frame scattering, in conjunction with the symmetrical scattering of all three products relative to the velocity of the dication in the COM frame, therefore confirms that the collision complex, $[N_2O_2]^{2+}$, decays via neutral loss, followed by charge separation.

Considering the magnitudes of the product velocities can also help to confirm the reaction mechanism. Although the N product appears quite dispersed in the scattering diagrams the average velocity of the N fragment is about 0.6 cm μs^{-1}. Thus, by conservation of momentum, the velocity of the NO_2^{2+} ion formed in the initial neutral loss step should be 0.18 cm μs^{-1}. If the "neutral-loss" mechanism, (5.8), is operating we would expect the NO_2^{2+} to be moving away from the COM at 0.18 cm μs^{-1} in the opposite direction to the N atom. Satisfyingly, as shown in Figure 5.8, the centres of the isotropic distributions of the charged species are indeed displaced from the velocity of the COM by 0.18 cm μs^{-1} which is the expected value.

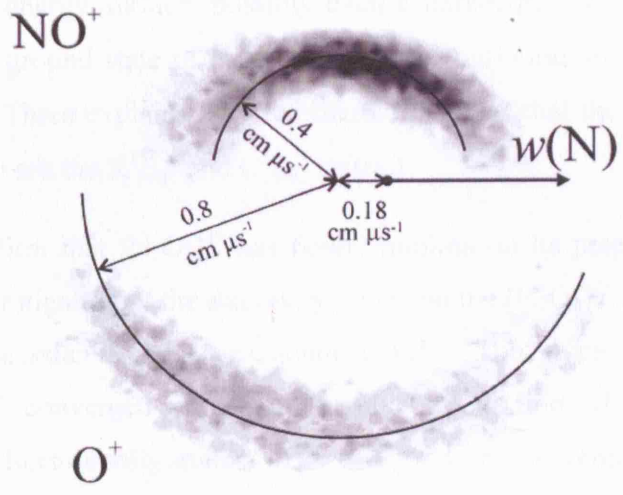

Figure 5.8 An internal frame scattering diagram derived from the PSCO data for reaction (5.4), showing the displacement velocity of NO^+ and O^+ from the COM (0.18 cm μs^{-1}), as well as the velocities of the NO^+ (0.4 cm μs^{-1}) and O^+ (0.8 cm μs^{-1}) from this displacement.

When the velocities of the NO^+ and the O^+ ions are measured from the displaced centre, as shown in Figure 5.8, the velocities of these ionic products are consistent with the two-body dissociation of an NO_2^{2+} ion; that is, the magnitudes of the momenta of the NO^+ and the O^+ ions are equal (approximately 12 amu cm μs^{-1}). Indeed, the velocities of the O^+ and NO^+ indicate an average kinetic energy release upon dissociation of 7.8 eV, in

excellent agreement with the energy release of 8 eV which has been reported for the dissociation of long-lived NO_2^{2+} ions. [8,9]

The PSCO angular scattering data therefore clearly indicates that this reactive channel proceeds, as indicated in equation (5.8), via initial neutral loss from a long-lived collision complex, $[N_2O_2^{2+}]$, followed by charge separation of the resulting NO_2^{2+} dication. To confirm this mechanism, an important consideration is whether there is an $N_2O_2^{2+}$ species that has a bound minimum on its potential energy surface, and hence could be 'long-lived'. To the best of our knowledge there are no published experimental or theoretical studies of the $N_2O_2^{2+}$ dication in the literature. However investigations of N_4 and $[N_3O]^+$, which are isoelectronic with $N_2O_2^{2+}$, have been published. [10-12] Quantum chemical investigations and Matrix Isolation Spectra show that N_4 has a tetrahedral ground singlet state. However, the literature shows that the $[N_3O]^+$ ion, which has been detected in mass spectrometric experiments, has a lifetime of at least 520 ns. Quantum chemical calculations on $[N_3O]^+$ reveal a "tetrahedral" (C_{3v}) minimum on the singlet surface and a "linear" (C_s, N-N-N-O) minimum on the triplet surface. Therefore the literature information hints that the isoelectronic $[N_2O_2]^{2+}$ may possess one or more bound minima on its potential energy surface, possibly even a tetrahedral configuration when formed from the $X^1\Sigma_g^+$ ground state of N_2^{2+} and a linear configuration from the $C^3\Sigma_u^+$ state of N_2^{2+}. (Chapter Three explains how the literature shows that the main reacting states of the N_2^{2+} dication are the $X^1\Sigma_g^+$ and $C^3\Sigma_u^+$ states.)

In order to confirm that $[N_2O_2]^{2+}$ has bound minima on its potential energy surface an independent investigation of the stationary points on the $[N_2O_2]^{2+}$ potential energy surface (PES), using Gaussian98, has been conducted. [7] The investigation showed that the singlet $[N_2O_2]^{2+}$ converged on a tetrahedral configuration while the triplet $[N_2O_2]^{2+}$ converged on a linear configuration. This study was not a complete investigation of the $[N_2O_2]^{2+}$ potential energy surface but does show that the $[N_2O_2]^{2+}$ dication does have minima on the potential energy surface. The study confirms the predictions made from the literature information which hinted that the singlet $[N_2O_2]^{2+}$ has a tetrahedral configuration while the triplet $[N_2O_2]^{2+}$ has a linear configuration. The rotational period for both these geometries was calculated to be of the order of 20 fs. Thus, estimating that the $[N_2O_2]^{2+}$ collision complex must survive for at least 100 fs or so before dissociating. Indeed, given that the angular distributions are quite close to isotropic, the lifetime of the $[N_2O_2]^{2+}$ species may be significantly longer than this estimate if it is formed in a low lying rotational state. [7]

Hence the angular scattering diagrams derived from the PSCO data, and the computation study on the geometry and lifetime of the proposed $[N_2O_2^{2+}]$ intermediate, both clearly indicate that this reactive channel proceeds via initial neutral loss from a long-lived collision complex, $[N_2O_2^{2+}]$, which is then followed by charge separation of the resulting NO_2^{2+} dication. The next section discusses the angular scattering of other bond-forming channel, $NO^+ + N^+ + O$, observed following the collision of N_2 with O_2^{2+}.

5.3.1.2.2 The formation of $NO^+ + N^+ + O$ (5.5)

To extract the dynamical data for this channel, (5.5), where an N^+ product is formed, the false coincidences were removed from the ion pairs corresponding to the $NO^+ + N^+$ events in the coincidence spectra as previously described. The scattering diagrams extracted from the $NO^+ + N^+$ events look exceptionally similar to those for the formation of $NO^+ + O^+ + N$, channel (5.4), as can be seen by comparison of the scattering with respect to the velocity of N_2^{2+} in the COM frame in Figure 5.3 (a), channel (5.4), with Figure 5.9 (a), channel (5.5), and by comparison of the scattering in the internal frame in Figure 5.7 (b), channel (5.4), with Figure 5.9 (b), channel (5.5).

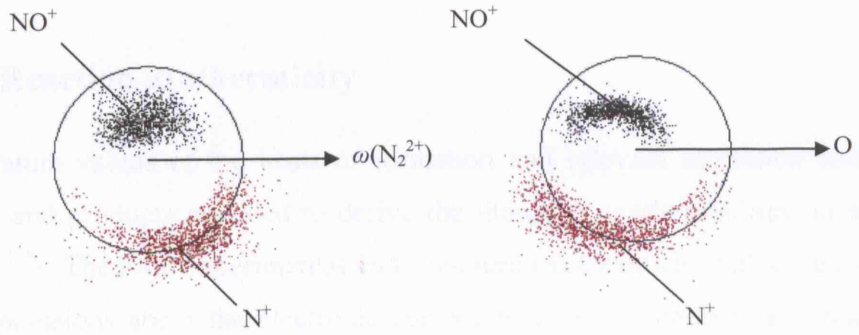

Figure 5.9 The scattering diagrams, circle radius 1.0 cm μs^{-1}, for (a) NO^+ and N^+ with respect to the velocity of N_2^{2+} in the COM frame and (b) NO^+ and N^+ relative to O in the internal frame recorded following collisions of N_2^{2+} with O_2 at 7.1 eV, 300 V repeller plate.

The scattering diagrams show again that the products NO^+, N^+ and O are symmetrically scattered relative to N_2^{2+}. Again, as described above, this symmetrical scattering is a strong indication that the products have been formed from the break-up of a collision complex, $N_2O_2^{2+}$, which has had time to rotate before dissociation. The data show that there is a strong anti-correlation between the velocities of the charged products, NO^+ and N^+, while the velocity of the neutral fragment, O in this case, is not correlated with either of the charged products. Hence, analogous to the reaction forming NO^+, N^+ and O, the data strongly indicate that the mechanism for the formation of $NO^+ + N^+ + O$ is:

$$[N_2O_2]^{2+} \rightarrow N_2O^{2+} + O \quad \text{then } N_2O^{2+} \rightarrow NO^+ + N^+ \qquad (5.9)$$

The N_2O^{2+} dication is well known to possess long-lived metastable states, which could readily survive for several hundred picoseconds before dissociating to $NO^+ + N^+$. It is also well established that the ground state of N_2O^{2+} dissociates to $N_2^+ + O^+$ as well as to $NO^+ + N^+$. [13, 14] However, $N_2^+ + O^+$ ion pairs from the dissociation of N_2O^{2+} would be swamped in the PSCO spectra by coincidences between the same ions formed by dissociative electron transfer (5.2).

Therefore, to summarise, we have concluded that both the bond-forming reactions in the N_2^{2+} with O_2 proceed via a long-lived collision complex $[N_2O_2^{2+}]$ which rotates for a period of time at least comparable with its rotational period. The collision complex, $[N_2O_2^{2+}]$, then decays via neutral loss, either N or O to form a second long-lived collision complex, $[NOX^{2+}]$ with X being O or N respectively. This second collision complex also lives for a period of time also likely to be at least comparable with its rotational period. The second collision complex then dissociates to yield two singly charged species, either NO^+ paired with O^+ or NO^+ paired with N^+. The next section discusses the reaction exothermicity for these two bond-forming channels detected following the collision of N_2^{2+} with O_2.

5.3.1.3 Reaction exothermicity

The literature values of the heats of formation and relevant ionisation energies of the reactants and products are used to derive the literature exothermicities, in each specific reaction. [15] Then the experimental and literature exothermicity values are compared to make conclusions about the electronic composition of the products and reactants. The translational exothermicity spectra generated for the bonding-forming reactions, channels (5.4) and (5.5), are broad and unresolved even when recorded at the low repeller plate voltage of 100 eV. A broad and unresolved spectrum can be indicative of the involvement of a significant number of reactant, or product, electronic or vibronic states. Generally the resolution of the exothermicity spectra can be increased by applying a lower voltage to the repeller plate however it is difficult to collect a significant number of pairs for these reactions when using a low repeller plate voltage. As previously mentioned the low number of pairs for these bond-forming reactions at low repeller voltages is because these bond-forming reactions are 'sideways' scattered as shown in section 3.3.1.2. In the PSCO experiment sideways scattered products can not be detected at lower repeller plate voltages as the longer flight times mean the ions fly beyond the

detector or hit the walls of the drift tube. Firstly the exothermicity spectrum of channel (5.4) is presented in section 4.3.1.3.1, followed by the exothermicity spectrum of channel (5.5) in section 4.3.1.3.2.

5.3.1.3.1 The exothermicity of $NO^+ + O^+ + N$

Figure 5.10 shows the broad reaction exothermicity spectra from the pairs data for NO^+ paired with O^+ and N, indicating that the translational exothermicity is distributed between approximately 1 and 12 eV with a maximum at approximately 4 eV. The lack of resolution means no definitive conclusions can be drawn about the electronic channels participating in this bond-forming channel. However some observations can be made.

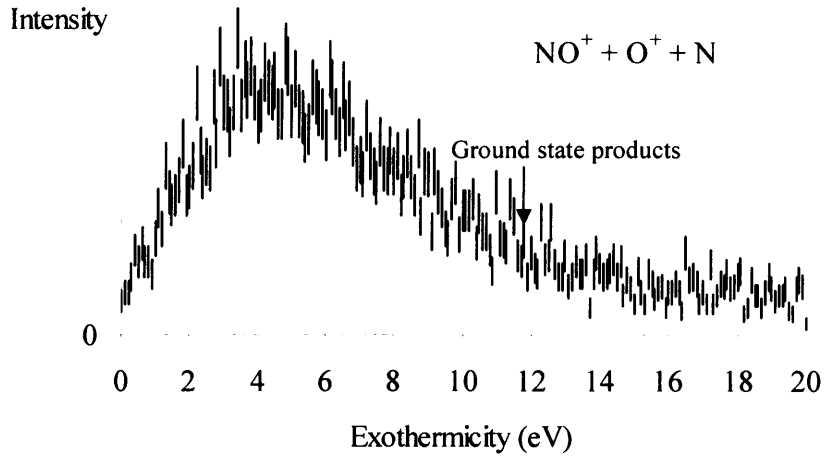

Figure 5.10 The exothermicity spectra for the bond-forming channel $NO^+ + O^+ + N$ showing the calculated exothermicity of the reaction of ground state N_2^{2+} to form ground state products.

The reaction of ground electronic state N_2^{2+} with O_2 to form ground electronic state NO^+ with O^+ and N has a literature exothermicity of 11.7 eV. This ground state literature exothermicity is near to the limit of the exothermicity we observe; most of the reactive events have translational exothermicities less than 11.7 eV. We can therefore ascertain that in the majority of reactive events excited electronic or vibrational states of at least some of the products are populated.

First let us consider the vibrational excitation of the NO^+ product. The dissociation energy of the ground electronic state of NO^+ is approximately 11 eV. Thus, varying degrees of vibrational excitation of the NO^+ product in its ground electronic state can account for translational exothermicity signals from 11.7 to 0.7 eV, a range of exothermicities overlapping almost exactly the experimental spectrum. Considering the

possibility of the formation of electronically excited states of the products, the range of translational exothermicities observed experimentally encompasses the formation of excited states of the atomic products arising from their ground $2p^3$ configurations together with the ground electronic state of NO^+. Similarly, the experimentally observed range of translational exothermicities could also be explained by the formation of NO^+ in a number of its electronic excited states, which lie within 12 eV of the NO^+ ground state. In particular, a reaction of ground state reactants to form ground state O^+ and N together with NO^+ in the $^3\Sigma^+$ excited state has an exothermicity of 5.2 eV, which agrees well with the observed maximum of the exothermicity intensity.

The PSCO experimental exothermicity spectra cannot enable us to definitively between the different options of how the internal energy is distributed in and between the NO^+, O^+, and N products. The independent computational work deduces the collision complexes involved in the formation of the NO^+ product have N–O bond lengths markedly different from that of NO^+ re=1.06 Å in its ground electronic state.[7] Thus, one might expect a significant vibrational excitation of the NO^+ product. This observation, coupled with the good agreement between the range of translational exothermicities we observe and the dissociation energy of the $X^1\Sigma^+$ state of NO^+, perhaps hints that a significant number of reactive events involve the formation of the products in their ground electronic states with the NO^+ ion possessing a range of vibrational excitation. The next section discusses the reaction exothermicity of the other bond-forming reaction detected following the collisions of N_2^{2+} with O_2.

5.3.1.3.2 The exothermicity of $NO^+ + N^+ + O$

Figure 5.11 shows the reaction exothermicity spectra from the pairs data for NO^+ paired with N^+ and O. Again the spectrum is broad and unresolved, indicating that the translational exothermicity is distributed between approximately 1 and 12 eV with a maximum at approximately 6 eV.

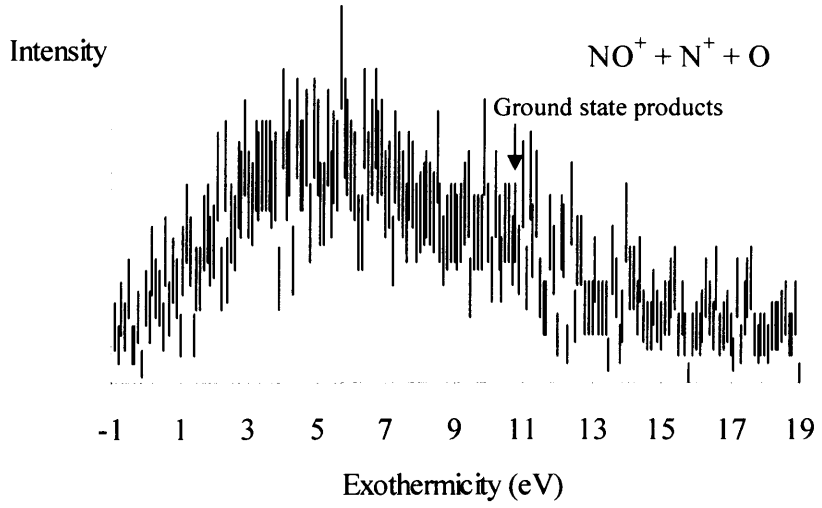

Figure 5.11 The exothermicity spectra for the bond-forming channel $NO^+ + N^+ + O$ showing the calculated exothermicity of the reaction of ground state N_2^{2+} to form ground state products.

A reaction of ground electronic state N_2^{2+} with O_2 to form ground electronic state NO^+ with N^+ and O has a literature exothermicity of 10.8 eV. Previously we observed that in the reaction to form NO^+ with O^+ and N, the literature exothermicity for a ground state reaction was near to the limit of the exothermicity we observe. Again this 'ground state' literature exothermicity of 10.8 eV is close to the limit. That is, most of the reactive events have translational exothermicities less than 10.8 eV. We can therefore ascertain that in the majority of reactive events, excited electronic or vibrational states of at least some of the products are populated. However the exothermicity spectrum shows intensity up to approximately 12 eV, therefore a small number of reactions must involve excited states of the reactants in order to explain this intensity. As previously mentioned N_2^{2+} beams are mainly composed of the ground state of N_2^{2+}, $X^1\Sigma_g^+$, as well as an excited state, $c^3\Sigma_u^+$. Reactions of the $c^3\Sigma_u^+$ state, to form products in their ground states, could therefore explain this small amount of intensity.

If we consider which product states could contribute to the exothermicity spectrum we find a range of options. The vibrational excitation of the NO^+ product can account for translational exothermicity signals from 10.8 to -0.8 eV. Again, as with the previous channel, (5.4), this range of exothermicities overlaps very well with the experimental spectrum which has intensity from approximately 1 to 12 eV. However the exothermicity spectrum could also encompass the formation of excited states of the atomic products together with the ground electronic state of NO^+. The formation of NO^+ in a number of its electronic excited states, which lie within 12 eV of the NO^+ ground state, together with ground state atomic products would also overlap well with the exothermicity spectrum

intensity. As previously mentioned we cannot distinguish between these options, but the independent computational work predicts that the collision complexes involved in the formation of the NO^+ product have N–O bond lengths different from that of the ground state of NO^+, hence, as previously mentioned, one might expect a significant vibrational excitation of the NO^+ product. As with the previous channel, (5.4), we conclude that the evidence hints that a significant number of reactive events involve the formation of the products in their ground electronic states with the NO^+ ion possessing a range of vibrational excitation, and given that again we see a reasonably good overlap of the vibrational excitation of NO^+ with the intensity in the exothermicity spectrum, it is quite likely that the range of vibrational states of NO^+ are the main contributing factor to the broad nature of the exothermicity spectra.

We have discussed the two bond-forming reactions, channels (5.4) and (5.5), detected following the collision of N_2^{2+} with O_2. Both reactions proceed via neutral loss from a collision complex, $[N_2O_2^{2+}]$, followed by charge separation of the resulting dication. Both reactions have broad exothermicity spectra, therefore it is difficult to assign how the internal energy is distributed between the products, however both exothermicity spectra could be explained almost entirely by vibrational excitation of the NO^+ product. The following section discusses the relative intensity, angular scattering and reaction exothermicity of the bond-forming reactions detected following the collisions of N_2^{2+} with CO_2.

5.3.2 N_2^{2+} with CO_2

Eight main reaction channels are observed in the coincidence spectrum following the reactions of N_2^{2+} with CO_2: non-dissociative charge transfer, (5.10), dissociative charge transfer, (5.11), (5.12), (5.16) and (5.17), dissociative double electron transfer, (5.13), and two bond-forming channels, (5.14) and (5.15).

$$N_2^{2+} + CO_2 \rightarrow N_2^+ + CO_2^+ \quad (5.10)$$
$$N_2^{2+} + CO_2 \rightarrow N_2^+ + CO^+ + O \quad (5.11)$$
$$N_2^{2+} + CO_2 \rightarrow N_2^+ + CO + O^+ \quad (5.12)$$
$$N_2^{2+} + CO_2 \rightarrow N_2 + CO^+ + O^+ \quad (5.13)$$
$$N_2^{2+} + CO_2 \rightarrow NO^+ + CO^+ + N \quad (5.14)$$
$$N_2^{2+} + CO_2 \rightarrow NO^+ + CO + N^+ \quad (5.15)$$
$$N_2^{2+} + CO_2 \rightarrow N^+ + CO_2^+ + N \quad (5.16)$$
$$N_2^{2+} + CO_2 \rightarrow N^+ + CO^+ + (N + O) \quad (5.17)$$

A section of the coincidence spectrum, recorded at 300 V repeller plate, for the reaction of N_2^{2+} with CO_2 is shown Figure 5.12, showing one of the chemical channels, (5.14), and one of the dissociative electron transfer reactions, (5.11).

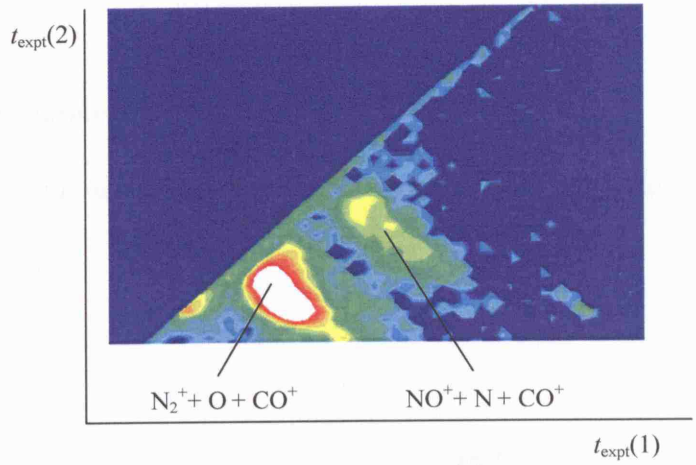

Figure 5.12 A section of the coincidence spectrum recorded following collisions of N_2^{2+} with CO_2 at COM 7 eV with a repeller plate voltage of 300 V showing a chemical channel, (5.14), and a dissociative electron transfer channel, (5.11). It is important to note that white signifies the most intensity, followed by red, orange, yellow, green and finally blue is the least intense.

The next section discusses the relative intensities of the various channels observed in this N_2^{2+} with CO_2 reaction system. This is then followed by the discussion of the angular scattering of the two bond-forming channels, (5.14) and (5.15), and subsequently the reaction exothermicity of these bond-forming channels is discussed.

5.3.2.1 Relative intensities

The relative intensities of the different reaction channels observed are measured by comparing the number of counts in each coincidence peak in the pairs spectrum after the false coincidences are extracted from the channels with an N^+ product. The eight channels, non-dissociative charge transfer, (5.10), dissociative charge transfer (5.11), (5.12), (5.16) and (5.17), dissociative double electron transfer (5.13), and the bond-forming channels (5.14) and (5.15), are formed in the ratio 9 : 6 : 2 : 8 : 2 : 1 : 1 : 2 (to 0 decimal places) at a COM collision energy of 7.0 eV. Therefore the non-dissociative electron transfer channel is 8.9 and 5.5 times more intense than the bond-forming channels respectively (5.14) and (5.15) respectively. However although the bond-forming channels (5.14) and (5.15), are weak, they contribute to a similar amount as some of the dissociative double and single electron transfer reactions (5.12),(5.17) and (5.13).

5.3.2.2 Angular scattering

The interpretation of angular scattering diagrams of the two bond-forming channels, (5.14) and (5.15), will be discussed in the next sections, 4.3.2.2.1 and 4.3.2.2.1 respectively.

5.3.2.2.1 The formation of $NO^+ + CO^+ + N$ (5.14)

Figure 5.13 shows the scattering of the three products, NO^+, CO^+ and N, relative to N_2^{2+} in the COM frame.

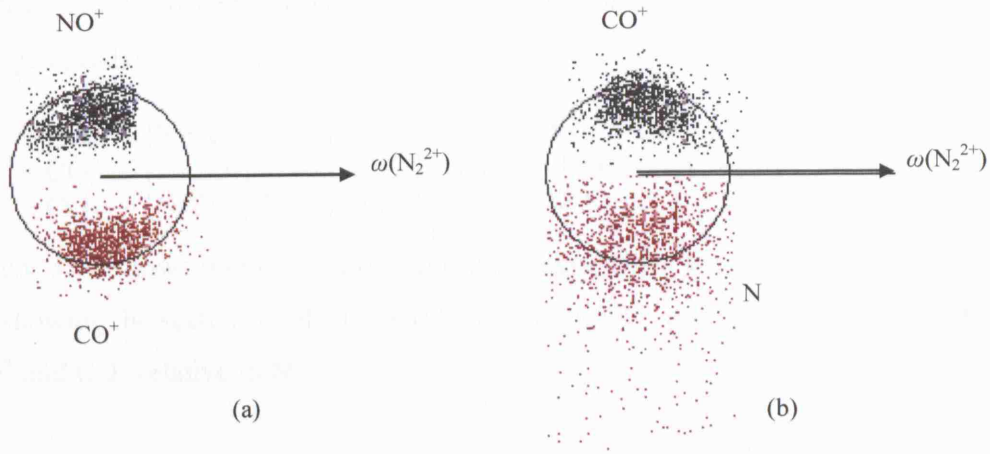

Figure 5.13 The scattering diagrams, circle radius 0.7 cm μs^{-1}, for (a) NO^+ and CO^+ and (b) CO^+ and N with respect to N_2^{2+} in the COM frame recorded following collisions of N_2^{2+} with CO_2 at 300 V repeller plate.

The scattering diagrams in Figure 5.13 show that the products, NO^+, CO^+ and N, are all sideways scattered over a large range of angles relative to N_2^{2+} in the COM frame. However, as can be seen in Figure 5.13, part of the forwards scattering area of the NO^+ intensity and part of the backwards scattering area of the CO^+ intensity are missing. This 'missing' area is due to similarities in the *TOF* of the NO^+ and CO^+ ions; the forwards scattered NO^+ has *m/z* slightly lower than the 'normal' *m/z* of 30 while the CO^+ has an *m/z* slightly higher than the 'normal' *m/z* of 28. In the PSCO experiment, the dead time of the electronics after the detection of an ion is very quick (30 ns). However, when the *m/z* of the ions in an ion pair is within 30 ns, as for forwards scattered NO^+ and the backwards scattered CO^+, it is not possible to detect both ions. Specifically, after the detection of the first ion, there is a dead time in the electronics where the signal must return to baseline before the arrival of the second ion; hence in this case where there was not enough time to return to baseline it would appear as if only one ion was detected and

therefore it cannot be processed into the pairs spectrum. Therefore although it is evident that NO^+ and CO^+ are scattered over a range of angles, part of the scattering distribution appears to be missing.

The range of scattering angles of all the products is a primary indication that the products have been formed from the break-up of a complex $[N_2CO_2]^{2+}$. The scattering of all three of the products, over the large range of angles, indicates the complex lived for at least the life time of its rotation period. After the formation of an intermediate complex, $[N_2CO_2]^{2+}$, there are two obvious mechanistic routes for the formation of the products of this reaction. One route, (5.18) or (5.19), would proceed via the loss of a charged species followed by the separation of a neutral and second charged species. The other route, (5.20), would proceed via the loss of a neutral, followed by the separation of the two charged product species.

$$N_2^{2+} + CO_2 \rightarrow [N_2CO_2]^{2+} \rightarrow [N_2O]^+ + CO^+ \rightarrow NO^+ + CO^+ + N \quad (5.18)$$
$$N_2^{2+} + CO_2 \rightarrow [N_2CO_2]^{2+} \rightarrow [NCO]^+ + NO^+ \rightarrow NO^+ + CO^+ + N \quad (5.19)$$
$$N_2^{2+} + CO_2 \rightarrow [N_2CO_2]^{2+} \rightarrow [NCO_2]^{2+} + N \rightarrow NO^+ + CO^+ + N \quad (5.20)$$

Figure 5.14 shows internal frame scattering diagrams for the products of channel (5.14); (a) showing the scattering of CO^+ and N relative to NO^+ and (b) showing the scattering of NO^+ and CO^+ relative to N.

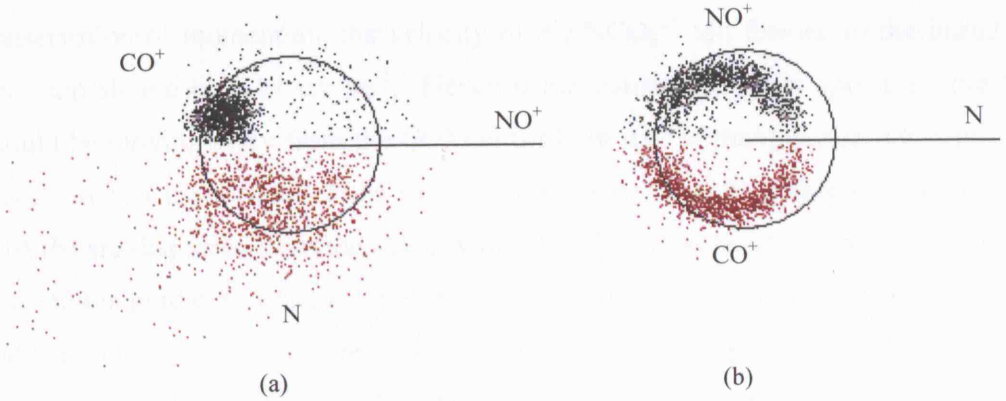

Figure 5.14 The internal frame scattering diagrams, circle radius 0.7 cm μs^{-1}, showing (a) CO^+ and N relative to NO^+ and (b) NO^+ and CO^+ relative to N, recorded following collisions of N_2^{2+} with CO_2 at 300 V repeller plate.

The internal frame scattering diagram in Figure 5.14 (a), shows strong anti-correlation between the velocities of the charged products NO^+ and CO^+, while the neutral product, N, shows no correlation with either of the charged species in both Figure 5.14 (a) and (b). If the neutral product, N, had been formed in the charge dissociation reaction step we would expect to see some correlation in the velocity of either the N and CO^+ or the N and

NO^+ because the Coulomb repulsion in the charge separating step would define the scattering in the scattering diagrams. However, since we see no correlation of the N with either of the charged species, it appears the neutral must have resulted from the dissociation of the intermediate complex, $[N_2CO_2]^{2+}$, first. A second intermediate, $[NCO_2]^{2+}$ would then be formed which dissociates to yield the NO^+ and CO^+. The lack of correlation between the neutral and the charged species indicates that the neutral loss reaction step was mechanistically distinct from the charge separation step, hence there was also complex rotation of the second intermediate complex $[NCO_2]^{2+}$ after the N dissociated from $[N_2CO_2]^{2+}$.

The fact that there is no correlation between the velocity of the neutral N atom and either of the charged species in conjunction with that obvious correlation of the charged species, means that we can rule out the possibility of the formation of the neutral in the same step as the charged species, such as in the mechanisms of (5.18) or (5.19). Hence to conclude, the mechanism for channel (5.14) proceeds via the formation of a doubly charged intermediate, followed by neutral loss then charge separation of the second doubly charged intermediate:

$$N_2^{2+} + CO_2 \rightarrow [N_2CO_2]^{2+} \rightarrow [NCO_2]^{2+} + N \rightarrow NO^+ + CO^+ + N \qquad (5.20)$$

The reaction mechanism is also confirmed by considering the magnitudes of the products velocities. The average velocity of the N fragment is about 0.6 cm μs^{-1}. Thus, by conservation of momentum, the velocity of the NCO_2^{2+} ion formed in the initial neutral loss step should be 0.14 cm μs^{-1}. Hence if mechanism (5.20) is operating, the NCO_2^{2+} should be moving away from the COM at 0.14 cm μs^{-1} in the opposite direction to the N atom. In fact the centres of the isotropic distributions of the charged species in Figure 5.14 (b) are displaced from the velocity of the COM by approximately 0.15 cm μs^{-1}, very close to the predicted velocity of NCO_2^{2+}. When the velocities of the NO^+ (0.51 cm μs^{-1}) and the CO^+ (0.54 cm μs^{-1}) ions are measured from this displacement, the magnitudes of the momenta of the NO^+ and the CO^+ ions are equal (approximately 15 amu cm μs^{-1}). Therefore the velocities of these ionic products are consistent with the two-body dissociation of an NCO_2^{2+} ion.

In order to further confirm that the reaction mechanism involves a long-lived collision complex, it is important to probe the potential energy surface of the $N_2CO_2^{2+}$ species for a bound minimum. These calculations will not form part of this thesis and to the best of our knowledge no literature information is available regarding experimental or theoretical studies of the $N_2CO_2^{2+}$ species. However the isoelectronic, linear species C_3O_2 (OC_3O), a

compound believed to be of astrochemical significance, is stable. [16] This may suggust that the $N_2CO_2^{2+}$ species could have a level of stability.

5.3.2.2.2 The formation of $NO^+ + N^+ + (CO)$ (5.15)

When NO^+ was detected paired with CO^+, (5.14), there was no ambiguity in the identity of the third product, N. In the case of channel (5.15) the neutral product(s) could be either CO or C and O. However, given that NO^+ has been detected as a pair with CO^+, (5.14), it seems plausible that the neutral product in channel (5.15) is CO so for consistency the neutral product will be referred to as CO. In fact, when we consider the energetics later in section 4.3.2.3.2 we can confirm that the neutral is in fact CO. Figure 5.15 shows the scattering of this channel with respect to the velocity of the dication in the COM frame.

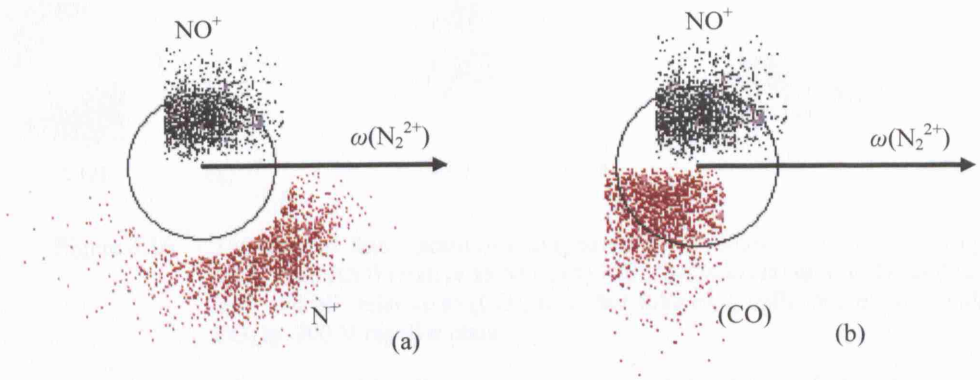

Figure 5.15 The scattering diagrams, circle radius 1 cm μs^{-1}, for (a) NO^+ and N^+ and (b) NO^+ and (CO) with respect to the velocity of the dication in the COM frame, recorded following collisions of N_2^{2+} with CO_2 at 300 V repeller plate.

Before analysis of this channel, (5.15), the false coincidences have been extracted from the data set. However the scattering diagrams are 'noisy'. This noise is attributed to the collection of a weak channel close to the false coincidences. The scattering diagrams also appear to look as if the peaks have been 'cut off' but in fact this is only due to the cutting off of the noise rather than real reaction channel signal which while noisy is easily distinguishable when selecting the peak from the coincidence spectrum. As can been seen from the scattering diagrams in Figure 5.15 and Figure 5.16, when compared with the diagrams in Figure 5.13 and Figure 5.14, the scattering for channel (5.15) is not exactly the same as that for channel (5.14). There are, however, some similarities. NO^+ is certainly scattered symmetrically relative to N_2^{2+} in the COM frame (upper half of Figure 5.15 (a) and (b)). This certainly implies the NO^+ species has been involved in

some sort of long-lived collision complex. A heavy species like NO^+ would be unlikely to appear isotropically scattered otherwise. However the CO neutral product appears to be slightly backwards scattered with respect to the velocity of the dication in the COM frame, while the scattering of the N^+ is slightly forwards scattered. Whilst certainly the scattering of both the CO and N^+ species is not clear forwards/backwards scattering, it is neither symmetrically scattered as seen in the previous channel. This could imply that if a collision complex $[N_2CO_2^{2+}]$ was involved it did not live as long as the collision complexes formed in the bond-forming channels previously discussed in this Chapter.

In the internal frame, Figure 5.16, the scattering diagrams again are not as clear as for channel (5.14).

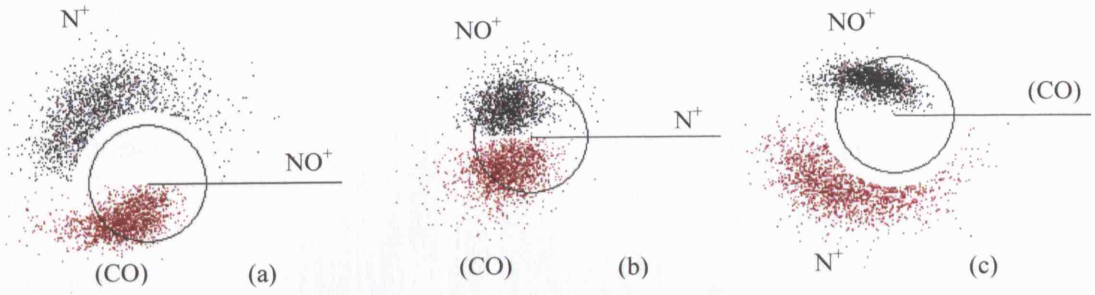

Figure 5.16 The internal frame scattering diagrams, circle radius 1 cm μs^{-1}, showing (a) N^+ and (CO) relative to NO^+, (b) NO^+ and (CO) relative to N^+ and (c) NO^+ and N^+ relative to (CO), recorded following collisions of N_2^{2+} with CO_2 at 300 V repeller plate.

The upper halves of the scattering diagrams in Figure 5.16 (a) and (b) show scattering with some signs of an anti-correlation between the two charged species, NO^+ and N^+, although it is certainly not as clearly defined as in the previously discussed bond-forming channels. In Figure 5.16 (c), the NO^+ and N^+ show little relationship with the neutral species, CO, although, the lower halves of the scattering diagrams in Figure 5.16 (a) and (b) appear to show an anti-correlation of CO with both the charged species. The most illuminating scattering diagram is that of Figure 5.16 (b), here NO^+ and CO are clearly anti-correlated with N^+. This certainly implies that the NO^+ and CO were formed in the same reaction mechanism step, after the formation of N^+. In conclusion, the analysis of the scattering for channel $NO^+ + N + CO^+$ (5.15), does not lead to a definitive mechanism however it does shows signs of a different mechanism to that of channel $NO^+ + CO^+ + N$ (5.14). While the formation of a complex $[N_2CO_2]^{2+}$ happens in the first step, as in channel (5.14), this complex is not as long-lived as that of the previous reaction mechanism and seems to dissociate via loss of a charged species, N^+, followed by dissociation into NO^+ and CO:

$$N_2^{2+} + CO_2 \rightarrow [N_2CO_2]^{2+} \rightarrow [NCO_2]^+ + N^+ \rightarrow NO^+ + N + CO^+ \quad (5.21)$$

5.3.2.3 Energetics

Sections 4.3.2.3.1 and 4.3.2.3.2 discuss the exothermicity of channels (5.14) and (5.15) respectively.

5.3.2.3.1 Energetics of $NO^+ + CO^+ + N$

Although for some systems the PSCO technique can be used to derive accurate information on the exothermicity of the reactive events detected in the pairs spectrum, for reaction (5.14), at repeller plate 300 V, the exothermicity spectra are broad and unresolved, as shown in Figure 5.17.

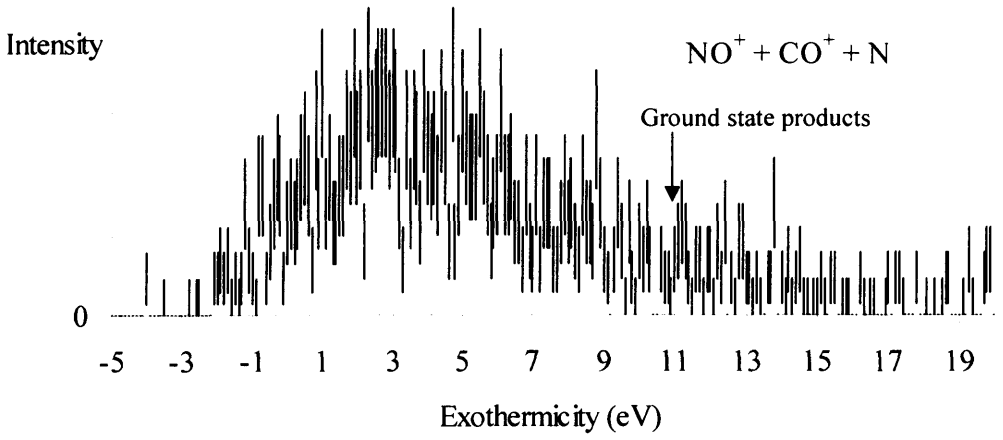

Figure 5.17 The exothermicity spectra for the bond-forming channel $NO^+ + CO^+ + N$ recorded using a 300 V repeller plate showing the calculated exothermicity of the reaction of ground state N_2^{2+} to form ground state products.

For the formation of $NO^+ + CO^+ + N$, the exothermicity spectra indicate an exothermicity from approximately -1 to 12 eV at repeller plate voltage 300 V, with a maximum at approximately 3 eV. Beyond 12 eV the signals observed in the spectra can just be attributed noise. The angular scattering diagrams for this reaction, shown in Figure 5.13, show that a large proportion of the products are sideways scattered. Therefore, as previously mentioned, at lower repeller voltages these sideways scattered products will fly past the detector and hence not be detected. Therefore it is not surprising that when using a 50 V repeller plate, where normally better exothermicity spectra can be derived from the data, this reaction channel, (5.14), was not detectable at a viable signal level.

Previous studies have shown that ion beams of N_2^{2+} are mainly composed of two electronic states: the ground $X^1\Sigma_g^+$ and the $c^3\Sigma u^+$ states, at 43 e V and 44.5 eV above the ground state of N_2. Even if we only consider the $X^1\Sigma_g^+$ and the $c^3\Sigma u^+$ states of N_2^{2+}, over 150 different combinations of reactant and product electronic channels could contribute intensity to the broad exothermicity spectrum recorded for this channel. Therefore, although some of these electronic channels are not necessarily present, we can be certain there are a large number of vibronic and/or electronic reactant or product states involved in this reaction channel.

However, for the reaction of N_2^{2+} with CO_2, even the broad exothermicity spectrum can provide some information. The reaction of N_2^{2+} with CO_2 in the ground states to form $NO^+ + CO^+ + N$ in the ground states has a literature exothermicity of 11 eV. Since there is intensity in the exothermicity spectrum up to 12 eV, we can be certain there must be at least a very small amount of either N_2^{2+} in an excited electronic state, most likely the $c^3\Sigma_u^+$ state. A reaction of the $c^3\Sigma_u^+$ state of N_2^{2+} to form ground state products has a literature exothermicity of 12.5 eV, or N_2^{2+} in high vibrational levels of the ground state may be present and reacting to form products in their ground states. However the majority of the reactive events have exothermicities between 0 and 6 eV. Exothermicities in this 0 and 6 eV range must be due to the population of excited electronic or vibrational states of the products. We can therefore say that for the majority of the reactive events, at least one of the products were excited either electronically or vibrationally. For the formation of $NO^+ + O^+ + N$, in the previously discussed N_2^{2+} with O_2 system, the variation of the ground state vibrational excitation of NO^+, with the other products in the ground electronic and vibrational states, overlapped almost exactly with the range of exothermicities observed. Again in the formation of $NO^+ + CO^+ + N$ the variation of the ground state vibrational excitation of NO^+, with the other products in the ground electronic and vibrational states, (CO^+ $X^2\Sigma^+$ and N $2s^2 2p^3$, $^4S^0$), overlaps with the majority of the exothermicity observed. However many other combinations of vibronic and electronic states of any of the products, such as ground state CO^+ with a range of excited state NO^+ (most likely the lower states $a^3\Sigma^+$ and $b^3\Pi_p$ and) and N (most likely $2s^2 2p^3$, $^2D^0$ and $^2P^0$) or ground state NO^+ with a range of excited states of CO^+ (most likely $A^2\Pi_i$ and $B^2\Sigma^+$) and N (most likely $2s^2 2p^3$, $^2D^0$ and $^2P^0$), can also account for the observed exothermicity. Vibrations of CO^+, which span several eV, are another possibility. [17] But, as with the previously discussed bond-forming reactions of N_2^{2+} with O_2, the variation of the NO^+ ground state vibration overlaps well with the intensity of the exothermicity spectrum. This overlap of the NO^+ ground state vibration with the

observed exothermicity intensity does seem like a good agreement. The next section discusses the exothermicity spectrum of the other bond-forming reaction, (5.15), observed following the collisions of N_2^{2+} with CO_2.

5.3.2.3.2 Energetics of $NO^+ + N^+ + CO$

Again, for channel (5.15), the exothermicity spectrum is broad and unresolved as shown in Figure 5.18.

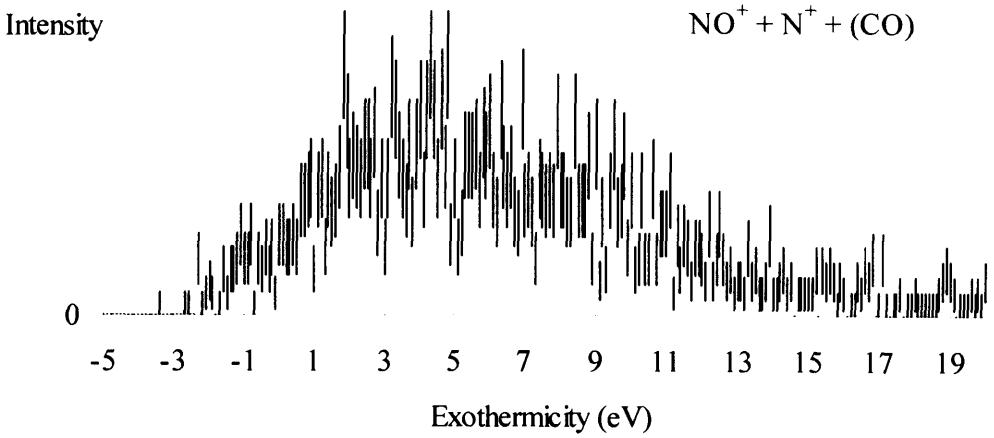

Figure 5.18 The exothermicity spectra for the bond-forming channel $NO^+ + N^+ + CO$, after false coincidence extraction, recorded using a 300 V repeller.

The exothermicity spectrum indicates an exothermicity from approximately -1 to 12 eV, with a maximum at approximately 4 eV, and the majority of events between 1 and 9 eV. The reaction of $N_2^{2+} + CO_2$ in the ground states to form $NO^+ + N^+ + CO$ in the ground states has a literature exothermicity of 10.43 eV. While the reaction of ground state N_2^{2+} with CO_2 to form $NO^+ + N^+ + C + O$ in their ground states has a literature exothermicity of -0.7 eV. Even if we consider the $c^3\Sigma u^+$ state of N_2^{2+} reacting to form ground state products, $NO^+ + N^+ + C + O$, the literature exothermicity is only 0.8 eV. Since the majority of the intensity in the exothermicity spectrum is above these values we can be certain that in this reaction the identity of the neutral product is CO.

As with the previous channel $NO^+ + CO^+ + N$ (5.14), once again the spectra indicates that at least a small amount of either N_2^{2+} in excited electronic states or N_2^{2+} in high vibrational levels of the ground state is present to account for the intensity from 10.43 eV up to approximately 12 eV. This intensity above 10.43 eV is most likely to be due to a small amount of reactions of the $c^3\Sigma u^+$ state of N_2^{2+} to form products in their ground states, which would have an exothermicity of 11.9 eV. But the majority of reactive

events have exothermicities associated with the population of excited electronic or vibrational states of at least one of the products. Again a variety of options could account for the intensity such as several low lying excited states of NO^+ together with ground state N^+ and CO, or ground state NO^+ with a variety of low lying excited states of N^+ and CO. Alternatively as for the previously discussed exothermicity spectra in the chapter, another very likely option is the variation of the vibration of ground state NO^+ with ground state N^+ and CO. Once again, the broad exothermicity spectrum hinders a definitive assignment of states to the reactants and products in this reaction channel.

To conclude, we have discussed the two bond-forming reactions, channels (5.14) and (5.15), detected following the collision of N_2^{2+} with CO_2. While the reaction mechanisms appear to be different, both reactions proceed via the formation of a collision complex, $[N_2CO_2^{2+}]$. In both cases the nitrogen species, N or N^+, is lost from the collision complex first, followed by dissociation of the NO^+ and the CO species, CO^+ or CO. Both reactions have broad exothermicity spectra, therefore, as with the previously discussed bond-forming reactions of N_2^{2+} with O_2, it is difficult to assign how the internal energy is distributed between the products, however again both exothermicity spectra could be explained almost entirely by vibration excitation of the NO^+ product. Certainly the majority of the exothermicities detected can only be associated with vibrationally or electronically excited products. The following section discuses the relative intensity, angular scattering and reaction exothermicity of three of the bond-forming reactions detected following the collisions of N_2^{2+} with H_2O.

5.3.3 N_2^{2+} with H_2O

Ten dominant bimolecular reactions can clearly be seen in the coincidence (pairs) spectra following collisions of N_2^{2+} with H_2O. The reactions observed are listed below and correspond to non-dissociative electron transfer (5.22), dissociative electron transfer (5.23), (5.24), (5.25) and (5.26), dissociative double electron transfer (5.27) and four bond-forming channels (5.28), (5.29), (5.30) and (5.31).

Non-dissociative electron transfer

$$N_2^{2+} + H_2O \rightarrow N_2^+ + H_2O^+ \qquad (5.22)$$

Dissociative electron transfer

$$N_2^{2+} + H_2O \rightarrow N_2^+ + HO^+ + H \qquad (5.23)$$
$$N_2^{2+} + H_2O \rightarrow N_2^+ + H_2^+ + O \qquad (5.24)$$

$$N_2^{2+} + H_2O \rightarrow N_2^+ + H^+ + OH \quad (5.25)$$
$$N_2^{2+} + H_2O \rightarrow H_2O^+ + N^+ + N \quad (5.26)$$

Dissociative double electron transfer

$$N_2^{2+} + H_2O \rightarrow OH^+ + H^+ (+N_2) \quad (5.27)$$

Bond-forming

$$N_2^{2+} + H_2O \rightarrow NO^+ + H_2^+ + N \quad (5.28)$$
$$N_2^{2+} + H_2O \rightarrow NO^+ + NH^+ + H \quad (5.29)$$
$$N_2^{2+} + H_2O \rightarrow NO^+ + H^+ (+ NH) \quad (5.30)$$
$$N_2^{2+} + H_2O \rightarrow NO^+ + N^+ (+ H_2) \quad (5.31)$$

Channel (5.24) is a dissociative electron transfer reaction with an H_2^+ product. The production of H_2^+ is not considered a 'bond-forming' product because electron ionisation cross sections of H_2O show that H_2^+ is undoubtedly a dissociation product of H_2O^+. [18]

The coincidence spectrum for the N_2^{2+} with H_2O system was recorded under the early version of the data acquisition program where it was necessary to exclude the N_2^{2+}/N^+ false coincidences in order to extend the collection time of the system. As previously mentioned, unfortunately, this exclusion also excluded the data collection of this real reaction which involved N^+. The program was subsequently adapted to extend the number of pairs it was possible to collect and hence it was no longer necessary to cut the false coincidences from collection. However channel (5.31) was not fully recorded and the data collection of the N_2^{2+} with H_2O system was not repeated in order to collect a full data set for channel (5.31) because this channel was very weak and there is a wealth of other bond-forming channels observed in the coincidence spectrum. Channel (5.31) may also be a four-body channel depending on whether the neutral product is H_2 or 2H. It is important to realize that if the reaction is a 4-body process our methodology of deriving the momentum of the neutral species from the ionic moments does not work. What will be derived is the vector sum of the momenta of the two neutrals. The scattering information derived for the two ions is unaffected, but care must be exercised when interpreting the "neutral velcoity" in the scattering diagrams. However, with this caveat some useful informtion for 4 body processes can be derived. In this case however it was deemed unnecessary to repeat the data collection, just for channel (5.31), when there were full data sets for the three other bond-forming channels detected in the N_2^{2+} with H_2O system.

Figure 5.19 shows a lower section of the coincidence spectrum recorded following the collisions of N_2^{2+} with H_2O. Five reactions can be observed in this area; including two bond-forming reactions, (5.28) and (5.30).

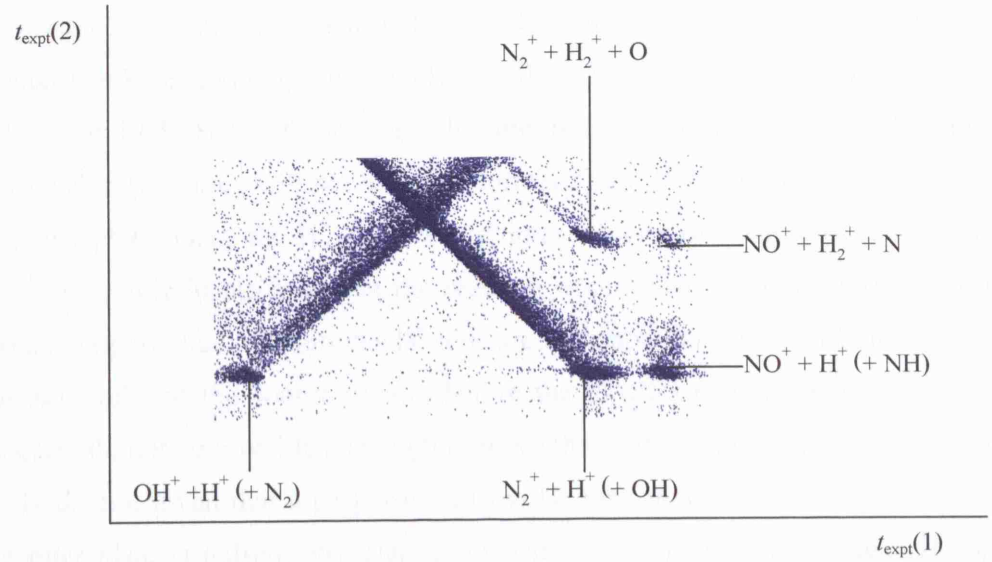

Figure 5.19 The lower section of the coincidence spectrum, showing five reaction channels including two bond-forming channels, recorded following collisions of N_2^{2+} with H_2O, with a 300 V repeller plate.

The next section explains the relative intensities of the various channels observed in this N_2^{2+} with H_2O reaction system, which is then followed by the discussion of the angular scattering of the three bond-forming channels, (5.29), (5.28) and (5.30) which have been recorded with full data sets.

5.3.3.1 Relative intensities

The relative intensities of the different reaction channels observed are derived by the comparing the number of counts in each coincidence peak in the pairs spectrum. As previously mentioned the data sets for the two channels with an N^+, (5.26) and (5.31), have not been fully recorded. However we estimate, from the recorded area, that the intensity of the bond-forming channel (5.31) is approximately twice as intense as the bond-forming channel (5.29). The method by which we make these estimations is described in the previous chapter, Chapter Four, section 4.3.2.1. The intensity of the dissociative electron transfer channel (5.26) is difficult to estimate as there are no other channels with similar peak shapes to use in the estimation. The relative intensities of the other eight channels, where full data sets have been recorded, have been derived. The non-dissociative charge transfer reaction, (5.22), the dissociative charge transfer

reactions, (5.23), (5.24) and (5.25), dissociative double electron transfer reaction, (5.27), and bond-forming reactions, (5.28), (5.29) and (5.30), are formed in the ratio 211 : 50 : 3 : 14 : 5 : 1 : 8 : 4.

The channels with a H^+ ((5.25), (5.27) and (5.30)) or H_2^+ ((5.24) and (5.28)) pair might be expected be weak. H^+ ions, and even H_2^+, are so light that, if they have significant transverse kinetic energy, they could actually leave the source region before the repeller plate is pulsed. Hence these ions will either not be detected at all or will not be detected as efficiently as they will not have the correct *TOF*. If the reaction occurs just before the repeller plate pulse, the H^+ ions will be detected with the same probability as any other ion. However in the case that the reaction occurs just as the dication pulse enters the source region, then certainly the H^+ ions are fast enough to fly out of the source region, or hit the walls of the source region, before the repeller plate is pulsed. Larger, heavier species do not be travel fast enough to leave the source region before the repeller plate is pulsed. So, given that a proportion of the H^+ ions may be lost in the period before the repeller plate is pulsed, the relative intensities of reactions involving a H^+ product are lowered relative to reactions not involving a H^+ product. We can therefore confidently postulate that in the source region channels (5.25), (5.27), (5.30), (5.24) and (5.28), which all have a H^+ or H_2^+ product, are formed to a relatively larger extent than their relative intensities imply.

5.3.3.2 Angular scattering

The following section describes the angular scattering for the three bond-forming channel, (5.29), (5.28) and (5.30) in sections 4.3.3.2.1, 4.3.3.2.2 and 4.3.3.2.3 respectively, where full scattering data has been recorded.

5.3.3.2.1 The formation of $NO^+ + NH^+ + H$ (5.29)

This bond-forming channel, (5.29), is weak; hence the scattering diagrams appear to be very noisy. However interpretation of the scattering can still yield clear mechanistic conclusions since the scattering of the true reaction peak can easily be distinguished from the background noise.

Figure 5.20 (a) and (b) show the scattering of the products, NO^+, NH^+ and H, relative to the velocity of N_2^{2+} in the COM frame.

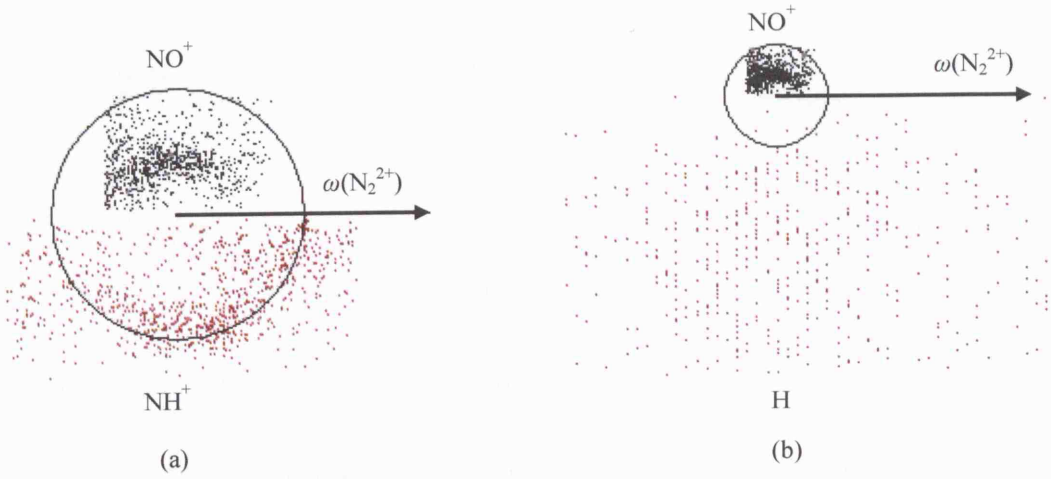

Figure 5.20 The scattering diagrams for (a) NO^+ and NH^+ and (b) NO^+ and H with respect to the velocity of N_2^{2+} in the COM frame, recorded following collisions of N_2^{2+} with H_2O at 300 V repeller plate. The scattering diagrams are shown on different scales, as will be seen throughout this N_2^{2+} with H_2O section, but both have a circle radius 1 cm μs^{-1}.

All three products are obviously symmetrically scattered relative to the velocity of N_2^{2+} in the COM frame. As observed and described in the previously discussed bond-forming reactions of N_2^{2+} with O_2 and one of the bond-forming reactions of N_2^{2+} with CO_2, this isotropic scattering of all three reaction products is a strong indication that all the products have been formed from the dissociation of a collision complex, in this case $[N_2\text{-}H_2O]^{2+}$.

As discussed for the similar bond-forming reactions of N_2^{2+} with O_2 and one of the N_2^{2+} with CO_2 bond-forming reactions, this collision complex must have lived for a period of time at least equal with its rotational period since the scattering diagrams in Figure 5.20 show the products have been scattered through the whole range of angles, relative to N_2^{2+} in the COM frame, upon the dissociation of the collision complex.

Figure 5.21 shows the internal frame scattering diagrams for channel (5.29), showing each of the products relative to the other products.

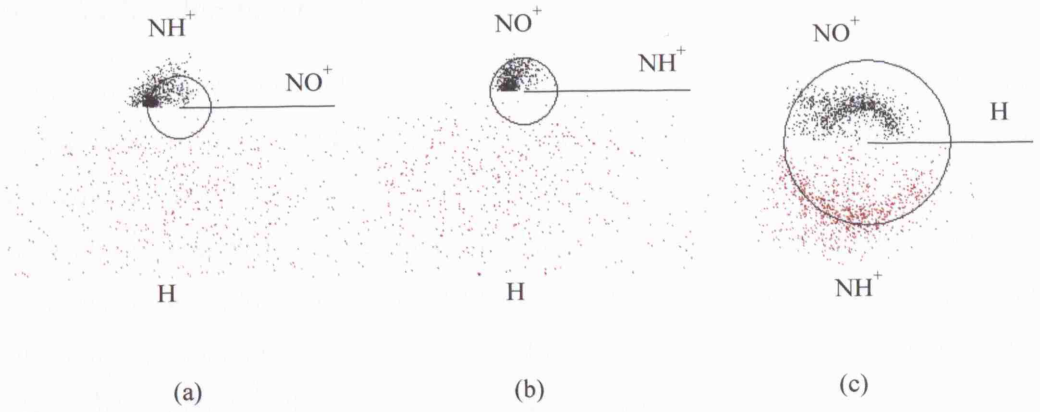

Figure 5.21 The internal frame scattering diagrams, circle radius 1 cm μs^{-1}, showing (a) NH^+ and H relative to NO^+, (b) NO^+ and H relative to NH^+ and (c) NO^+ and NH^+ relative to H, recorded following collisions of N_2^{2+} with H_2O at 300 V repeller plate.

The upper halves of the internal frame scattering diagrams in Figure 5.21 (a) and (b) show that the two charged species, NH^+ and NO^+, are clearly anti-correlated with each other. The neutral species, H, however appears to have no correlation with either of the charged species. As previously explained for the bond-forming reactions of N_2^{2+} with O_2 and one of the bond-forming reactions of N_2^{2+} with CO_2, this lack of correlation of the neutral species with either of the charged species is indicative that the neutral species was formed before the charge separating step. If the neutral had been formed after the charge separating step, we would expect to see some correlation of the velocity of the H with one of the charged products. Figure 5.21 (c) clearly shows that the charged species have no relationship with the H product, suggesting that the neutral loss was a distinct mechanistic step. Therefore the second intermediate complex $[N_2OH^{2+}]$ had time to rotate before the charge separation.

To conclude, the reaction mechanism of this bond-forming channel proceeds via formation of an intermediate collision complex, $[N_2H_2O]^{2+}$. The isotropic scattering of the products relative to N_2^{2+} in the COM frame shows that this complex lives for a period of time at least as long as its rotational period. The neutral species, H, then dissociates from the collision complex. A second complex, $[N_2HO]^{2+}$, is formed, which may also live for a period of time at least as long as its rotational period, before dissociation into the two charged species, NO^+ and NH^+.

$$N_2^{2+} + H_2O \rightarrow [N_2H_2O]^{2+} \rightarrow [N_2OH]^{2+} + H \rightarrow NO^+ + NH^+ + H \qquad (5.32)$$

5.3.3.2.2 The formation of $NO^+ + H_2^+ + N$ (5.28)

This bond-forming channel, (5.28), is weak. However, there was significantly less noise in the area of the coincidence spectrum for this reaction compared to the area of the coincidence spectrum for the previous channel (5.29). This is because far fewer background counts in the coincidence spectrum will arise from the false coincident detection of low *m/z* species such as H_2^+. As explained above, low *m/z* species are less likely to be detected as they may leave the source region or hit the walls of the source region before the repeller plate pulse. Therefore the scattering diagrams appear 'cleaner' than those of the previous reaction discussed.

Figure 5.22 (a) and (b) shows the scattering of all the products relative to N_2^{2+} in the COM frame. The H_2^+ and N product shows a hint of forward scattering with respect to the velocity of the dication in the COM frame in Figure 5.22 (a) and Figure 5.22 (b) respectively, while the NO^+ is scattered slightly in the opposite direction to the dication in both Figure 5.22 (a) and (b). This is certainly different to the previously discussed reaction mechanisms of the bond-forming reactions of N_2^{2+} with O_2 and one of the bond-forming reactions of N_2^{2+} with CO_2, as well as the previously discussed reaction of N_2^{2+} with H_2O in section 4.3.3.2.3. The scattering in Figure 5.22 suggests that no long-lived complex was formed which has a timescale comparable with its rotational period. The slight forwards scattering of the neutral product hints that the neutral product was formed after the charge separating step, hence its scattering has been influenced by the Coulomb repulsion in the charge separating step. The fact the H_2^+ is also slightly forwards scattered hints that the H_2^+ and the N were formed together (as NH_2^+), later dissociating.

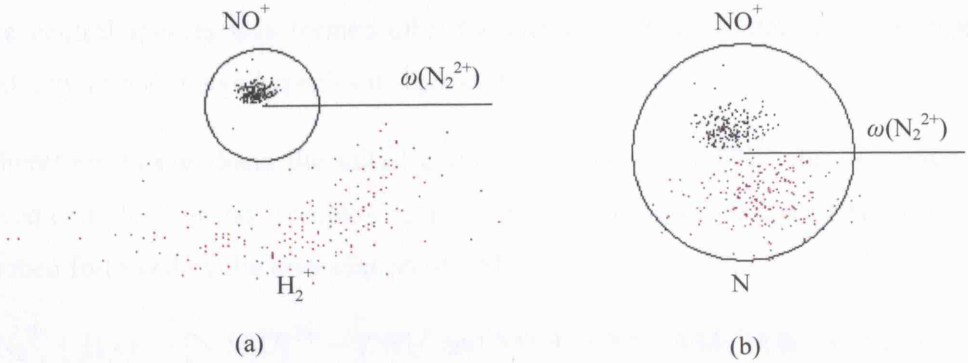

Figure 5.22 The scattering diagrams, circle radius 1 cm μs^{-1}, for (a) NO^+ and H_2^+ and (b) NO^+ and N with respect to the velocity of the dication in the COM frame, recorded following collisions of N_2^{2+} with H_2O at 300 V repeller plate.

The internal frame scattering diagrams in Figure 5.23 yield even more information to confirm that this channel follows a different reaction mechanism to those seen previously in the bond-forming reactions of N_2^{2+} with O_2 and one of the bond-forming reactions of N_2^{2+} with CO_2, as well as that of the previously described channel, (5.29), of N_2^{2+} with H_2O.

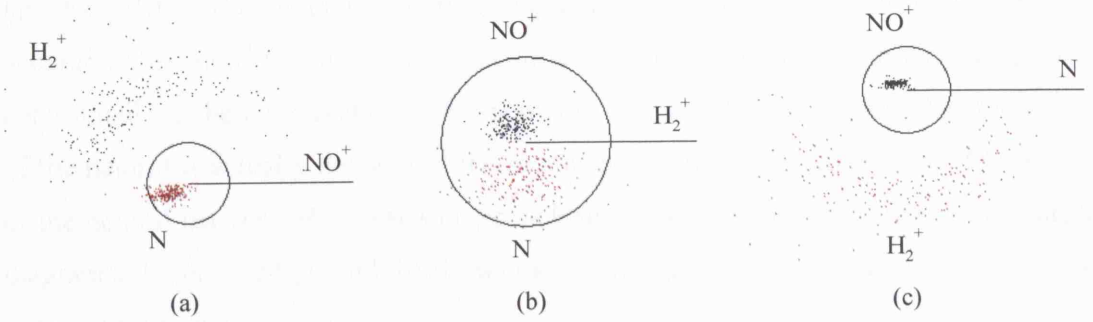

Figure 5.23 The internal frame scattering diagrams, circle radius 1 cm μs^{-1}, showing (a) H_2^+ and N relative to NO^+, (b) NO^+ and N relative to N_2^+ and (c) NO^+ and N_2^+ relative to N, recorded following collisions of N_2^{2+} with H_2O at 300 V repeller plate.

The upper half of the scattering diagrams in Figure 5.23 (a) and (b) show that the two charged species, H_2^+ and NO^+, are subtly anti-correlated with each other. In the internal frame, both the neutral species, N and the H_2^+, appear to have little correlation with each other, as can be seen in the lower halves of Figure 5.23 (b) and (c). However the velocity of N and NO^+ appear to be anti-correlated with each other, as seen in the lower half of Figure 5.23 (a) and upper half of Figure 5.23 (c). While the anti-correlation of the two charged species in the internal frame is not unexpected, irrespective of the mechanism, the correlation or anti-correlation of the neutral species with a charged species hints that the neutral species was formed after the charge separating step and hence retained the velocity of the charged species it separated with.

Therefore, to conclude, the initial collision to form $[N_2H_2O]^{2+}$ did not result in a long-lived complex but the 'complex' quickly charge separated to form NH_2^+ and NO^+, which is then followed by the dissociation of NH_2^+ into N and H_2^+;

$$N_2^{2+} + H_2O \rightarrow [N_2H_2O]^{2+} \rightarrow [NH_2^+ \text{ and } NO^+] \rightarrow NO^+ + H_2^+ + N \qquad (5.33)$$

5.3.3.2.3 The formation of $NO^+ + H^+$ (+ NH) (5.30)

This channel, (5.30), could be a three or a four-body channel depending on whether the neutral species is an NH molecule or a N atom and a H atom. Unfortunately in this case we can not use the energetics to determine which the more likely option is. The fact that we do detect NO^+ paired with NH^+ may suggust that the identity of the neutral species is NH although this is only conjecture. Therefore for consistency alone the neutral is labelled (NH). The angular scattering diagrams we derive can only truly be considered accurate when used for three-body reactions since the velocity of the neutral species is determined via the conservation of momentum. Therefore, what is plotted as the velocity of the neutral is actually the sum of the momenta of the two neutrals divided by the sum of the neutral masses. However some conclusions can still be drawn from the scattering diagrams. Figure 5.24 (a) and (b) shows the scattering of all three vectors relative to N_2^{2+} in the COM frame.

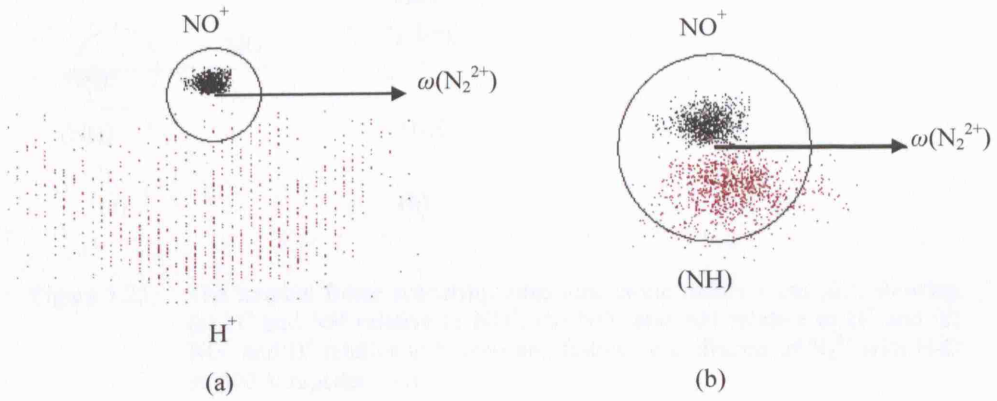

Figure 5.24 The scattering diagrams, circle radius 1 cm μs^{-1}, for (a) NO^+ and H^+ and (b) NO^+ and (NH) with respect to the velocity of the dication in the COM frame, recorded following collisions of N_2^{2+} with H_2O at 300 V repeller plate.

Upon first impression, the scattering of all the products in Figure 5.24 appears to be across a full range of scattering angles. However, on closer inspection, the NO^+ in fact seems to be scattered slightly in the opposite direction to the velocity of the dication in the COM frame while the H^+ and the (NH) seem to be scattered slightly in the same direction as the dication. Given how close the products are to isotropic it most probable that a complex, $[N_2H_2O]^{2+}$, was formed which on average dissociated before completion of a full rotational period and hence the scattering of products shows a range of velocities which are not quite isotropic. So this scattering hints that any collision complex formed was short-lived. In section 4.3.1.2.1 the rotational lifetime of $[N_2O_2]^{2+}$ was stated to be of

the order of 20 fs, it is likely that the lifetime of the short-lived complex, $[N_2H_2O]^{2+}$, is of the order of 20 fs. The fact the H^+ and the (NH) both appear to be slightly forwards scattered while the NO^+ is scattered in the opposite direction implies that the short-lived collision complex decayed via charge separation with the H^+ and the (NH) dissociating together as $[NH_2^+]$. The neutral species will retain some of the velocity derived from the Coulomb repulsion in the charge separating step hence why if the H^+ and the (NH) are formed together they appear to be scattering in the same direction. Figure 5.25 shows the internal frame scattering diagrams for each of the products relative to each other. These scattering diagrams provide more convincing evidence that supports a similar reaction mechanism to that of the previous reaction discussed, channel (5.28).

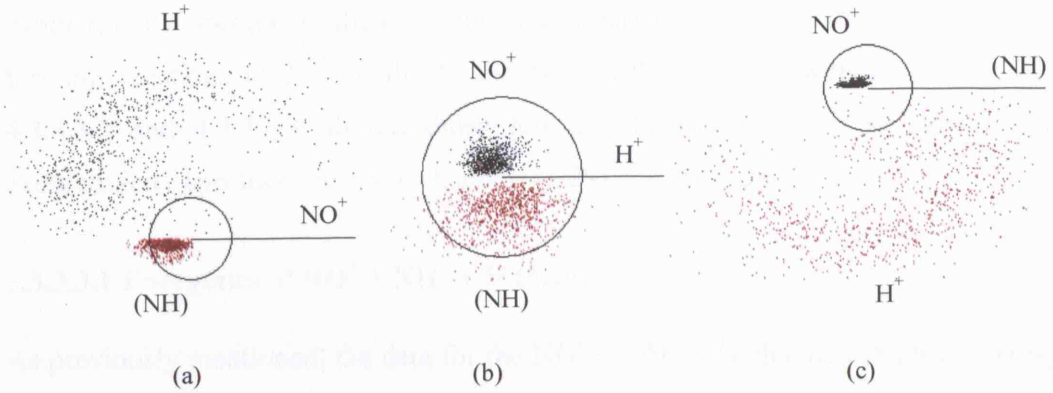

Figure 5.25 The internal frame scattering diagrams, circle radius 1 cm μs^{-1}, showing (a) H^+ and NH relative to NO^+, (b) NO^+ and NH relative to H^+ and (c) NO^+ and H^+ relative to N recorded following collisions of N_2^{2+} with H_2O at 300 V repeller plate.

The upper half of the scattering diagrams in Figure 5.25 (a) and (b) show that the two charged species, H^+ and NO^+, are anti-correlated with each other. The velocity of the neutral species in the internal frame appears to be anti-correlated with that of the NO^+ and correlated with that of the H^+. This therefore confirms that the initial mechanistic step was the charge dissociation step of the short lived complex, $[N_2H_2O]^{2+}$, to form NO^+ and $[NH_2^+]$ followed by further dissociation of $[NH_2^+]$ to yield H^+ and (NH);

$$N_2^{2+} + H_2O \rightarrow [N_2H_2O]^{2+} \rightarrow [NH_2^+ \text{ and } NO^+] \rightarrow NO^+ + (NH) + H^+ \qquad (5.34)$$

5.3.3.2.4 Summary

To summarise, there are two different reaction mechanisms in the bond-forming reactions of N_2^{2+} with H_2O. The reaction mechanism of channel (5.30) is the same as the reaction mechanism for the previously discussed reaction mechanisms of N_2^{2+} with O_2 and CO_2.

That is the reaction proceeds via neutral loss from a long-lived collision complex, followed by charge dissociation of the remaining second complex. The second mechanism observed for the bond-forming reactions of N_2^{2+} with H_2O forms a "short-lived" collision complex, with a lifetime of the order of less than 20 fs, which dissociates via charge separation followed by dissociation of one of the monocations to form a singly charged species and one or more neutral species. The next section briefly discusses the exothermicity spectra derived from the PSCO data for these bond-forming reactions.

5.3.3.3 Energetics

As previously mentioned the bond-forming reactions detected following the collisions of N_2^{2+} with H_2O are weak; therefore it is harder to derive any conclusions from the exothermicity spectra of these reactions compared to the previously discussed bond-forming reactions of N_2^{2+} with O_2 and N_2^{2+} with CO_2. However sections 4.3.3.3.1, 4.3.3.3.2 and 4.3.3.3.3 discuss those few conclusions that can be drawn from the exothermicity spectra of reaction channels (5.29), (5.28) and (5.30).

5.3.3.3.1 Energetics of $NO^+ + NH^+ + H$ (5.29)

As previously mentioned, the data for the $NO^+ + NH^+ + H$ channel, (5.29), is 'noisy' due to the weak nature of the reaction which lay very near to the false coincidence strip in the coincidence spectrum. Therefore the background noise of the false coincidences with any random background ions, with *m/z* close to that of NO^+ and NH^+, were almost as intense as the reaction peak itself. While the reaction peak was still easily distinguishable in the coincidence spectrum, and conclusions about the reaction mechanism could still be drawn from the angular scattering diagrams, the exothermicity spectrum appears so noisy that no meaningful conclusions can be drawn for the energetics of this channel. Hence there will be no further discussion of the exothermicity spectrum derived from the PSCO data for this channel. However information can be found in the exothermicity spectra of the two other bond-forming channels, (5.28) and (5.29), as follows.

5.3.3.3.2 Energetics of $NO^+ + H_2^+ + N$ (5.28)

This channel was particularly weak, in fact it was the weakest channel detected as can be seen from the relative intensities. Therefore the exothermicity spectrum appears very weak as can be seen from Figure 5.26. However this channel was recorded in a 'clean' area of the coincidence spectrum where there were few false coincidence detections, as

previously mentioned, therefore true reaction intensity can be observed in the exothermicity spectrum.

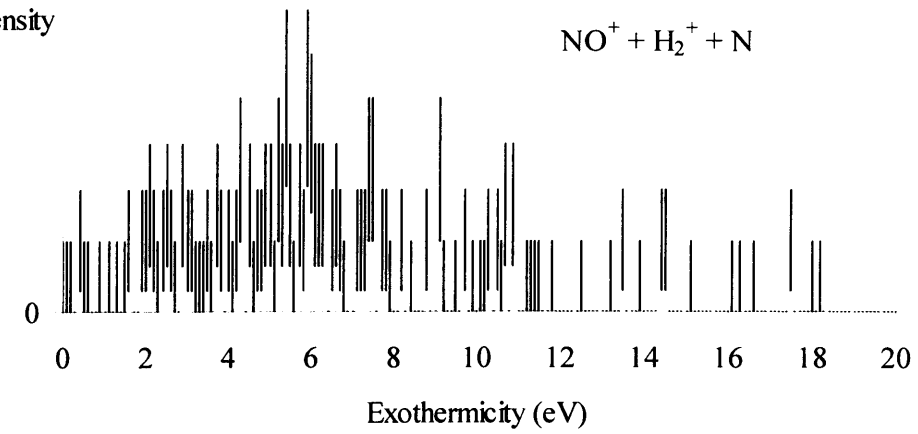

Figure 5.26 The exothermicity spectrum for channel (5.28) derived from the data recorded using a 300 V repeller plate.

Despite the very weak nature of this spectrum we can still observe that the exothermicity has intensity between approximately 2 and 8 eV. A reaction of ground state reactants to form ground state products for this channel has an exothermicity of approximately 15 eV. There is virtually no intensity at this exothermicity therefore certainly this reaction proceeded to form products almost entirely in excited electronic or vibrational states. In addition, unlike the previously discussed bond-forming reactions of N_2^{2+} with O_2 and CO_2, this means we do not see a good overlap of the exothermicity spectrum with the formation of all the products in their ground states but with NO^+ in a full range of vibrational states. Therefore the reaction could proceed to form products in a range of excited electronic and/or vibrational states, but we can not distinguish between this range of excited states which could contribute to the exothermicity spectrum.

5.3.3.3.3 Energetics of $NO^+ + H^+$ (+ NH) (5.30)

This channel, (5.30), was also weak, but significantly stronger than the previous channel.

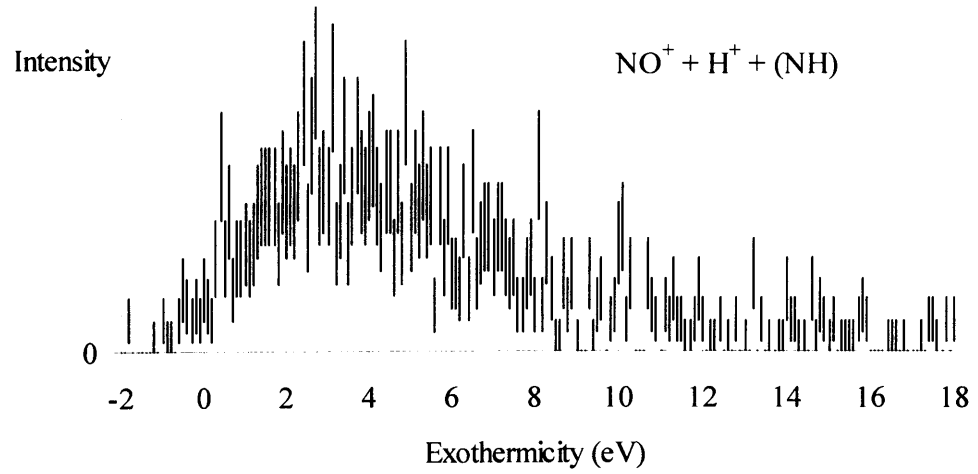

Figure 5.27 The exothermicity spectrum for channel (5.30) derived from the data recorded using a 300 V repeller plate.

The intensity of the exothermicity spectrum for channel (5.30) is between approximately 0 and 7 eV. A reaction of ground state reactants to form ground state products for this channel has an exothermicity of approximately 15 eV or 18 eV depending on whether the neutral product is NH or N and H. As with the previous channel there is virtually no intensity at these ground state exothermicities in the exothermicity spectrum derived from the PSCO data. Therefore, irrespective of the identity of the neutral product, at least one of the products is formed in an excited vibrational and/or electronic state in all the reactions.

For the bond-forming reactions of N_2^{2+} with O_2 and N_2^{2+} with CO_2 we concluded that the reaction mechanism involved a long-lived collision complex and that the independent computational work deduced that these collision complexes have N–O bond lengths different from that of the ground state of NO^+, therefore one might expect a significant vibrational excitation of the NO^+ product. The vibrations of the ground state NO^+ product, together with the other products in their ground states, overlapped very well with the observed reaction exothermicity spectra for the bond-forming reactions of N_2^{2+} with O_2 and N_2^{2+} with CO_2. However we do not conclude any involvement of a long-lived collision complex for this channel, $NO^+ + H^+$ (+ NH). Interestingly the intensity in the exothermicity does not overlap as well with the vibrations of the ground state NO^+ product. While this does not give us any information regarding the electronic or vibrational channels of this channel $NO^+ + H^+$ (+ NH), it does hint that the energetics conclusions, regarding the variation of the vibration of the NO^+ product, in the bond-forming reactions of N_2^{2+} with O_2 and N_2^{2+} with CO_2, could be correct.

5.4 Conclusion

We have studied the reaction between N_2^{2+} and O_2, CO_2 and H_2O, which are potentially significant in the terrestrial ionosphere, using position sensitive coincidence spectroscopy. We observe non-dissociative and dissociative electron transfer, dissociative double electron transfer reactions as well as several bond-forming channels. Notably all of the bond-forming channels involve the formation of NO^+. The NO^+ is formed together with a second charged species and one or two neutral products. NO^+ is one of the most abundant components of the terrestrial ionosphere so it particularly interesting that all of the bond-forming reactions produced NO^+ in this study of the potentially terrestrially significant reactions between N_2^{2+} with O_2, CO_2 and H_2O.

The scattering diagrams derived from the PSCO data for both of the bond-forming reactions of N_2^{2+} with O_2, one of the bond-forming reactions of N_2^{2+} with CO_2, and for one of the bond-forming reactions of N_2^{2+} with H_2O, showed the products are all approximately symmetrically scattered in the Centre Of Mass frame. In the internal frame it is clear that the velocities of the charged products are generally anti-correlated whilst the velocities of the neutral products are generally not correlated with the velocities of the charged products. The scattering data clearly indicates that the bond-forming reactions proceed via a collision complex $[N_2XO]^{2+}$, where X = O, CO or H_2. This collision complex then decays by loss of a neutral atom to form a daughter dication which then decays by charge-separation to yield the observed products. One of the bond-forming reactions of N_2^{2+} with CO_2 and two of the bond-forming reactions of N_2^{2+} with H_2O do not appear to follow this 'neutral loss' mechanism. In the case of the reaction of N_2^{2+} with CO_2 to form NO^+ with N^+ and CO the reaction mechanism proceeds via the formation of a collision complex which dissociates via charge separation followed by dissociation of one of the monocations to form NO^+ and CO or C and O. While in the case of the two bond-forming reactions of N_2^{2+} with H_2O, the reaction mechanism proceeds via the formation of a short-lived collision complex which dissociates via charge separation followed by dissociation of one of the monocations to form a singly charged species and one or more neutral species.

The exothermicity spectra for the bond-forming reactions do not yield as much information as the scattering diagrams, however we can still make some conclusions, particularly for the bond-forming reactions involving the long-lived collision complex. In these bond-forming reactions involving a long-lived collision complex (N_2^{2+} with O_2 and

CO_2) it appears that the energetics could be dominated by the formation of the NO^+ products in their ground electronic state but with a full range of vibrational levels whereas the other products are all in their ground electronic states. Therefore we can make only a few conclusions about the energetics but the analysis of the scattering diagrams provides a significant amount of information about the reaction dynamics of the reactions of N_2^{2+} and O_2, CO_2 and H_2O.

5.5 References

[1] Simon, C., Lilensten, J., Dutuit, O., Thissen, R., Witasse, O., Alcaraz, C., and Soldi-Lose, H., 2005, Annales Geophysicae, 23, 3, 781.
[2] Lilensten, J., Witasse, O., Simon, C., Solidi-Lose, H., Dutuit, O., Thissen, R., and Alcaraz, C., 2005, Geophysical Research Letters, 32, 3.
[3] Savage, H. F. and Wittebor, F. C., 1968, Journal of Chemical Physics, 48, 4, 1872.
[4] Kamber, E. Y., Akgungor, K., Safvan, C. P., and Mathur, D., 1996, Chemical Physics Letters, 258, 3-4, 336.
[5] Dutuit, O., Thissen, R., and Soldi-Lose, H., 2005, -Unpublished.
[6] Hu, W. P., Harper, S. M., and Price, S. D., 2002, Measurement Science & Technology, 13, 10, 1512.
[7] Ricketts, C. L., Harper, S. M., Hu, S. W. P., and Price, S. D., 2005, Journal of Chemical Physics, 123, 13, 134322-1.
[8] Fournier, P. G., Eland, J. H. D., Millie, P., Svensson, S., Price, S. D., Fournier, J., Comtet, G., Wannberg, B., Karlsson, L., Baltzer, P., Kaddouri, A., and Gelius, U., 1988, Journal of Chemical Physics, 89, 6, 3553.
[9] Masuoka, T. and Kobayashi, A., 2004, Chemical Physics, 302, 1-3, 31.
[10] Glukhovtsev, M. N. and Laiter, S., 1996, Journal of Physical Chemistry, 100, 5, 1569.
[11] Engelke, R., Blais, N. C., and Sander, R. K., 1999, Journal of Physical Chemistry A, 103, 28, 5611.
[12] Zheng, J. P., Waluk, J., Spanget-Larsen, J., Blake, D. M., and Radziszewski, J. G., 2000, Chemical Physics Letters, 328, 1-2, 227.
[13] Price, S. D., Eland, J. H. D., Fournier, P. G., Fournier, J., and Millie, P., 1988, Journal of Chemical Physics, 88, 3, 1511.
[14] Harris, F. M., Reid, C. J., Ballantine, J. A., and Parry, D. E., 1991, Journal of the Chemical Society-Faraday Transactions, 87, 11, 1681.
[15] NIST Chemistry WebBook, National Institute Of Standards and Technology, 2003, - http://webbook.nist.gov.
[16] Gerakines, P. A. and Moore, M. H., 2001, Icarus, 154, 2, 372.
[17] Krupenie, P. H. and Weissman, S., 1965, Journal of Chemical Physics, 43, 5, 1529.
[18] Straub, H. C., Lindsay, B. G., Smith, K. A., and Stebbings, R. F., 1998, Journal of Chemical Physics, 108, 1, 109.

Chapter 6 The reactions of the Nitrogen Dication Part III: Bond-forming reactions of N_2^{2+} with C_2H_2, H_2, CH_4 and Ar

6.1 Introduction

Modelling has suggested that N_2^{2+} ions are present in the nitrogen rich ionosphere of Titan. [1] These dications are believed to be lost by electron recombination and chemical reactions with neutral species such as Ar, H_2 and hydrocarbons, for example CH_4 and C_2H_2. In a study of the reactions of N_2^{2+} with ionospherically relevant neutrals by Dutuit *et al*, several bond forming products were observed in the reaction of N_2^{2+} with CD_4, including ND^+, ND_2^+, DCN^+ and D_2CN^+. [2] Dutuit *et al* also studied the reaction of N_2^{2+} with Ar but did not observe a bond forming channel. The reaction of N_2^{2+} with Ar was first studied in the 1960s by Savage *et al* and has since been studied by several other groups including Kamber *et al*, Koslowski *et al* and Schulz *et al*. [3-6] However, these studies concentrate on the electron transfer reactions and do not discuss any observation of a bond forming channel. A more detailed introduction to the ionosphere of Titan is given in Chapter One and to N_2^{2+}, and its reactions, in Chapter Three.

In this Chapter, the reactions of C_2H_2, H_2, CH_4 and Ar with N_2^{2+} at low collision energies, between approximately 1 eV and 11 eV in the COM frame, are discussed. These reactions have been grouped together due to similarities in the observed reaction mechanisms for the bond forming channels, as well as their common relevance to the atmosphere of Titan. The reactions of N_2^{2+} with Ar, CH_4 and H_2 may also be of relevance to the ionosphere of Earth. [7]

6.2 Experimental

Details of the experimental methodology are given in Chapter Two together with details of the data processing. Specific details of the experiments discussed in this Chapter are as follows. The reactions of N_2^{2+} with C_2H_2 have been studied using the PSCO technique at a range of COM collision energies (4.81, 5.78, 6.74, 8.67 and 10.59 eV), at a repeller plate voltage of 300 V. The PSCO spectrum following the reaction of N_2^{2+} with CH_4 was recorded at a 300 V repeller plate voltage, (7.46 eV COM collision energy) and 50 V

repeller plate voltage, (4.8 eV COM collision energy). The PSCO spectrum following the reaction of N_2^{2+} with H_2 was recorded at a 300 V repeller plate voltage (0.93 eV COM collision energy). Finally the PSCO spectrum resulting from the reaction of N_2^{2+} with Ar was recorded at a 300 V repeller plate voltage (8.24 eV COM collision energy).

6.3 Results and discussion

This section presents the results of the PSCO studies of the reactions of N_2^{2+} with C_2H_2, H_2, CH_4 and Ar. As previously mentioned, due to the vast amount of chemistry observed in this survey of the reactions of N_2^{2+} with neutrals, only the bond forming reactions are discussed in detail; other reaction types have been well rationalised previously (for details on typical electron transfer reactions see Chapter Four). Details of the relative intensities of the different channels, and, for the bond-forming reactions only, the reaction energetics and reaction mechanisms are discussed. Further experimental details related to the deviation of the relative intensities of the different channels, the reaction energetics and the angular scattering is given in the experimental Chapter, Chapter Two. Chapter Three details experimental features such as 'tails' in the coincidence spectrum and the extraction of false coincidences. Sections 6.3.1, 6.3.2, 6.3.3 and 6.3.4 cover the bond forming reactions of N_2^{2+} with C_2H_2, H_2, CH_4 and Ar respectively. As will become apparent, the result from the PSCO study of the bond-forming reactions of N_2^{2+} with CH_4 and H_2 are slightly ambiguous so are only discussed briefly, while the more definitive data on the bond forming reactions of N_2^{2+} with C_2H_2 are discussed in detail. Finally, the dynamics of the novel '2 body' bond-forming reaction between N_2^{2+} and Ar is presented; this is the first investigation of the dynamics of a bond-forming reaction between a dication and a rare gas atom.

6.3.1 N_2^{2+} with C_2H_2

Many bimolecular reactions can clearly be seen in the coincidence spectra recorded following collisions of N_2^{2+} with C_2H_2. The observed reactions are listed below, according to the types of reactions.

Non-dissociative electron transfer:

$$N_2^{2+} + C_2H_2 \rightarrow N_2^{+} + C_2H_2^{+} \quad (6.1)$$

Dissociative electron transfer:

$$N_2^{2+} + C_2H_2 \rightarrow N_2^{+} + C_2H^{+} + H \quad (6.2)$$
$$N_2^{2+} + C_2H_2 \rightarrow N^{+} + C_2H_2^{+} + N \quad (6.3)$$
$$N_2^{2+} + C_2H_2 \rightarrow N_2^{+} + H^{+} + (C_2H) \quad (6.4)$$
$$N_2^{2+} + C_2H_2 \rightarrow N^{+} + C_2H^{+} (+ N + H) \quad (6.5)$$

Dissociative double electron transfer:

$$N_2^{2+} + C_2H_2 \rightarrow H^{+} + C_2H^{+} (+ N_2) \quad (6.6)$$
$$N_2^{2+} + C_2H_2 \rightarrow H^{+} + C^{+} (+ N_2 + CH) \quad (6.7)$$
$$N_2^{2+} + C_2H_2 \rightarrow H^{+} + CH^{+} (+ C + N_2) \quad (6.8)$$
$$N_2^{2+} + C_2H_2 \rightarrow H^{+} + C_2^{+} (+ H + N_2) \quad (6.9)$$

Bond-forming:

$$N_2^{2+} + C_2H_2 \rightarrow H^{+} + C_2NH^{+} + N \quad (6.10)$$
$$N_2^{2+} + C_2H_2 \rightarrow N^{+} + C_2NH^{+} + H \quad (6.11)$$
$$N_2^{2+} + C_2H_2 \rightarrow H^{+} + C_2N^{+} (+ H + N) \quad (6.12)$$
$$N_2^{2+} + C_2H_2 \rightarrow N^{+} + C_2N^{+} (+ H + H) \quad (6.13)$$

Figure 6.1 shows a section of a typical coincidence spectrum recorded following collisions of N_2^{2+} with C_2H_2 at 6.74 eV, showing two bond-forming reactions, $N^+ + C_2N^+$ (+ H + H) (6.13) and $N^+ + C_2NH^+ + H$ (6.11). The peaks due to the bond-forming reactions can clearly be distinguished even with the strip of false coincidences running through the peaks.

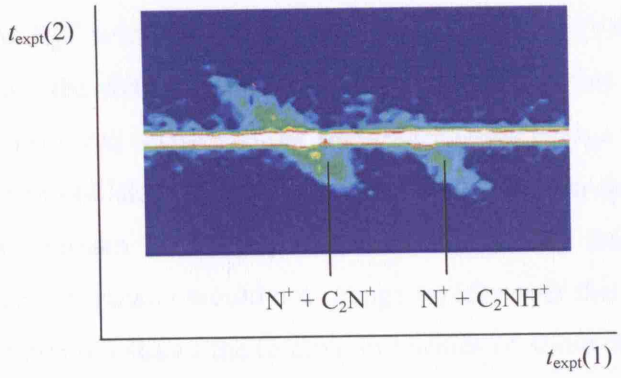

Figure 6.1 A section of a coincidence spectrum showing two bond-forming channels (6.13) and (6.11) with the horizontal line of false coincidences running through the reaction channels recorded using 300 V repeller plate and at E_{com} 6.74 eV.

Figure 6.2 shows a second section of the coincidence spectrum, now focusing on two different bond-forming channels, $H^+ + C_2N^+$ (+ H + N) (6.12) and $H^+ + C_2NH^+ + N$ (6.10). This section of the coincidence spectrum also shows two dissociative double

electron transfer reactions, $H^+ + C^+$ (+ N_2 + CH) (6.7) and $H^+ + CH^+$ (+ C + N_2) (6.8), and a dissociative electron transfer channel, $N_2^+ + H^+ + (C_2H)$ (6.4).

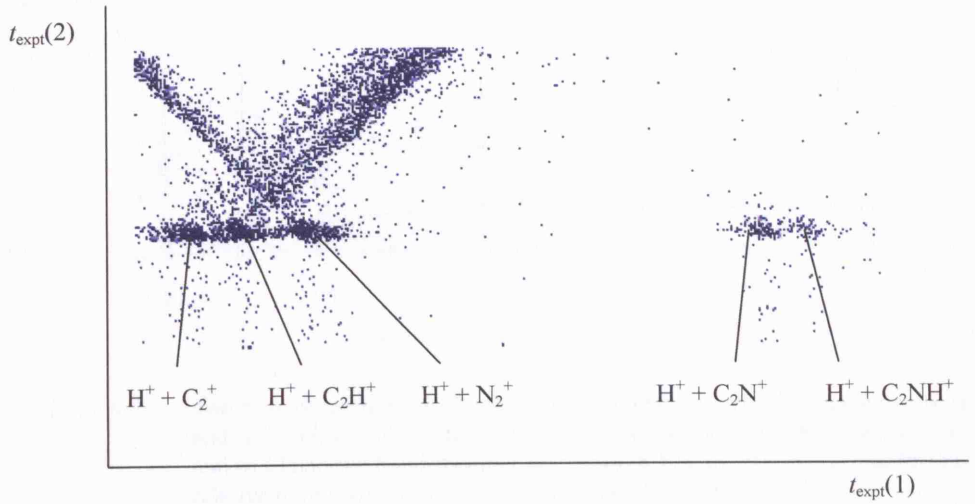

Figure 6.2 A section of a coincidence spectrum showing two bond-forming channels, (6.12) and (6.10), two dissociative double electron transfer reactions, (6.7) and (6.8), and a dissociative electron transfer channel (6.4) recorded using 300 V repeller plate and at E_{com} 6.74 eV.

The following section discusses the relative intensities of the channels detected following the collisions of N_2^{2+} with C_2H_2.

6.3.1.1 Relative intensities of different reactive channels

The reaction of N_2^{2+} with C_2H_2 was studied at a range of COM collision energies. In order to compare the change in the intensities of the channels at different energies, the intensities are measured relative to the non-dissociative charge transfer channel. At this restricted range of collision energies, the intensity of the non-dissociative charge transfer channel should remain reasonably constant. That is, the cross-section for non-dissociative electron transfer would not change rapidly over this narrow range of collision energies. [8] Figure 6.3 shows the relative intensities of some of the dissociative electron transfer channels, (6.4) and (6.2) (the dissociative electron transfer reactions, $N^+ + C_2H_2^+$ + N and $N^+ + C_2H^+$ (+ N + H), which include an N^+ product, are excluded as this area of the coincidence spectrum was particularly noisy due to false coincidences), dissociative double electron transfer channels, (6.7), (6.8), (6.9) and (6.6), and the bond-forming channels (6.12), (6.10), (6.13) and (6.11), at each of the measured COM collision energies.

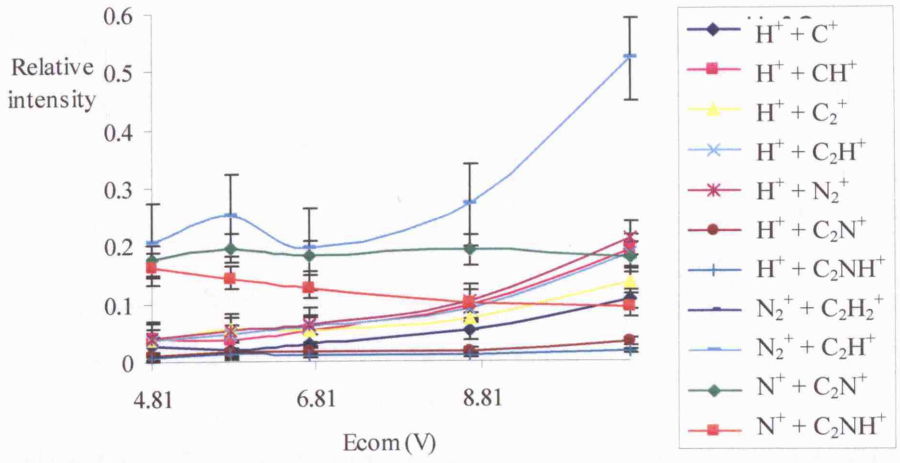

Figure 6.3 The relative intensities of the dissociative electron transfer channels, (6.4) and (6.2), dissociative double electron transfer channels, (6.7), (6.8), (6.9) and (6.6) and the bond-forming reactions (6.12), (6.10), (6.13) and (6.11), relative to the non-dissociative charge transfer channel, (6.1).

We observe that the dissociative electron transfer and double dissociative electron transfer reactions, featured in the graph in Figure 6.3, slightly increase in intensity as the collision energy is increased, relative to the non-dissociative charge transfer channel. This behaviour is not surprising because as the collision energy increases, the additional energy in the system makes it is more likely that excited states of the primary product monocations will be populated. [9] The curve crossings of the asymptotes of the reactants with the asymptotes of the excited state product channels move into the Landau-Zener Reaction Window, as discussed in Chapter One, hence the probability of populating the excited states of the primary product monocations increases. Due to the excitation of the molecule, these excited state primary product monocations are more likely to dissociate and hence an increase in dissociative electron transfer, relative to non-dissociative electron transfer, is observed. The bond-forming reactions however do not appear to differ in intensity as the collision energy increases. Figure 6.4 focuses on the relative intensities of these bond-forming channels, (6.12), (6.10), (6.13) and (6.11), at each of the measured COM collision energies.

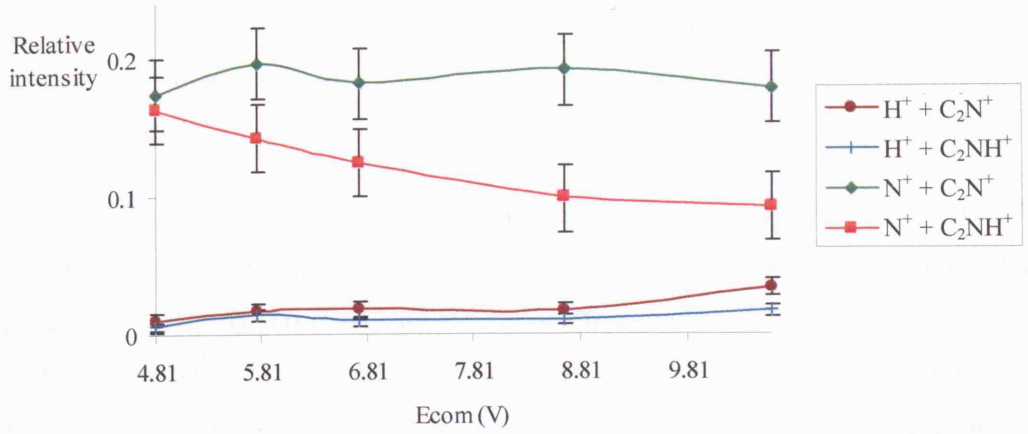

Figure 6.4 The relative intensity of the bond-forming channels, (6.12), (6.10), (6.13) and (6.11), relative to non-dissociative charge transfer channel, (6.1).

With the exception of bond-forming channel, $N^+ + C_2NH^+ + H$ (6.11), which decreases slightly in relative intensity as the collision energy is raised, we can see in Figure 6.4 that at this range of COM collision energies most of the bond-forming channels vary little in intensity, relative to the non-dissociative electron transfer channel. We might expect to see the relative intensities drop as the collision energy increases, mainly because the increased collision energy makes dissociation of the molecular products more likely due to their increased vibrational excitation. However, it is possible that this expected sharp drop in intensity, of the bond-forming channels, in fact occurred at collision energy lower than those studied. Therefore the relative intensities of the bond-forming channels can be determined from an average ratio, over all the COM collision energies studied. After subtraction of false coincidences, the four bond-forming channels, $H^+ + C_2NH^+ + N$ (6.10), $N^+ + C_2NH^+ + H$ (6.11), $H^+ + C_2N^+$ (+ H + N) (6.12) and $N^+ + C_2N^+$ (+ H + H) (6.13), (Figure 6.4), are formed in the relative intensity of 1 : 14 : 2 : 20 relative to the weakest bond-forming channel. It is important to note that the two significantly weaker bond-forming channels, $H^+ + C_2NH^+ + N$ (6.10) and $H^+ + C_2N^+$ (+ H + N) (6.12), involve the product H^+. H^+ ions are so light that, if they have significant transverse kinetic energy, they could actually leave the source region before the repeller plate is pulsed and hence will not be detected as efficiently. That is, if the reaction occurs just before the repeller plate pulse, the H^+ ions will be detected with the same probability as any other ion but if the reaction occurs just as the dication pulse enters the source region, then the H^+ ions are fast enough to fly out of the source region, or hit the walls of the source region, before the repeller plate is pulsed. Larger heavier species do not be travel fast enough to leave the source region before the repeller plate is pulsed. So, given that a proportion of the H^+ ions may be lost from the source region in the period before the

repeller plate is pulsed, the relative intensities of reactions involving a H^+ product are lowered relative to reactions that do not involve a H^+ product. We can therefore confidently say that our relative intensities of channels $H^+ + C_2NH^+ + N$ (6.10) and $H^+ + C_2N^+ (+ H + N)$ (6.12) are a lower limit.

Two of the bond-forming reactions $N^+ + C_2NH^+ + H$ (6.11) and $N^+ + C_2N^+ (+ H + H)$ (6.13) are, on average, significantly more intense than the dissociative electron transfer channel, $N_2^+ + H^+ + (C_2H)$ (6.4), and the dissociative double electron transfer channels $H^+ + C^+ (+ N_2 + CH)$ (6.7), $H^+ + CH^+ (+ C + N_2)$ (6.8), $H^+ + C_2^+ (+ H + N_2)$ (6.9) and $H^+ + C_2H^+ (+ N_2)$ (6.6). However these dissociative, single or double, electron transfer channels all involve a H^+ product, which as explained previously is perhaps not detected as efficiently as heavier ions. When we compare channels $N^+ + C_2NH^+ + H$ (6.11) and $N^+ + C_2N^+ (+ H + H)$ (6.13) with a dissociative electron transfer channel that does not involve H^+, $N_2^+ + C_2H^+ + H$ (6.2), we see the dissociative electron transfer channel is slightly more intense (see Figure 6.3). The non-dissociative electron transfer channel (6.1) is however approximately 100 times more intense than the bond-forming channels $H^+ + C_2NH^+ + N$ (6.10) and $H^+ + C_2N^+ (+ H + N)$ (6.12) which means it is about five times as intense as channel $N^+ + C_2N^+ (+ H + H)$ (6.13), the most intense bond-forming channel.

The four bond-forming reactions (6.10), (6.11), (6.12) and (6.13) are formed in different intensities and with a different number of products. Channels $H^+ + C_2NH^+ + N$ (6.10) and $N^+ + C_2NH^+ + H$ (6.11) can only have three products, whilst channels $H^+ + C_2N^+ (+ H + N)$ (6.12) and $N^+ + C_2N^+ (+ H + H)$ (6.13) posses some ambiguity as to whether there is one or two neutral products. However some conclusions can be drawn about the reaction mechanisms of these possible four-body channels, at the least via comparison of the scattering diagrams.

6.3.1.2 Angular Scattering

The following section discusses the angular scattering of each of the bond-forming channels in turn.

6.3.1.2.1 The formation of $H^+ + C_2NH^+ + N$ (6.10)

As mentioned above the intensity of channel (6.10) is low. However, despite the weak nature of the signals, clear mechanistic conclusions can be drawn from the form of the

scattering diagrams we derive from the PSCO data. First the scattering with respect to $\omega(N_2^{2+})$ will be considered, as shown in Figure 6.5.

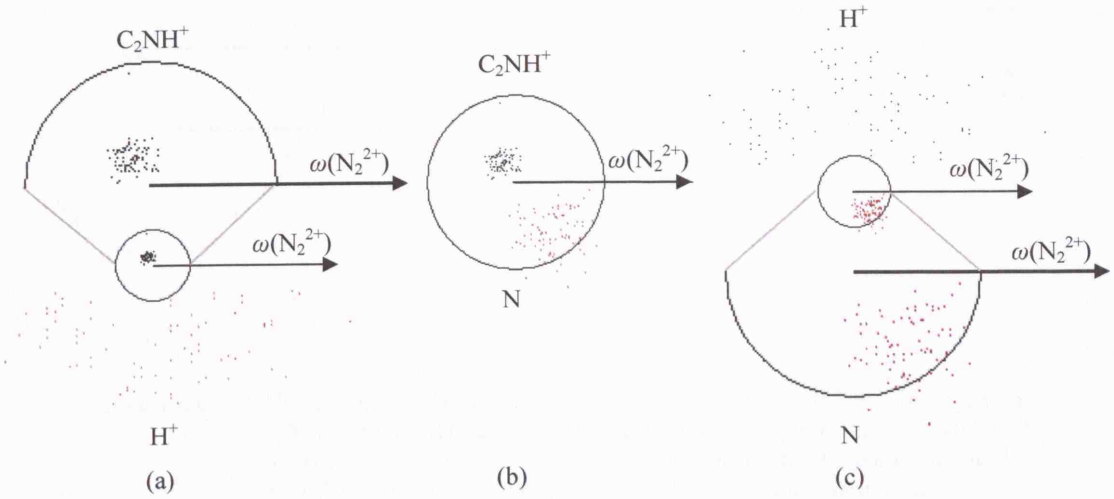

Figure 6.5 The scattering diagrams, circle radius 1 cm μs^{-1}, for the velocities of (a) H^+ and C_2NH^+, (b) C_2NH^+ and N, and (c) H^+ and N with respect to $\omega(N_2^{2+})$, derived from the data recorded following the collisions of N_2^{2+} with C_2H_2 at 300 V repeller plate and E_{com} 6.74 eV.

The scattering of the velocity of the H^+ appears to be close to symmetrical over the scattering angles with respect to $\omega(N_2^{2+})$, with a slight inclination towards forwards scattering. The velocity of the neutral species, N, however is clearly forwards scattered, and the velocity of C_2NH^+ is clearly backwards scattered, again with respect to the direction of $\omega(N_2^{2+})$; a strong indication that the reactants did not form a long-lived intermediate complex. If a long-lived complex had formed, the velocity of N and C_2NH^+ would be scattered over a wide range of angles (both forward and backward) due to the rotation of the complex. The internal frame scattering diagrams as shown in Figure 6.6 reveal more conclusive support for this initial mechanistic conclusion.

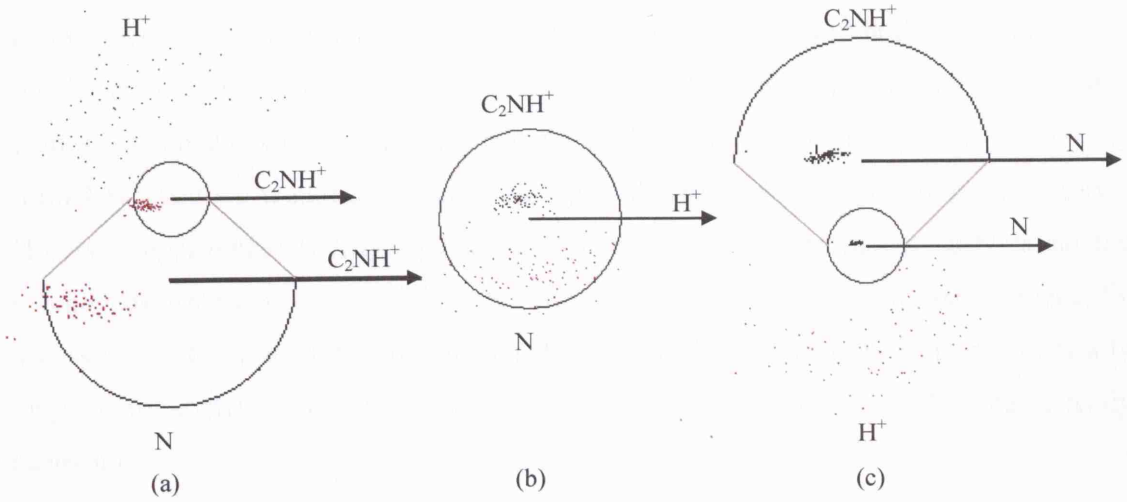

Figure 6.6 The scattering diagrams of the velocities of (a) H^+ and N with respect to C_2NH^+, (b) C_2NH^+ and N with respect to H^+, (c) H^+ and C_2NH^+ with respect to N, derived from the data recorded following collisions of N_2^{2+} with C_2H_2, 300 V repeller plate, E_{com} 6.74 eV, circle radius 1 cm μs^{-1}.

The internal frame scattering diagrams in Figure 6.6 show that the velocities of the products N and C_2NH^+ are clearly anti-correlated with each other, as are the velocities of H^+ and C_2NH^+, and hence, the velocity of H^+ is correlated with the velocity of N. The products formed in the charge separating step of a reaction almost invariably have strongly anti-correlated velocities. The energy provided by the Coulomb repulsion involved in charge separation is usually significantly greater than the energy release from dissociations to form a dication and a neutral species. In dissociations to form a dication and a neutral, the neutral species will typically show no correlation with either of the subsequently formed monocations. Therefore given that the velocity of the neutral species, N, does show a strong anti-correlation with the velocity of C_2NH^+, as opposed to symmetrical scattering, we can conclude that the neutral species was formed after the charge separating step. In addition, the energy typically provided by the Coulomb repulsion involved in charge separation is also usually greater than the energy release from dissociations to form a monocation and a neutral species. Therefore given the velocities of the N and H^+ are both anti-correlated with the velocity of the C_2NH^+, we can conclude that the N and H^+ were formed together (as NH^+) and subsequently dissociated (6.14);

$$N_2^{2+} + C_2H_2 \rightarrow C_2NH^+ + NH^+ \rightarrow C_2NH^+ + N + H^+ \qquad (6.14)$$

Compared with the strong repulsion of the like charges on formation of C_2NH^+ and NH^+ in the charge separation step, the dissociation of NH^+ would not be expected to have a large energy release. Hence, also given the mass difference, the N would only receive a

small velocity kick from the dissociation of NH^+. We would therefore expect N and H^+ to retain correlated velocities, hence correlated scattering, as observed in the experiment. In the literature only five electronic states of NH^+ have been observed and all were bound. If these bound states were populated it is likely that the reaction mechanism would only form NH^+, and we would to detect C_2NH^+ paired with NH^+, which we do not observe. However, approximately fifty repulsive states of NH^+ have been theoretically calculated recently by Amero *et al.* [10] Of course most of these states would not be energetically accessible in this system but an unbound state which dissociates to N + H^+ lies vertically only approximately 8 eV above the ground state of NH^+ so would be energetically accessible.

The internal frame scattering diagrams show that the velocities of the N and the H^+ are not distributed evenly about the nascent velocity vector of the NH^+. This provides evidence that the dissociation of NH^+ occurs rapidly after formation, as would be expected from the population of a repulsive state. Given that the life-times of 'long-lived' complexes are of the order of at least approximately 100 fs (see Chapter Five, section 5.3.1.2.1), we can therefore speculate that the time-scale of this dissociation is significantly less than 100 fs.

To the best of our knowledge, the C_2NH^+ ion has not been intensively studied in the literature. However it has been detected previously in a mass spectrometric and theoretical study of the glycine cation by Lu *et al.* Here the author's proposed the lowest energy formation of C_2NH^+ was in an $[N\text{-}C\text{-}C\text{-}H]^+$ configuration, which is close to linear with bond angles of 178° (N-C) and 169° (C-H). [11]

6.3.1.2.2 The formation of $N^+ + C_2NH^+ + H$ (6.11)

Before analysis of the channel $N^+ + C_2NH^+ + H$ the false coincidences were subtracted as detailed in Chapter Three. Figure 6.7 shows the scattering of the product ions with respect to $\omega(N_2^{2+})$.

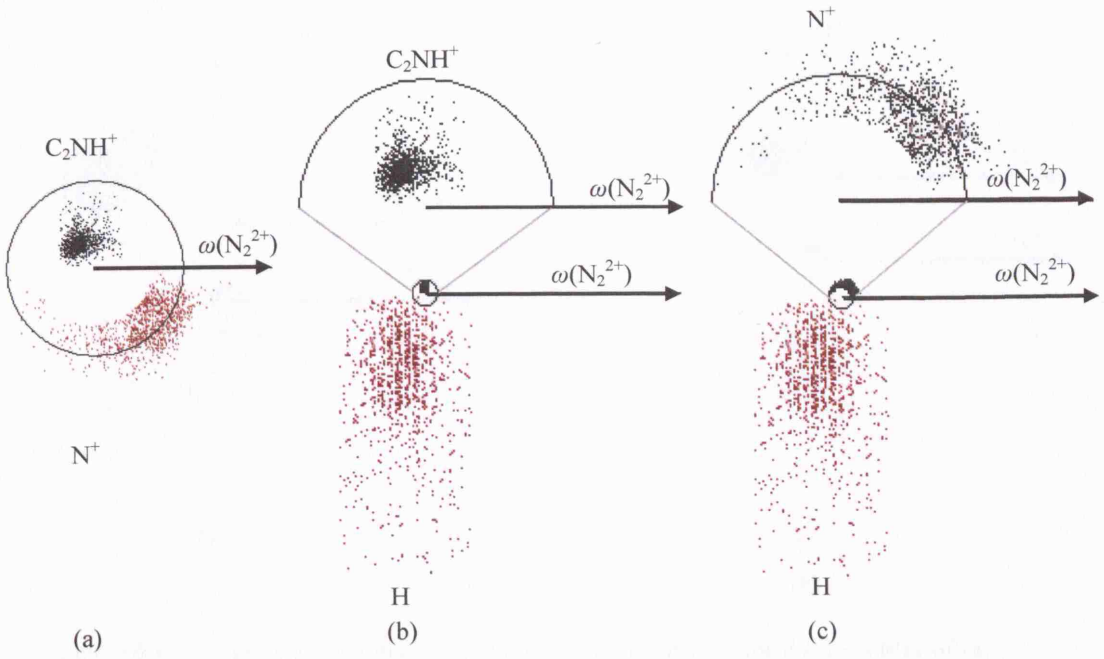

Figure 6.7 The scattering diagrams, circle radius 1 cm μs^{-1}, for the velocities of (a) N^+ and C_2NH^+, (b) C_2NH^+ and H, and (c) N^+ and H with respect to $\omega(N_2^{2+})$, derived from the data recorded following the collisions of N_2^{2+} with C_2H_2 at 300 V repeller plate and E_{com} 6.74 eV.

The velocity of N^+ is distinctly, but not very strongly, forward scattered with respect to $\omega(N_2^{2+})$. The velocity of C_2NH^+ is backwards scattered with respect to $\omega(N_2^{2+})$, again with a small amount of sideways scattering. H is slightly backwards scattered with respect to $\omega(N_2^{2+})$. Because the hydrogen species has a large velocity, due to low mass, the scattering velocities of the H atoms relative to $\omega(N_2^{2+})$ show a considerable spread compared to those for the N^+ and C_2NH^+ products. This is in addition to the fact that the velocity of the neutral species is determined via the conservation of momentum of the ionic species and hence there will be greater uncertainty in the velocity vector of the neutral species. Still, this backwards scattering of the H suggusts that the H was formed together with the C_2NH^+, as $[NC_2H_2^+]$, before this 5-atomic ion dissociated, since the C_2NH^+ is also backwards scattered with respect to the velocity of the dication in the COM frame. However, if this is correct, the $[NC_2H_2^+]$ must be very short lived, of the order of significantly less than 100 fs (see section 5.3.1.2.1) because there can be no long-lived complexation of $[NC_2H_2^+]$ as this would result in symmetric scattering of C_2NH^+ and H relative to $\omega(N_2^{2+})$, about the point of the nascent velocity vector of $[NC_2H_2^+]$, due to rotation of the complex. Figure 6.8 shows two internal frame scattering diagrams for this channel.

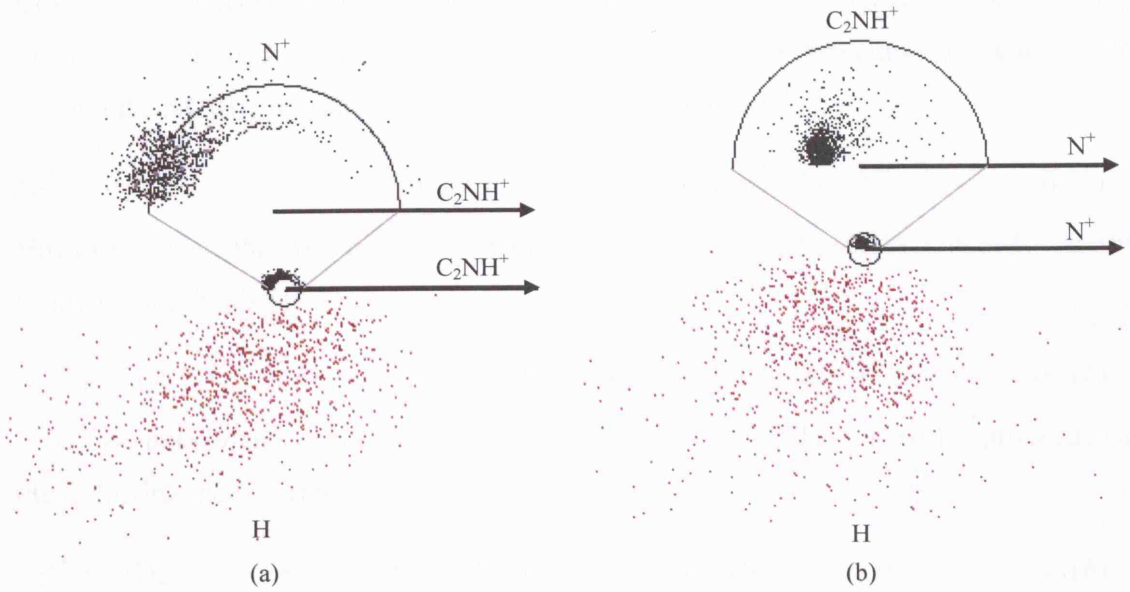

Figure 6.8 The scattering diagrams, circle radius 1 cm μs^{-1}, for the velocities of (a) N^+ and H with respect to C_2NH^+, (b) C_2NH^+ and H with respect to N^+, and (c) N^+ and C_2NH^+ with respect to H, derived from the data recorded following the collisions of N_2^{2+} with C_2H_2 at 300 V repeller plate and E_{com} 6.74 eV.

As expected, in the internal frame the scattering shows the velocities of the charged species, N^+ and C_2NH^+, are anti-correlated with each other. The velocity of H in this case shows little correlation with either of the charged species. However on closer inspection it appears that the scattering observed for this channel is in fact quite unusual because both the velocity of the H with respect to the velocity of C_2NH^+ and the velocity of the H with respect to the velocity of N^+ appears to be very slightly anti-correlated. This slight anti-correlation leads to two tentative conclusions. Firstly, the anti-correlation of the velocity of N^+ and H may lead to the conclusion that because the velocities of the H and the C_2NH^+ are both anti-correlated with the N^+, H and the C_2NH^+ were initially formed together as $[NC_2H_2^+]$. Then, if H was thrown of the $[NC_2H_2^+]$ with a big energy release, we may see this slight anti-correlation of the velocity of H with the velocity of C_2NH^+. Given that on average the velocities of the H are relatively high (approximately 6 cm μs^{-1}), and hence the H has high energy, it is feasible that the H was thrown off the $NC_2H_2^+$ with a signficant energy release. Therefore given that the velocity of the H would be anti-correlated with the velocity of the N^+ from the initial charge separating step, and then anti-correlated with C_2NH^+, from the dissociation of $[NC_2H_2^+]$ we might see this slight anti-correlation of H with both of the charged species. In addition the scattering diagrams in Figure 6.8 clearly show that the velocities of C_2NH^+ and H are backwards scattered respect to the velocity of the dication in the COM frame, while the velocity of the N^+ is forwards scattered with respect to the velocity of the dication in the

COM frame, suggesting that C_2NH^+ and H were initially formed together. The scattering diagrams therefore suggest that the reaction proceeds via the formation of $NC_2H_2^+$ with N^+, and the $NC_2H_2^+$ then dissociated to yield H and the C_2NH^+;

$$N_2^{2+} + C_2H_2 \rightarrow (NC_2H_2^+) + N^+ \rightarrow C_2NH^+ + H + N^+ \quad (6.15)$$

However, given that the previous channel $H^+ + C_2NH^+ + N$ (6.10) proceeds via the following mechanism;

$$N_2^{2+} + C_2H_2 \rightarrow C_2NH^+ (+ NH^+) \rightarrow C_2NH^+ + N + H^+ \quad (6.14)$$

would we not perhaps expect that the mechanism for $N^+ + C_2NH^+ + H$ (6.11) proceeds via the following mechanism?

$$N_2^{2+} + C_2H_2 \rightarrow C_2NH^+ + (NH^+) \rightarrow C_2NH^+ + N^+ + H \quad (6.16)$$

Here the C_2NH^+ is formed with NH^+, and the NH^+ can then dissociate to yield either N and H^+ or N^+ and H. This mechanism is the second possibility because if the C_2NH^+ was formed with NH^+, and the NH^+ subsequently dissociated with a moderate energy release, the velocity of the H would appear to be slightly anti-correlated with the velocity of the N^+ as we see in the internal frame scattering diagrams. However we might have then still expected the velocity of the H to be forwards scattered with respect to the velocity of the dication in the COM fame, as the velocity of the N^+ was, given that the internal frame anti-correlation is only slight although certainly is not enough evidence to exclude mechanism (6.16). We can however consider the energetics of NH^+. The lowest energy unbound state of NH^+ dissociates to form N and H^+, so therefore it is possible that the reaction to form C_2NH^+ with NH^+ always proceeds via the N and H^+ dissociative state of NH^+ and hence $N^+ + H$ cannot be formed from NH^+ in this channel. However the only way to know if this speculation is correct is by calculation of the bond length of the intermediate NH^+. If the bond-length of the NH^+ is similar to that of the ground state NH^+ then it is most likely that only N and H^+ can be formed from NH^+. If the bond length of the NH^+ is considerably longer than that of ground state NH^+, then it would be possible to form an unbound electronic state which could dissociate to N^+ and H and is energetically accessible. However these calculations will not form part of this thesis.

6.3.1.2.3 The formation of $H^+ + C_2N^+ (+ H + N)$ (6.12)

As with the previous channel, this channel is also very weak, but again the form of the scattering diagrams can still be observed. In this channel the identity of the neutral is uncertain; H and N or NH. In section 5.3.1.3.2 the energetics are considered and they

hint that this reaction may be a four-body process. In addition we do not observe H^+ or C_2N^+ paired with NH^+, and so this may further suggest that the neutral products are likely to be an H and a N. For clarity we will therefore call the neutral product N+H. Figure 6.9 shows the scattering of the velocities of the products H^+, C_2N^+ and 'H+N' relative to $\omega(N_2^{2+})$.

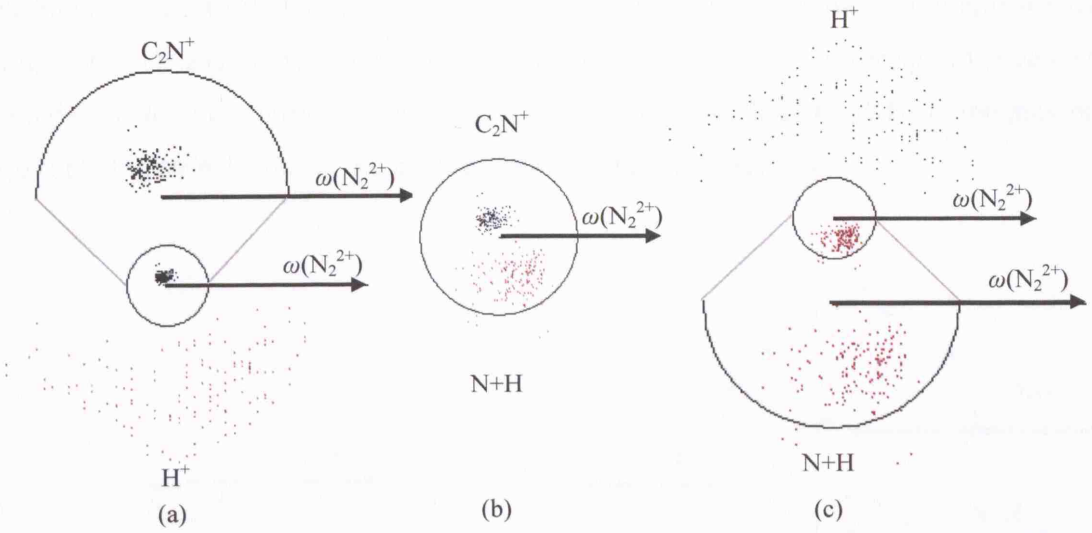

Figure 6.9 The scattering diagrams , circle radius 1 cm μs^{-1}, for the velocities of (a) H^+ and C_2N^+, (b) C_2N^+ and N+H, and (c) H^+ and N+H with respect to $\omega(N_2^{2+})$, derived from the data recorded following the collisions of N_2^{2+} with C_2H_2 at 300 V repeller plate and E_{com} 6.74 eV.

The velocity of H^+ is close to symmetrically scattered with respect to the velocity of the dication in the COM frame. However there is perhaps a inclination towards forwards scattering. The velocity of C_2N^+ is backwards scattered, in the opposite direction to $\omega(N_2^{2+})$. As seen with the previous channel, this forwards/backwards scattering is a strong indication that the reaction is very fast without a long-lived complexation of the reactants. As previously mentioned, the velocity of the neutral species is determined using conservation of momentum. Therefore in a four-body product reaction the velocity is determined from the sum of the masses and momenta of the two neutral species. In a four-body product reaction it is very unlikely that the two neutral species would be travelling in exactly the same direction, therefore one would perhaps expect that the derived velocity of the "neutral" we derive would appear to be broadly scattered over a range of angles in the scattering diagrams. However, we see that the velocity of the neutral species, N+H, is markedly forward scattered, with respect to $\omega(N_2^{2+})$. This directional localisation of the velocity of the neutral species strongly hints that the neutral species was in fact initially formed as one entity, whether it then separates or not would not affect the scattering dynamics we derive. Given that the velocity of the neutral

species is forwards scattered, and there appears to be some forward scattering of the H^+, this suggusts that the neutral species and H^+ were initially formed as NH_2^+, with the NH_2^+ then dissociating to form H^+ and NH, with the NH then possibly further dissociating.

Perhaps further evidence for this mechanism is the fact the velocity of the C_2N^+ appears to be very sharply angularly constrained, similarly to that of the C_2NH^+ in the previous channel. If the C_2N^+ had not been formed 'directly', for example if initially we had formed C_2NH^+ and the H had then separated, we may expect the scattering of the velocity of the C_2N^+ to have appeared more angularly scattered than that of C_2NH^+ in the previous channel. Figure 6.10 shows the internal frame scattering diagrams.

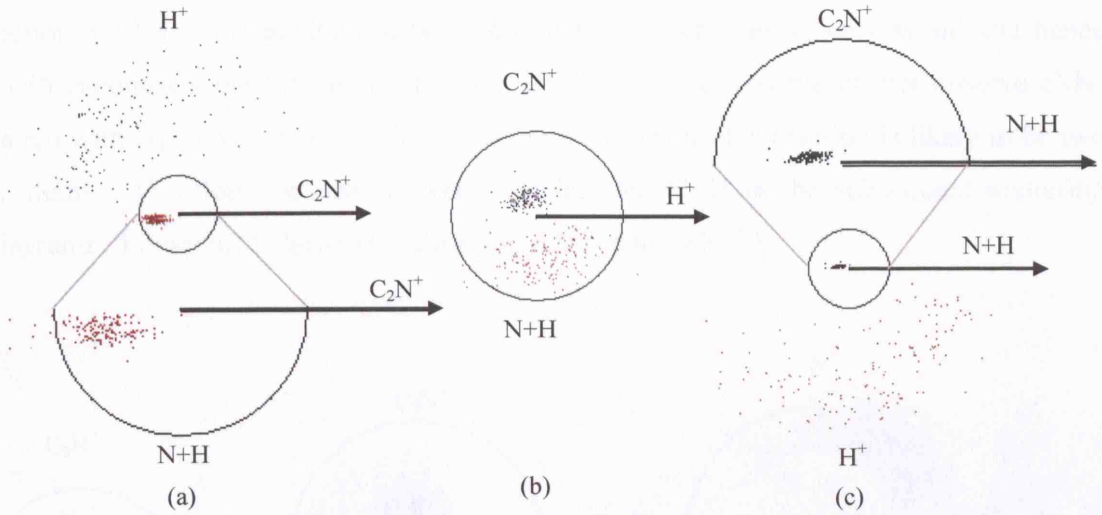

Figure 6.10 The scattering diagrams, circle radius 1 cm μs^{-1}, for the velocities of (a) H^+ and N+H with respect to C_2N^+, (b) C_2N^+ and N+H with respect to H^+, and (c) H^+ and C_2N^+ with respect to N+H, derived from the data recorded following the collisions of N_2^{2+} with C_2H_2 at 300 V repeller plate and E_{com} 6.74 eV.

The internal frame scattering diagrams show a clear anti-correlation in the velocities of the neutral(s) and C_2N^+. There is also a clear anti-correlation of the scattering of the velocity of H^+ with the velocity of C_2N^+, and correlated scattering of the velocity of H^+ with the velocity of N+H. As previously mentioned this clear directionally localised scattering of the velocity of the 'N+H' certainly indicates that the N and H were formed together as NH. The clear correlation of the velocity of H^+ with the velocity of NH, confirms the previous indications that the H^+ initially formed with the NH. As previously mentioned, the energetics and the fact with do not observe any NH^+ products perhaps hints that the NH then dissociated, although whether or not this happened would not have an effect on the scattering we detect. Again the initial formation of NH_2^+ with C_2N^+ is confirmed by the very clearly localised scattering of the velocity of the of C_2N^+ with

respect to the velocity of the N+H, indicating the C_2N^+ was not initially formed as C_2NH^+ in the charge separating step. Therefore the scattering is consistent with the following mechanism to yield C_2N^+ with NH_2^+, with the NH_2^+ further dissociating;

$$N_2^{2+}+C_2H_2 \rightarrow C_2N^+ + (NH_2^+) \rightarrow (NH_2^+) \rightarrow H^+ + (NH \text{ or } N+H) \qquad (6.17)$$

Little is known about the structure of C_2N^+.

6.3.1.2.4 The formation of $N^+ + C_2N^+ (+ H + H)$ (6.13)

Again, before the analysis of the data from this channel, the false coincidences were subtracted as described in Chapter Three. Energetically we cannot distinguish whether the neutral species is H+H or H_2, both are energetically accessible. As discussed in section 5.3.1.3.2, the exothermicity spectrum for this channel is very broad and hence could encompass the formation of either H+H or H_2. Given we do not observe C_2N^+ paired with H_2^+, this could hint that the neutral species in this reaction is likely to be two H atoms. Therefore the neutral species is labelled H+H in the subsequent scattering diagrams. Figure 6.11 shows the scattering relative to $\omega(N_2^{2+})$.

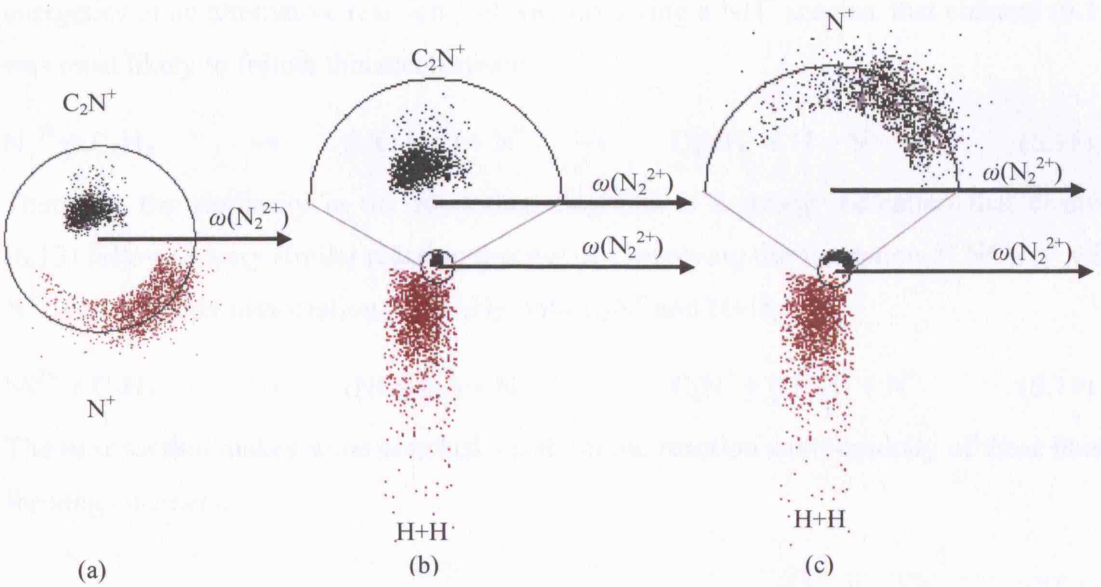

Figure 6.11 The scattering diagrams, circle radius 1 cm μs^{-1}, for the velocities of (a) N^+ and C_2N^+, (b) C_2N^+ and H+H, and (c) N^+ and H+H with respect to the velocity of $\omega(N_2^{2+})$, derived from the data recorded following the collisions of N_2^{2+} with C_2H_2 at 300 V repeller plate and E_{com} 6.74 eV.

Figure 6.11 shows the H+H velocity is very slightly backwards scattered with respect to the velocity of the dication in the COM frame, which, as we discussed previously, may indicate that the two H were formed in the same reaction step. Figure 6.12 shows the internal frame scattering diagrams.

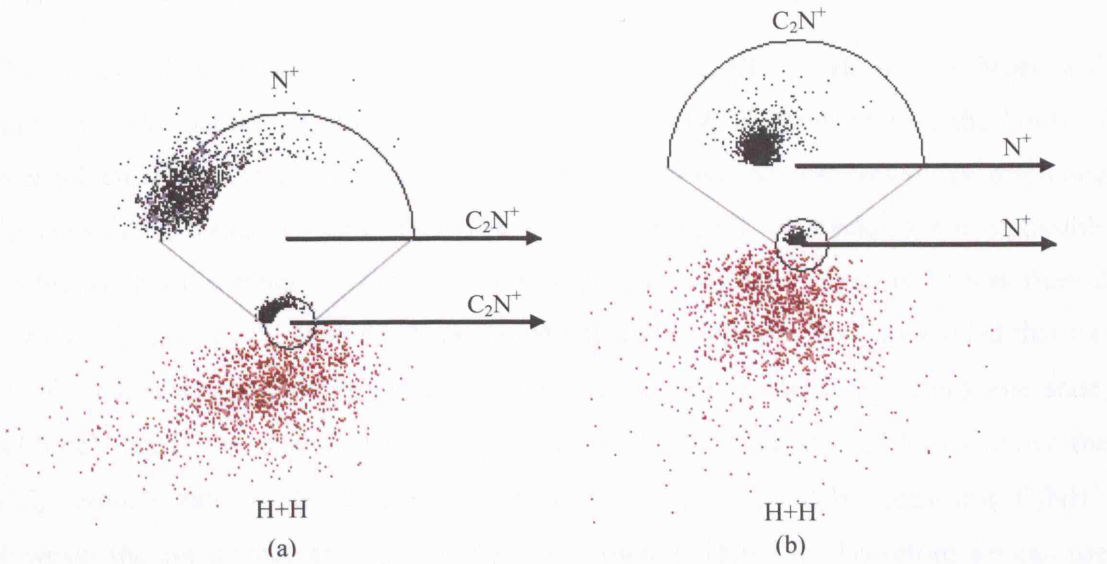

Figure 6.12 The scattering diagrams, circle radius 1 cm μs^{-1}, for the velocities of (a) N^+ and H+H with respect to C_2N^+, (b) C_2N^+ and H+H with respect to N^+, and (c) N^+ and C_2N^+ with respect to H+H, derived from the data recorded following the collisions of N_2^{2+} with C_2H_2 at 300 V repeller plate and E_{com} 6.74 eV.

The scattering diagrams are incredibly similar to those of channel $C_2NH^+ + H + N^+$ (6.11). We showed via analysis of these earlier scattering diagrams, and by consideration of the energetics of an alternative reaction pathway involving a NH^+ species, that channel (6.11) was most likely to follow this mechanism:

$$N_2^{2+} + C_2H_2 \rightarrow (NC_2H_2^+) + N^+ \rightarrow C_2NH^+ + H + N^+ \quad (6.15)$$

Therefore the similarity in the scattering diagrams is a strong indication that channel (6.13) follows a very similar reaction mechanism involving the formation of $NC_2H_2^+$ with N^+, with a further dissociation of $NC_2H_2^+$ into C_2N^+ and H+H;

$$N_2^{2+} + C_2H_2 \rightarrow (NC_2H_2^+) + N^+ \rightarrow C_2N^+ + (H+H) + N^+ \quad (6.18)$$

The next section makes some conclusions about the reaction exothermicity of these bond-forming channels.

6.3.1.3 Reaction Exothermicity

Although the PSCO technique has previously been used to successfully derive information on the exothermicity of the reactive events that are detected in the pairs spectrum, [12, 13] the exothermicity spectra generated for reactions the four bond-forming channels (6.10), (6.11), (6.12) and (6.13) are very broad and unresolved. However, with some assumptions, several conclusions can be drawn.

6.3.1.3.1 The energetics of $H^+ + C_2NH^+ + N$ (6.10) and $N^+ + C_2NH^+ + H$ (6.11)

The exothermicity spectrum for channel (6.11) $N^+ + C_2NH^+ + H$, is very broad and unresolved, in fact the spectrum is so noisy that it is even difficult to state the limits of over which range the exothermicity is distributed, unlike all the previously discussed channels in this thesis. Channel, (6.10) $H^+ + C_2NH^+ + N$, is even weaker but it is possible to observe that the majority of the intensity in the exothermicity spectrum ranges from 2 to 7 eV. As previously mentioned, experimental studies of N_2^{2+} have concluded that ion beams of this dication are principally composed of ions in the $X^1\Sigma_g^+$ electronic state, (43.00 eV above the ground state of N_2), and the $c^3\Sigma_u^+$ excited state (1.51 eV above the $X^1\Sigma_g^+$ ground state of N_2^{2+}). There is limited information available regarding C_2NH^+. However the appearance energy of C_2NH^+ is known at 15.9 eV. Therefore we can use this value, together with the known values for H^+ and N to determine the exothermicity of the reaction. A reaction of ground state N_2^{2+} to form H^+, C_2NH^+ and N in their ground states has an exothermicty of 8.7 eV which is just slightly higher than the limit of the intensity in the weak exothermicity spectrum for this channel. The observed lower exothermicties can be accounted for by excitation of the products.

6.3.1.3.2 The energetics of $H^+ + C_2N^+$ (+ H + N) and $N^+ + C_2N^+$ (+ H + H)

We can obtain literature values for the heat of formation and first ionisation energy of C_2N^+ (NCC^+) as well as all other relevant products for these reactions. We can therefore derive the thermodynamic exothermicity for the reactions forming $H^+ + C_2N^+$ (+ H + N) (6.12) and $N^+ + C_2N^+$ (+ H + H) (6.13) from literature values of the heats of formation of the relevant neutrals and monocations and the double ionisation energy of the ground states and excited states of N_2^{2+}. The exothermicity spectra derived from the pairs data for the formation of reaction (6.12), $H^+ + C_2N^+$ paired with either NH or H and N, indicate that the reaction exothermicity is mostly distributed between 0 and 5 eV. A reaction from $N_2^{2+} + C_2H_2$ in their ground electronic states to form $H^+ + C_2N^+ + H + N$ in their ground electronic states has a literature exothermicity of 4.5 eV. While a reaction of $N_2^{2+} + C_2H_2$ in the ground electronic states to form ground state $H^+ + C_2N^+ + HN$ has a literature exothermicity of 7.8 eV. When considering the reaction of the excited state $c^3\Sigma_u^+$ of N_2^{2+} with ground state C_2H_2 to form ground state $N^+ + C_2N^+ + H + H$ or $H^+ + C_2N^+ + HN$ the literature exothermicities are 6.0 eV and 9.3 eV respectively. The values for the reaction to form HN as the neutral product as opposed to N and H are higher than

the detected exothermicity. This may hint that the neutral product is N and H but could also be attributed to the formation of products in excited vibrational or electronic states.

The exothermicity spectra we derive from the pairs data for the formation of reaction (6.13), $N^+ + C_2N^+ + H + H$ or $N^+ + C_2N^+ + H_2$, are very broad. A reaction from N_2^{2+} and C_2H_2 in their ground electronic states to form $N^+ + C_2N^+ + H + H$ or H_2 in their ground electronic states has a literature exothermicity of 3.6 eV and 8.1 respectively, depending on the neutral identity. If we consider the reaction of the excited state $c^3\Sigma_u^+$ of N_2^{2+} reacting with C_2H_2 in the ground electronic state to form $N^+ + C_2N^+ + H + H$ or H_2 in the ground electronic states, the literature exothermicity is 5.1 and 9.1 eV respectively. However we cannot distinguish between the two identities of the neutral species because the exothermicity spectrum is too noisy and broad.

6.3.1.4 Summary

None of the respective scattering diagrams of the four bond-forming channels discussed show any isotropic scattering. This is a strong indication that the reaction mechanisms did not involve any long-lived complexation and therefore were very rapid. Although the exact time scales of the reactions have not been calculated we can speculate that the time scale was significantly less than 100 fs because the long-lived complex observed in the reaction mechanisms in Chapter Five only lived for approximately 100 fs. It appears two reaction mechanisms are operating depending on the identity of the atomic monocation. In both mechanisms the neutral species is formed after the charge dissociation step, and only one of the initially formed charged species dissociates further to form a singly charged species and one or two neutral species. In the first mechanism the N^+ is initially formed with a $[NC_2H_2^+]$ species, the $[NC_2H_2^+]$ then further dissociates to lose one or two H atoms;

$$N_2^{2+} + C_2H_2 \rightarrow (NC_2H_2^+) + N^+ \rightarrow C_2NH^+ + H + N^+$$
$$\rightarrow C_2N^+ + (H + H) + N^+$$

In the second mechanism an NH^+ or NH_2^+ species is initially formed, with the NH^+ dissociating to form H^+ with N, and the NH_2^+ dissociating to form H^+ with NH or N and H;

$$N_2^{2+} + C_2H_2 \rightarrow C_2NH^+ + (NH^+) \rightarrow C_2NH^+ + H^+ + N$$
$$\rightarrow C_2N^+ + (NH_2^+) \rightarrow C_2N^+ + H^+ + (NH \text{ or } N+H)$$

As discussed in section 5.3.1.3.2 the energetics hint that the NH_2^+ dissociates to form H^+ with N and H. The next section discusses the reactions of N_2^{2+} with H_2.

6.3.2 N_2^{2+} with H_2

In the PSCO spectra recorded following collisions of N_2^{2+} with H_2 five reactions have been clearly observed. These reactions are listed below and shown in the pairs spectrum in Figure 6.13. These reactions are a non-dissociative electron transfer channel (6.19), three dissociative electron transfer channel (6.21), (6.22) and (6.23), and an 'ambiguous' channel, (6.24), which could be either an isotopic dissociative electron transfer reaction, involving the reaction of the small amount of $^{14}N^{15}N^{2+}$ present in the system, or a bond-forming reaction. As will be shown below, analysis of isotopic intensities shows that in fact (6.24) is a bond-forming process.

$$N_2^{2+} + H_2 \rightarrow N_2^{+} + H_2^{+} \quad (6.19)$$
$$N_2^{2+} + H_2 \rightarrow {}^{14}N^{15}N^{+} + H_2^{+} \quad (6.20)$$
$$N_2^{2+} + H_2 \rightarrow N_2^{+} + H^{+} + H \quad (6.21)$$
$$N_2^{2+} + H_2 \rightarrow N^{+} + H_2^{+} + N \quad (6.22)$$
$$N_2^{2+} + H_2 \rightarrow N^{+} + H^{+} + (N + H) \quad (6.23)$$
$$N_2^{2+} + H_2 \rightarrow {}^{15}N+ + H^{+} + (N + H) \text{ or } NH^{+} + H^{+} + N \quad (6.24)$$

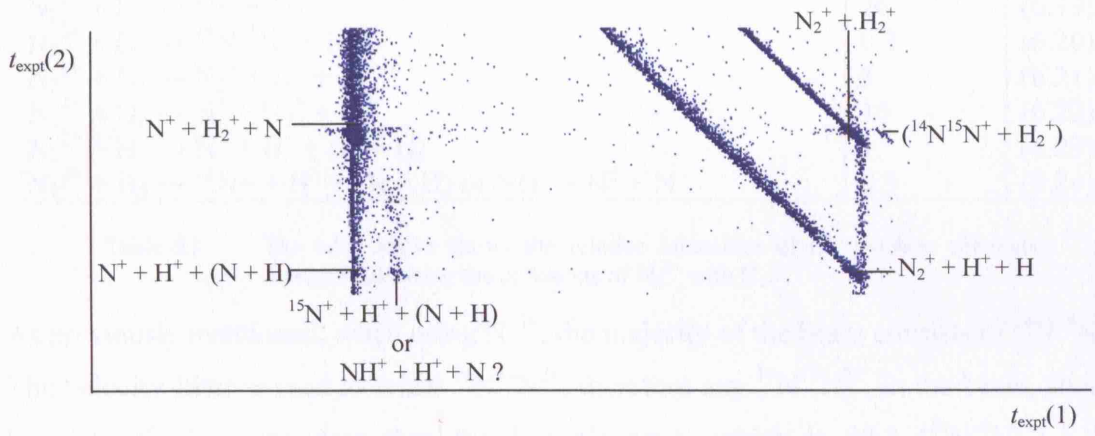

Figure 6.13 A coincidence spectrum of the N_2^{2+} with H_2 system at 300 V repeller plate, E_{com} 0.93 eV.

The tails from reaction peaks in the coincidence spectrum can provide strong clues to differentiate channels. As explained in Chapter Three, the peak tails are mainly due to reactions that occur beyond the source region of the *TOF-MS*, where the dication is travelling considerably faster than when entering the source region. Unlike electron transfer reactions, the cross section for bond-forming reactions rapidly drops off as the collision energy increases therefore bond-forming reactions are only likely to occur in the low collision energy conditions of the source region. [8] Thus, bond-forming channels are rarely observed to have tails in the coincidence spectrum. The 'ambiguous' channel, (6.24), has a tail, although it is less instance than some of the other tails, which is very indicative of a dissociative electron transfer reaction. However it may be possible that the

specific mechanism for this channel may make allow this reaction to occur at higher energies than typical bond-forming reactions. Whatever the identity of this channel, using D_2, instead of H_2, would provide a simple way to solve the ambiguity of the $^{15}N^+ + H^+ + (N + H)$ or $NH^+ + H^+ + N$, channel. Using D_2 means the reactions would not be in the same position in the pairs spectrum since the m/z of $^{15}N^+$ would remain 15, while the m/z of ND^+ would be 16. However the relative intensities and scattering diagrams can also be used to provide more definitive information to differentiate the two possible channels.

6.3.2.1 Relative intensities

The different reaction channels are shown in Table 6.1, relative to the weakest (non-isotopic) electron transfer reaction, $N^+ + H^+$, (6.23).

Reaction channel	Relative Intensity	
$N_2^{2+} + H_2 \rightarrow N_2^+ + H_2^+$	26	(6.19)
$N_2^{2+} + H_2 \rightarrow {}^{14}N^{15}N^+ + H_2^+$	0.3	(6.20)
$N_2^{2+} + H_2 \rightarrow N_2^+ + H^+ + H$	5	(6.21)
$N_2^{2+} + H_2 \rightarrow N^+ + H_2^+ + N$	16	(6.22)
$N_2^{2+} + H_2 \rightarrow N^+ + H^+ + (N + H)$	1	(6.23)
$N_2^{2+} + H_2 \rightarrow {}^{15}N+ + H^+ + (N + H)$ or $NH^+ + H^+ + N$	0.3	(6.24)

Table 6.1 The table above shows the relative intensities of the reaction channels detected following the collisions of N_2^{2+} with H_2.

As previously mentioned, when using N_2^{2+}, the majority of the beam consists of $^{14}N^{14}N^{2+}$. The velocity filter is used to select $^{14}N^{14}N^{2+}$, therefore any $^{14}N^{15}N^{2+}$, in the beam, should be distinctly less abundant than the isotopic ratio, which is 99.3 ($^{14}N^{14}N^{2+}$) : 0.7 ($^{14}N^{15}N^{2+}$). However there is always a small percentage of $^{14}N^{15}N^{2+}$ present in the ion beam, which is revealed in the coincidence spectrum by the weak non-dissociative electron transfer channel forming, $^{14}N^{15}N^+ + H_2^+$, (6.20), directly next to the non-dissociative electron transfer channel, $^{14}N^{14}N^+ + H_2^+$, (6.19). As expected, the relative intensities in Table 6.1, show that the non-dissociative electron transfer channel, $N_2^+ + H_2^+$ (6.19), is considerably stronger than the isotopic channel, $^{14}N^{15}N^+ + H_2^+$, (6.20), at approximately 100 times more intense. It is rare that the presence of isotopes can cause any difficulty in channel assignment. However in this N_2^{2+} with H_2^+ system, as with the subsequently discussed N_2^{2+} with CH_4^+ system, there is an ambiguity, from simple inspection of the pairs spectrum, as to whether channel (6.24) is a simple dissociative electron transfer reaction with an isotope product, $^{15}N^+$, or a bond-forming reaction with an NH^+ product. If the ambiguous, $^{15}N^+ + H^+ + (N + H)$ or $NH^+ + H^+ + N$, channel (6.24)

is assigned as $^{15}N^+ + H^+ + (N + H)$ we would expect it to be in the region of 99 times less intense than $^{14}N^+ + H^+ + (N + H)$ (6.23). However it is evident from the relative intensities in that this ambiguous channel (6.24) is only approximately three times less intense than $^{14}N^+ + H^+ + (N + H)$ (6.23). The relative intensity evidence therefore clearly shows that channel (6.24) is not an isotopic channel but is in fact the bond-forming channel:

$$N_2^{2+} + H_2 \rightarrow NH^+ + H^+ + N \qquad (6.24)$$

The angular scattering, and hence reaction mechanism, of this bond–forming channel will be discussed in the next section.

6.3.2.2 Angular scattering

Figure 6.14 shows two scattering diagrams for the bond-forming channel (6.24) with respect to the velocity of N_2^{2+} in the COM frame.

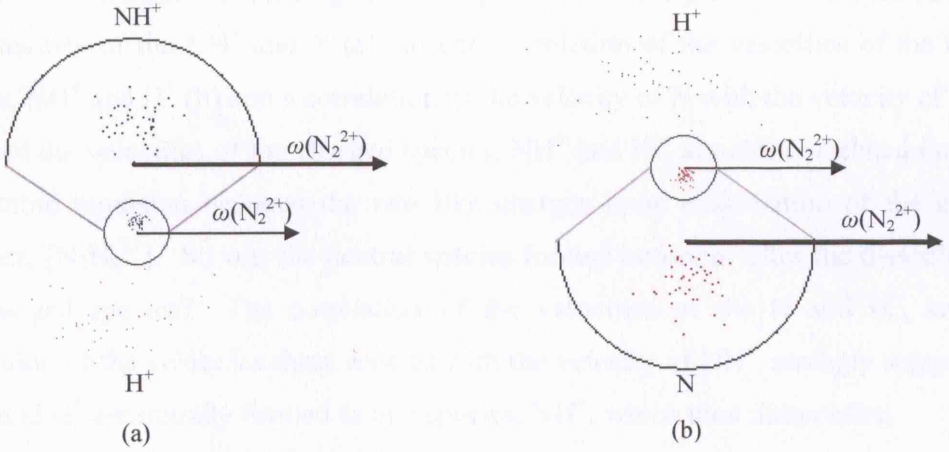

Figure 6.14 The scattering diagrams of channel (6.24). (a) shows the scattering of the velocity of the two ions relative to $\omega(N_2^{2+})$, (b) shows the scattering of the velocity of the H^+ and the neutral species, N, relative to $\omega(N_2^{2+})$. The scattering diagrams both have a circle radius of 1 cm μs^{-1}, including enlarged section, and both derived from data recorded using a 300 V repeller plate and at E_{com} 0.93 eV.

The scattering diagrams in Figure 6.14 show that there is very little correlation, or anti-correlation, of the velocity of any of the products with respect to the velocity of the N_2^{2+} in the COM frame. That is, the products are mostly sideways scattered with respect to the velocity of the dication in the COM frame. As previously mentioned sideways scattering of all three products is a very strong indication that the products were involved in a

collision complex, $[N_2H_2^{2+}]$, which had time to rotate before dissociation. Figure 6.15 shows the internal frame scattering diagrams of the three products relative to each other.

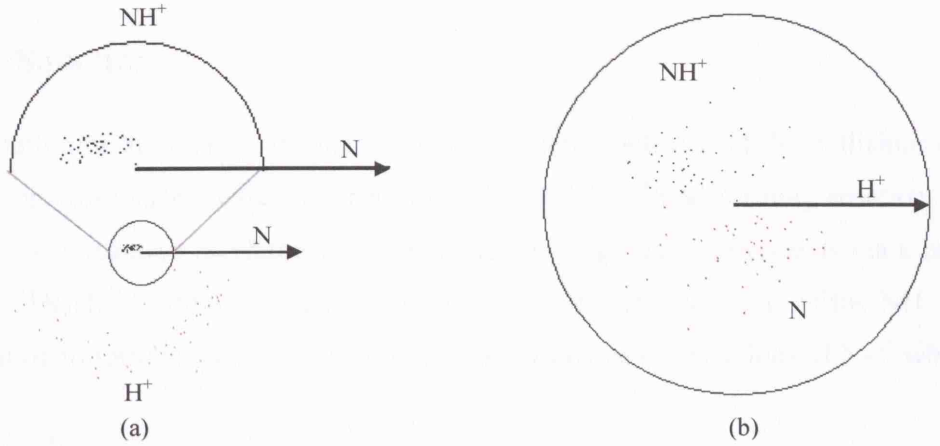

Figure 6.15 The internal frame scattering diagrams of bond-forming channel (6.24). (a) shows the scattering of the two ions relative to N, (b) show the scattering of the NH^+ and the neutral species, N, relative to H^+. The scattering diagrams both have a circle radius of 1 cm μs^{-1}, both derived from data recorded using a 300 V repeller plate and at E_{com} 0.93 eV.

The internal frame scattering diagrams, in Figure 6.15, clearly show an anti-correlation of the velocities of the NH^+ and N (a), an anti-correlation of the velocities of the charged species, NH^+ and H^+ (b) and a correlation of the velocity of N with the velocity of H^+. As expected the velocities of the charged species, NH^+ and H^+, are anti-correlated due to the Coulombic repulsion between the two like charges upon dissociation of the collision complex, $[N_2H_2^{2+}]$. So was the neutral species formed before or after the dissociation of the charged species? The correlation of the velocities of the N and H^+, and anti-correlation of the velocities these species with the velocity of NH^+, strongly suggests that the N and H^+ are initially formed as one species, NH^+, which then dissociates;

$$N_2^{2+}+H_2 \rightarrow [N_2H_2^{2+}] \rightarrow NH^+ + NH^+ \rightarrow NH^+ + N + H^+ \quad (6.25)$$

6.3.2.3 Reaction energetics

The exothermicity spectrum for the bond-forming channel, $NH^+ + H^+ + N$ (6.24), is very weak. However the intensity is mainly distributed between approximately 4 and 7 eV, which agrees well with the calculated 5.1 eV literature exothermicity of a reaction of ground state reactants to form ground state products. If we also consider the $c^3\Sigma_u^+$ state of N_2^{2+}, then a reaction to form ground state NH^+ with either the ground state or first excited state of N, has an exothermicity of 6.6 and 4.2 eV respectively, which also agrees with the experimentally observed exothermicity spectrum. NH^+ is an unusual molecule in that its

first excited state, $a^4\Sigma^-$, lies only 0.04 eV above its ground state, $X^2\Pi_r$. Thus the population of the NH^+ $a^4\Sigma^-$ state with the ground or $c^3\Sigma_u^+$ state of N_2^{2+}, and ground state or first excited state of N also agrees well with the observed exothermicity.

6.3.2.4 Summary

Interpretation of the relative intensities of the ion pairs detected in the collisions of N_2^{2+} with H_2 provides strong evidence that channel (6.24) is a bond forming reaction, $NH^+ + H^+ + N$. The reaction mechanism of this bond-forming channel proceeds via a collision complex, $[N_2H_2^{2+}]$, which dissociates to form NH^+ and NH^+ with one of the NH^+ further dissociating to form N and H^+. The next section discusses the reactions of N_2^{2+} with CH_4.

6.3.3 N_2^{2+} with CH_4

At least sixteen channels are observed in the PSCO spectra recorded following the collisions of N_2^{2+} with CH_4. These reactions are listed as follows.

Non-dissociative electron transfer

$$N_2^{2+} + CH_4 \rightarrow N_2^+ + CH_4^+ \quad (6.26)$$

Dissociative electron transfer

$$N_2^{2+} + CH_4 \rightarrow N_2^+ + CH_3^+ + H \quad (6.27)$$
$$N_2^{2+} + CH_4 \rightarrow N_2^+ + CH_2^+ (+ H_2) \quad (6.28)$$
$$N_2^{2+} + CH_4 \rightarrow N_2^+ + CH^+ (+ H_2 + H) \quad (6.29)$$
$$N_2^{2+} + CH_4 \rightarrow N_2^+ + H_2^+ (+ CH_2) \quad (6.30)$$
$$N_2^{2+} + CH_4 \rightarrow N_2^+ + H^+ (+ CH_3) \quad (6.31)$$

Dissociative double electron transfer

$$N_2^{2+} + CH_4 \rightarrow (N_2 +) CH_2^+ + H_2^+ \quad (6.32)$$
$$N_2^{2+} + CH_4 \rightarrow (N_2 +) CH^+ + H_2^+ (+ H) \quad (6.33)$$
$$N_2^{2+} + CH_4 \rightarrow (N_2 +) C^+ + H_2^+ (+H_2) \quad (6.34)$$
$$N_2^{2+} + CH_4 \rightarrow (N_2 +) CH_3^+ + H^+ \quad (6.35)$$
$$N_2^{2+} + CH_4 \rightarrow (N_2 +) CH_2^+ + H^+ (+ H) \quad (6.36)$$
$$N_2^{2+} + CH_4 \rightarrow (N_2 +) CH^+ + H^+ (+ H_2) \quad (6.37)$$
$$N_2^{2+} + CH_4 \rightarrow (N_2 +) C^+ + H^+ (+ H_2 + H) \quad (6.38)$$

Isotopic dissociative electron transfer or bond-forming? (see below)

$$N_2^{2+} + CH_4 \rightarrow {}^{14}N^{15}N^+ + H_2^+ (+ CH_2) \text{ or } N_2H^+ + H_2^+ (+ CH) \quad (6.39)$$
$$N_2^{2+} + CH_4 \rightarrow {}^{14}N^{15}N^+ + H^+ (+ CH_3) \text{ or } N_2H^+ + H^+ (+ CH_2) \quad (6.40)$$

The identity of the products in the last two channels are not clear from the coincidence spectrum, the product with an *m/z* of 29 could either be a trace of $^{14}N^{15}N^+$ or a bond-forming product, N_2H^+, since both have the same mass. We discuss this further below and conclude that in fact this channel is a bond-forming channel.

As can be seen from the above list a non-dissociative electron transfer channel along with many dissociative single and double electron transfer channels are observed following collisions of N_2^{2+} with CH_4. Many of these channels may be more than three-body. That is, for several of these reactions we cannot definitely assign what the identity of the neutral product. Therefore, in the list of reactions a suggestion is given in brackets. Two additional 'ambiguous', potentially bond-forming channels have also been observed which will be discussed in more detail. The products of the double dissociative electron transfer reactions, CH_3^+, CH_2^+, CH^+, C^+, H^+ and H_2^+, are typical of the products observed from the dissociative double ionisation of CH_4 [14-18] As mentioned above the reactions of N_2^{2+} with CH_4 have been previously studied by Dutuit *et al.* [2] In the reaction of N_2^{2+} with CD_4 they detect ND^+, ND_2^+, DCN^+, D_2CN^+, $C_2D_4^+$ and $C_2D_5^+$ However as can be seen from the list of observed channels we do not observe any of these products. Operating under single collision conditions we would not expect to detect secondary reaction products, such as $C_2D_4^+$ and $C_2D_5^+$. The lack of detection of ND^+, ND_2^+, DCN^+ and D_2CN^+ may be attributed to 'crowding' of the PSCO coincidence spectra in the region where these reaction peaks would lie. Bond-forming channels tend to be less intense than charge transfer channels so if they lie in the same region of the coincidence spectrum, the intensity of the charge transfer channel 'swamps' the bond-forming channel. For example if H_2CN^+ was paired with H^+ or H_2^+ the peaks would lie in exactly the same position in the coincidence spectrum as N_2^+ paired with H^+ or H_2^+. Over 14 electron transfer channels (non-dissociative electron transfer, dissociative electron transfer and dissociative double electron transfer) are detected, many in the same position, or within only one mass unit, of the isotopic bond forming reactions observed by Dutuit *et al* following the collision of N_2^{2+} with CD_4. An obvious next step in the study of this collision system would involve reacting N_2^{2+} with CD_4, as performed by Dutuit *et al*, to separate the reactions further. For example, if H_2CN^+ is produced with H^+ or H_2^+, by using CD_4 the D_2CN^+ paired with D^+ or D_2^+, would move two mass units away from the electron transfer products, and hence the two reactions would easily be distinguished.

The pairs spectrum in Figure 6.16 has been collected using a pulsed beam. However, two sections have been cut from the pairs collection where the false coincidences lie. A full discussion of false coincidences, and why they have omitted from some coincidence spectra, has been given in Chapter Three. It is also important to note that these 'spot' plots over emphasize the reaction peak tails, as discussed in Chapter Three.

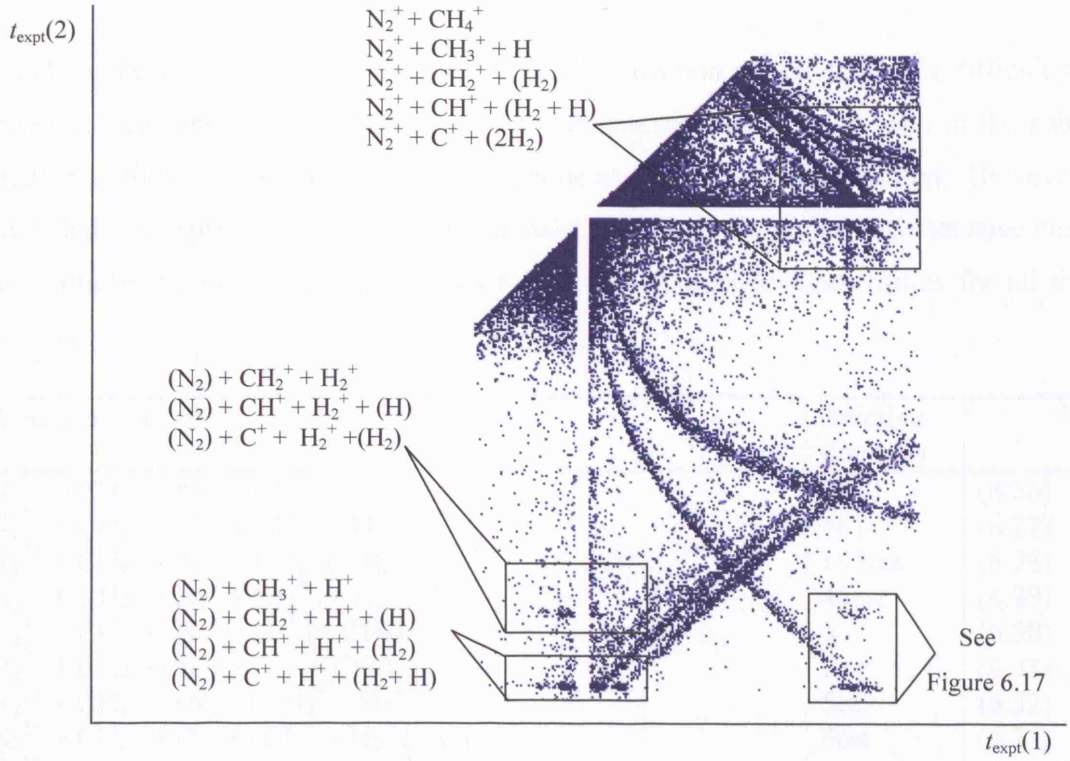

Figure 6.16 A coincidence spectrum recorded following collisions of N_2^{2+} and CH_4, at E_{com} 5.08 eV, using a 300 V repeller plate.

Figure 6.17 shows the section of the pairs spectrum of the area with the 'possible' bond-forming reactions.

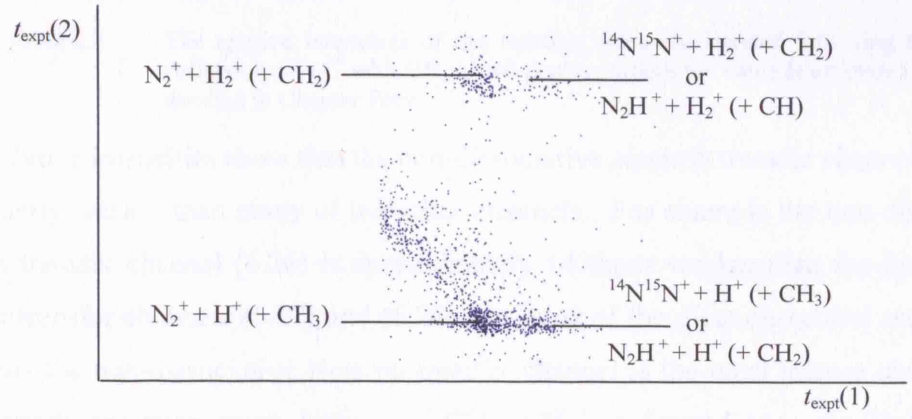

Figure 6.17 A section of coincidence spectrum of N_2^{2+} with CH_4, focusing on the 'possible' bond-forming reactions, E_{com} 5.08 eV, recorded using a 300 V repeller plate.

The following section details the relative intensities of the different channels.

6.3.3.1 Relative intensities

Excluding the false coincidences from the pairs collection means that it is difficult to derive the true relative intensities of all the channels since, as can be seen in the pairs spectrum in Figure 6.16, some of the channels lie in areas cut from collection. However, as detailed in Chapter Four, it is possible to make estimates of the channels that have only been partially recorded. Table 6.2 shows the calculated relative intensities for all the channels.

Reaction channel	Relative Intensity	
$N_2^{2+} + CH_4 \rightarrow N_2^+ + CH_4^+$	12	(6.26)
$N_2^{2+} + CH_4 \rightarrow N_2^+ + CH_3^+ + H$	161	(6.27)
$N_2^{2+} + CH_4 \rightarrow N_2^+ + CH_2^+ (+ H_2)$	165est	(6.28)
$N_2^{2+} + CH_4 \rightarrow N_2^+ + CH^+ (+ H_2 + H)$	45est	(6.29)
$N_2^{2+} + CH_4 \rightarrow N_2^+ + H_2^+ (+ CH_2)$	3	(6.30)
$N_2^{2+} + CH_4 \rightarrow N_2^+ + H^+ (+ CH_3)$	7	(6.31)
$N_2^{2+} + CH_4 \rightarrow (N_2 +) CH_2^+ + H_2^+$	5est	(6.32)
$N_2^{2+} + CH_4 \rightarrow (N_2 +) CH^+ + H_2^+ (+ H)$	6est	(6.33)
$N_2^{2+} + CH_4 \rightarrow (N_2 +) C^+ + H_2^+ (+H_2)$	1	(6.34)
$N_2^{2+} + CH_4 \rightarrow (N_2 +) CH_3^+ + H^+$	13	(6.35)
$N_2^{2+} + CH_4 \rightarrow (N_2 +) CH_2^+ + H^+ (+ H)$	30est	(6.36)
$N_2^{2+} + CH_4 \rightarrow (N_2 +) CH^+ + H^+ (+ H_2)$	11est	(6.37)
$N_2^{2+} + CH_4 \rightarrow (N_2 +) C^+ + H^+ (+ H_2 + H)$	3	(6.38)
$N_2^{2+} + CH_4 \rightarrow {}^{14}N^{15}N^+ + H_2^+ (+ CH_2)$ or $N_2H^+ + H_2^+ (+ CH)$	1	(6.39)
$N_2^{2+} + CH_4 \rightarrow {}^{14}N^{15}N^+ + H^+ (+ CH_3)$ or $N_2H^+ + H^+ (+ CH_2)$	4	(6.40)

Table 6.2 The relative intensities of the reaction channels detected following the collisions of N_2^{2+} with CH_4. 'est' denotes where the value is estimated as detailed in Chapter Four.

These relative intensities show that the non-dissociative electron transfer channel (6.26) is significantly weaker than many of the other channels. For example the non-dissociative electron transfer channel (6.26) is approximately 14 times weaker than the dissociative electron transfer channels (6.27) and (6.28). In most of the dication-neutral reactions in this thesis the non-dissociative electron transfer channel is the most intense channel. In the electron ionisation cross section of CH_4, CH_4^+ is formed to a similar order of magnitude as CH_3^+, and is more abundant in formation that CH_2^+. [18] However in low energy reactions of the monocation N_2^+ with CH_4 and N^+ with CH_4, CH_3^+ is the most dominant product which is attributed to the dominant population of CH_4^+ in states which readily dissociate to $CH_3^+ + H$. [19, 20] It is likely that a similar process is occurring in the reaction of N_2^{2+} with CH_4.

A second 'unusual' feature refers to the H_2^+ products; one may not expect the formation of H_2^+ from a dissociative electron transfer reaction of N_2^{2+} with CH_4. However H_2^+ is in fact a reasonably abundant product in the electron ionisation of CH_4, formed with a similar order of magnitude as C^+. The abundance of H_2^+ formed from the ionisation of CH_4 explains why it appears to be a common product in the dissociative electron transfer reaction in this system; H_2^+ is simply formed from the dissociation of excited states of CH_4^+, rather than through bond-forming processes. [18] However electron ionisation cross sections of CH_4 show the H^+ product ions are typically 10 times more abundant than H_2^+ product ions. But in the collision of N_2^{2+} + CH_4, the H^+ channels $N_2^+ + H^+$ (+ CH_3) (6.31), (N_2 +) $C^+ + H^+$ (+ H_2 + H) (6.38), (N_2 +) $CH_2^+ + H^+$ (+ H) (6.36), (N_2 +) $CH^+ + H^+$ (+ H_2) (6.37) and $^{14}N^{15}N^+ + H^+$ (+ CH_3) or $N_2H^+ + H^+$ (+ CH_2) (6.40), are only 2 to 7 times more intense than the most similar H_2^+ channels $N_2^+ + H_2^+$ (+ CH_2) (6.30), (N_2 +) $C^+ + H_2^+$ (+ H_2) (6.34), (N_2 +) $CH_2^+ + H_2^+$ (6.32), (N_2 +) $CH^+ + H_2^+$ (+ H) (6.33) and $^{14}N^{15}N^+ + H_2^+$ (+ CH_2) or $N_2H^+ + H_2^+$ (+ CH) (6.39), respectively. However, as explained in section 5.3.1.1, this difference can be attributed to the fact that a distinct proportion of the H^+ ions can leave the region source region before the repeller plate is pulsed and hence will not be detected, reducing the recorded relative intensities of these channels.

As with the previous collision system, the relative intensities can also help to differentiate the ambiguous channels, $^{14}N^{15}N^+ + H_2^+$ (+ CH_2) or $N_2H^+ + H_2^+$ (+ CH), (6.39), and $^{14}N^{15}N^+ + H^+$ (+ CH_3) or $N_2H^+ + H^+$ (+ CH_2), (6.40). When using N_2^{2+}, the majority of the beam consists of $^{14}N^{14}N^{2+}$. $^{14}N^{14}N^{2+}$ is selected using the velocity filter therefore any $^{14}N^{15}N^{2+}$, in the beam, should be no higher than the expected isotopic abundance, which is 99.3 ($^{14}N^{14}N^{2+}$) : 0.7 ($^{14}N^{15}N^{2+}$), and in fact should be much weaker than this due to losses in the velocity filter. If channels (6.39) and (6.40) were simply isotopic channels of (6.30) and (6.31), then channels (6.30) and (6.31) would be expected to be significantly more intense, in the region of 100 times more, than (6.39) and (6.40). However channels $^{14}N^{15}N^+ + H_2^+$ (+ CH_2) or $N_2H^+ + H_2^+$ (+ CH) (6.39), $^{14}N^{15}N^+ + H^+$ (+ CH_3) or $N_2H^+ + H^+$ (+ CH_2) (6.40), $N_2^+ + H_2^+$ (+ CH_2) (6.30) and $N_2^+ + H^+$ (+ CH_3) (6.31) are formed in the ratio of 1 : 4 : 3 : 7. That is, channel (6.30) is only about 3 times stronger than channel (6.39) and channel (6.31) is only 2 times stronger than channel (6.40). Thus this evidence from the relative intensities strongly suggests we have observed bond forming processes:

$$N_2^{2+} + CH_4 \rightarrow N_2H^+ + H_2^+ (+ CH) \quad (6.39)$$
$$N_2^{2+} + CH_4 \rightarrow N_2H^+ + H^+ (+ CH_2) \quad (6.40)$$

6.3.3.2 Angular scattering

The scattering diagrams of the two bond-forming channels, (6.39) and (6.40), are very similar to each other as can be seen from the scattering diagrams in Figure 6.18 which show the scattering of the velocities of each of the products, in each of the two reactions, relative to $\omega(N_2^{2+})$. This strongly suggests that the reactions follow a similar mechanism and so they will hence be discussed together in this section.

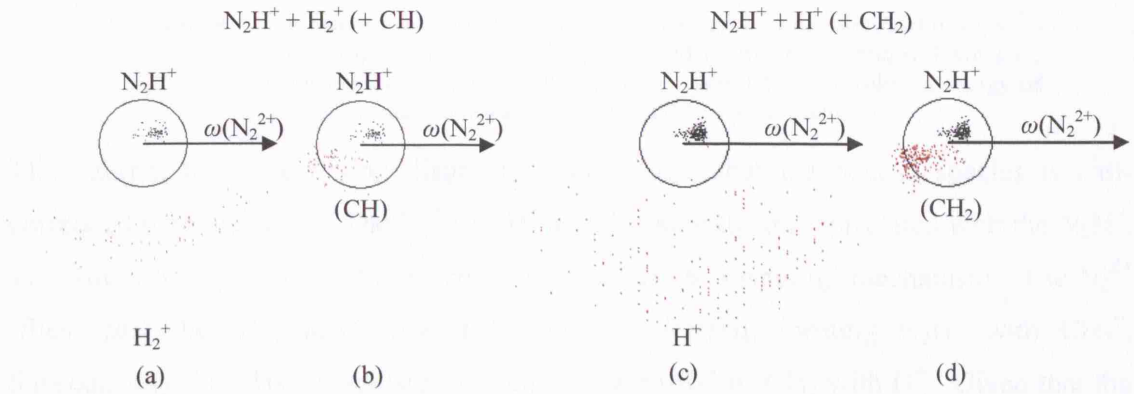

Figure 6.18 The scattering of the velocities of each of the product, relative to the velocity of the dication, N_2^{2+}, in the COM frame, for bond-forming channels, (6.39) and (6.40), circle radius 1 cm μs^{-1}, recorded following the collision of N_2^{2+} with CH_4 at a collision energy of 5.08 eV in the COM frame, using a 300 V repeller plate.

The scattering diagrams in Figure 6.18 show that the velocity of the N_2H^+ is dominantly forwards scattered, while the velocity of the (CH) or (CH_2) is dominantly backwards scattered. The scattering of the velocity of the H_2^+ or H^+ appears to be close to symmetrical. Of course we do not know the true identity of the neutral species in either reaction. However, as previously discussed, the directional, localised low velocity of the neutral species is a strong indication that it was formed in the same reaction step. Whether the neutral species then separates is unlikely to affect the scattering so the reaction can be treated as a three-body product reaction. Given that we detect CH^+ and CH_2^+ in other channels following the collision of N_2^{2+} with CH_4, it is quite likely that the neutral is CH or CH_2 in these bond forming channels. Figure 6.19 shows two internal frame scattering diagrams, one for each of the bond-forming channels.

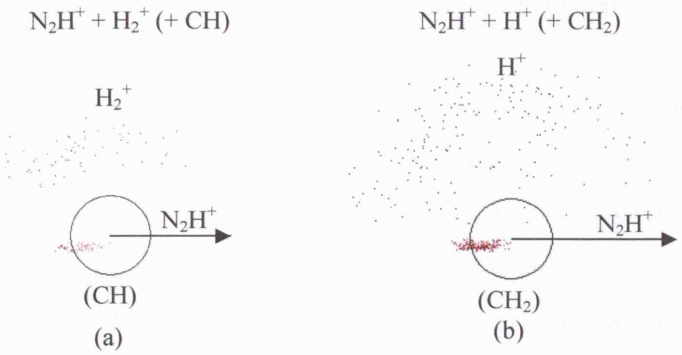

Figure 6.19 The scattering of the two product ions relative to the direction of $\omega(N_2^{2+})$ for bond-forming channels, (6.39) and (6.40), circle radius 1 cm μs^{-1}, recorded following the collision of N_2^{2+} with CH_4 at a collision energy of 5.08 eV in the COM frame, using a 300 V repeller plate.

The internal frame scattering diagrams clearly show that the neutral species is anti-correlated with the N_2H^+. The H_2^+ and H^+ are also slightly anti-correlated with the N_2H^+. This strongly suggests that the reaction occurred via a 'stripping' mechanism. The N_2^{2+} 'flies' past the CH_4 and strips a H and an electron, forming N_2H^+ with CH_3^+. Subsequently the CH_3^+ dissociates to form CH with H_2^+ or CH_2 with H^+. Given that the velocities of the H_2^+/H^+ and CH/CH_2 are not isotropically scattered centred about the same velocity, the nascent velocity of CH_3^+, the dissociation will have occurred rapidly after the formation of the species before it had time to rotate. This 'stripping' mechanism has previously been observed using the PSCO experiment in the reaction of CF_2^{2+} with H_2O to form HCF_2^+ with H^+ and O.

6.3.3.3 Reaction energetics

The exothermicity spectra for the bond forming reactions detected following the collisions of N_2^{2+} with CH_4 are broad and unresolved. For channel $N_2H^+ + H_2^+ (+ CH)$, (6.39), the exothermicity is distributed between 2 to 14 eV, although the intensity is so weak that it is difficult to define a peak in the spectrum. The calculated literature exothermicity of a reaction of the ground and the $c^3\Sigma_u^+$ of N_2^{2+} to form the products N_2H^+, H_2^+ and CH in their ground state, is 9.6 eV and 11.1 eV respectively. Although the scattering diagrams certainly hint that the neutral product is CH we have also considered the formation of C and H. A reaction of the ground state, and the $c^3\Sigma_u^+$, of N_2^{2+} to form the products, N_2H^+, H_2^+, C and H, in their ground states has an exothermicity of 6.1 and 7.6 eV respectively. Given that we observe exothermicity up to 14 eV and the fact that a reaction to form N_2H^+, H_2^+, C and H has a lower exothermicity than that of a reaction to form N_2H^+, H_2^+ and CH may hint that the identity of the neutral is CH. Exothermicities

lower than those calculated to form products in their ground states can be easily accounted form by vibrational or electronic excitation of the molecular products. However exothermicities at a higher value than the calculated exothermicity to form products in their ground states can only be accounted for by excitation of the dication. As previously mentioned studies show that N_2^{2+} is primarily only formed in the ground and the $c^3\Sigma_u^+$ state. Therefore it appears that a reaction to form N_2H^+, H_2^+ and CH accounts for intensity observed in the exothermicity spectrum more than a reaction to form N_2H^+, H_2^+, C and H would.

The exothermicity spectra of channel $N_2H^+ + H^+$ (+ CH_2) (6.40) has intensity distributed between 2 and 14 eV with a peak in intensity at approximately 8 eV. Table 6.3 shows the calculated exothermicities for each of the neutral combinations in this channel.

Electronic state of N_2^{2+}	Exothermicity (eV)			
	$N_2H^+ + H^+ + CH_2$	$N_2H^+ + H^+ + C + H_2$	$N_2H^+ + H^+ + CH + H$	$N_2H^+ + H^+ + C + H + H$
$X^1\Sigma g^+$	11.3	7.9	6.9	3.4
$c^3\Sigma_u^+$	12.8	9.4	8.4	4.9

Table 6.3 The calculated exothermicity (eV) to form products in their ground states for each of the different possible neutral identities in channel (6.40).

Table 6.3 shows that a reaction of ground or $c^3\Sigma_u^+$ state N_2^{2+} to form the products N_2H^+, H^+ and CH_2 in there ground states has the highest exothermicity. Again, as with the previous channel, this hints that the calculated exothermicities of a reaction of ground or $c^3\Sigma_u^+$ state N_2^{2+} to form the products N_2H^+, H^+ and CH_2 in there ground or excited states would agree the most with the observed exothermicity spectrum. [21, 22]

6.3.3.4 Summary

To conclude, the evidence from the relative intensities discussed above certainly suggests that channels (6.39) and (6.40) and are bond-forming channels. The reaction mechanism of the bond-forming channels follows a 'stripping' mechanism where the N_2^{2+} 'flies' past the CH_4, and strips an H and electron. The CH_3^+ then rapidly dissociates to yield CH and H_2^+ or CH_2 and H^+. The following section will discuss the reactions of N_2^{2+} with Ar.

6.3.4 N_2^{2+} with Ar

Previous work studying the consequences of collisions between N_2^{2+} and Ar was described in section 5.1. Using the PSCO three channels are observed; non-dissociative electron transfer, dissociative electron transfer and a bond-forming channel.

$$N_2^{2+} + Ar \rightarrow N_2^{+} + Ar^{+} \quad (6.41)$$
$$N_2^{2+} + Ar \rightarrow N^{+} + Ar^{+} + N \quad (6.42)$$
$$N_2^{2+} + Ar \rightarrow NAr^{+} + N^{+} \quad (6.43)$$

The pairs spectrum in Figure 6.20 shows these three reactions.

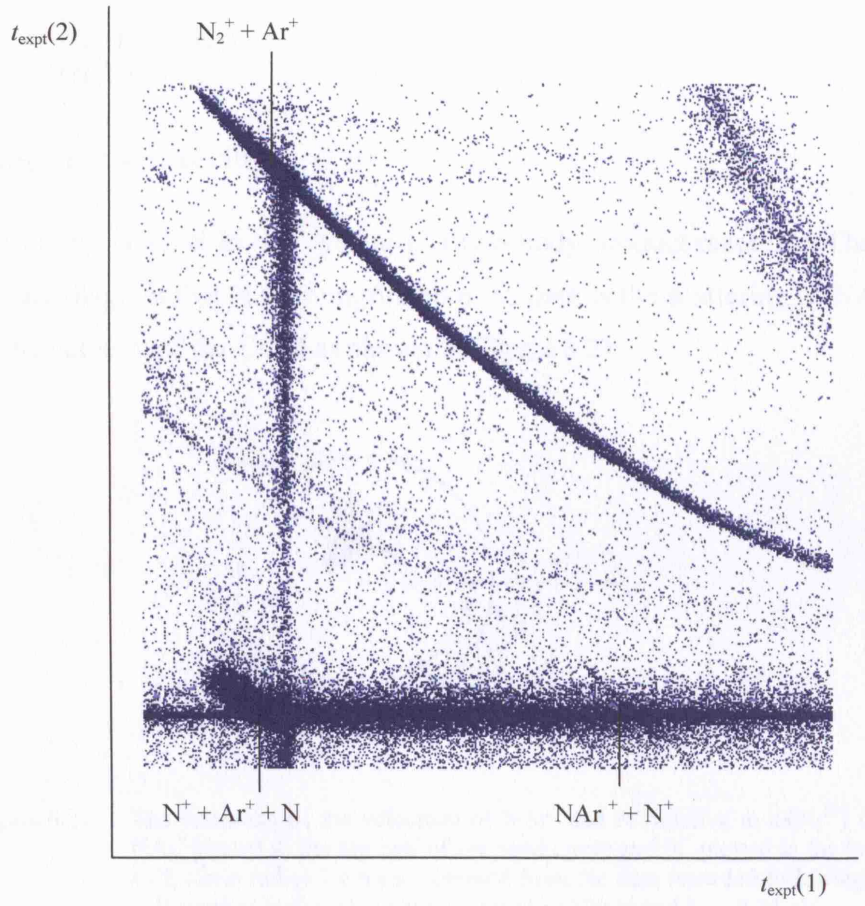

Figure 6.20 The coincidence spectrum of the N_2^{2+} with Ar system at 300 V repeller plate and E_{com} 8.24 eV.

The relative intensities of these channels are discussed in the next section, before the discussion of the angular scattering and exothermicity spectrum of the bond-forming channel.

6.3.4.1 Relative intensities

The three channels, non-dissociative electron transfer (6.41), dissociative electron transfer (6.42) and bond-forming (6.43), are formed in the ratio of 22:21:1 respectively. The bond-forming channel is therefore distinctly weaker compared with the electron transfer channels, while the two electron transfer channels occur with comparable intensities. Dication-neutral bond-forming reactions involving rare gases have been previously reported, involving either the production of monocation pairs, such as (6.44) by Lambert *et al*, or a dicationic species, such as (6.45) by Bassi *et al*, the latter of which has been discussed in more detail in Chapter One. [23-26]

$$Ar^{2+} + NH_3 \rightarrow ArNH^+ + (H_2)^+ \quad (6.44)$$
$$Ar^{2+} + N_2 \rightarrow ArN^{2+} + N \quad (6.45)$$

6.3.4.2 Angular scattering

The bond-forming channel in this system is a two-body product reaction. Therefore the only scattering diagram that is meaningful from the data is the scattering of NAr^+ and N^+ relative to the velocity of the COM as shown in Figure 6.21.

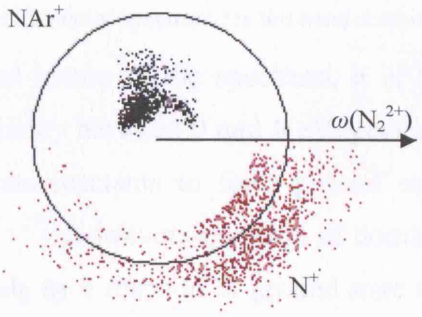

Figure 6.21 The scattering of the velocities of NAr^+ and N^+ relative to $\omega(N_2^{2+})$ with NAr^+ plotted in the top half of the semi circle and N^+ plotted in the lower half, circle radius 1 cm μs^{-1}, derived from the data recorded following the collisions of N_2^{2+} with Ar at repeller plate 300 V and E_{com} 8.24 eV.

The scattering diagram in Figure 6.21 shows that the scattering of the velocities of the products is over a range of scattering angles, indicating participation of a collision complex, ArN_2^{2+}, in the reaction mechanism. However the scattering certainly is not isotropic, therefore the average lifetime of the collision complex must be of the order of its rotational lifetime. Computational calculations have shown that minima exist for linear and C_{2v} geometries on the singlet and triplet ArN_2^{2+} surface, lying 7.8 eV and 1.5 eV below the ground state and 'c' state reaction asymptote of N_2^{2+}, respectively.

Therefore collision complexes, ArN_2^{2+}, are certainly energetically accessible for the N_2^{2+} and Ar reactants.

6.3.4.3 Reaction energetics

The exothermicity spectrum for the bond-forming channel, $NAr^+ + N^+$ (6.43), is broad and unresolved as shown in (6.20).

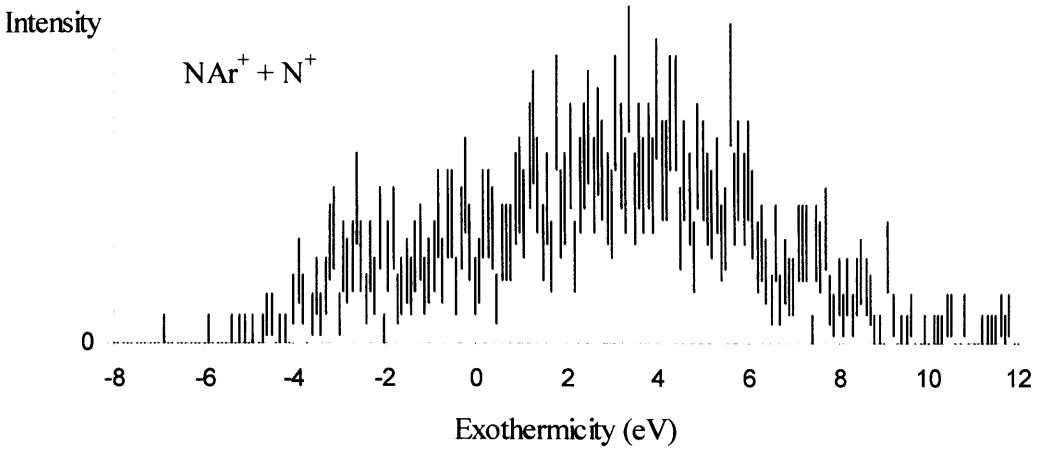

Figure 6.22 The exothermicity spectrum for the bond-forming channel $NAr^+ + N^+$.

However, despite the broad nature of the spectrum, it is clear that the majority of the reactions have an exothermicity between 0 and 6 eV, peaking at approximately 3 eV. A reaction of the ground state reactants to form ground state products has a literature exothermicity of 6.3 eV. [22, 27] However, the range of dominant exothermicities observed can be accounted for entirely by a reaction of ground state reactants to form ground state NAr^+ with the $2p^2$ states of N^+.

6.4 Conclusion

Chapter Six has discussed four collision systems, N_2^{2+} with C_2H_2, H_2, CH_4 and Ar, which may all be of relevance to the ionosphere of Titan, where N_2^{2+} has recently been modelled. [1] The reactions N_2^{2+} with CH_4, H_2 and Ar may also be of relevance to the ionosphere of Earth. [7] All these systems display significant levels of electron transfer reactions (both dissociative and non-dissociative) and double dissociative electron transfer reactions for N_2^{2+} with CH_4 and C_2H_2. Most significantly to this thesis however, is the fact all the collision systems in this Chapter result in 'bond forming' reactions.

Despite the fact that only a few conclusions can be drawn from the reaction exothermicity spectra, analysis of the angular scattering yielded some strong evidence towards deriving reaction mechanisms for each these bond forming reactions. All these reactions appear to follow a non-complexation reaction mechanism, with the exception of the bond-forming reaction of N_2^{2+} with Ar. This is evident from the lack of isotopic scattering from all the species, with the exception of, in some cases, the H species.

6.5 References

[1] Lilensten, J., Witasse, O., Simon, C., Solidi-Lose, H., Dutuit, O., Thissen, R., and Alcaraz, C., 2005, Geophysical Research Letters, 32, 3.
[2] Dutuit, O., Thissen, R., and Soldi-Lose, H., 2005, -Unpublished.
[3] Kamber, E. Y., Akgungor, K., Safvan, C. P., and Mathur, D., 1996, Chemical Physics Letters, 258, 3-4, 336.
[4] Koslowski, H. R., Lebius, H., Staemmler, V., Fink, R., Wiesemann, K., and Huber, B. A., 1991, Journal of Physics B-Atomic Molecular and Optical Physics, 24, 23, 5023.
[5] Savage, H. F. and Wittebor, F. C., 1968, Journal of Chemical Physics, 48, 4, 1872-&.
[6] Schulz, P. A., 1985, Journal of Chemical Physics, 83, 11, 5673.
[7] Simon, C., Lilensten, J., Dutuit, O., Thissen, R., Witasse, O., Alcaraz, C., and Soldi-Lose, H., 2005, Annales Geophysicae, 23, 3, 781.
[8] Roithova, J., Herman, Z., Schroder, D., and Schwarz, H., 2006, Chemistry-A European Journal, 12, 9, 2465.
[9] Rogers, S. A., Price, S. D., and Leone, S. R., 1993, Journal of Chemical Physics, 98, 1, 280.
[10] Amero, J. M. and Vazquez, G. J., 2005, International Journal of Quantum Chemistry, 101, 4, 396.
[11] Lu, H. F., Li, F. Y., and Lin, S. H., 2004, Journal of Physical Chemistry A, 108, 42, 9233.
[12] Harper, S. M., Hu, W. P., and Price, S. D., 2002, Journal of Physics B-Atomic Molecular and Optical Physics, 35, 21, 4409.
[13] Hu, W. P., Harper, S. M., and Price, S. D., 2002, Measurement Science & Technology, 13, 10, 1512.
[14] Benitzhak, I., Carnes, K. D., Ginther, S. G., Johnson, D. T., Norris, P. J., and Weaver, O. L., 1993, Physical Review A, 47, 5, 3748.
[15] Dujardin, G., Winkoun, D., and Leach, S., 1985, Physical Review A, 31, 5, 3027.
[16] Fiegele, T., Hanel, G., Torres, I., Lezius, M., and Mark, T. D., 2000, Journal of Physics B-Atomic Molecular and Optical Physics, 33, 20, 4263.
[17] Orient, O. J. and Srivastava, S. K., 1987, Journal of Physics B-Atomic Molecular and Optical Physics, 20, 15, 3923.
[18] Straub, H. C., Lin, D., Lindsay, B. G., Smith, K. A., and Stebbings, R. F., 1997, Journal of Chemical Physics, 106, 11, 4430.
[19] Alcaraz, C., Nicolas, C., Thissen, R., Zabka, J., and Dutuit, O., 2004, Journal of Physical Chemistry A, 108, 45, 9998.
[20] Carrasco, N., Dutuit, O., Thissen, R., Banaszkiewicz, M., and Pernot, P., 2007, Planetary and Space Science, 55, 1-2, 141.
[21] Dibeler, V. H., Franklin, J. L., and Reese, R. M., 1959, Journal of the American Chemical Society, 81, 1, 68.
[22] NIST Chemistry WebBook, National Institute Of Standards and Technology, 2003, - http://webbook.nist.gov.
[23] Burnside, P. W. and Price, S. D., 2006, International Journal of Mass Spectrometry, 249, 279.
[24] Lambert, N., Kearney, D., Kaltsoyannis, N., and Price, S. D., 2004, Journal of the American Chemical Society, 126, 11, 3658.
[25] Tosi, P., Lu, W. Y., Correale, R., and Bassi, D., 1999, Chemical Physics Letters, 310, 1-2, 180.
[26] Tosi, P., Correale, R., Lu, W. L., Falcinelli, S., and Bassi, D., 1999, Physical Review Letters, 82, 2, 450.
[27] Price, S. D., 2007, International Journal of Mass Spectrometry, 260, 1, 1.

Chapter 7 Conclusions and Future Work

The current PSCO experimental arrangement has been successfully used to provide detailed information regarding the reactivity of gas–phase molecular dications with neutrals. [1, 2] The experiment has been used to successfully determine the ion pairs formed in these reactions, giving a greater insight to the product partners than conventional, single ion detection techniques. In addition to the reactivity information, often a detailed insight can be gained into the reaction dynamics, as shown in the results Chapters of this thesis.

Bond-forming reactions were observed following the collisions of N_2^{2+} and O_2, CO_2, H_2O, C_2H_2, H_2, CH_4 and Ar. All these reactions are potentially of relevance to the ionospheres of Earth or Titan. Notably for the reactions between N_2^{2+} and O_2, CO_2 and H_2O all of the bond-forming channels involve the formation of NO^+. NO^+ is one of the most abundant components of the terrestrial ionosphere so it particularly interesting that all of the bond-forming reactions produced NO^+ in this study of the potentially terrestrially significant reactions.

The scattering diagrams derived from the PSCO data for both of the bond-forming reactions of N_2^{2+} with O_2, one of the bond-forming reactions of N_2^{2+} with CO_2, and one of the bond-forming reactions of N_2^{2+} with H_2O, indicate that the bond-forming reactions proceed via a long-lived collision complex $[N_2XO]^{2+}$, where X = O, CO or H_2. This collision complex then decays by loss of a neutral atom to form a daughter dication which then decays by charge-separation to yield the observed products. One of the bond-forming reactions of N_2^{2+} with CO_2 and two of the bond-forming reactions of N_2^{2+} with H_2O do not appear to follow this 'neutral loss' mechanism. In the case of the reaction of N_2^{2+} with CO_2 to form NO^+ with N^+ and CO, the reaction mechanism proceeds via the formation of a collision complex which dissociates via charge separation followed by dissociation of one of the monocations to form NO^+ and CO or C and O. While in the case of the two bond-forming reactions of N_2^{2+} with H_2O, the reaction mechanism proceeds via the formation of a short-lived collision complex which dissociates via charge separation followed by dissociation of one of the monocations to form a singly charged species and one or more neutral species.

The scattering diagrams of the bond-forming reaction of N_2^{2+} with Ar to form ArN^+ with N^+, indicate the participation of a collision complex, ArN_2^{2+}, although not quite as long-

lived as those previously mentioned. The reactions of N_2^{2+} with C_2H_2, H_2 and CH_4 do not appear to involve any long-lived complexation and are very rapid. In the reaction of N_2^{2+} and C_2H_2, it appears two reaction mechanisms are operating. In one mechanism the N^+ is initially formed with a $[NC_2H_2^+]$ species, the $[NC_2H_2^+]$ then further dissociates to lose one or two H atoms. In the other mechanism an NH^+ or NH_2^+ species is initially formed, with the NH^+ dissociating to form H^+ with N, and the NH_2^+ dissociating to form H^+ with NH or N and H. In the reaction of N_2^{2+} with H_2 the reaction proceeds via a short-lived collision complex, $[N_2H_2^{2+}]$, which dissociates to form NH^+ and NH^+ with one of the NH^+ further dissociating to form N and H^+. While the reactions of N_2^{2+} with CH_4 follows a 'stripping' mechanism where the N_2^{2+} 'flies' past the CH_4, and strips an H and electron, the CH_3^+ then rapidly dissociates to yield CH and H_2^+ or CH_2 and H^+.

7.1 Future Work

The research for this thesis has therefore yielded a detailed insight to the bond-forming reactivity of ionospherically relevant dication-neutral reactions. However, while some energetics information can be gained from the reaction exothermicity spectra, it is often not as informative as the angular scattering diagram. Some conclusions can be made, for example for the bond-forming reactions involving the long-lived collision complex (such as N_2^{2+} with O_2, CO_2 and H_2O) it appears that the energetics could be dominated by the formation of the NO^+ products in their ground electronic state but with a full range of vibrational levels whereas the other products are all in their ground electronic states. But as is seen from the unresolved exothermicity spectra shown throughout this thesis, there is still room for improvement regarding the energetics, in order to discover even more about dication-neutral reactions. In addition computational studies could also further the knowledge of some of the systems studied experimentally in this thesis.

7.1.1 Improving the PSCO energy resolution

There are several methods by which the PSCO experiment could be modified to improve the energy resolution, such as improving the delivery of the neutral gas, increasing the detector size and Velocity Map Imaging (VMI) the products. These improvements are described as follows.

7.1.1.1 Neutral gas beam

In the current PSCO arrangement the neutral gas is introduced into the reaction source region by a simple effusive jet. This means there is little control over the position of the neutral species in the reaction region as well as the fact that there is a thermal distribution of the velocity of the neutral species. Both of these factors can broaden the exothermicity spectra. A more sophisticated beam source for the delivery of the neutral gas reactant would dramatically restrict the velocity and positional distribution of the neutral reactant in the reaction region and would hence improve the energy resolution.

7.1.1.2 Increasing the detector size

Most of the results discussed in this thesis were recorded using a 300 V repeller plate. By lowering the repeller plate voltage to 50 V, a significant improvement is seen in the resolution of the exothermicity spectra. However, at this lower repeller plate voltage, the ions travel much slower from the reaction region to the detector and so ions with any sideways scattering are not detected because they simply fly past the detector. Hence when studying bond-forming reactions, which often have a level of sideways scattered products as seen in the results Chapters, it is not practical to lower the repeller plate voltage. By increasing the size of the detector many more of these sideways scattered ions could be detected when using the lower voltage repeller plate, and so the resolution of the exothermicity spectra will be significantly improved. Furthermore, the increased sensitivity provided by the larger detector means the pass energy of the hemispherical energy analyser could be reduced. This would lead to an even smaller spread in the velocities of the dications in the ion pulses, which would also improvement the energy resolution.

7.1.1.3 Velocity Map Imaging

'Velocity Map Imaging' (VMI) maps all particles with the same initial velocity vector onto the same point on the detector using electrostatic ion lens optics and 2D detection, irrespective of their position of creation in the ionisation volume. Ions (or electrons) of all velocities are detected simultaneously to yield a three dimensional velocity distribution of scattered particles in a single image. Therefore, the kinetic energy and angular velocity distributions of the ion can be determined from one 2D image.

A typical VMI experiment uses a pulsed molecular beam which passes through a skimmer, then a small hole in a repeller plate electrode, before propagating along the axis

of a *TOF* tube. [3, 4] Between the repeller and extractor electrode, the molecular beam is crossed with a laser beam. Following the photoabsorption events, ions and electrons are produced and since each production channel has a particular associated kinetic energy release, a number of concentric ion spheres are created. By using certain electric fields in the *TOF-MS*, the ions can be focused so that all ions of the same velocity arrive at the same point on the detector. An electric field between the repeller and extractor accelerates the ion spheres into the *TOF* region where acceleration voltages 'pancake' the ion spheres along the flight tube so the ions of the same mass all arrive at the detector at the same time. This gives each fragment the same velocity upon arrival at the microchannel plate-phosphor screen detector. The images are then recorded with a CCD camera and analyzed. By using open lens optics as opposed to grid electrodes, VMI can yield excellently resolved images without significant reduction in transmission, trajectory deflections or blurring.

The conventional VMI design described above would not be suitable for studying dication-neutral reactions using PSCO, as the resolving power would not be great enough to resolve the large number of potential reaction products. However, a new variant of the VMI design which uses slightly different electric fields may be suitable for the PSCO. VMI could be implemented by the addition of one extra electrostatic lens and by changing the voltages on the existing lens in the acceleration region. Since the implementation requires so little change to the current arrangement, the experiment could be easily switched from the current mode, to VMI mode, and back again, simply by changing the voltages applied to the lens.

7.1.2 Computational Studies

In Chapter Four the angular scattering shows that the reaction of N_2^{2+} with O_2 to form NO^+ with O^+ or N^+ proceeds via a long-lived collision complex, $[N_2O_2^{2+}]$. A brief study of the potential energy surface of $N_2O_2^{2+}$ is presented, showing that $N_2O_2^{2+}$ does in fact have bound minima. Calculations also show that the collision complex $[N_2O_2^{2+}]$ has a lifetime of at least 100fs. No further calculations were presented in the thesis. However, calculations of the potential surfaces of other collision complexes such as those of $[N_2CO_2^{2+}]$ and $[N_2H_2O^{2+}]$, which are also predicted to be long-lived, could provide further supporting information for the reaction mechanisms proposed in this thesis. In addition further calculations regarding the lifetimes of the 'long' or 'short' lived collision-complexes could be useful for the confirmation of the reaction mechanisms.

7.2 Summary

The experimental improvements described above should improve the energy resolution of the PSCO, to electronically state resolve, possibly even to vibronic resolution, the reactions of molecular dications with neutrals as well as providing valuable new information about the dications themselves. The computational studies will yield more information about the collision complexes in dication-neutral bond-forming reactions.

7.3 References

[1] Harper, S. M., Hu, S. W. P., and Price, S. D., 2004, Journal of Chemical Physics, 121, 8, 3507.
[2] Ricketts, C. L., Harper, S. M., Hu, S. W. P., and Price, S. D., 2005, Journal of Chemical Physics, 123, 13, 134322-1
[3] Eppink, A. T. J. B. and Parker, D. H., 1997, Review of Scientific Instruments, 68, 9, 3477.
[4] Parker, D. H. and Eppink, A. T. J. B., 1997, Journal of Chemical Physics, 107, 7, 2357.

Appendix A

A.1 Time-Of-Flight Mass spectrometry

The basis of *TOF* mass spectrometry is that when ions are all accelerated to the same energy, the velocity of each ion depends on its mass. Hence, given that the ions of different mass take different times to travel the length of a given path, by recording the *TOF* of an ion its mass can be derived. Figure A. 1 shows a schematic of a simple "two-field" TOF-MS.

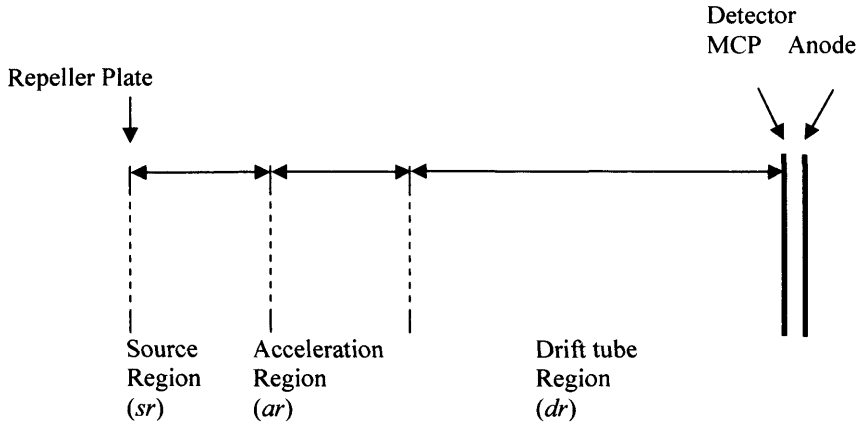

Figure A. 1 Schematic of a *TOF-MS*.

The *TOF* of an ion is composed of the sum of the *TOF* of the ion in each region of the mass spectrometer, ($t_{(sr)}$, $t_{(ar)}$ and $t_{(dr)}$) (A.1) [1];

$$TOF = t_{(sr)} + t_{(ar)} + t_{(dr)} \quad \text{(A.1)}$$

In the source region, *sr*, of the spectrometer, the $t_{(sr)}$ can be derived using the equation of motion (A.2);

$$t_{(sr)} = (v_{sr1} - v_{sr0}) / a \quad \text{(A.2)}$$

where v_{sr0} is the initial velocity of the ion on entering the region, v_{sr1} is the final velocity and a_{sr} is the acceleration of the ion in the source field. v_{sr1} can be determined using the equation of motion (A.3)

$$v_{sr1}^2 = v_{sr0}^2 + 2\, a_{sr}\, s_{sr} \quad \text{(A.3)}$$

where s_{sr} is the distance from the centre of the source region to the start of the acceleration region. Hence;

$$t_{(sr)} = ((v_{sr0}^2 + 2\, a_{sr}\, s_{sr})^{½} - v_{sr0}) / a \quad \text{(A.4)}$$

The acceleration, a_{sr}, can be determined using Newton's second law;

$$F = ma \quad \text{(A.5)}$$

The force F acts on the ion due to the electric field in the particular region, E_{sr} and the charge on the ion, q;

$$a_{sr} = (q\, E_{sr}) / m \quad \text{(A.6)}$$

Hence;

$$t_{(sr)} = ((v_{sr0}^2 + 2 s_{sr} ((q\, E_{sr}) / m))^{½} - v_{sr0}) / ((q\, E_{sr}) / m) \quad \text{(A.7)}$$

The initial velocity of the ion v_{sr0}, can be determined from the kinetic energy of the ion K, (A.8), where V is the potential of the ion at the relevant point:

$$K = q\, V = ½\, m\, v_{sr0}^2 \quad \text{(A.8)}$$

Thus

$$v_{sr0} = (2\, q\, V / m)^{½} \quad \text{(A.9)}$$

Hence;

$$t_{(sr)} = (((2\, q\, V / m) + 2 s_{sr} (q\, E_{sr} / m))^{½} - ((2\, q\, V / m)^{½})) / ((q\, E_{sr}) / m) \quad \text{(A.10)}$$

which simplifies to;

$$t_{(sr)} = (((2m)^{½}) / (q\, E_{sr}))((q\, V + q\, s_{sr} E_{sr})^{½} - (q\, V)^{½}) \quad \text{(A.11)}$$

Since;

$$q = z\, e \quad \text{(A.12)}$$

where z is the charge number and e is the electronic charge. Then;

$$t_{(sr)} = (((2m)^{½}) / (z\, e\, E_{sr}))((z\, e\, V + z\, e\, s_{sr} E_{sr})^{½} - (z\, e\, V)^{½}) \quad \text{(A.13)}$$

simplifying to;

$$t_{(sr)} = (m/z)^{½} (2^{½} / (e^{½} E_{sr}))) ((V + s_{sr} E_{sr})^{½} - V^{½}) \quad \text{(A.14)}$$

A very similar argument can be used to derive $t_{(ar)}$;

$$t_{(ar)} = (v_{ar} - v_{sr1}) / a_{ar} \quad \text{(A.15)}$$

where v_{sr1} is the initial velocity of the ion on entering the region, that is the final velocity of the ion leavening the source region, v_{ar} is the final velocity and a_{ar} is the acceleration of the ion in the acceleration field, E_{ar}. v_{ar} can be determined using the equation of motion;

$$v_{ar}^2 = v_{sr1}^2 + 2s_{ar}\,(q\,E_{ar}) / m \qquad \text{(A.16)}$$

where s_{ar} is the length of the acceleration region. Hence;

$$t_{(ar)} = ((v_{sr1} + 2s_{ar}\,(q\,E_{ar}) / m)^{1/2} - v_{sr1}) / (q\,E_{ar}) / m \qquad \text{(A.17)}$$

Given;

$$v_{sr1}^2 = v_{sr0}^2 + 2a_{sr}s_{sr} \qquad \text{(A.3)}$$
$$v_{sr0} = (2\,q\,V/m)^{1/2} \qquad \text{(A.9)}$$
$$q = z\,e \qquad \text{(A.12)}$$

Hence;

$$t_{(ar)} = ((((2\,z\,e\,V/m) + (2s_{sr}\,(z\,e\,E_{sr}) / m) + (2s_{ar}\,(z\,e\,E_{ar}) / m))^{1/2}) - (((2\,z\,e\,V/m) + (2s_{sr}\,(z\,e\,E_{sr}) / m))^{1/2})) / ((z\,e\,E_{ar}) / m) \qquad \text{(A.18)}$$

which simplifies to;

$$t_{(ar)} = (m/z)^{1/2}\,(2^{1/2} / (e^{1/2}\,E_{ar}))\,(((V + s_{sr}E_{sr} + s_{ar}E_{ar})^{1/2}) - ((V + s_{sr}E_{sr})^{1/2})) \qquad \text{(A.19)}$$

However, in the drift region there is no acceleration so the time is derived using the length of the drift tube, s_{dr}, and the velocity, v_{ar},

$$t_{(dr)} = s_{dr} / v_{ar} \qquad \text{(A.20)}$$

Given;

$$v_{ar}^2 = v_{sr1}^2 + 2s_{ar}\,(q\,E_{ar}) / m \qquad \text{(A.16)}$$
$$v_{ar}^2 = ((2\,e\,z\,V) / m) + (2s_{sr}\,(e\,z\,E_{sr}) / m) + (2s_{ar}\,(e\,z\,E_{ar}) / m)) \qquad \text{(A.21)}$$

Hence;

$$t_{(dr)} = s_{dr} / (((2\,e\,z\,V / m) + (2s_{sr}\,(e\,z\,E_{sr}) / m) + (2s_{ar}\,(e\,z\,E_{ar}) / m))^{1/2}) \qquad \text{(A.22)}$$

which simplifies to;

$$t_{(dr)} = (m/z)^{1/2}\,(1 / 2\,e)^{1/2}\,(s_{dr} / (V + s_{sr}\,E_{sr} + s_{ar}\,E_{ar})^{1/2}) \qquad \text{(A.23)}$$

The total *TOF*, (A.1), is therefore derived from the addition of equations, (A.14), (A.19) and (A.23);

$$t_{(sr)} = (m/z)^{1/2}\,(2^{1/2} / (e^{1/2}\,E_{sr}))\,((V + s_{sr}E_{sr})^{1/2} - V^{1/2}) \qquad \text{(A.14)}$$
$$t_{(ar)} = (m/z)^{1/2}\,(2^{1/2} / (e^{1/2}\,E_{ar}))\,(((V + s_{sr}E_{sr} + s_{ar}E_{ar})^{1/2}) - ((V + s_{sr}E_{sr})^{1/2})) \qquad \text{(A.19)}$$
$$t_{(dr)} = (m/z)^{1/2}\,(1 / 2\,e)^{1/2}\,(s_{dr} / (V + s_{sr}\,E_{sr} + s_{ar}\,E_{ar})^{1/2}) \qquad \text{(A.23)}$$

To conclude, if the electric fields, and of course the experimental geometry, remains constant then the terms V, e, s_{sr}, s_{ar}, s_{dr}, E_{sr}, E_{ar} and the numerical terms can be combined into one term 'c'. Therefore the TOF, is proportional to the square root of the mass to charge ratio;

$$TOF = c\,(m/z)^{1/2} \tag{A.24}$$

As previously mentioned Wiley and McLaren discovered that by applying a certain set of electric fields in a two-field TOF-MS the variation of ionic TOFs with source position could be dramatically reduced. [1] In principle, about the centre of the source the ionic TOF no longer depends on the ions initial position in space (to first order). This property is known as 'first order' space focusing;

$$(\mathrm{d}TOF / \mathrm{d}s) = 0 \tag{A.25}$$

where s is the position of the ion in the source region. (A.25) is only valid when s is the centre of the source region and assuming the ions have zero kinetic energy. However Eland discovered that in fact it was possible to derive conditions which generated 'second order space focusing'. [2] As discussed in Chapter Two, second order space focusing is used in the PSCO;

$$(\mathrm{d}^2TOF / \mathrm{d}s^2) = 0 \tag{A.26}$$

As with the first order space focusing, (A.26) is valid when s is the centre of the source region and assuming the ions have zero kinetic energy.

A.2 References

[1] Wiley, W. C. and Mclaren, I. H., 1955, Review of Scientific Instruments, 26, 12, 1150.
[2] Eland, J. H. D., 1993, Measurement Science & Technology, 4, 12, 1522.

Appendix B Other bond-forming reactions of dications with neutrals

B.1 Introduction

The reactions of the nitrogen dication, studied using the PSCO experiment, have been discussed in detail in Chapters Four, Five and Six. However several other dication-neutral-collision systems were studied using the PSCO experiment throughout the course of this thesis. In particular the reactions of the CO_2^{2+} and O_2^{2+} dications were probed. CO_2^{2+} has been predicted to be present in the Martian ionosphere and O_2^{2+} has been predicted to be present in the terrestrial ionosphere, in addition to N_2^{2+} and O^{2+}.[1, 2] Background information on the prediction of ionospheric dication abundances is given in Chapter One. In light of these recent predictions, the reactions of CO_2^{2+} with N_2, H_2O, N_2O, NO, CO, CO_2 and O_2, and O_2^{2+} with O_2, NO, N_2O and C_2H_2 have been studied using the PSCO technique. Electron transfer reactions, non-dissociative and dissociative, were detected in all these collision systems. However, bond-forming reactions were only observed following the collisions of CO_2^{2+} with N_2 and H_2O, and O_2^{2+} with N_2 and C_2H_2. After the detailed discussion of the nitrogen dication in the three results Chapters, this Appendix will serve only to briefly display some coincidence spectra, showing some of these bond-forming reactions of other dications, in order to give an impression of the reactivity of these other ionospherically relevant dications. First, however, an overview of the previously studied reactions of CO_2^{2+} and O_2^{2+} with neutral gases is given.

Isolated dications of CO_2^{2+} have been reasonably well studied which can mainly be attributed to the fact that CO_2^{2+} is a particularly stable dication. [3-17] Storage ring experiments in the last decade showed that the ground state of CO_2^{2+} has a lifetime of approximately 4.2 seconds. [18] The reactions of CO_2^{2+} with neutrals CO_2, CO, H_2, D_2, He, Ne, Ar, Kr and Xe have been previously studied, generally making the bimolecular reactivity of CO_2^{2+} one of the most intensively studied. Franceschi *et al* studied the reactions of CO_2^{2+} in collisions with CO_2 and CO. These authors used synchrotron radiation, to obtain the dication by photoionising CO_2, and the CERISES guided beam apparatus (which is described in Chapter One) and observed dissociative charge transfer reaction products CO^+ and O^+ in the reactions of CO_2^{2+} with neutral gases CO_2 and CO.[19] Mrazek *et al* studied the reaction of CO_2^{2+} with Ar and Ne using a crossed-beam

scattering apparatus and observed non-dissociative single electron transfer at low collision energy (3-10 eV).[20] Mrazek *et al* have also studied the low energy collisions of CO_2^{2+} with D_2, which yield CO_2^+, CO^+, O^+ and the bond-forming reaction products CO_2D^+ and COD^+.[21] Price *et al* studied the collisions of CO_2^{2+} with He, Ne, Ar, Kr and Xe at a collision energy of 49 eV, producing a dication beam using electron ionisation, mass selection using a quadrupole mass spectrometer and monitored the reaction products using *TOF-MS*. Price *et al* observed reaction products of rare gas ions, O^+, CO^+ and CO_2^+, and found the dominant reaction channel of CO_2^{2+} with He was collision-induced dissociation. In the reaction between Ne and Ar, the dominant reaction channel was charge transfer forming stable CO_2^+ and with Kr and Xe it was charge transfer forming unstable CO_2^+, which dissociated to O^+ and CO^+. Price *et al* rationalized this reactivity using the Landau-Zener theory, which is discussed in Chapter One and also observed the product XeO^+, a bond-forming product in the reaction of CO_2^{2+} with Xe.[22] Reid *et al* also studied the reactions of CO_2^{2+} with rare gases using mass analyzed ion kinetic energy spectroscopy and observed dissociative and non-dissociative electron transfer reaction channels at 6 and 10 keV collision energies. [23] Mrazek *et al* have studied computationally a bond-forming reaction of CO_2^{2+} with H_2, (B.1), by calculating the stationary points on the potential energy surface.

$$CO_2^{2+} + H_2 \rightarrow HCO^+ + H^+ + O \qquad \text{(B.1)}$$

Their proposed reaction mechanism, Figure B.1, shows how the dication and neutral associate first to form an intermediate collision complex (A). An H atom then migrates to form a second intermediate (B) which then loses a proton (C) and the remaining monocation dissociates.[21]

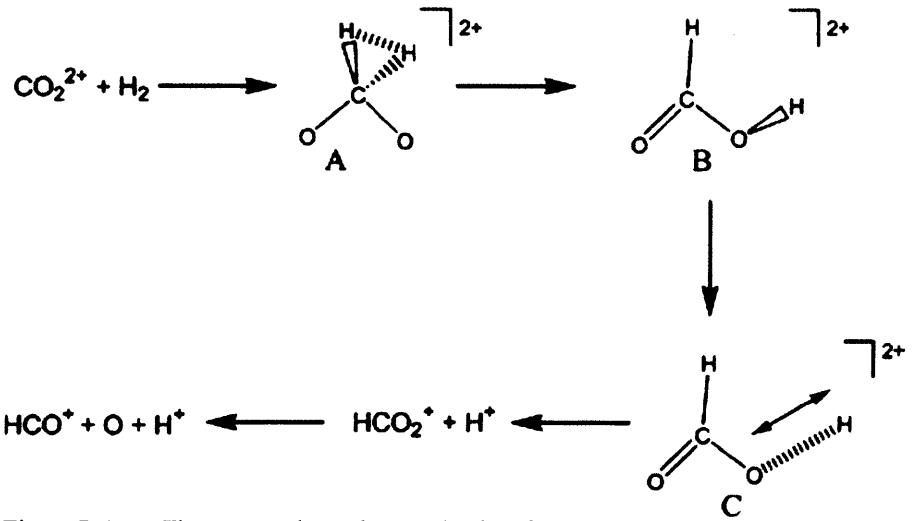

Figure B.1 The proposed reaction mechanism for (B.1) taken from [21].

Tafadar *et al* studied the intramolecular isotope effects in the bond-forming reaction collisions of CO_2^{2+} with HD. They found a strong intramolecular isotope effect favouring the formation of DCO^+ as opposed to HCO^+ at low collision energies; this could be explained using the computationally proposed mechanism for the reaction of CO_2^{2+} with H_2 and an analysis of the factors affecting the competition between the bond-forming channels.[24] The molecular oxygen dication has not been studied as intensively as CO_2^{2+}; but there have been some previous studies. The double ionisation of O_2 to form isolated O_2^{2+} dications has been studied theoretically and experimentally with vibrational resolution.[25-28] Chatterjee *et al* studied the reactions of O_2^{2+} ions with O_2, N_2, CO_2, NO and Ne, and observed one of the first bond-forming reactions (B.2).[29]

$$O_2^{2+} + NO \rightarrow NO_2^+ + O^+ \qquad \text{(B.2)}$$

The next section will show some coincidence spectra from CO_2^{2+} and O_2^{2+} collision systems which display bond-forming channels.

B.2 Results and discussion

Experimental detail is given in Chapter Two with details of the data processing. Details of the features of the coincidence spectrum are given in Chapter Three.

B.2.1 CO_2^{2+} with N_2

Six dominant bimolecular reactions can be seen in the coincidence spectra following collisions of CO_2^{2+} with N_2. The reactions observed are listed below and correspond to one non-dissociative electron transfer, (B.3), three dissociative electron transfer, (B.4), (B.5) and (B.6), and two bond-forming channels, (B.7) and (B.8).

$$CO_2^{2+} + N_2 \rightarrow CO_2^+ + N_2^+ \qquad \text{(B.3)}$$
$$CO_2^{2+} + N_2 \rightarrow CO^+ + N_2^+ + O \qquad \text{(B.4)}$$
$$CO_2^{2+} + N_2 \rightarrow O_2^+ + N_2^+ + C \qquad \text{(B.5)}$$
$$CO_2^{2+} + N_2 \rightarrow O^+ + N_2^+ + CO \qquad \text{(B.6)}$$
$$CO_2^{2+} + N_2 \rightarrow N_2O^+ + O^+ + C \qquad \text{(B.7)}$$
$$CO_2^{2+} + N_2 \rightarrow N_2O^+ + CO^+ \qquad \text{(B.8)}$$

A section of a typical coincidence spectrum recorded following the collisions of CO_2^{2+} and N_2 is shown in Figure B.2 which displays one of the bond-forming reactions (B.7) along with the typical non-dissociative electron transfer reaction.

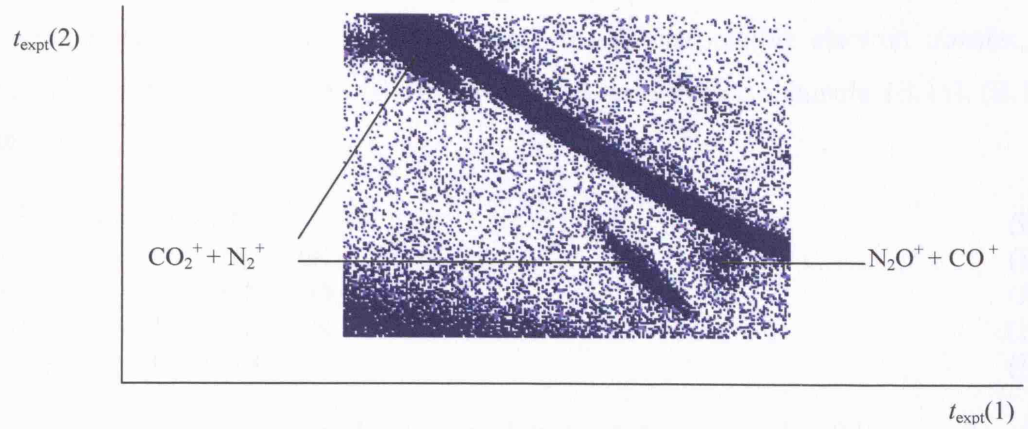

Figure B.2 A coincidence spectrum recorded following collisions of CO_2^{2+} and N_2 using a 50 V repeller plate, E_{com} 3.5 eV, showing reaction channels (B.3) and (B.7).

Figure B.3 shows a second section of the coincidence spectrum recorded following the collisions of CO_2^{2+} and N_2, showing the other bond-forming channel, (B.8).

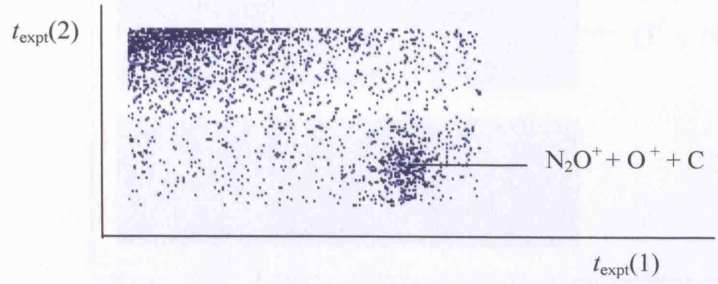

Figure B.3 The coincidence spectrum recorded following collisions of CO_2^{2+} and N_2 using a 50 V repeller plate, E_{com} 3.5 eV.

No mechanistic details can be given about the bond-forming reactions detected following the collisions of CO_2^{2+} and N_2. Channel (B.7) was only observed when using a 50 V repeller plate. As previously mentioned in Chapter Three, full scattering data is not recorded when using a 50 V repeller plate, making it difficult to draw conclusions about the reaction mechanism. Channel (B.8) is a two-body product reaction, hence products will also be scattered at 180° to each other, due to the conservation of momentum, and therefore scattering diagrams do not reveal significant information about the reaction mechanism.

B.2.2 O_2^{2+} with N_2

The reactions of O_2^{2+} may be relevant to the terrestrial ionosphere, particularly the reaction of O_2^{2+} and N_2.[2] Five dominant bimolecular reactions that can be seen in the

coincidence spectra recorded following collisions of O_2^{2+} with N_2. The reactions observed are listed below and correspond to non-dissociative electron transfer, (B.9), dissociative electron transfer, (B.10) and three bond-forming channels, (B.11), (B.12) and (B.13).

$$O_2^{2+} + N_2 \rightarrow O_2^{+} + N_2^{+} \quad \text{(B.9)}$$
$$O_2^{2+} + N_2 \rightarrow O^{+} + N_2^{+} + O \quad \text{(B.10)}$$
$$O_2^{2+} + N_2 \rightarrow NO^{+} + N^{+} + O \quad \text{(B.11)}$$
$$O_2^{2+} + N_2 \rightarrow NO^{+} + O^{+} + N \quad \text{(B.12)}$$
$$O_2^{2+} + N_2 \rightarrow O^{+} + N_2O^{+} \quad \text{(B.13)}$$

Figure B.4 shows a section of the coincidence spectrum recorded following the collision of O_2^{2+} and N_2, showing the two body bond-forming channel, (B.13).

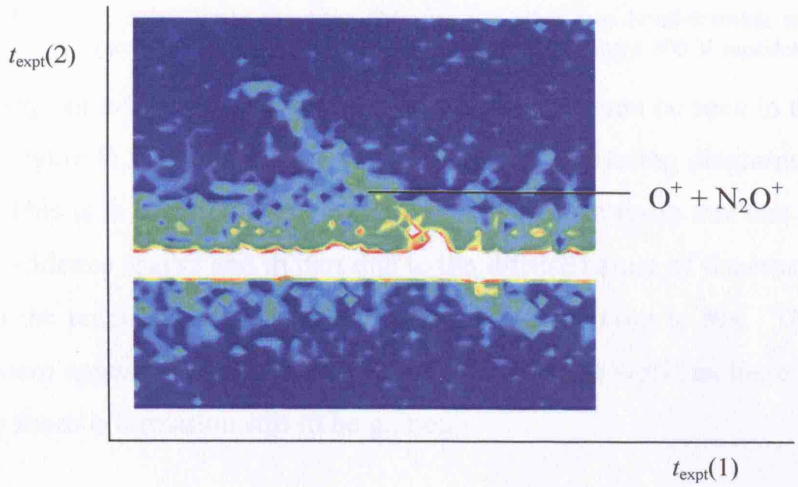

Figure B.4 A coincidence spectrum showing one of the bond-forming reactions recorded following collisions of O_2^{2+} and N_2 using a 300 V repeller plate.

As previously discussed, no informative mechanistic information can be obtained from the scattering diagrams of channel (B.13), as there are only two products. The following Figure B.5 is more noisy than most of the previously displayed coincidence spectra, but shows the other two bond-forming channels recorded following the collisions of O_2^{2+} and N_2, (B.11) and (B.12), along with the dissociative electron transfer reaction, (B.10).

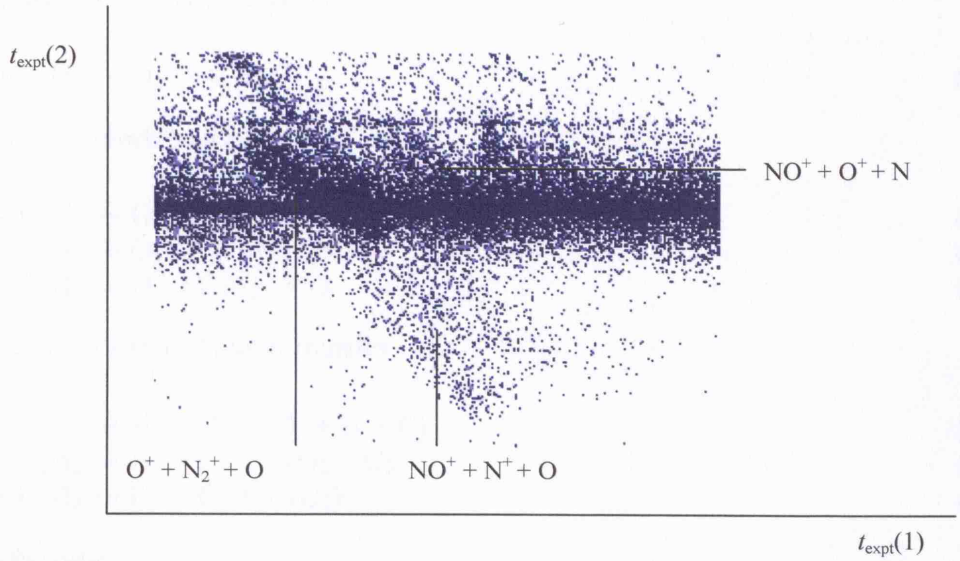

Figure B.5 A coincidence spectrum showing the other two bond-forming reactions recorded following collisions of O_2^{2+} and N_2 using a 300 V repeller plate.

The three-body bond-forming channels, (B.11) and (B.12), can be seen in the coincidence spectrum in Figure B.5. However deriving meaningful scattering diagrams from this data is difficult. This is in part due to the reasonably significant noise that can be observed in the false coincidence region and in part due to the diffuse nature of the reaction pair peaks compared to the reaction peaks discussed in the Chapters Four to Six. The O_2^{2+} and N_2 collision system appears to be the ideal candidate for future work, as there is undoubtedly significantly more information still to be gained.

The O_2^{2+} and N_2 collision system is potentially very significant in the terrestrial ionosphere, where, as previously discussed in Chapter One, O_2^{2+} has been predicted. This ionospheric O_2^{2+} is predicted at an altitude where neutral species, particularly N_2, are still present; hence ion-neutral reactions can play an important role in the ionospheric chemistry of Earth. NO^+ is known to be one of the major ions in the terrestrial ionosphere and hence the reaction channels to form NO^+ detected following the collisions of O_2^{2+} with N_2, may play a part in the chemistry of the Earth's atmosphere.

B.2.3 O_2^{2+} with C_2H_2

Twelve clear bimolecular reactions can be seen in the coincidence spectra following collisions of O_2^{2+} with C_2H_2, which are listed below according to the reaction class. Note there are five bond-forming reactions in this collision system.

Non-dissociative electron transfer

$$O_2^{2+} + C_2H_2 \rightarrow O_2^{+} + C_2H_2^{+} \quad \text{(B.14)}$$

Dissociative electron transfer

$$O_2^{2+} + C_2H_2 \rightarrow O_2^{+} + C_2H^{+} + H \quad \text{(B.15)}$$
$$O_2^{2+} + C_2H_2 \rightarrow O_2^{+} + H^{+} + (C_2H) \quad \text{(B.16)}$$
$$O_2^{2+} + C_2H_2 \rightarrow O^{+} + C_2H_2^{+} + O \quad \text{(B.17)}$$

Double dissociative electron transfer

$$O_2^{2+} + C_2H_2 \rightarrow H^{+} + C^{+} + (O_2 + H + C) \quad \text{(B.18)}$$
$$O_2^{2+} + C_2H_2 \rightarrow H^{+} + CH^{+} + (O_2 + C) \quad \text{(B.19)}$$
$$O_2^{2+} + C_2H_2 \rightarrow H^{+} + C_2H^{+} + (O_2) \quad \text{(B.20)}$$

Bond-forming

$$O_2^{2+} + C_2H_2 \rightarrow H^{+} + C_2OH^{+} + O \quad \text{(B.21)}$$
$$O_2^{2+} + C_2H_2 \rightarrow H^{+} + C_2O^{+} + (O + H) \quad \text{(B.22)}$$
$$O_2^{2+} + C_2H_2 \rightarrow H^{+} + COH^{+} + (C + O) \quad \text{(B.23)}$$
$$O_2^{2+} + C_2H_2 \rightarrow H^{+} + CO^{+} + (H + C + O) \quad \text{(B.24)}$$
$$O_2^{2+} + C_2H_2 \rightarrow CH^{+} + COH^{+} + O \quad \text{(B.25)}$$

Figure B.6 shows two of the bond-forming reactions of O_2^{2+} and C_2H_2, (B.23) and (B.24), along with a double dissociative electron transfer reaction and a dissociative electron transfer reaction.

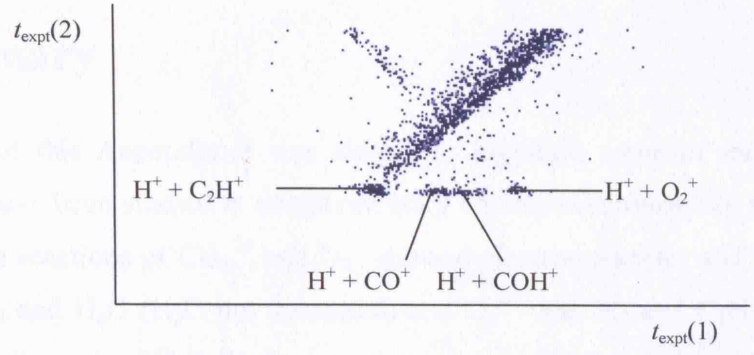

Figure B.6 A Coincidence spectrum showing some of the bond-forming reactions recorded following collisions of O_2^{2+} and C_2H_2 using a 300 V repeller plate.

As can be seen from the above list, three of the five bond-forming channels have more than three products, making scattering analysis more uncertain. The most intense three-body channel is channel (B.25), forming COH^+ and CH^+ with O. Figure B.7 shows some of the scattering diagrams derived from the data for this channel.

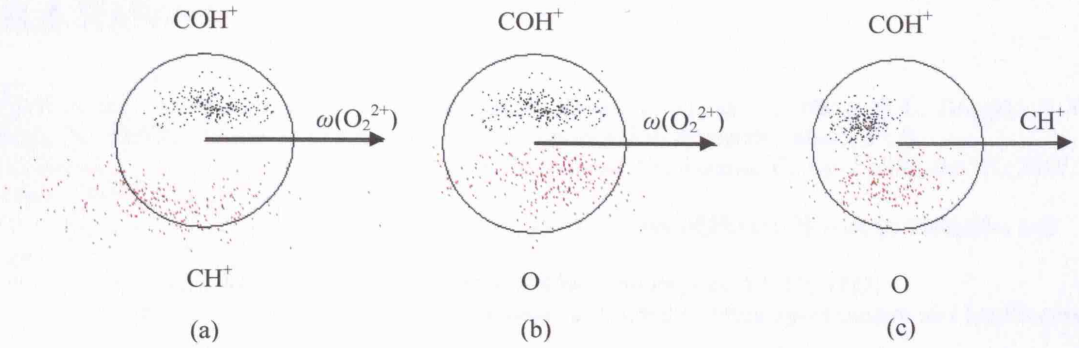

Figure B.7 The scattering diagrams for channel (B.25), recorded following the collision of O_2^{2+} and C_2H_2, circle radius 1 cm μs^{-1}.

The scattering relative to O_2^{2+}, Figure B.7 (a) and (b), shows a significant level of sideways scattering from all three products. This could hint towards complex formation, $[O_2C_2H_2]^{2+}$, and that the complex has time to rotate before dissociation. The internal frame scattering diagram, Figure B.7 (c) very clearly shows that the two ions, COH^+ and CH^+, are scattered in opposite directions while the neutral, O, has little correlation with either ion. If indeed the mechanism does involve a complex that lives for a period of time at least comparable with its rotational period, then the lack of correlation of the O neutral species, with either product ions, hints that the O dissociated from the complex first, and subsequently the $[OC_2H_2]^{2+}$ then dissociated to yield the two monocations.

B.3 Summary

The purpose of this Appendix B was simply to highlight some of the other reaction systems that have been studied in complementary studies accompanying the work of this thesis. All the reactions of CO_2^{2+} and O_2^+ showed electron transfer and the reactions of CO_2^{2+} with N_2 and H_2O (H_2O not discussed) and O_2^{2+} with N_2 and C_2H_2 also displayed bond-forming channels. While limited mechanistic or energetic information is discussed in this Appendix, the coincidence spectra displayed show that bond-forming reactions are common not only in the ionospherically reactions of N_2^{2+} as discussed in the Chapters Four to Six, but also with the ionospherically relevant molecular dications CO_2^{2+} and O_2^{2+}.[1, 2, 30]

B.4 References

[1] Witasse, O., Dutuit, O., Lilensten, J., Thissen, R., Zabka, J., Alcaraz, C., Blelly, P. L., Bougher, S. W., Engel, S., Andersen, L. H., and Seiersen, K., 2002, Geophysical Research Letters, 29, 8.
[2] Simon, C., Lilensten, J., Dutuit, O., Thissen, R., Witasse, O., Alcaraz, C., and Soldi-Lose, H., 2005, Annales Geophysicae, 23, 3, 781.
[3] Cornaggia, C., Schmidt, M., and Normand, D., 1994, Journal of Physics B-Atomic Molecular and Optical Physics, 27, 7, L123.
[4] Dujardin, G. and Winkoun, D., 1985, Journal of Chemical Physics, 83, 12, 6222.
[5] Griffiths, W. J. and Harris, F. M., 1989, International Journal of Mass Spectrometry and Ion Processes, 87, 3, 349.
[6] Hall, R. I., Avaldi, L., Dawber, G., Mcconkey, A. G., Macdonald, M. A., and King, G. C., 1994, Chemical Physics, 187, 1-2, 125.
[7] Harris, F. M., 1992, International Journal of Mass Spectrometry and Ion Processes, 120, 1-2, 1.
[8] Hogreve, H., 1995, Journal of Physics B-Atomic Molecular and Optical Physics, 28, 8, L263.
[9] Jalbout, A. F., 2002, International Journal of Quantum Chemistry, 86, 6, 541.
[10] Jonathan, P., Hamdan, M., Brenton, A. G., and Willett, G. D., 1988, Chemical Physics, 119, 1, 159.
[11] Langford, M. L., Harris, F. M., Reid, C. J., Ballantine, J. A., and Parry, D. E., 1991, Chemical Physics, 149, 3, 445.
[12] Leach, S., Devoret, M., and Eland, J. H. D., 1978, Chemical Physics, 33, 1, 113.
[13] Masuoka, T., 1994, Journal of Chemical Physics, 101, 1, 322.
[14] Newton, A. S. and Sciamann, A. F., 1964, Journal of Chemical Physics, 40, 3, 718.
[15] Seiersen, K., Al-Khalili, A., Heber, O., Jensen, M. J., Nielsen, I. B., Pedersen, H. B., Safvan, C. P., and Andersen, L. H., 2003, Physical Review A, 68, 2,
[16] Shields, G. C. and Moran, T. F., 1983, Chemical Physics Letters, 101, 3, 287.
[17] Slattery, A. E., Field, T. A., Ahmad, M., Hall, R. I., Lambourne, J., Penent, F., Lablanquie, P., and Eland, J. H. D., 2005, Journal of Chemical Physics, 122, 8,
[18] Mathur, D., Andersen, L. H., Hvelplund, P., Kella, D., and Safvan, C. P., 1995, Journal of Physics B-Atomic Molecular and Optical Physics, 28, 15, 3415.
[19] Franceschi, P., Thissen, R., Zabka, J., Roithova, J., Herman, Z., and Dutuit, O., 2003, International Journal of Mass Spectrometry, 228, 2-3, 507.
[20] Mrazek, L., Zabka, J., Dolejsek, Z., and Herman, Z., 2003, Collection of Czechoslovak Chemical Communications, 68, 1, 178.
[21] Mrazek, L., Zabka, J., Dolejsek, Z., Hrusak, J., and Herman, Z., 2000, Journal of Physical Chemistry A, 104, 31, 7294.
[22] Price, S. D., Rogers, S. A., and Leone, S. R., 1993, Journal of Chemical Physics, 98, 12, 9455.
[23] Reid, C. J., Ballantine, J. A., and Harris, F. M., 1989, International Journal of Mass Spectrometry and Ion Processes, 93, 1, 23.
[24] Tafadar, N., Kearney, D., and Price, S. D., 2001, Journal of Chemical Physics, 115, 19, 8819-8827.
[25] Dorman, F. H. and Morrison, J. D., 1963, Journal of Chemical Physics, 39, 7, 1906.
[26] Price, S. D. and Eland, J. H. D., 1991, Journal of Physics B-Atomic Molecular and Optical Physics, 24, 20, 4379.
[27] Fournier, J., Fournier, P. G., Langford, M. L., Mousselmal, M., Robbe, J. M., and Gandara, G., 1992, Journal of Chemical Physics, 96, 5, 3594.
[28] Hall, R. I., Dawber, G., Mcconkey, A., Macdonald, M. A., and King, G. C., 1992, Physical Review Letters, 68, 18, 2751.
[29] Chatterjee, B. K. and Johnsen, R., 1989, Journal of Chemical Physics, 91, 2, 1378.
[30] Lilensten, J., Witasse, O., Simon, C., Solidi-Lose, H., Dutuit, O., Thissen, R., and Alcaraz, C., 2005, Geophysical Research Letters, 32, 3.